HOKKAIDO UNIVERSITY

Title	Synthesis of W-based Complex Metal Oxide Catalysts and Transformation of Glycerol
Author(s)	小俣, 香織
Degree Grantor	北海道大学
Degree Name	博士(工学)
Dissertation Number	甲第11478号
Issue Date	2014-03-25
DOI	https://doi.org/10.14943/doctoral.k11478
Doc URL	https://hdl.handle.net/2115/58196
Type	doctoral thesis
File Information	Kaori_Omata.pdf

Hokkaido University Collection of Scholarly and Academic Papers : HUSCAP

Synthesis of W-based Complex Metal Oxide Catalysts and Transformation of Glycerol

by

KAORI OMATA

Thesis submitted in partial fulfillment

of the requirements for the degree of

Doctor of Engineering

2013

Graduate School of Chemical Sciences and Engineering

Hokkaido University

Promoter: Prof. Dr. Wataru Ueda
Referees: Prof. Dr. Atsushi Fukuoka
Prof. Dr. Takao Masuda
Prof. Dr. Shin Mukai
Prof. Dr. Ken-ichi Shimizu

TABLE OF COTETS

Chapter 1 General Introduction

1-1 Synthesis of acrolein and acrylic acid from glycerol 1

1-1-1 Why glycerol has been targeted? 1

1-1-1-1 Oil dependence and utilization of biomass

1-1-1-2 Biodiesel production and glycerol

1-1-1-2-1 Production of biomass

1-1-1-2-2 Glycerol

1-1-2 Transformation of glycerol 3

1-1-2-1 Oxidation

1-1-2-2 Reforming

1-1-2-3 Hydrogenolysis

1-1-2-4 Esterification

1-1-2-5 Other processes

1-1-3 Synthesis of acrolein from glycerol 5

1-1-3-1 Demand of acrolein and ongoing process

1-1-3-2 Synthesis of acrolein from glycerol

1-1-3-2-1 Production mechanisms of acrolein and by-products

1-1-3-2-2 Proposed catalysts and problems

1-1-4 Synthesis of acrylic acid from glycerol 13

1-1-4-1 Synthesis of acrylic acid from acrolein

1-1-4-2 Direct transformation of glycerol to acrylic acid

1-1-4-2-1 Proposed catalysts and problems

1-2 Synthesis of W-based complex metal oxide catalysts and transformation of glycerol ―The outline of this thesis― 17

1-3 References 19

Chapter 2 Hydrothermal Synthesis of W-based Complex Metal Oxide

2-1 Introduction 45

2-2 Experimental 47

2-2-1 Chemicals 47

2-2-2 Catalyst preparation 47

2-2-2-1 Preparation of W-Nb-O by hydrothermal method

2-2-2-2 Preparation of WO_3/Nb_2O_5 by impregnation method

2-2-2-3 Preparation of $Cs_{0.5}[Nb_{2.5}W_{2.5}O_{14}]$ by solid-state reaction

2-2-2-4 Preparation of hexagonal WO_3

2-2-2-5 Preparation of W-V-O and W-Ta-O

2-2-3 Catalyst characterization 48

2-2-3-1 XRD

2-2-3-2 Nitrogen adsorption

2-2-3-3 SEM-EDS

2-2-3-4 STEM

2-2-3-5 TEM

2-2-3-7 Raman

2-2-3-8 Rietveld analysis

2-3 Results and discussion 50

2-3-1 $Cs_{0.5}[Nb_{2.5}W_{2.5}O_{14}]$ 50

2-3-2 Hydrothermal synthesis of W-Nb-O 50

2-3-2-1 Effect of the W/Nb ratio

2-3-2-2 Effect of the concentration of precursor solution

2-3-2-3 Effect of the calcination temperature

2-3-3 Characterization of layer-structured W-Nb-O 53

2-3-4 Synthesis of W-V-O and W-Ta-O 54

2-4 Conclusion 56

2-5 References 57

Chapter 3 Solid Acid Property of W-based Complex Metal Oxide and Dehydration of Glycerol to Acrolein

3-1 Introduction 81

3-2 Experimental 82

3-2-1 Chemicals 82

3-2-2 Catalyst preparation 82

3-2-2-1 Preparation of W-Nb-O by hydrothermal method

3-2-2-2 WO_3/ZrO_2

3-2-2-3 H-ZSM-5

3-2-2-4 Treatment of $Cs_{0.5}[Nb_{2.5}W_{2.5}O_{14}]$ with acid

3-2-3 Catalyst characterization 84

3-2-3-1 NH_3-TPD

3-2-3-2 FT-IR spectroscopy of adsorbed pyridine

3-2-3-3 Determination of coke amount

3-2-4 Catalytic testing 84

3-2-4-1 Transformation of glycerol

3-3 Results and discussion 86

3-3-1 Effect of crystal structure on selectivity in glycerol transformation 86

3-3-1-1 Acid properties

3-3-1-2 Catalytic glycerol dehydration

3-3-1-3 Catalytic deactivation

3-3-2 Effect of the W/Nb ratio on activity for glycerol transformation 88

3-3-2-1 Surface properties of catalysts

3-3-2-2 Activity for glycerol transformation

3-3-3 Transformation of glycerol over W-V-O and W-Ta-O 89

3-3-3-1 Acid properties

3-3-3-2 Glycerol transformation

3-4 Conclusion 91

3-5 References 92

Chapter 4 Glycerol Transformation over the W-Nb Complex Metal Oxide Catalyst

4-1 Introduction 109

4-2 Experimental 111

4-2-1 Chemicals 111

4-2-2 Catalyst preparation 111

4-2-2-1 Preparation of W-Nb-O by hydrothermal method

4-2-3 Catalyst characterization 112

4-2-3-1 FT-IR spectroscopy of adsorbed pyridine

4-2-4 Catalytic testing 112

4-2-4-1 Transformation of glycerol

4-3 Results and discussion 114

4-3-1 Reaction pathway 114

4-3-2 Effect of reaction atmosphere on catalytic property 115

4-3-2-1 Effect of water on catalytic activity

4-3-2-1-1 Glycerol transformation

4-3-2-1-2 FT-IR of adsorbed pyridine

4-3-2-1-3 Cumene cracking

4-3-2-2 Effect of partial pressure of O_2 on catalytic activity

4-4 Conclusion 119

4-5 References 120

Chapter 5 Direct Oxidative Transformation of Glycerol to Acrylic Acid over W-based Complex Metal Oxide Catalysts

5-1 Introduction 131

5-2 Experimental 133

5-2-1 Chemicals 133

5-2-2 Catalyst preparation 133

5-2-2-1 Preparation of W-V-Nb-O by hydrothermal method

5-2-2-2 Addition of V to W-Nb-O by impregnation method

5-2-2-3 Reference catalysts

5-2-3 Catalyst characterization 134

5-2-3-1 XRD

5-2-3-2 Nitrogen adsorption

5-2-3-3 SEM-EDS

5-2-3-4 STEM

5-2-3-5 NH_3-TPD

5-2-3-6 FT-IR spectroscopy of adsorbed pyridine

5-2-3-7 Raman

5-2-3-8 ESR

5-2-4 Catalytic testing 136

5-2-4-1 Transformation of glycerol

5-2-4-2 Oxidation of acrolein

5-3 Results and discussion 138

5-3-1 W-Nb-O and W-V-O catalysts 138

5-3-2 Addition of V to W-Nb-O 139

5-3-3 Effect of V content and reaction conditions on the yield of acrylic acid 142

5-3-4 Effect of V addition on life time 145

5-4 Conclusion 146

5-5 References 147

Chapter 6 Transformation of Glycerol over Phosphoric Acid Added W-based Complex Metal Oxide Catalysts

6-1 Introduction 179

6-2 Experimental 180

6-2-1 Chemicals 180

6-2-2 Catalyst preparation 180

6-2-2-1 Addition of phosphoric acid to W-Nb-O and W-V-Nb-O

6-2-3 Catalyst characterization 181

6-2-3-1 XRD

6-2-3-2 Nitrogen adsorption

6-2-3-3 STEM

6-2-3-4 NH_3-TPD

6-2-3-5 FT-IR spectroscopy of adsorbed pyridine

6-2-4 Catalytic testing 182

6-2-4-1 Transformation of glycerol

6-2-4-2 Oxidation of acrolein

6-3 Results and discussion 184

6-4 Conclusion 186

6-5 References 187

Chapter 7 General Conclusion 195

Chapter 1

General Introduction

1-1 Synthesis of acrolein and acrylic acid from glycerol

1-1-1 Why glycerol has been targeted?

1-1-1-1 Oil dependence and utilization of biomass

An oil is a vital resource for our life. Fig. 1.1 illustrates a primary energy supply and their composition in Japan.[1] Primary energy is an energy form found in nature that has not been subjected to any conversion or transformation process such as oil and coal. Oil dependence (the ratio of oil in primary energy) is about 15% in 1953, and continued to increase at a rapid rate, and then reached 77.4% in 1973. Since the oil shock of the 1973, oil dependence has decreased gradually. Nevertheless, the dependence remained above 40% as of 2011. Reducing dependence on oil is extremely important globally because the excess use of oil have the problems such as emission of air pollution or CO_2 with their combustion, localization of regions with oil reserves, change in price, and reserve-production ratio.

Petrochemicals are the refined components of crude oil and the chemical products made from them. The use as material for chemical product accounts for about 20% in domestic demand for oil.[2] The development of chemical process for effective utilization of oil is a global challenge.

Under this situation, biomass utilization of as an alternative to oil has attracted attention. “Biomass” is renewable organic animal- or plant-derived resource.[3]

Because plants absorb carbon dioxide generated from the combustion of biomass during photosynthesis, there is no increase in the amount of carbon dioxide in the atmosphere (Carbon neutral). Besides, biomass energy is renewable because it is derived solar energy adsorbed by plants. Utilization of biomass as an energy source or material for petrochemical products has been expanding globally.

In USA, Energy Policy Act of 2005 went into effect. The government gave subsidy of $3.2 billion and preferential treatment for development of renewable energy. In Japan, the action program called “Biomass Nippon Strategy” to promote biomass utilization was also approved in a Cabinet meeting in 2010.

1-1-1-2 Biodiesel production and glycerol

1-1-1-2-1 Production of biomass

Bioethanol and biodiesel are the most common biomass resource and used as biofuel. Fig. 1.2 illustrates ethanol and biodiesel global production.[4] The capacities of ethanol and biodiesel productions are expanding year after year. In 2012, the production capacities of ethanol and biodiesel were 83.1 and 22.5 billion liters, respectively.

Bioethanol is ethanol produced by fermentation method. 95% of ethanol produced worldwide is bioethanol. About 80% of bioethanol is used as fuel.[5]

Biodiesel fuel (BDF) is animal- or plant- derived diesel fuel. It has been used as fuel for cars in Europe and Brazil. In Japan, "Act on the Quality Control of Gasoline and Other Fuels" standardized quantity of light diesel oil on the assumption that it contains the 5% of biodiesel, and went into effect in 2007. Biodiesel has been used as fuel for public cars or buses in some local communities.

1-1-1-2-2 Glycerol

Development of biodiesel production process based on transesterification of plant oils and animal fat has progressed greatly as described above.[6] This growth is accompanied by a significant increase in glycerol production, as this a significant by-product (~10 wt%) of the biodiesel process (Scheme 1.1).

As biodiesel production increases, the price of glycerol is expected to drop significantly from the actual cost, which has already decreased by half in the last few years.[7] Under this situation, the reuse of glycerol as chemical feedstock was studied widely. However, the crude glycerol contains water, methanol, unconverted oil and alkali derived from the catalysts such as sodium and potassium hydroxide for the transesterification. Therefore, the crude glycerol that is not refined generally burned or treated as industrial waste.[8]

Recently, solid base catalysts such as CaO[9], $Ca_2(Al(OH)_6)Cl \cdot 2H_2O$[8] and La_2O_3/ZrO_2[10] as alternative to water-soluble base such as for sodium hydroxide have been reported. These catalyst gave high yield of biodiesel of 74.6~97.5% in transesterification.

In parallel with these techniques, the process which transforms glycerol into high value-added product should be developed.

1-1-2 Transformation of glycerol

The transformation of glycerol into other desirable chemicals by various reactions has been attempted by many researchers.

1-1-2-1 Oxidation

Oxidation of glycerol is one of the most important processes, and gives various products as shown in Scheme 1.2. Kimura *et al*. has reported the oxidation of glycerol to dihydroxyacetone which used as ingredient of cosmetics over Bi-Pt based catalysts.[11] Then it has been reported that other products such as glyceric acid and glyceraldehyde are able to be formed with controlling reaction conditions.[12-17] Pd, Pt, Au and their alloy is efficient for these reactions. Because carbonic acids as products are decomposed by decarboxylation, the selective formation of desirable products which are intermediates in sequential reaction is important.

1-1-2-2 Reforming

Growing energy demands in a time of dwindling fossil fuel supplies has attracted much attention to hydrogen as an energy carrier. Hydrogen has been mainly produced by steam reforming of natural gas and other hydrocarbons (Scheme 1.3). The hydrogen production from glycerol decreases fossil resources. The topic of glycerol reforming for hydrogen production has received some attention in the literature.

It has been reported that Ni supported catalysts used for reforming of hydrocarbon industrially gave 98% of glycerol conversion and 63% of hydrogen selectivity in the glycerol reforming.[18] The kind of active metals and supports are investigated aiming enhancement of the catalytic activity and suppression deactivation of catalysts by carbon deposition.[19-21]

1-1-2-3 Hydrogenolysis

Scheme 1.4 illustrates pathways of hydrogenolysis of glycerol.[22] Among the products in the glycerol hydrogenolysis, 1,3-propanediol (1,3-PD), 1,2-propanediol (1,2-PD; propylene glycol), 1-propanol (1-PrOH), 2-propanol (2-PrOH) and ethylene glycol (EG) are industrially important. Propanediols have applications as antifreeze, lubricant or a starting monomer of polyesters. In particular, 1,3-PD is the most attractive target in the conversion of glycerol because of the high price and large demands.

The catalysts containing noble metals having an ability to activate hydrogen molecules, Ni, Co and Cu has been reported for hydrogenolysis.In particular, Cu-based catalysts gave high yield of 1, 2-PrD of more than 90%.[23] However, this process has not been conducted industrially in Japan due to the small difference in the price between glycerol and 1, 2-PrD. Recently, Nakagawa et al. has been reported the Ir-ReOx/SiO_2 as an efficient catalyst for the synthesis of 1, 3-PrD from glycerol (1, 3-PrD selectivity, 70%; yield, 38%).[24]

1-1-2-4 Esterification

Glycerol can be esterified with carbonic acid to obtain value added products of mono-, di- and tri-acetyl glycerol (named as MAG, DAG and TAG, respectively), which have found versatile industrial applications (Scheme 1.5).

MAG and DAG obtained by esterification with acetic acid have applications in cosmetics, medicines and as a starting monomer for the production of biodegradable polyesters [26, 27]; whereas TAG has salutary application as a fuel/biodiesel additive.[28] Besides, MAG obtained by esterification with higher fatty acid such as palmitic acid ($C_{15}H_{31}COOH$) is amphipathic molecule which is one of the most widely used emulsifiers in food, pharmaceutical and cosmetic industries.[29] It is important to suppress the formation of DAG and TAG as by-product. The solid acid catalysts such as complex metal oxides, zeolites and heteropoly acids have been reported for liquid phase reaction.[30-33]

1-1-2-5 Other processes

Other processes such as etherification to glycerol t-butylether used as a fuel/biodiesel additive or octane booster,[34] oligomerization to diglycerol, triglycerol or polyglycerols used as additives in food industry and cosmetic applications[35, 36] have been also reported.

1-1-3 Synthesis of acrolein from glycerol

1-1-3-1 Demand of acrolein and ongoing process

Most acrolein is used for synthesis of acrylic acid which is used in the manufacture of plastics, coatings, adhesives and so on. In particular, the demand of acrylic acid as a starting material for synthesising sodium polyacrylate increased (Scheme 1.6(a)). According to its physical properties, this polymer, classified as a superabsorbent, finds uses in hygiene products, such as diapers. The annual worldwide market for this superabsorbent polymer (SAP) is estimated at 1.9 million tonnes for 2010.27. [6] The second largest consumer of acrolein is represented by the synthesis of DL-methionine via 3-methylthio-propionaldehyde as an intermediate (Scheme 1.6(b)). DL-Methionine is an essential amino-acid, which cannot be synthesised by living organisms, and is widely used in meat production to accelerate animal growth. The annual worldwide production capacity of DL-methionine is about 500 000 tonnes. As natural methionine sources like plants and microorganisms provide concentrations that are too low, it has to be synthesised on the industrial scale. It is estimated that the global demand will increase by 3–7% in the near future.

The synthesis of acrolein is currently based on the selective oxidation of propene over complex multicomponent $BiMoO_x$-based catalysts (Scheme 1.7). The selectivity reached in this process is close to 85% at 95% conversion.[37]

1-1-3-2 Synthesis of acrolein from glycerol

Acrolein can be obtained by dehydration of glycerol by a double-dehydration of glycerol (Scheme 1.8). It is expected to reduce dependence on oil and increase in demand of propene by the synthesis of acrolein from biomass-derived glycerol.

In 2009, NIPPON SHOKUBAI CO., LTD. announced that they have developed a high-performance catalyst for manufacturing acrolein, an intermediate at manufacturing acrylic acid, from glycerine obtained as a by-product when biodiesel fuel is manufactured from vegetable oils.[38] Their technology was adopted as a subject of 2009 Subsidy for Development Cost of Industrial Technology of Innovation Promotion Program of NEDO and has been demonstrated in pilot plant.

The dehydration of glycerol into acrolein has been known since the twentieth century. As early as 1918, Sabatier and Gaudion[39] reported the synthesis of acrolein (10% yield) from glycerol by gas-phase dehydration on Al_2O_3 or UO_2 catalysts at 360 and 350◦C, respectively, with ethanol, water, and allyl alcohol as other products. In 1928, Freund reported that pure acrolein could be produced from glycerol at 180 ◦C using diatomaceous silica.[40] After that, various solid acid catalysts such as activated bauxite,[41] solid phosphoric acid[42] and phosphoric acid supported on alumina[43] have been applied to this reaction in gas phase.

The utilization of solid acid catalysts in liquid-phase dehydration of glycerol has been also reported. [44-47] However, the number of publications dealing with liquid-phase dehydration is quite less than that with gas-phase dehydration. Their activity is lower than that of homogeneous catalysts such as sulfuric acid or potassium sulphate. Besides, the reaction must be carried out under about 30 MPa of pressure at temperature above 573 K to obtain high acrolein selectively.

1-1-3-2-1 Production mechanisms of acrolein and by-products

Formation of acrolein and acetol

A first proposal was made by Bühler *et al*. for the glycerol activation in the liquid phase.[48] Two pathways were claimed, either via an ionic or a radical mechanism (Scheme 1.9). The ionic reaction (Scheme 1.9(a)) begins with the protonation of glycerol either on one primary hydroxyl group or on the

secondary hydroxyl group. Consequently, the elimination of a water molecule leads to the formation of a carbocation. In the case of the secondary carbocation, the only possible product after release of H_3O+ is acrolein, whereas either acrolein or acetaldehyde + formaldehyde can be formed starting from the primary carbocation. The radical pathway (Scheme 1.9(b)) starts with the abstraction of a hydrogen atom from a primary carbon using an OH· radical. The resulting radical species further loses an hydroxyl radical (OH·), which leads to the formation of acrolein.

Tsukuda *et al*. –who performed the dehydration in the gaseous phase – developed a more formal reaction framework (Scheme 1.10).[49] The first dehydration step leads to the formation of two enols, which are in tautomeric equilibrium with the corresponding ketone (hydroxyacetone) and aldehyde (3-hydroxypropionaldehyde). The latter may subsequently react in a second dehydration reaction to yield acrolein, or undergoes a retroaldol reaction to liberate formaldehyde + acetaldehyde, which – in the presence of oxygen – can easily be oxidised to acetic acid. In agreement with the previous proposal of Bühler *et al*., Tsukuda et al. confirmed that the key to obtain high acrolein selectivity lies in the control of the first dehydration step, whereby the formation of 3-hydroxypropionaldehyde must be favored over the formation of hydroxyacetone, which is identified as the main by-product of the process.

Chai *et al*. screened numerous catalysts, which were classified into four different groups according to their acidity.[50] As shown in Fig. 1.3, the most effective acid strength for the selective dehydration of glycerol to form acrolein appeared between $-8.2<H_0<-3.0$, with which acrolein was produced at a selectivity of 60–70 mol%. The catalysts having very strong acid sites ($H_0<-8.2$) effected a lower acrolein selectivity (40–50 mol%) due to more severe coke deposition in the reaction. Solid acids holding medium strong and weak acid sites ($-3.0<H_0<+6.8$) were found to be not selective for the acrolein production, the acrolein selectivity being less than 30 mol%. Solid base catalysts were shown not to be effective for acrolein production. Nevertheless, because the catalytic performance was not depend on only acid strength, the authors have been also suggested that Brönsted acid sites are advantageous over Lewis acid sites in catalyzing the selective synthesis of acrolein from glycerol dehydration.

Alhanash *et al.* compared a pure Brönsted acid catalyst (acidic caesium salts of phosphotungstic acid

(CsPW)) to a pure Lewis acid catalyst (Zn-Cr mixed oxide).[51]

Because the acrolein selectivity over Zn-Cr mixed oxide (acrolein serectivity, 30-34%; aceotol selectivity, 31-42%) was lower than that over CsPW, they concluded that Lewis acid catalysts give a larger selectivity for hydroxyacetone. However, the pathway where acrolein forms over Lewis acid site is suggested because acrolein was also obtained over the Zn-Cr mixed oxide catalyst.

They have proposed the reaction mechanisms shown in Scheme 1.11. Since proton transfer is not limited by steric constrains, interaction of glycerol with a proton site should mainly lead to the protonation of the internal oxygen in the glycerol molecule possessing a higher negative charge compared to the terminal oxygens (Scheme 1.11(a)). Subsequent steps involve elimination of H_3O^+ to give 1,3-dihydroxypropene and its tautomerisation to 3-hydroxypropanal. The latter undergoes further acid-catalysed dehydration to yield acrolein. Finally, the proton site is regenerated by interaction of its conjugate base with H_3O^+.

Interaction of glycerol with Lewis acid sites, in contrast to the glycerol protonation above, is bound to be affected by steric constrains. As a result, it is the terminal OH group of glycerol rather than the internal one that is more likely to interact with Lewis acid site as shown in Scheme 1.11(b), where two oxo-bridged metal ions (M) represent the Lewis acid site in the Zn–Cr oxide. Concerted transfer of the terminal OH group of glycerol to the M and migration of the H^+ from the internal carbon atom to the bridging O atom of the oxide gives 2,3-dihydroxypropene together with the hydrated active site in the catalyst. The 2,3-dihydroxypropene is then tautomerised to yield hydroxyacetone, and the Lewis acid site is regenerated by thermal dehydration of its hydrated form.

Kinage *et al*. investigated the selective dehydration of glycerol to hydroxyacetone and proposed a reaction mechanism over basic catalysts.[52] The Na/CeO_2 catalyst gave hydroxyacetone in yield of about 80%. Proposed pathway is shown in Scheme 1.12. The reaction over basic catalysts begins with a dehydrogenation step. The resulting 2,3-dihydroxypropanal can either further react via consecutive dehydration and hydrogenation to yield hydroxyacetone, or can form– via a retro-aldol reaction – formaldehyde and hydroxyacetaldehyde, which can be subsequently hydrogenated to ethylene glycol.

Stošić *et al*.[53-55] has been reported about relation between catalytic activity and surface acid–base features. Besides Fig. 1.4 presents acrolein selectivity as a function of the ratio of acid to basic sites ($V_{irr}(SO_2)/V_{irr}(NH_3)$). This ratio has been calculated for each catalyst from microcalorimetry results by dividing the amount of irreversibly adsorbed NH_3 by the amount of irreversibly adsorbed SO_2. As can be observed in Fig. 1.4, the higher this parameter is (which corresponds to a decrease in basicity) the higher the selectivity towards acrolein is, and after a certain value further increase of this ratio does not influence selectivity which remains constant. However, the catalysts having high acid amount exhibited high glycerol conversion corresponding with acrolein selectivity. The selectivity should be compared at iso-conversion of glycerol.

As discussed above, it is considered that the strength and the type of the catalyst acidity are of utmost importance for obtaining high catalytic performances.

Calculation for pathway to acrolein and hydroxyacetone

Nimlos *et al*. calculated energies for the neutral and the protonated reaction pathways.[59] For the so-called 'neutral glycerol', they found a very high activation barrier of 70.9 kcal mol^{-1} for the dehydration of the secondary hydroxyl-group (Fig. 1.5). In contrast, the second dehydration step – starting from the intermediate 3-hydroxy-propionaldehyde – required only 29.7 kcal mol^{-1}. The dehydration of the primary OH-group, leading to the formation of hydroxyacetone, was found to be energetically even more unfavorable, with an activation energy of 73.2 kcal mol^{-1}. Nevertheless, the formation of hydroxyacetone is exothermic and liberates 4.0 kcal mol^{-1}, whereas acrolein requires +9.3 kcal mol^{-1}.

The calculations for the protonated glycerol – as proposed by Bühler *et al*.[48] – show that the activation energies aremuch lower than for the non-protonated one. Starting from the protonated secondary hydroxyl group of glycerol, the activation energy of the transition state of the first dehydration is only 22.4 kcal mol^{-1} *vs*. 70.9 kcal mol^{-1} without proton. The second dehydration step, which is calculated to 24.6 kcal

mol^{-1} in the presence of a proton, is also 5.1 kcal mol^{-1} lower than without (29.7 kcal mol^{-1}). Furthermore, the reaction pathway for protonated glycerol leads to the exothermic formation of acrolein with an energy release of 18.0 kcal mol^{-1}. As in the case of the nonprotonated reaction, the formation of hydroxyacetone requires a higher activation energy of 24.9 kcal mol^{-1} compared to that required for the formation of acrolein (22.4 kcal mol^{-1}). Moreover, the differences in the final energy states of the two products are quite low (hydroxyacetone: -18.3 kcal mol^{-1}; acrolein: -18.0 kcal mol^{-1}). From these results, one can conclude that the formation of hydroxyacetone is thermodynamically less favored than the formation of acrolein, due to the associated higher barrier of activation energy. Nevertheless, the difference is rather small, which suggests that it might be difficult to entirely suppress the formation of hydroxyacetone.

By-products other than hydroxyacetone

The various products form from glycerol besides acrolein and hydroxyacetone. Chai *et al*.[50] indicated two hydrogenation steps, one starting from acrolein and the other from hydroxyacetone to yield allylic alcohol and 1,2-propanediol, respectively.

Corma *et al*. investigated sequential products by using hydroxyacetone as a reactant at 350◦C.[56] The products were classified into three groups: acids (9.4%), other aldehydes (52.0%) and coke (27.7%). Based on this result, they have proposed the pathway shown in Scheme 1.13. Nevertheless, the conversion of hydroxyacetone did not exceed 25%, which means that this compound is quite stable and does not easily undergo consecutive reactions. This explains why it is usually identified as the major by-product in the reaction of dehydration of glycerol to acrolein.

Suprun *et al.*[57] demonstrated the formation of formaldehyde and acetaldehyde issuing from 3-hydroxypropionaldehyde. Additionally, significant amounts of coke were found, which was ascribed to the formation of cyclic C6 compounds identified by GC–MS analysis (Scheme 1.14(a)). The authors further identified numerous furan derivatives as products from hydroxyacetone (Scheme 1.14(b)).

Deleplanque *et al*.[58] has reported that the presence of oxygen results in a new type of product distribution (Scheme 1.15). In addition to dehydration, which yields the already known products like

hydroxyacetone and acrolein, or their reductions to acetone and allylic alcohol, the authors postulate some new oxidation reactions. Starting from formaldehyde, originating from the aforementioned retroaldol reaction, oxidation leads to the formation of formic acid, which is easily over-oxidised to CO or CO_2. When acrolein is oxidised, acrylic acid is observed, which may further react to give acetic acid by decarbonylation. Although the presence of oxygen has a positive impact on the long-term performances of the catalyst, it results in a much higher number of by-products.

1-1-3-2-2 Proposed catalysts and problems

Various solid acid catalysts have been reported for the gas-phase glycerol dehydration (Table 1.1). Typical proposed catalysts and problems are shown below.

Heteropoly acid

Keggin heteropoly acids (*i.e.* HSiW, HPW, HPMo on silica supports), possessing very strong Brönsted acidity, have been found amongst the most efficient catalysts for glycerol to acrolein conversion in the gas phase.[49] In particular, with 12-tungstosilicic acid, $H_4SiW_{12}O_{40}$, possessing a higher water tolerance compared to other Keggin heteropoly acids, acrolein yields of 80% have been achieved at an optimum temperature of 548 K.

The caesium 12-tungstophosphate $Cs_{2.5}H_{0.5}PW_{12}O_{40}$ (CsPW) catalyst gave acrolein yield of up to 98% at 548 K, which is the highest performance ever reported. However, it should be noted that regeneration of heteropoly acid catalysts by combustion of coke is difficult because of relatively low thermal stability of heteropoly acids.[60] Doping CsPW with platinum group metals (PGM), such as Ru, Pd and Pt, and co-feeding hydrogen to the reaction system has been reported to enhance catalyst lifetime and reduce coke deposition.

Zeolites and SAPO

Kim *et al*. studied the influence of the silica/alumina ratio in zeolites of the H-ZSM-5 type,[61] and

reported that H-ZSM-5 catalysts with SiO_2/Al_2O_3＝150 exhibited the highest yield for acrolein synthesis from glycerol (glycerol conversion, 94%; acrolein yield, 54% at 613 K).[61] Besides, Y- or Beta-Zeolites has been also reported although their activity was lower than that of H-ZSM-5.[56, 62]

Suprun *et al*.[57] has been reported the acrolein formation from glycerol over SAPO-11 and SAPO-34. SAPO-34 gave acrolein in selectivity of 72% at the glycerol conversion of 59% at 553 K.[57]

However, deactivation of the catalysts due to the formation of coke and internal diffusion limitations are problems for these catalysts. To suppress the pore blockage by coke, various approaches such as the using small-sized zeolites,[63] expanding external surface area with alkali treatment[64] and using fluidized bed reactor[56] have been examined.

Metal oxides, complex metal oxides and phosphate

・Nb_2O_5 and Ta_2O_5

Niobium oxide (Nb_2O_5) and tantalum oxide (Ta_2O_5) have been used as a water-tolerant solid acid catalyst for various water-involving reactions, such as esterification, hydrolysis, dehydration, and hydration.[65] A key to the acidic and catalytic properties of Nb_2O_5 is its calcination or pretreatment temperature.[66]

Chai *et al.* has been reported the dehydration of glycerol over Nb_2O_5[67] and Ta_2O_5.[68] Nb_2O_5 gave acrolein in selectivity of 88% at glycerol conversion of 88%. On the other hand, Ta_2O_5 gave acrolein in selectivity of 75% at glycerol conversion of 60%. In both cases, calcination temperature affected the catalytic performances and the catalysts calcined at a temperature below 673 K exhibited high activity.

・WO_3/ZrO_2

WO_3/ZrO_2 is well-known as a solid superacid catalyst and has been used as the catalyst for the glycerol dehydration. Ulgen *et al*. has been reported that 19wt.%WO_3/ZrO_2 gave selectivity for aclorein of 69% at glycerol conversion of 83%.[69]

Dubois injected 250 ppm of sulfur dioxide into the feed in order to slow down the deactivation.[70]

The addition of SO_2 even induced a slight positive impact on the selectivity for acrolein (73% vs. 72% without SO_2) and significantly inhibited the formation of hydroxyacetone (selectivity of 0.2% vs. 2.4% without SO_2). Besides, the addition of SO_2 exhibited the effect for suppression of catalytic deactivation.

・VPO, $Fe_x(PO_4)_y$

Wang *et al*.[71] have reported vanadium pyrophosphate calcined at 800◦C, which gave selectivity for acrolein of 64% at full conversion at 573 K.

Deleplanque *et al*. have reported that $Fe_x(PO_4)_y$ synthesized by hydrothermal reaction or precipitation gave acrolein in yield of 92.1%.[58] With co-feeding of molecular oxygen, the selectivity for acrolein decreased to 62.5% at full conversion, due to the total oxidation to carbon oxide species (CO_x) as an important side reaction.

As described above, some compounds, like niobium oxide, tungsten oxide and pyrophosphates, offer the possibility of controlling their acid strength via the calcination step. This thermal treatment generally also has an influence on the specific surface area and the pore size due to sintering. In comparison to the aforementioned zeolites and supported heteropoly acids, the control of the physical properties of the mixed metal oxides and phosphates seems nevertheless less straightforward.

1-1-4 Synthesis of acrylic acid from glycerol

1-1-4-1 Synthesis of acrylic acid from acrolein

As described above, acrylic acid produced by the oxidation of acrolein is an important intermediate. Mo-V-O based complex oxides have been used as catalysts for the selective oxidation of acrolein to acrylic acid. The yield of acrylic acid has been achieved above 98% by using these catalysts.[72, 73]

Andrushkevich[74] and Tichy *et al*.[75] focus on the effect of composition in V-Mo oxide catalysts on their structures and catalytic properties. Fig 1.6 illustrates the catalytic properties and phase composition of a V-Mo oxide systems supported on SiO_2. The relation between the composition and catalytic

properties is able to categorized into the following three regions.

1. V_2O_4 0~3 mol%, MoO_3 97~100 mol%

MoO_3 and binaly compositions containing less than 3 mol% of V_2O_4 characterized by low activity: Their selectivity grows with the increasing vanadium content.

2. V_2O_4 7-30 mol%, MoO_3 70~97 mol%

Composition containing 7-30 mol% of V_2O_4, with high activity and selectivity toward acrylic acid formation.

3. V_2O_4 40~100 mol%, MoO_3 0~60 mol%

Composition enrich with vanadium (>40 mol% V_2O_4), with medium activity in complete oxidation.

They considered that the phase contained the catalysts in group 2 is more active. The sample with (14.5 mol% V_2O_4, 85.5 mol% MoO_3) composition included in group 2 was individual monoclinic VMo_3O_{11+x} phase. Therefore, they concluded monoclinic VMo_3O_{11+x} phase is active phase. Besides, they has described V^{4+} plays important role in selective oxidation of acrolein based on the relation amongst crystal phase, catalytic properties and the ratio of V^{4+} (Table 1.2)

Fig. 1.7 illustrates the mechanism of acrylic acid formation assisted by V-Mo catalyst proposed by Andrushkevich *et al*.. First, carbonyl oxygen atom of aclorein coordinates on Mo. Second, nucleophilic oxygen on the surface abstracts hydrogen from aldehyde group. And then attack of this fragment on the oxygen of catalyst leads to the formation of the carbonyl bound compound SI-III and its very fast conversion into the symmetrical acrylate SI-IV possessing an equivalent oxygen atom. The surface acrylate is stabilized on V^{4+} and accepts hydrogen, followed by desorption as acrylic acid.

Sadakane *et al.*[76] have reported the orthorhombic-Mo_3VO_x and trigonal-Mo_3VO_x catalysts which exhibit a high yield of acrolein of more than 90% in the acrolein oxidation. Because the orthorhombic and trigonal phase which have similar structure show similar catalytic properties, they have advocated their local structure (the layered structure comprising 6- and 7-rings of metal-oxide octahedral and pentagonal

columns) is important for high oxidation activity.

1-1-4-2 Direct transformation of glycerol to acrylic acid

Direct transformation of glycerol to acrylic acid brings about simplification of process and reduction of energy. Standard enthalpy change of the glycerol dehydration to acrolein and the acrolein oxidation to acrylic acid are 18.0 kJ·mol^{-1} and -298.3 kJ·mol^{-1}, respectively.[77] The direct transformation of glycerol to acrylic acid may be energy-efficient process if the energy exhausted in the latter reaction can be used for the first reaction. Moreover, because it has been reported that the co-feeding of oxygen has a positive impact on the long-term performances of the catalysts, the suppression of the catalytic deactivation is expected simultaneous dehydration and oxidation.

1-1-4-2-1 Proposed catalysts and problems

The direct transformation of glycerol to acrylic acid has been first reported by Deleplanque *et al*.[58] in 2010. Proposed catalysts are listed in Table 1.3.

Use of two-bed reactor (H-ZSM-5 and V-Mo oxides on silicic acid support)

Witsuthammakul *et al*. demonstrate a practical two-bed system consisting of zeolite and vanadium–molybdenum mixed oxides as catalysts for direct conversion of glycerol to acrylic acid.[78] The separate bed system gives 40% yield of acrylic acid with about 40% yield of acrolein, while the mixed one gives considerable amounts of acetic acid and acetaldehyde, together with only 30 mol% yield of acrylic acid.

This report clarified that it is possible to match up the reaction conditions of both dehydration and oxidation.

Orthorhombic Mo-V-O and Mo-V-Te-Nb-O

Deleplanque *et al.* have been reported that Mo-V-O based catalysts which show high selectivity to

acrylic acid in acrolein oxidation gave acrylic acid directly from glycerol.[58] The orthorhombic Mo-V-O and Mo-V-Te-Nb-O catalysts gave acrylic acid in yield of 26.3 and 28.4% with acrolein in yield of 3.0 and 1.7%, respectively.

Although these catalysts exhibited high acrylic acid selectivity in acrolein oxidation, the acrylic acid yield from glycerol was below 30% due to low acrolein selectivity in glycerol dehydration.

Hexagonal W-V-O

Deleplanque *et al.*, at the same time as the Mo-V-O based catalysts, have been reported that hexagonal W-V-O gave acrylic acid in yield of 26.3% in glycerol transformation with acrolein in yield of 0.1%.[58]

Soliano *et al.* prepared hexagonal W-V-O having various composition, and have been reported that the catalyst with V/(W+V)＝0.21 gave acrylic acid in yield of 25% with acrolein in yield of 11%.[79]

Hexagonal W-V-Nb-O

Chieregato *et al*. have been reported the introduction of Nb to hexagonal W-V-O.[80] The catalyst with composition V/(W + V + Nb) = 0.13 and Nb/(W + V + Nb) = 0.13 (atomic ratios) gave 34% yield to acrylic acid (with overall selectivity to acrylic acid and acrolein of 51%), at 290◦C; this is the best result obtained so far for the one-pot transformation of glycerol into acrylic acid. They have been considered that the increase of acrylic acid yield is due to the increase catalytic acid strength by introduction of Nb.

The efficient catalyst for the direct transformation glycerol to acrylic acid must be the efficient catalyst for both the dehydration of glycerol to acrolein and the oxidation of acrolein to acrylic acid. Besides the improvement of selectivity for each reaction, the tune of optimum conditions for each reaction is also required to achieve higher acrylic acid yield. Therefore, the direct transformation of glycerol to acrylic acid is challenging process.

1-2 Synthesis of W-based complex metal oxide catalysts and transformation of glycerol －The outline of this thesis－

This study aims at developing new complex metal oxide catalysts composed of W and group 5 elements such as V, Nb or Ta and their application to the synthesis of acrolein or acrylic acid from glycerol.

In Chapter 2, hydrothermal synthesis of complex metal oxide composed of W and Nb (W-Nb-O) and analysis of their structure were investigated. Effect of preparation conditions such as composition, calcination temperature and concentration of precursor solution on structure of W-Nb-O was examined. W-Nb-O was analyzed of by X-ray diffraction and spectrophotometric method. Structure of W-Nb-O was discussed based on comparisons with crystalline complex metal oxides. Besides, W-V-O and W-Ta-O was also synthesized by hydrothermal method.

Chapter 3 described solid acid property of W-Nb-O and dehydration of glycerol to acrolein over the W-Nb-O catalyst. Effects of structure and the W/Nb ratio of the W-Nb-O catalyst on their acidity and selectivity in glycerol transformation were investigated. First, catalytic performance of W-Nb-O synthesized by hydrothermal method was compared with those of WO_3/ZrO_2 and H-ZSM-5 which are typical acid catalysts. Second, product selectivity over W-Nb complex metal oxides, which have the same layered structure in the *c*-axis direction were tested at comparable glycerol conversion rates. Besides, effect of a combination W and Nb on acidity was investigated by the reaction over W-Nb-O having various W/Nb ratio.

In Chapter 4, reaction pathway of glycerol transformation over the W-Nb-O catalyst was discussed based on effect of contact time on product distribution and reaction starting from intermediates. Effect of co-feeding gas on catalytic performance of the W-Nb-O catalyst was also examined.

Chapter 5 indicated direct oxidative transformation of glycerol to acrylic acid over W-based complex metal oxide catalysts. Introduction of V to W-Nb-O aiming at development of the catalyst for direct transformation to acrylic acid was investigated. Effect of additional method of V on state of V, catalytic

acidity and selectivity in glycerol transformation was discussed. The balance between acid and oxidative capability was optimized toward high acrylic acid selectivity by control of the V content and reaction conditions. Moreover, Reaction pathway of glycerol transformation over the W-V-Nb-O catalyst was proposed.

In Chapter 6, the addition of phosphoric acid to the W-V-Nb-O catalyst was attempted toward enhancement of acrylic acid yield. Effect of the phosphoric acid addition on acid properties of W-Nb-O and the catalytic performance of W-V-Nb-O for the acrolein oxidation and the glycerol transformation were investigated.

In Chapter 7, finally, I summarized overall conclusions of the present thesis.

1-3 References

[1] Agency for Natural Resources and Energy, Comprehensive energy statistics, *domestic energy supplies in 2011* **2013**.

[2] Oil information center, *OIL NOW 2010* **2010**.

[3] Ministry of Agriculture, Forestry and Fisheries, *Biomass Nippon Strategy* **2002**.

[4] Renewable Energy Policy Network for the 21st Century, *RENEWABLS GLOBAL STATUS REPORT 2013* **2013**.

[5] T. Koyama, T. Baba, *PETROTECH* **2008**, 31 (9), 697.

[6] B. Katryniok, S. Paul, V. Belli`ere-Baca, P. Reye and F. Dumeignil, *Green Chem*. **2010**, 12, 2079.

[7] M. McCoy, *Chem. Eng. News* **2005**, 83 (8), 19.

[8] T. Suzuki, E, Murakami, A. Kimura, *research report in Gunma Industrial Technology Center* **2010**.

[9] A.C. Alba-Rubio, M.L. Alonso Castillo, M.C.G. Albuquerque, R. Mariscal, C.L. Cavalcante Jr., M. López Granados, *Fuel* **2012**, 95, 464.

[10] Hui Sun, Yuqi Ding, Jinzhao Duan, Qijun Zhang, Zhiyong Wang, Hui Lou, Xiaoming Zheng *Bioresource Technology* **2010**, 101(3), 953.

[11] H. Kimura, K. Tsuto, *Appl. Catal. A* **1993**, 96, 217.

[12] W. Hu, B. Lowry, A. Varma, *Appl. Catal. B* **2011**, 106, 123.

[13] S. Gil, M. Marchena, L. S-Silva, A. Romero, P. Sánchez, J. L. Valverde, *Che. Eng. J.* **2011**, 178, 423.

[14] S. Carrettin, P. McMorn, P. Johnston, K. Griffin, G.J. Hutchings, *Chem. Commun.* **2002**, 7, 696.

[15] Ch.-H. Zhou, J.N. Beltramini, Y.-X. Fana, G.Q. Lu, *Chem. Soc. Rev.* **2008**, 37, 527.

[16] N. Dimitratos, J.A. Lopez-Sanchez, G. J. Hutchings, *Top. Catal.* **2009**, 52, 258.

[17] Y. Zheng, X. Chen, Y. Shen, *Chem. Rev.* **2008**,108, 5253.

[18] T. Suzuki, E, Murakami, A. Kimura, S. Takigami, *research report in Gunma Industrial Technology Center* **2008**.

[19] A. J. Byrd, K.K. Pant, R. B. Gupta, *Fuel* **2008**, 87, 2956.

[20] K. S. Avasthi, R. N. Reddy, S. Patel, *Procedia Eng.* **2013**, 51, 423.

[21] T. Pairojpiriyakul, E. Croiset, W. Kiatkittipong, K. Kiatkittipong, A. Arpornwichanop, S. Assabumrungrat, *Int. J. Hydrogen Energ*. **2013**, 38, 4368.

[22] Y. Nakagawa, M. Tamura, K Tomishige, *Catalysis* **2012**, 54(7), 439.

[23] M. Akiyama, S. Sato, R. Takahashi, K. Inui, M. Yokota, *Appl. Catal. A* **2009**, 371, 60.

[24] Y. Nakagawa, Y. Shinmi, S. Koso, K. Tomishige, *J. Catal.*, **2010**, 272, 191.

[25] M.S. Khayoon, B. H. Hameed, *Appl. Catal. A* **2012**, 433, 152.

[26] E. Li, Z.P. Xu, V. Rudolph, *Appl. Catal. B* **2009**, 88, 42.

[27] P. Ferreira, I.M. Fonseca, A.M. Ramos, J. Vital, J.E. Castanheiro, *Appl. Catal. B* **2009**, 91, 416.

[28] P.C. Smith, Y. Ngothai, Q. Dzuy Nguyen, B.K. O'Neill, *Renewable Energy* **2010**, 35, 1145.

[29] M. Kapoor, M. N. Gupta, *Process Biochem. (Oxford, U. K.)* **2012**, 47, 503.

[30] M. Balaraju, P. Nikhitha, K. Jagadeeswaraiah, K. Srilatha, P.S. Sai Prasad, N. Lingaiah, *Fuel Process. Technol.* **2010**, 91, 249.

[31] I. Dosuna-Rodríguez, C. Adriany, E.M. Gaigneaux, *Catal. Today* **2011**, 167, 56.

[32] P. Ferreira, I.M. Fonseca, A.M. Ramos, J. Vital, J.E. Castanheiro, *Catal. Commun.* **2009**, 10, 481.

[33] P. Ferreira, I.M. Fonseca, A.M. Ramos, J. Vital, J.E. Castanheiro, *Catal. Commun.* **2011**, 12, 573.

[34] H. J. Lee, D. Seung, K. S. Jung, H. Kim, I. N. Filimonov, *Appl. Catal. A* **2010**, 390, 235.

[35] A. Martin, M. Richter, E. J. Lipid, *Sci. Technol.* **2011**, 113, 100.

[36] L. C. A. Oliveira, M. F. Portilho, A. C. Silva, H. A. Taroco, P. P. Souza, *Appl. Catal. B* **2012**, 29, 117.

[37] N. Nojii, Y. Sakai, Y. Watanabe, *Catal. Rev. Sci. Eng.* **1995**, 37, 145.

[38] NIPPON SHOKUBAI CO., LTD., *News Release* **2009**.

[39] P. Sabatier, G. Gaudion, *Compt. Rend.* **1918**, 166, 1033.

[40] E. Freund, US Patent 1672378, **1928**, to Chemische Fabrik Auf Actien.

[41] H. Heinemann, R.W. Wert, *Ind. Eng. Chem.* **1949**, 41, 2928.

[42] H.E. Hoyt, T.H. Manninen, US Patent 2558520, **1951**, to U.S. Industrial Chemicals.

[43] A. Neher, T. Haas, US Patent 5387720, **1993**, to Degussa Aktiengesellschaft.

[44] W. Buhler, E. Dinjus, J. Supercrit, *Fluids* **2002**, 22, 37.

[45] L. Ott, M. Bicker, *Green Chem.* **2006**, 8, 214.

[46] S. Ramayya, A. Brittain, *Fuel* **1987**, 66, 1364.

[47] E. Drent, W.W. Jager, US Patent 6080898, **2000**, to Shell Oil Company.

[48] W. Buhler, E. Dinjus, H.J. Ederer, A. Kruse, C. Mas, *J. Supercrit. Fluids* **2002**, 22, 37.

[49] E. Tsukuda, S. Sato, R. Takahashi, T. Sodesawa, *Catal. Commun.* **2007**, 8, 1349.

[50] S.-H. Chai, H.-P. Wang, Y. Liang, B.-Q. Xu, *Green Chem.* **2007**, 9, 1130.

[51] A. Alhanash, E. F. Kozhevnikova, I. V. Kozhevnikov, *Appl. Catal. A* **2010**, 378, 11.

[52] A. K. Kinage, P. P. Upare, P. Kasinathan, Y. K. Hwang, J.-S. Chang, *Catal. Commun.* 11 (2010) 620.

[53] D. Stošić, S. Bennici, J.-L. Couturier, J.-L. Dubois, A. Auroux, *Catal. Commun.* **2012**, 17, 23.

[54] D. Stošić, S. Bennici, S. Sirotin, C. Calais, J.-L. Couturier, J-L. Dubois, A. Travert, A. Auroux, *Appl. Catal. A* **2012**, 124, 447.

[55] D. Stošić, S. Bennici, S. Sirotin, C. Calais, J.-L. Couturier, J.-L. Dubois, A. Travert, A. Auroux, *ABC-7* **2013**, OB-14.

[56] A. Corma, G. W. Huber, L. Sauvanaud, P. O'Connor, *J. Catal.* **2008**, 257, 163.

[57] W. Suprun, M. Lutecki, T. Haber, H. Papp, *J. of Mol. Catal. A* **2009**, 309, 71.

[58] J. Deleplanque, J.-L. Dubois, J.-F. Devaux,W. Ueda, *Catal. Today* **2010**, 157, 351.

[59] M. R. Nimlos, S. J. Blanksby, X. Qian, M. E. Himmel, D. K. Johnson, *J. Phys. Chem. A* **2006**, 110, 6145.

[60] I.V. Kozhevnikov, *J. Mol. Catal. A* **2009**, 305, 104.

[61] Y. T. Kim, K.-D. Jung, E. D. Park, *Microporous Mesoporous Mater.* **2010**, 131, 28.

[62] Y.T. Kim, K.-D. Jung, E.D. Park, *Appl. Catal. A* **2011**, 393, 275.

[63] C.-J. Jiang, Y. Liu, W. Schmidt, A.-H. Lu, F. Schüth, *J. Catal.* **2010**, 269, 71.

[64] L. G. Possato, R. N. Diniz, T. Garetto, S. H. Pulcinelli, C. V. Santilli, L. Martins, *J. Catal.* **2013**, 300, 102.

[65] K. Tanabe, *CHEMTECH* **1991**, 21, 628.

[66] K. Tanabe, *Mater. Chem. Phys.* **1987**, 17, 217.

[67] S.-H. Chai, H.-P. Wang, Y. Liang, B.-Q. Xu, *J. Catal.* **2007**, 250, 342.

[68] L.-Z. Tao, B. Yan, Z. Hu,Y. Liang, B.-Q. Xu, *ABC-7* **2013**, OB-11.

[69] A. Ulgen, W. Hoelderich, *Catal. Lett.* **2009**, 131, 122.

[70] J.-L. Dubois (Arkema), WO 2009156664, **2009**.

[71] F. Wang, J.-L. Dubois, W. Ueda, *Appl. Catal. A* **2010**, 376, 25.

[72] N. Nojii, Y. Sakai, Y. Watanabe, *Catal. Rev. Sci. Eng.* **1995**, 37, 145.

[73] Y. Ono, M. Misono, Y. Moro-oka, *Dictionary of catalysis* **2000**, 1, 3.

[74] T. V. Andrushkevich, *Catal. Rev.-Sci. Eng.* **1993**, 35(2), 213.

[75] J. Tichy, *Appl. Catal. A* **1997**, 157, 363.

[76] M. Sadakane, N. Watanabe, T. Katou, Y. Nodasaka, W. Ueda, *Angew. Chem. Int. Ed.* **2007**, 46, 1493.

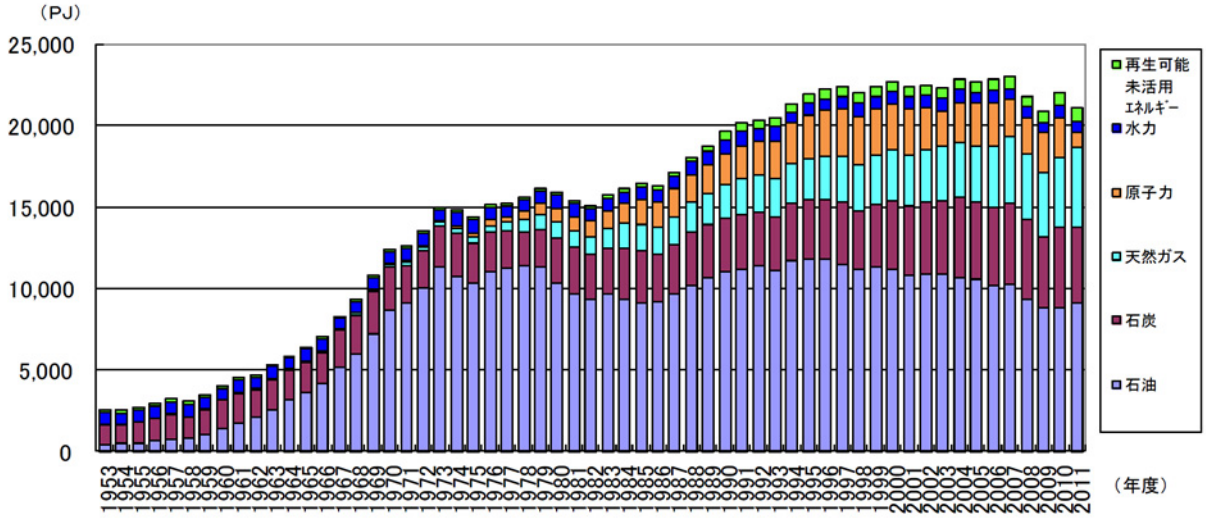
[77] J. A. Dean, *LANGE'S HANDBOOK OF CHEMISTRY*, **1985**, pp. 9-1f

[78] A. Witsuthammakul, T. Sooknoi, *Appl. Catal. A* **2012**, 413,109.

[79] M. D. Soriano, P. Concepci´on, J. M. L. Nieto, F. Cavani, S. Guidetti, C. Trevisanut, *Green Chem.* **2011**, 13, 2954.

[80] A. Chieregato, F. Basile, P. Concepción, S. Guidetti, G. Liosi, M. D. Soriano, C. Trevisanut, F. Cavani, J. M. L. Nieto, *Catal. Today* **2012**, 197, 58.

(a)



(b)

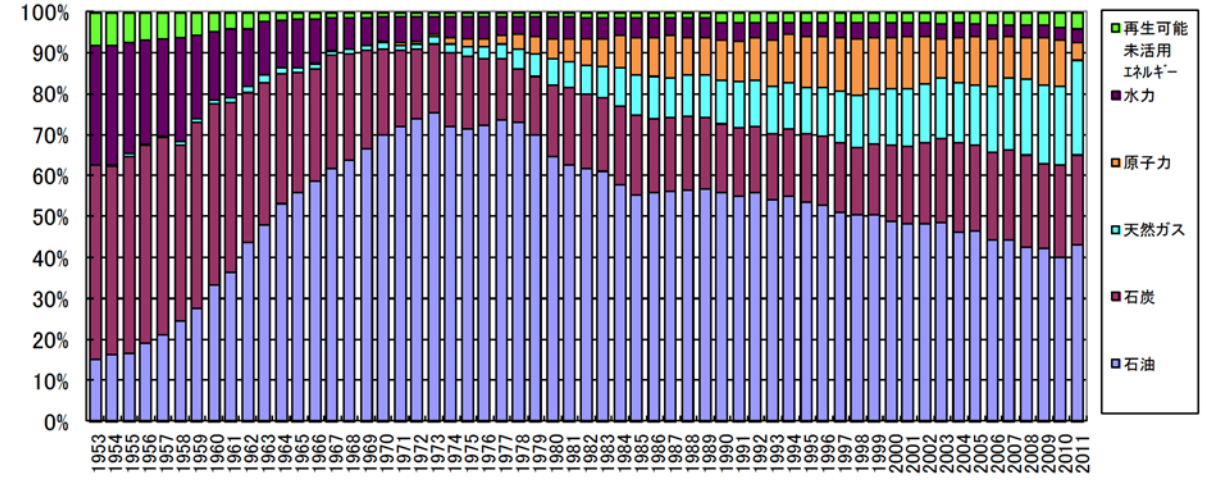


Fig. 1.1 Primary energy supply (a) and their composition (b) in Japan.

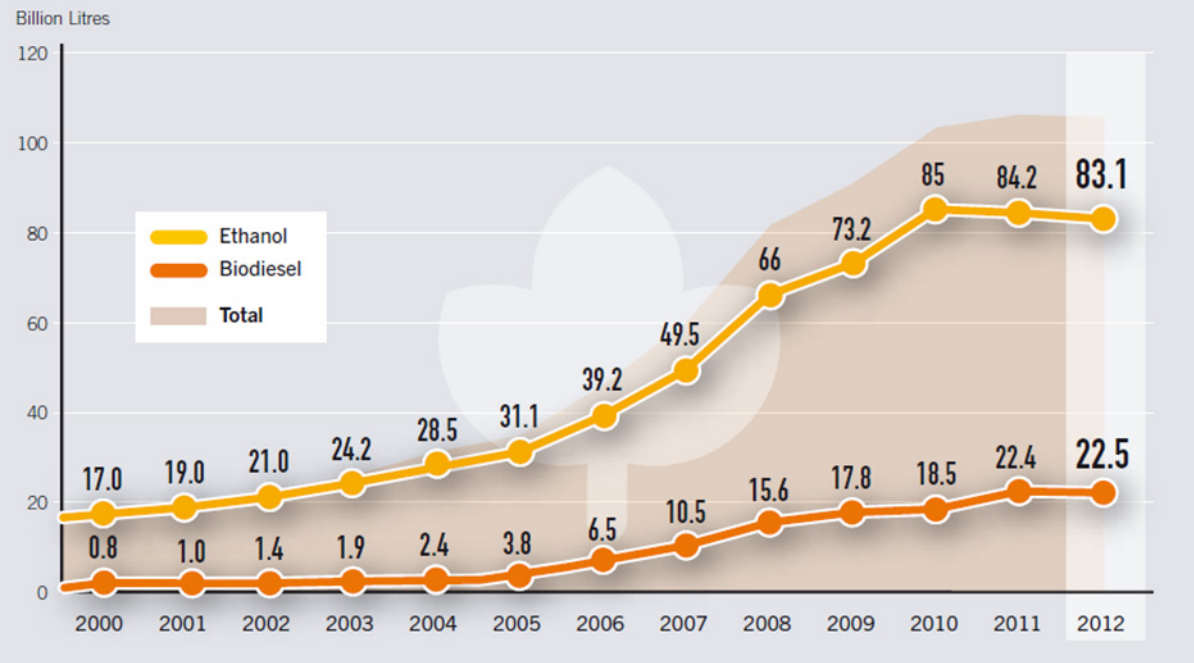
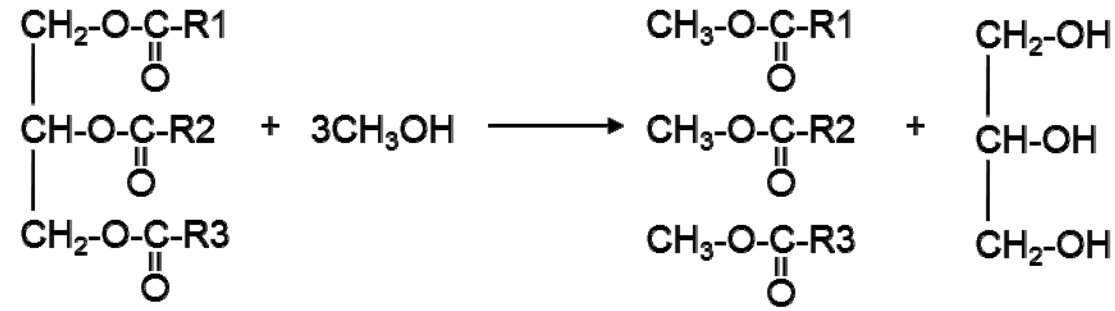
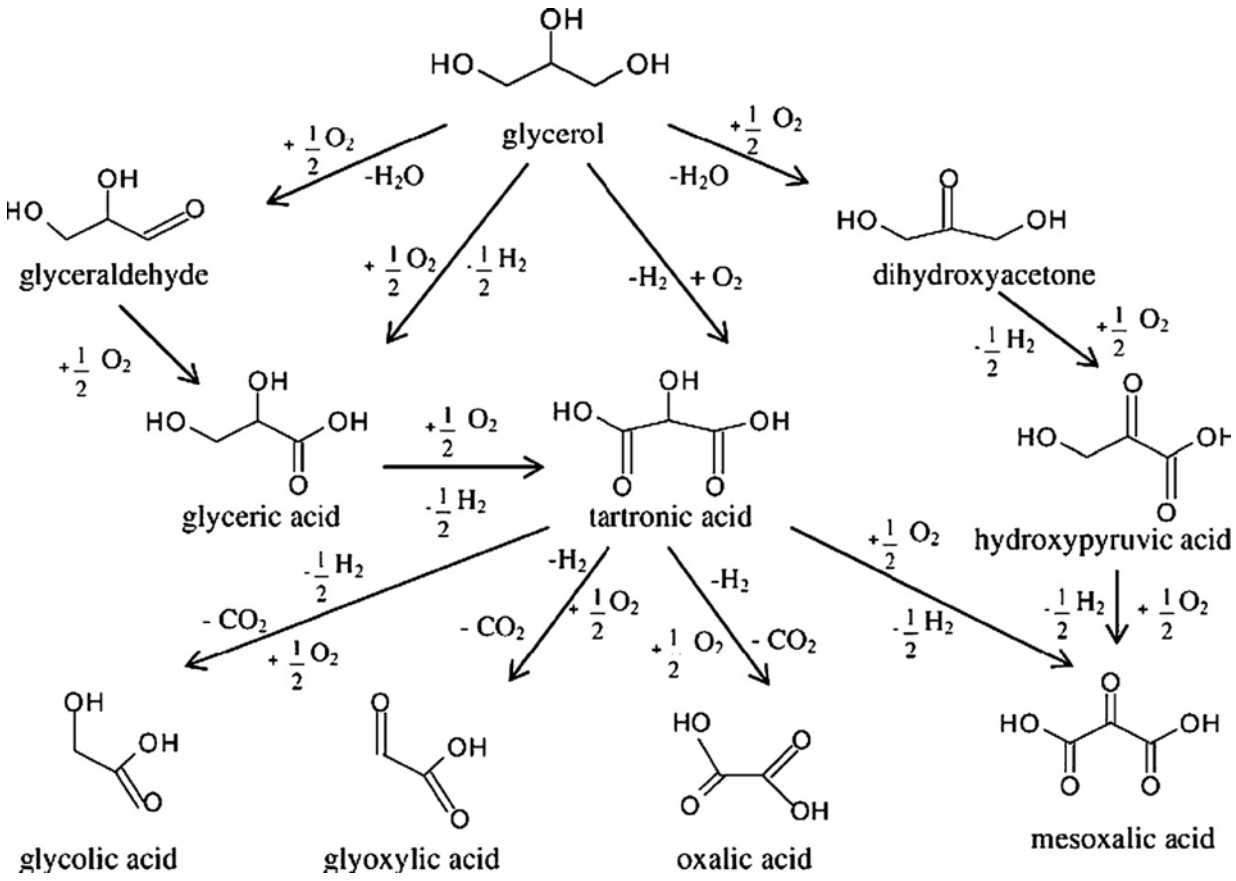


Fig. 1.2 Ethanol and biodiesel global production, 2000-2012.



Triacylglycerol Methanol Biodiesel Glycerol

Scheme 1.1 Transesterification of vegetable oils to yield biodiesel.



Scheme 1.2 General reaction network of the glycerol oxidation.

(a)

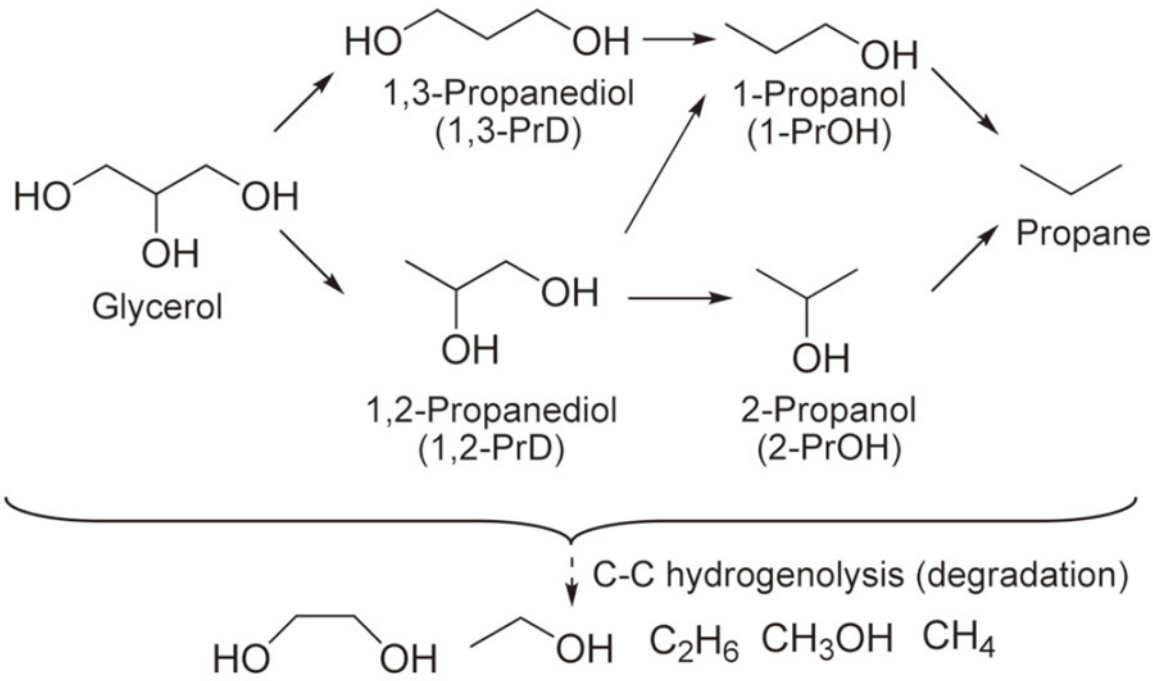
$$CH_4 + H_2O \rightarrow CO + 3H_2 \qquad \Delta H = +191.7\ kJ/mol$$

(b)

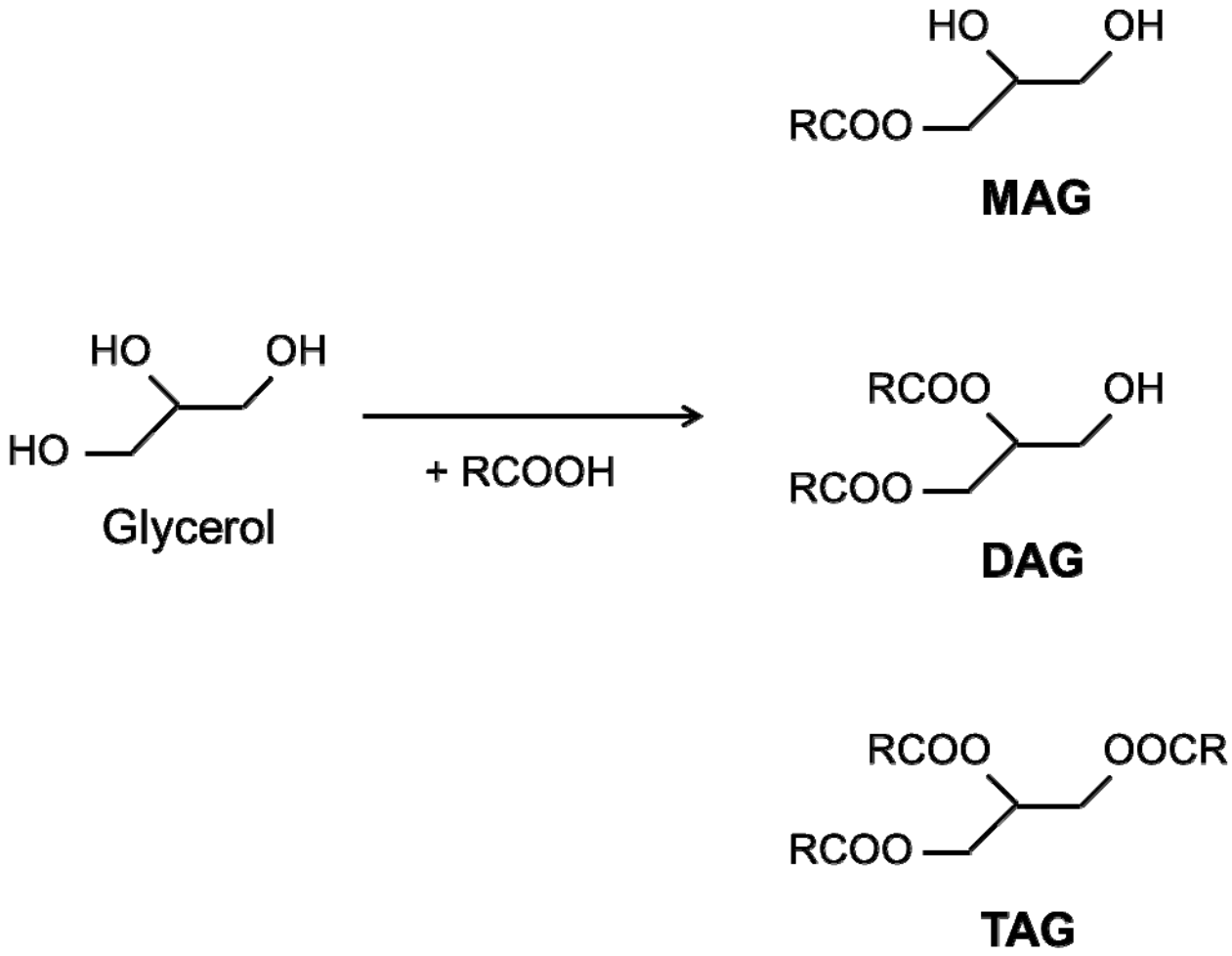
$$C_3H_8O_3(g) + 3H_2O(g) \leftrightarrow 7H_2(g) + 3CO_2(g)$$

$$\Delta H = 128\ kJ/mol$$

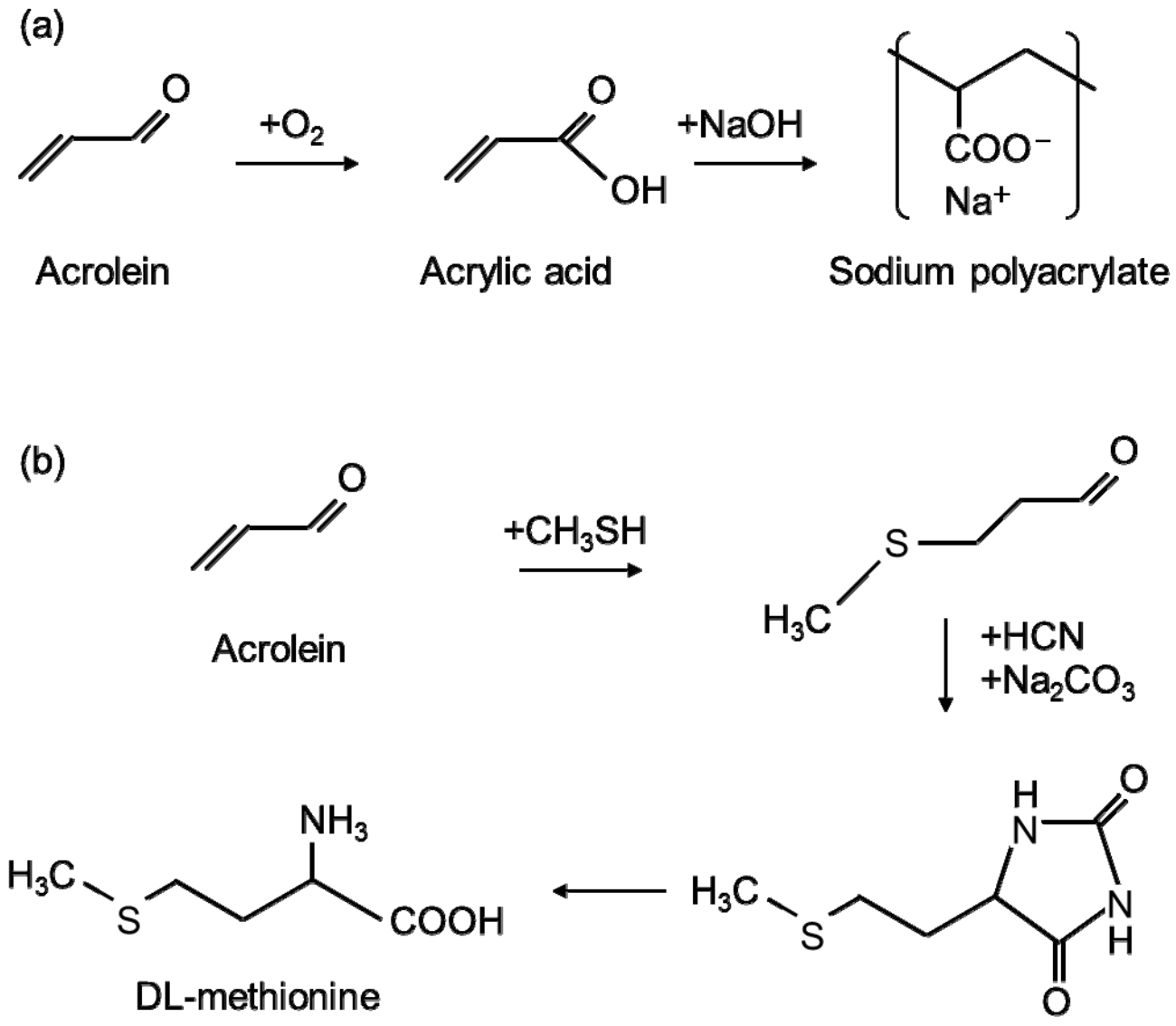
Scheme 1.3 Steam reforming of methane (a) and glycerol (b).



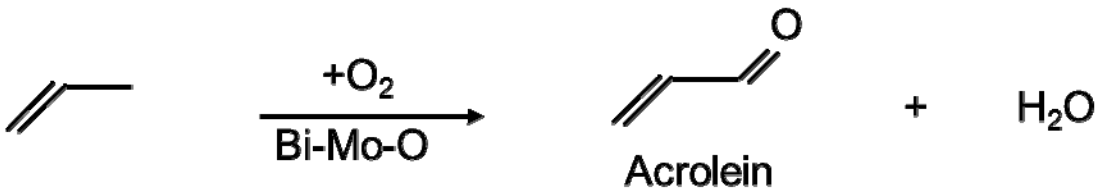
Scheme 1.4 Reaction pathways of glycerol hydrogenolysis.



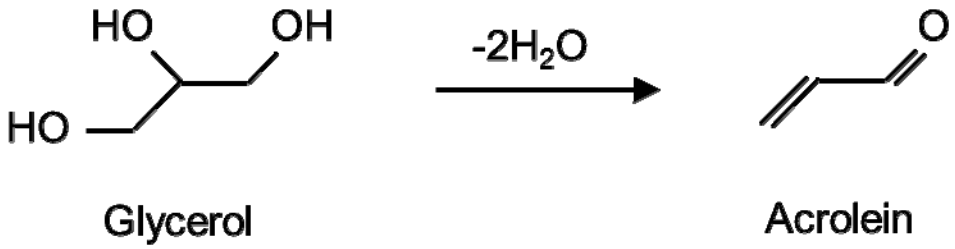
Scheme 1.5 Esterification of glycerol.



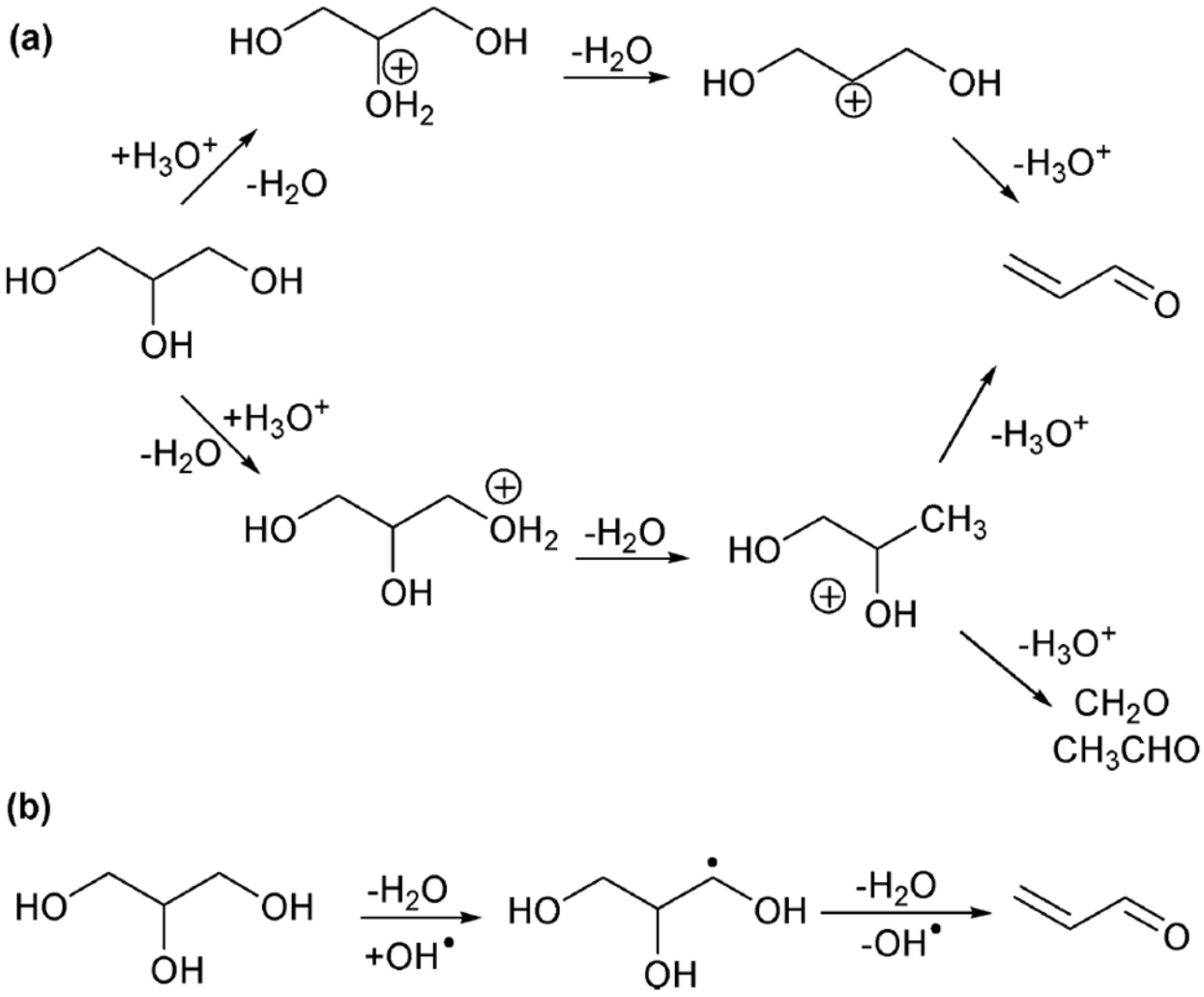
Scheme 1.6 Synthesis of superabsorbent polymer (a) and DL-methionine (b) from acrolein.



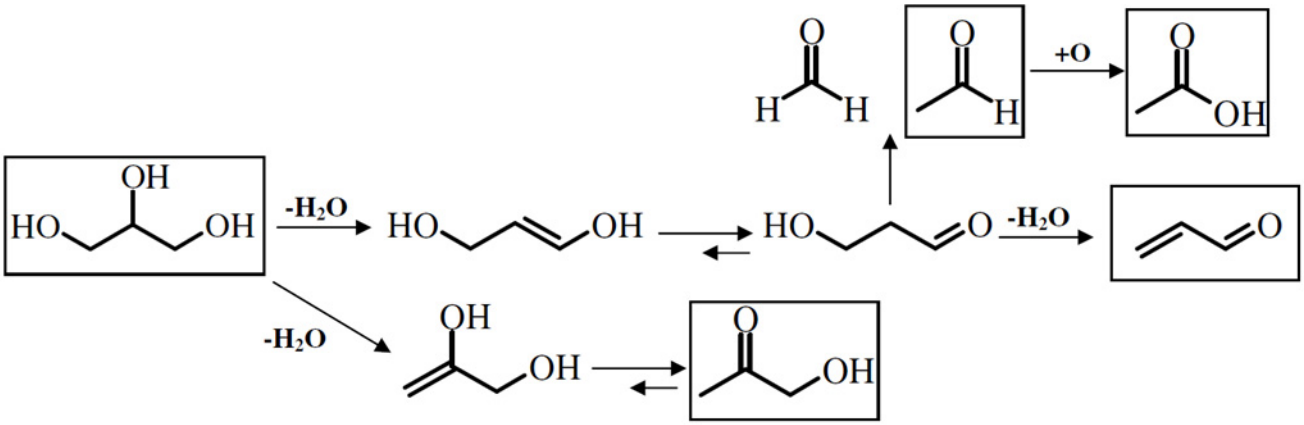
Scheme 1.7 Selective oxidation of propene to acrolein.



Scheme 1.8 Dehydration of glycerol to acrolein.



Scheme 1.9 Reaction pathways to the formation of acrolein considering (a) an ionic pathway and (b) a radical pathway.



Scheme 1.10 Reaction pathways to the formation of acrolein and acetol.

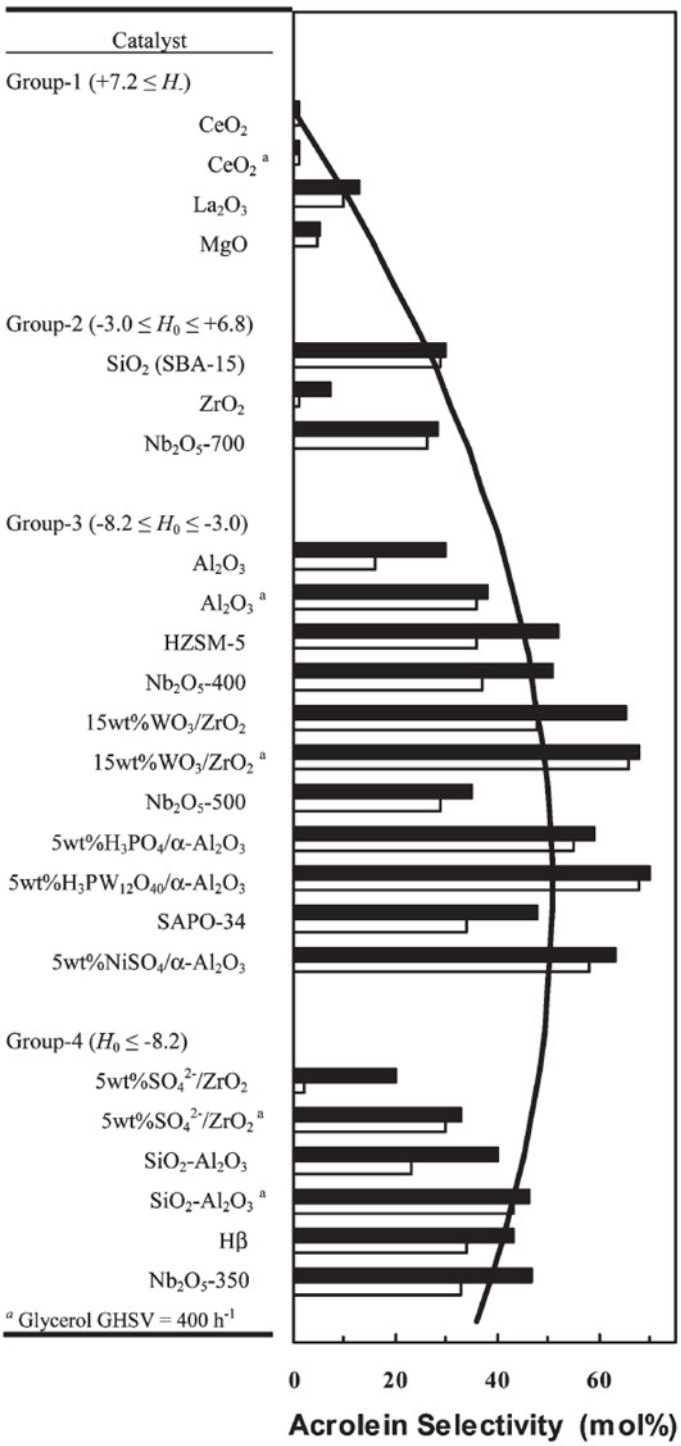
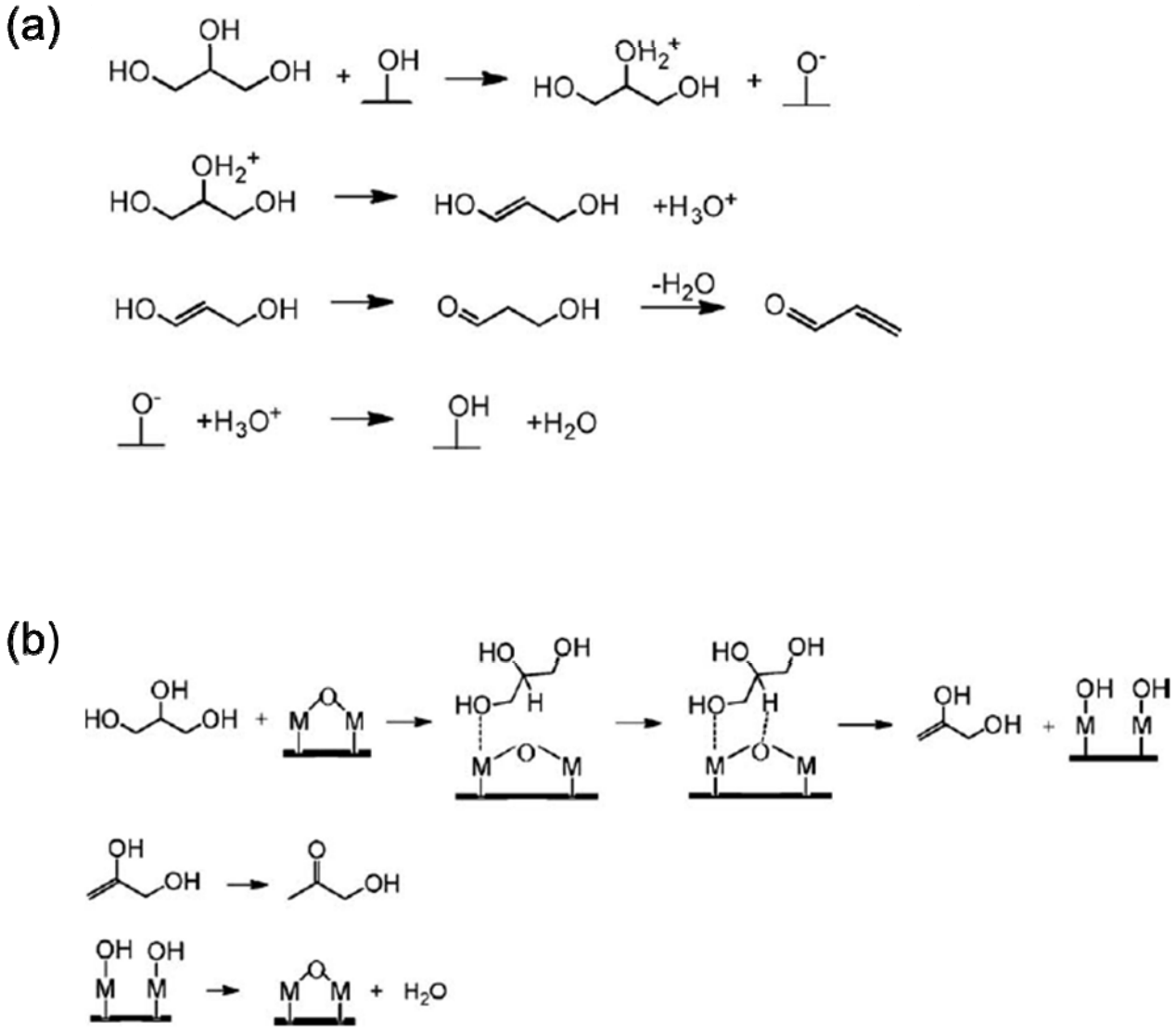
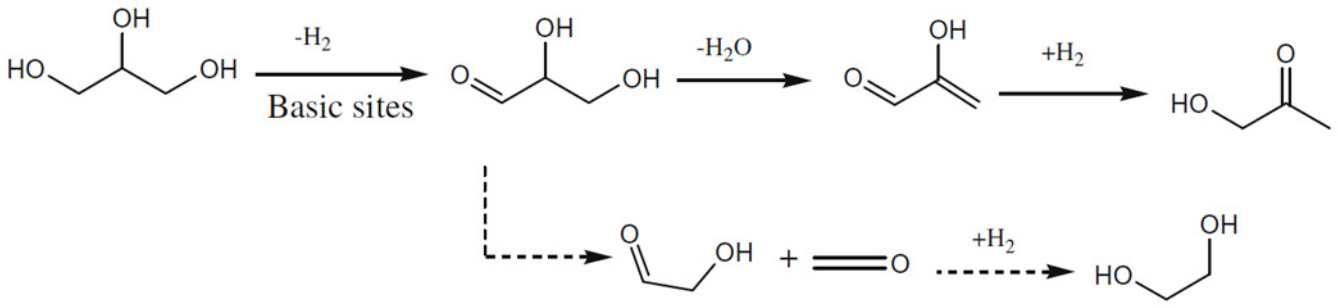


Fig. 1.3 Catalyst highest acid-base strength (H_0 or $H_$) and acrolein selectivity obtained at TOS = 1~2 h (open columns) and 9~10 h (solid columns). Reaction temperature: 315℃, glycerol GHSV: 80 h^{-1}.



Scheme 1.11 Mechanisms of glycerol dehydration on Brönsted (a) and Lewis (b) acid sites.



Scheme 1.12 Transformation of glycerol over basic catalysts.

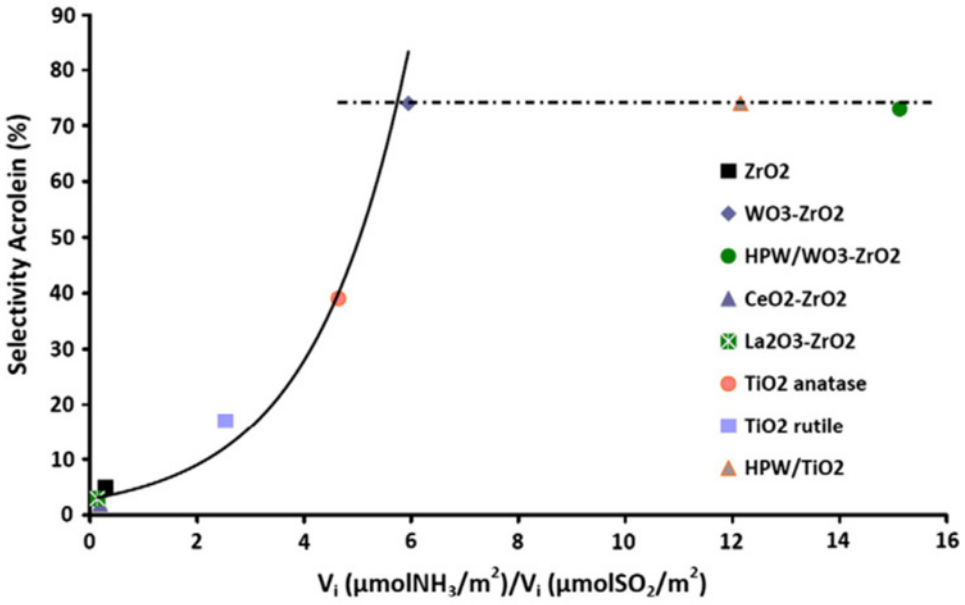


Fig. 1.4 Selectivity to acrolein as a function of V_i (μmolNH_3/m^2) / V_i (μmolSO_2/m^2) ratio.

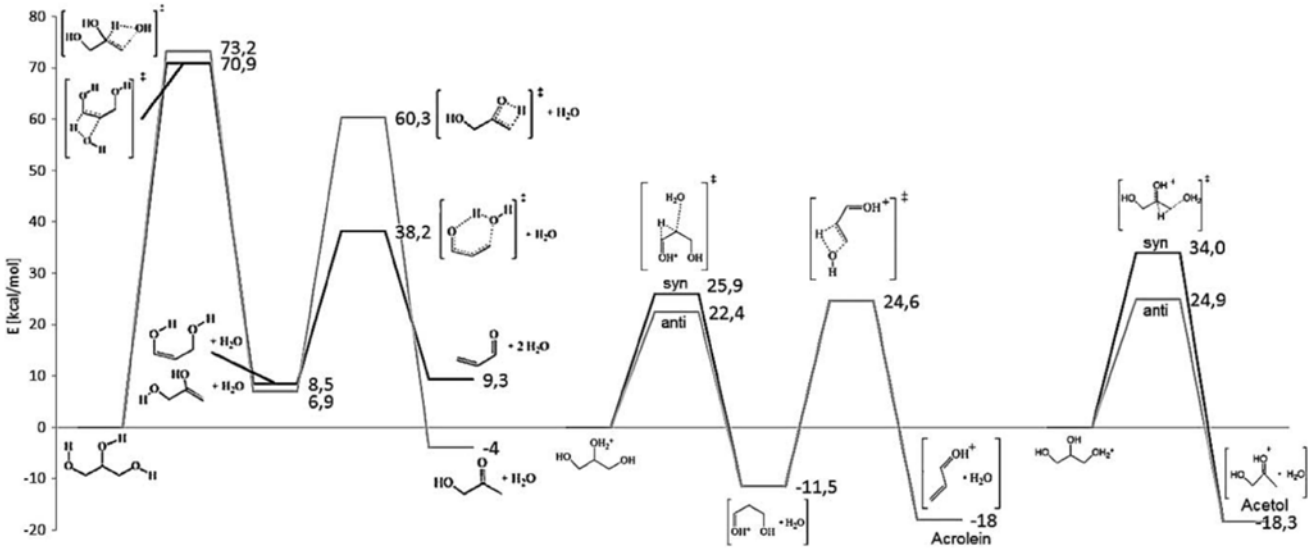
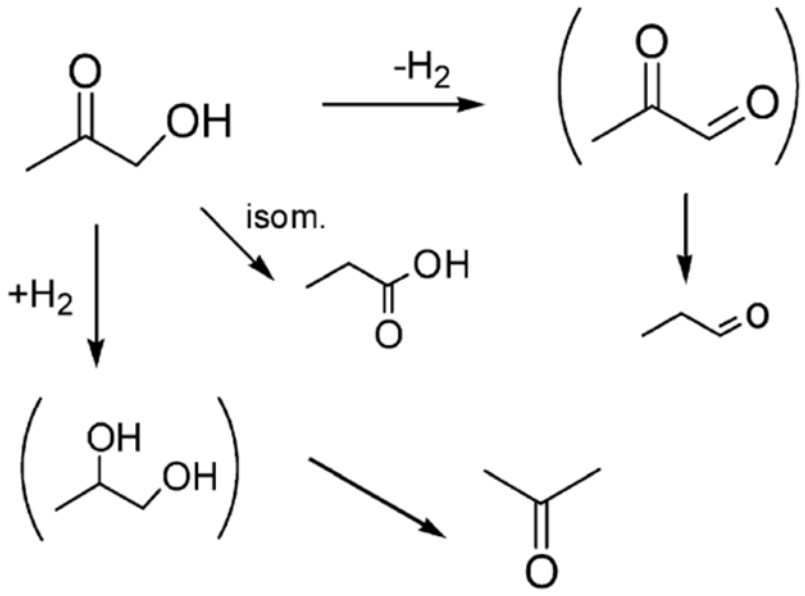
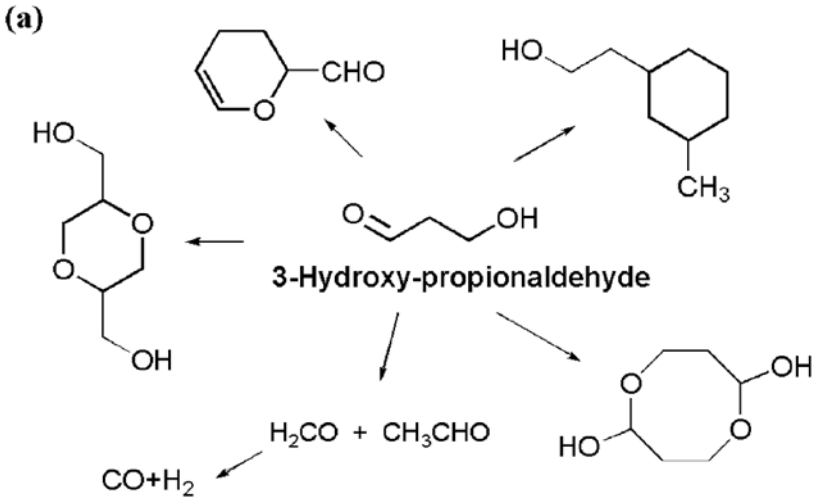


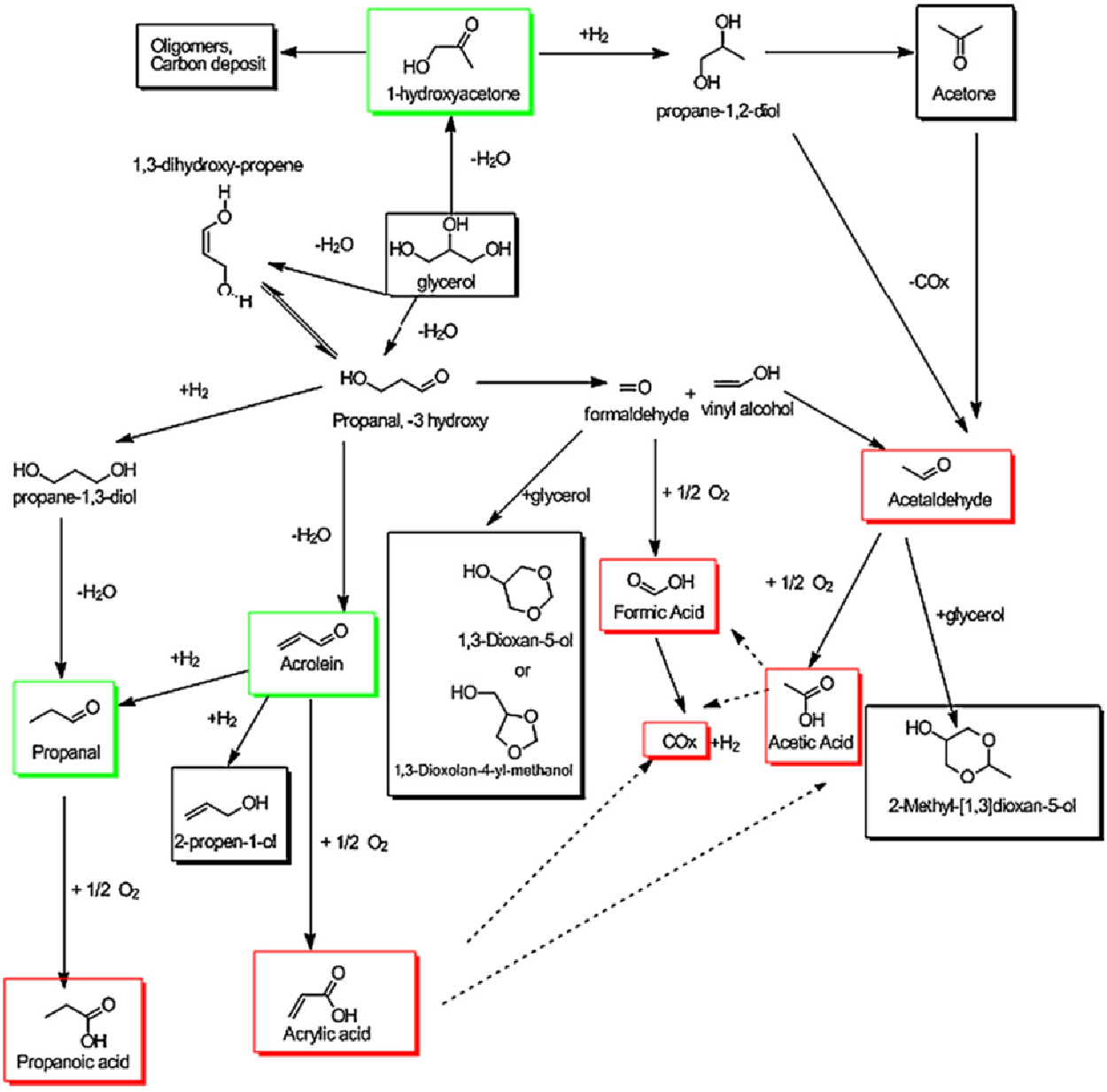
Fig. 1.5 Calculation for neutral and protonated reaction pathway to acrolein and acetol.



Scheme 1.13 By-products from acetol.



Scheme 1.14 By-products from 3-hydroxypropanl (a) and acetol (b).



Scheme 1.15 Transformation of glycerol in the presence of oxygen.

Table 1.1 Proposed catalysts for the dehydration of glycerol to acrolein

Catalyst	Yield of acrolein (STY[a])/ %	C_{glr}[b]	$S_{acrolein}$[c]	R. T.[d] / °C	Catal. wt. / g	TOS[e] / h	Carrier gas	P_{glr}/P_{total}	W_{water}/W_{glr}	Ref.
30wt.%SiW/SiO_2	85 (6.0)	98	86	275	0.3	5	He	0.02	9.0	49
$Cs_{2.5}H_{0.5}PW_{12}O_{40}$	98 (49.0)	100	98	275	0.3	1	N_2	0.02	9.0	51
H-ZSM-5 (150)[f]	54 (29.7)	94	57	340	0.3	2	He	0.08	1.8	61
H-Y (5.1)[f]	9 (5.0)	30	30	315	0.3	2	He	0.08	1.8	62
H-beta (25)[f]	35 (19.2)	76	46	315	0.3	2	He	0.08	1.8	62
SAPO-34	42 (0.9)	59	72	280	0.2	1	-	0.01	19.0	57
Nb_2O_5-400[g]	45 (1.6)	88	51	315	0.6	10	-	0.10	1.8	65
Ta_2O_5-350[g]	45 (1.7)	60	75	315	0.6	-	-	0.10	1.8	66
19wt.%WO_3/ZrO_2	69 (9.3)	83	83	280	5.0	-	-	0.05	4.0	67
VPO-800[g]	64 (7.1)	100	64	300	0.2	10	O_2/N_2	0.02	4.0	69
$Fe_x(PO_4)_y$	92 (4.1)	100	92	280	0.8	5	N_2	0.13	1.5	58

[a] Space-time yield / mmol $g^{-1}h^{-1}$. [b] Conversion of glycerol. [c] Selectivity of acrolein. [d] Reaction temperature. [e] Time on stream. [f] SiO_2/Al_2O_3. [g] Calcination temperature / °C.

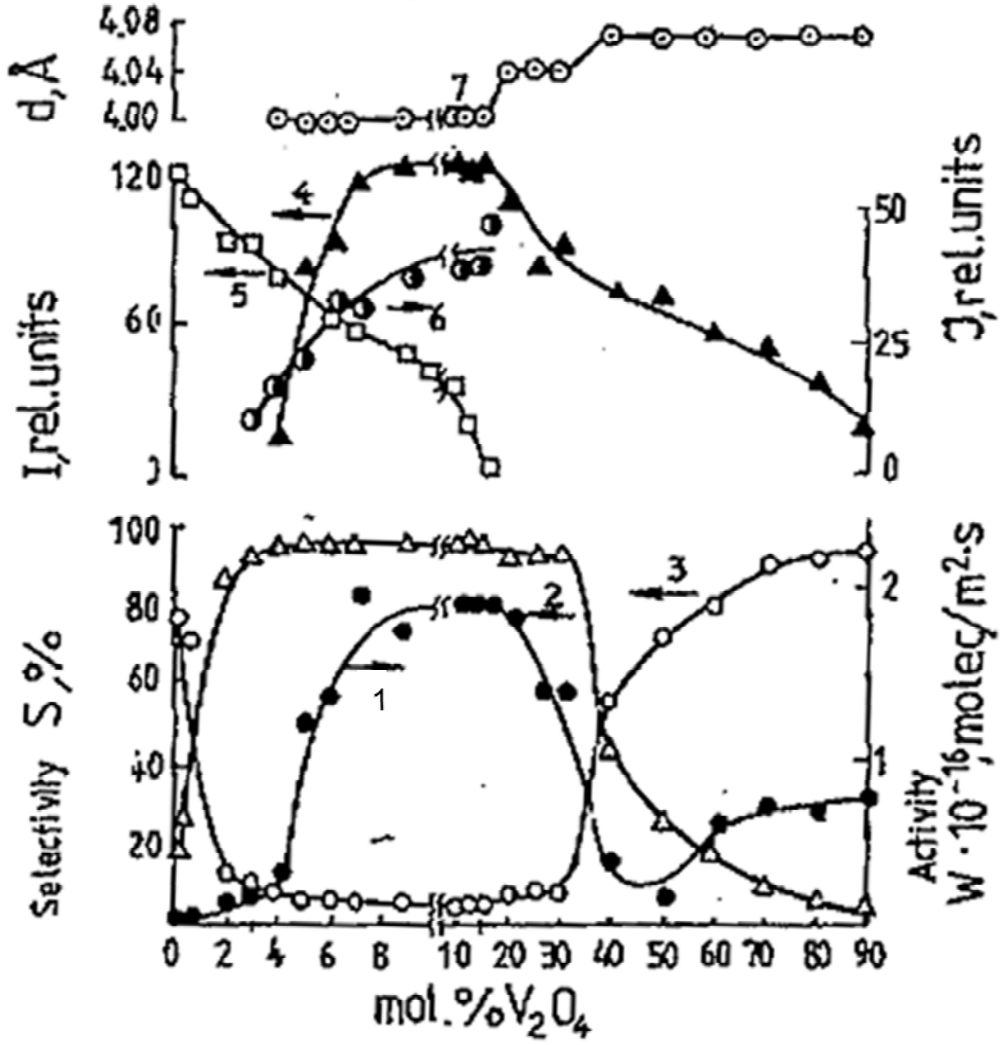


Fig. 1.6 Catalytic properties and phase composition of supported V-Mo oxide systems vs. V_2O_4 content: 1-activity, 2-selectivity toward acrylic acid, 3-selectivity toward the products of complete oxidation, 4-intensity of reflex with d = 4.00-4.07Å, 5-intensity of MoO_3 reflex with d =3.25Å, 6-intensity of ESR signal, 7-position of the most intensive diffraction maximum of vanadium-molybdenum compounds.

Table 1.2 Catalytic properties of unsuported V-Mo oxide compound

Compound	$V^{4+}/V^{4+}+V^{5+}$ (%)	X (%)	$W\times10^{-16}$ (molec/m^2s)	Selectivity (%)		
				C_3H_4O	$CO+CO_2$	$C_2H_4O_2$
VMo_3O_{11}	98.0	70.0	39.0	97.5	1.7	0.7
VMo_2O_{8-x}	75.0	70.0	35.0	26.0	4.0	1.5
$V_6Mo_4O_{25}$	67.0	73.0	3.7	25.9	64.7	9.4
V_2MoO_8	0.0	29.0	3.2	3.0	97.0	0.0
0.03 V_2O_4. 0.97 MoO_3[a] solid solution	100.0	65.0	0.3	92.8	6.5	0.7

[a] Supported on SiO_2 (30% of active mass), X – acrolein conversion, W – rate of acrolein total conversion.

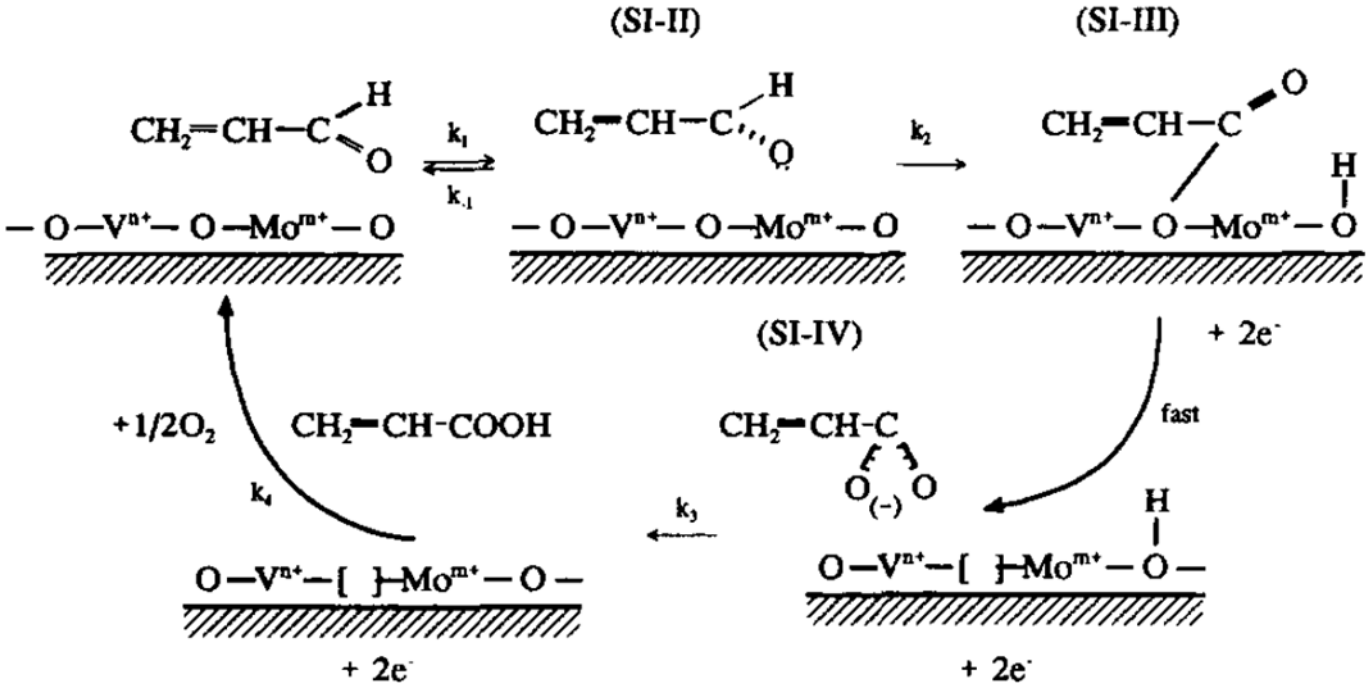


Fig. 1.7 Mechanisms of acrolein oxidation over Mo-V based catalyst.

Table 1.3 Proposed catalysts for the direct transformation of glycerol to acrylic acid

Catalyst	Yield of acrylic acid / %	Reaction temp. / K	Catal. wt. / g	TOS / h	Carrier gas	$P_{glycerol}/P_{total}$	$W_{water}/W_{glycerol}$
hexagonal W-V-O[a]	25	<603	0.5	2	O_2/He	0.02	3.9
hexagonal W-V-Nb-O[b]	34	563	0.5	-	O_2/He	0.02	3.9
MoVTeNbO	28	573	0.3	5	O_2/N_2	0.03	1.5

[a] V/(W+V) = 0.21. [b] V/(W+V+Nb) = 0.13, Nb/(W+V+Nb) = 0.13.

Chapter 2

Hydrothermal Synthesis of W-based Complex Metal Oxide

2-1 Introduction

Crystalline and porous mixed metal oxides such as zeolites have attracted attention because of their advantage in control of catalysis. Furthermore, these crystalline materials are helpful in revealing the relationship between structure of active sites and its catalysis.

W is constituent element of the catalysts such as WO_3-ZrO_2 and 12-tungstosilicic acid, which have high acid strength. The formation of uniform and strong active sites and revealing the relationship between structure and acidity are expected by the application of crystalline W-based complex metal oxide.

The synthesis of crystalline W-based complex oxides such as $Nb_8W_9O_{47}$[1-3] and $Cs_{0.5}[Nb_{2.5}W_{2.5}O_{14}]$ [4-7] by solid-state reaction has been reported.

$Nb_8W_9O_{47}$ crystallizes in a threefold tetragonal tungsten bronze (TTB) -type superstructure caused by the systematic occupation of 1/3 of the pentagonal tunnels with metal-oxygen strings (Fig. 2.1). The coordination of these cations are pentagonal bipyramids which are connected to five equatorial MO_6 octahedra each leading to the so-called PCs (pentagonal columns). This structure is obtained by the calcination of the mixture of WO_3 and Nb_2O_5 around 1473 K.

Lundberg *et al*. have been reported that $Cs_{0.5}[Nb_{2.5}W_{2.5}O_{14}]$ with an orthorhombic phase synthesized by solid-state reaction has a layered structure constructed with octahedral units consisting of a central six-coordinated metallic atom (*e.g.* W or Nb) surrounded by six oxygen atoms (Fig. 2.2). In order to obtain this kind of crystalline material, the introduction of Cs ions in the 6 and 7-membered ring pores and calcination at high temperature are required.

As shown above, these W-Nb complex oxides have been obtained by solid-state reaction at high temperature so far. Therefore, materials obtained through this method are unable to exhibit high catalytic functionality due to a low specific surface area and poor acidity.

Our group reported that Mo-V-O complex oxides (Mo_3VO_x) having crystal structures such as orthorhombic, trigonal and tetragonal system (Fig. 2.3) were synthesized with hydrothermal method.[8-10]

In particular, the orthorhombic and trigonal materials having micro pores consist of 7-membered rings were efficient catalysts for the partial and selective oxidation. Formation of Mo_3VO_x does not require high temperature calcination and can be carried out without addition of Cs, the materials synthesized by the hydrothermal method can possess high surface area, which is an advantage of this catalyst. The acid function of the Mo_3VO_x is expected to be enhanced by replacing the Mo cluster unit in the crystalline Mo_3VO_x with W cluster.

In this chapter, I attempted to synthesize the crystalline complex metal oxides composed of W and group 5 elements such as V, Nb or Ta by the hydrothermal method.

2-2 Experimental

2-2-1 Chemicals

Chemicals used in experiments are listed in Table 2.1.

Table 2.1 List of chemicals

chemical	formula or molar wt.	assay	manufacturer	No.
$Nb_2O_5 \cdot xH_2O$	265.82 (Nb_2O_5)	70.8% (Nb_2O_5)	Soekawa Chemical Co., Ltd.	02275B
$(NH_4)_6(H_2W_{12}O_{40}) \cdot nH_2O$ ($n \fallingdotseq 6$)	3064	90.8% (WO_3)	Nippon Inorganic Colour and Chemical Co., Ltd.	100114
$(NH_4)_{10}W_{12}O_{41} \cdot 5H_2O$	3132.52	-	Wako Pure Chemical Ind., Ltd.	013-03575
Cs_2CO_3	325.82	95.0~102.0%	Wako Pure Chemical Ind., Ltd.	036-06541
$Nb(HC_2O_4)_5 \cdot xH_2O$	-	-	Alfa Aesar	21348-59-4
$Ta_2O_5 \cdot nH_2O$	441.88	82.5% (Ta_2O_5)	Mitsuwa Chemicals Co., Ltd.	59678
$VOSO_4 \cdot nH_2O$	163.01	61.9%	Mitsuwa Chemicals Co., Ltd.	61595

2-2-2 Catalyst preparation

2-2-2-1 Preparation of W-Nb-O by hydrothermal method

The complex metal oxides catalysts of W and Nb were prepared by hydrothermal synthesis method. The mixed solution of $Nb_2O_5 \cdot nH_2O$ and $(NH_4)_6[H_2W_{12}O_{40}] \cdot nH_2O$ was put in a stainless steel autoclave with a Teflon liner and aged at 448 K for 72 h. The molar ratio between W and Nb was set at W/Nb = 1.35. The formed solid was filtered, washed with ion-exchanged water, dried at 353 K and then calcined at temperature of 673~1273 K for 4 h in air. The catalysts prepared by this method are represented by W–Nb–O (*X*, *Y*). The value *X* and *Y* in the parenthesis means W/Nb ratio and calcination temperature, respectively.

2-2-2-2 Preparation of WO_3/Nb_2O_5 by impregnation method

The mixed oxide catalyst of W and Nb was also prepared by impregnation of $Nb_2O_5 \cdot nH_2O$ with aqueous $(NH_4)_6[H_2W_{12}O_{40}] \cdot nH_2O$, followed by calcination at 673 or 973 K in air for 4 h. The catalyst

prepared by impregnation is represented by WO_3/Nb_2O_5. The atomic ratio of W/Nb was set to be 1.35.

2-2-2-3 Preparation of $Cs_{0.5}[Nb_{2.5}W_{2.5}O_{14}]$ by solid-state reaction

$Cs_{0.5}[Nb_{2.5}W_{2.5}O_{14}]$ was prepared by solid-state reaction according to the literature [16]. Aqueous suspension containing stoichiometric amount of $C_{10}H_5NbO_{20}\cdot nH_2O$, $(NH_4)_{10}W_{12}O_{41}\cdot 5H_2O$ and Cs_2CO_3 was evaporated with stirring and then dried at 353 K. Thus obtained material was calcined at 1273 K for 3 h in air. The $Cs_{0.5}[Nb_{2.5}W_{2.5}O_{14}]$ is represented by Cs-W-Nb-O.

2-2-2-4 Preparation of hexagonal WO_3

The aqueous solution of $(NH_4)_6(H_2W_{12}O_{40})\cdot nH_2O$ containing 24 mmol of W in 45 ml of H_2O was put in a stainless steel autoclave with a Teflon liner and heated at 448 K for 72 h. The formed solid was filtered, washed with ion-exchanged water, dried at 353 K and then calcined at 673 K for 4 h in air.

2-2-2-5 Preparation of W-V-O and W-Ta-O

The mixed aqueous solution of metal salts was put in a stainless steel autoclave with a Teflon liner and heated at 448 K for 72 h. The formed solid was filtered, washed with ion-exchanged water, dried at 353 K and then calcined at 673 K for 4 h in air. The atomic ratio of W/V or W/Ta was set to be 1.35.

2-2-3 Catalyst characterization

2-2-3-1 XRD

Powder X-ray diffraction (XRD) pattern of the catalysts was recorded on RINT2200 (Rigaku) with Cu Kα (λ = 0.154 nm) radiation (tube voltage: 40 kV, tube current: 20 mA).

2-2-3-2 Nitrogen adsorption

Surface area of the catalysts was estimated by BET method where nitrogen adsorption amount was

measured at 77 K with a BEL max 00094 (BEL Japan Inc.). Prior to the measurement, the samples were evacuated at 473 K for 2 h.

2-2-3-3 SEM-EDS

Scanning electron microscopy (SEM) images were obtained with a JSM-6360LA (JEOL). Composition of the catalysts was determined by simplified quantitative analysis of EDS with the ZAF method.

2-2-3-4 STEM

Scanning transmission electron microscopy (STEM) images were obtained with a HD-20000 (HITACHI).

2-2-3-5 TEM

Transmission electron microscopy (TEM) images were obtained on a JEM-2000FX (JEOL) electron microscope. The small amounts of the samples in ethanol were sonicated for 1min, and a few drops of the suspension were deposed on a micro grid, and then dried overnight.

2-2-3-7 Raman

The Raman spectra were recorded on an inVia Reflex (Renishaw) with a 2.5 mW semiconducting laser (excitation wavelength 532 nm).

2-2-3-8 Rietveld analysis

Rietveld analysis was carried out on a MATERIALS STUDIO (Accelrys).

2-3 Results and discussion

2-3-1 $Cs_{0.5}[Nb_{2.5}W_{2.5}O_{14}]$

Fig. 2.4 illustrates the X-ray diffraction patterns for orthorhombic Mo_3VO_x synthesized by hydrothermal method and $Cs_{0.5}[Nb_{2.5}W_{2.5}O_{14}]$ synthesized by solid-state reaction. $Cs_{0.5}[Nb_{2.5}W_{2.5}O_{14}]$ gave the characteristic diffraction pattern, particularly at low angle region, which is ascribable to that of the orthorhombic structure[5] as shown in Fig. 2.2. The pattern is comparable to that of Mo_3VO_x, however, there is slight difference in the 00*l* diffractions. In the case of Mo_3VO_x, the Mo octahedra can be highly stressed in the *c*-direction, so that the Mo-O-Mo bond length is about 0.4 nm. On the other hand, W-O-W bond length in the same direction is calculated to be about 0.39 nm, which is smaller than that in Mo-O-Mo, due to the W octahedral which tends to be more symmetric than Mo. It was considered that the W-O bond cannot elongate as with Mo-O.

2-3-2 Hydrothermal synthesis of W-Nb-O

2-3-2-1 Effect of the W/Nb ratio

The X-ray diffraction patterns WO_3/Nb_2O_5 and W-Nb-O (W/Nb=0~12) were illustrated in Fig. 2.5 (uncalcined samples) and 2.6 (samples calcined at 673 K). The simple impregnation and subsequent calcination only produced a mixture of WO_3 and Nb_2O_5. As shown in Fig. 2.5, on the other hand, all the catalysts synthesized by hydrothermal method exhibited the common peaks at 2θ=22 and 46°. Because these peaks were attributed to (001) and (002) planes of tungsten bronze structure, W-Nb-O having layered structure (liner arrangement of corner-shared octahedra) into the *c*-direction were synthesized. This result suggests that the hydrothermal method is in principle an effective method to promote octahedral arrangement of materials even in the case of W-Nb-O. However, the growth of *a*-*b* plane is not enough, because diffraction patterns ascribed to *a*-*b* plane of W-Nb-O was very broad appeared around 25~35°. While other low intensity diffractions assigned to pyrochlore were observed in Nb-O (W/Nb=0),

these peaks disappeared in the W containing catalyst. The intensity of the broad peaks at 14.6 and 28.2° increased with increasing the W/Nb ratio. The sharp peaks ascribed hexagonal structure were observed in W-Nb-O (W/Nb=12). The structures of these catalysts were maintained after calcination at 673 K (Fig. 2.6).

Fig. 2.7 illustrates the adsorption and desorption isotherms of W-Nb-O (W/Nb=0~12) calcined at 673 K. The isotherms of the W-Nb-O catalysts were type II. The BET surface area was listed in Table 2.2. The surface area of Nb-O without W was 89 m^2g^{-1}, and increased with increasing W/Nb ratio. The maximum surface area of W-Nb-O was 118 m^2g^{-1} with W/Nb=1.35. Further increase of W/Nb ratio decreased the surface area. The surface area of W-Nb-O (W/Nb=12) was 43 m^2 g^{-1}.

Fig. 2.8 illustrates the STEM images of WO_3/Nb_2O_5, W-Nb-O (W/Nb=0, 1.35, 12) and the hexagonal WO_3 synthesized by hydrothermal method. While the morphology of WO_3/Nb_2O_5 was amorphous, the W-Nb-O catalysts had rod-like shapes. The crystal size of Nb-O (W/Nb=0) varied from (*ca.* 20 nm×*ca.* 50 nm) to (*ca.* 80 nm×*ca.* 1000 nm). On the other hand, W-Nb-O (W/Nb=1.35) had uniform crystal size of (*ca.*10 nm×*ca.*100 nm). In W-Nb-O (W/Nb=12), crystal size growth was observed in diameter increasing to 50 nm. Besides, the crystal size of hexagonal WO_3 was about (*ca.* 200 nm×*ca.* 800 nm) which is larger than those of the samples containing Nb. Because deposition rate of WO_3 was lower than that of Nb_2O_5 due to the higher solubility of $(NH_4)_6[H_2W_{12}O_{40}]\cdot nH_2O$, the crystal size increased with increasing W/Nb ratio. However, excess increase of W content promoted the formation of the hexagonal phase. The surface area varies depending on crystal size.

2-3-2-2 Effect of the concentration of precursor solution

Fig. 2.9 illustrates the XRD patterns of uncalcined W-Nb-O (W/Nb=1.35) prepared from various concentrations of precursor solution. The catalysts prepared from the solution containing *x* mmol of W and *y* mmol of Nb in 45 ml of H_2O are denoted by W: Nb = *x*: *y*. The diffraction peaks attributed to a layered structure were observed in W-Nb-O (W: Nb = 0.7: 0.5~5.4: 4). In W: Nb=5.40: 4.00, the peaks attributed to pyrochlore and hexagonal phase were observed. Pyrochlore phase was formed by

hydrothermal treatment of $Nb_2O_5 \cdot nH_2O$ containing above 4 mmol of Nb in 45 ml of H_2O. On the other hand, hexagonal WO_3 was formed by hydrothermal treatment of the solution of $(NH_4)_6[H_2W_{12}O_{40}] \cdot nH_2O$ containing above 8 mmol of W in 45 ml of H_2O. Therefore, it was indicated that the preparation of W-Nb-O at high concentrations promote the formation of the stable phase of W and Nb individually.

The adsorption isotherms of all these catalysts were type II (Fig. 2.10). While The surface area of W-Nb-O from W: Nb=0.63: 0.50 to W: Nb=2.70: 2.00 was about 100 $m^2 \cdot g^{-1}$, that of W: Nb=5.40: 4.00 was 68 $m^2 \cdot g^{-1}$ (Table 2.3). It is indicated that the formation of pyrochlore or hexagonal decreases the surface area.

2-3-2-3 Effect of the calcination temperature

Fig. 2.11 illustrates the XRD patterns of W-Nb-O (W/Nb=1.35, W: Nb=2.70: 2.00) calcined at various temperature. The layered structure of W-Nb-O was maintained after calcination at a temperature of 973 K or below, however, this material transformed into a phase composed of $Nb_8W_9O_{47}$ at a temperature 1273 K or above. Firstly, we consider that the W-Nb-O material has high heat-resistance compared to the Mo_3VO_x materials in which complete structure decomposition was observed after heat-treatment at 973 K.[11] This phenomenon may originate from the high bond strength of W-O. Secondly, the phase transformation during the heat-treatment indicates that the same layered material with the $Nb_8W_9O_{47}$ phase was formed from W-Nb-O strongly infers that crystallization took place only in the *a-b* plane during the heat-treatment. This suggests that the non-structural identity in the *a-b* plane of W-Nb-O is thermodynamically meta-stable and is comparable to a high-dimensionally disordered structure.

Fig. 2.13 illustrates the nitrogen adsorption isotherm of W-Nb-O (W/Nb=1.35, W: Nb=2.70: 2.00) calcined at 673, 973 and 1273 K and the surface areas are summarized in Table 2.4. The surface area of the W-Nb-O (673 K) was 100 m^2g^{-1}. The surface area of the W-Nb-O decreased with an increase in calcination temperature and the surface area of W-Nb-O (973 K) and W-Nb-O (1273 K) which has the $Nb_8W_9O_{47}$ phase were 43 and 2 m^2g^{-1}, respectively. In W-Nb-O (673 K) and W-Nb-O (973 K), the nitrogen adsorption at

p/p_0 in the range of 10^{-6} was observed, indicating the presence of micropores in the material. In W-Nb-O (1273 K), on the other hand, the adsorption at p/p_0 in the range of 10^{-6} was not observed.

All catalysts were found to possess rod-like morphology in the STEM images (Fig. 2.13). The W-Nb-O (673 K) was found to be the small particle with sizes of 10~30 nm in diameter and of 0.1~0.3 μm in length. Following heat-treatment at 1273 K, crystal size growth was clearly observed both in diameter and length increasing to 1~2 μm and 3~10 μm, respectively. It is considered that the significant decrease of the surface area due to the disappearance of micropores and decrease of external surface corresponding to the increase of crystal size.

2-3-3 Characterization of layer-structured W-Nb-O

As shown in Fig. 2.14, the complex oxides having different crystal structures were obtained by preparation under various conditions. In these oxides, the layer-structured complex metal oxides synthesized by hydrothermal method such as W-Nb-O (673 K) and W-Nb-O (973 K) were discussed in detail. TEM images of W-Nb-O (673 K) confirmed the formation of layered structure (Fig. 2.16). The layer spacings were about 0.4 nm in agreement with the result of XRD. However, it was hard to observe the arrangement in *a*-*b* plane. Therefore, crystal structure in *a*-*b* plane was investigated by comparison with some complex metal oxides having structure ordered in *a*-*b* plane.

The low intensity diffractions were also observed over the range comparable to that of $Cs_{0.5}[Nb_{2.5}W_{2.5}O_{14}]$ (Fig. 2.16). However, they were very broad, indicating that the growth of *a*-*b* plane is not enough.

Fig. 2.17 illustrates the SEM images of $Cs_{0.5}[Nb_{2.5}W_{2.5}O_{14}]$ and W-Nb-O (673 K). Both catalysts were found to possess rod-like morphology. $Cs_{0.5}[Nb_{2.5}W_{2.5}O_{14}]$ was well-grown crystals with sizes of 0.5~1 μm in diameter and of more than 5 μm in length. The W-Nb-O (673 K) was found to be the smaller particle with sizes of 10~30 nm in diameter and of 0.1~0.3 μm in length. It is apparent that the crystal growth in the *a* and *b*-direction in this material is difficult as discussed on the basis of the XRD data.

As already described in 2-3-1, it is considered the W-O bond cannot elongate as with Mo-O. This property is crucial for determining the ease with which the orthorhombic structure forms. The formation of orthorhombic W-based complex oxide is difficult compared to that of the Mo-based oxide systems as the formation of the octahedral arrangement in the *a*-*b* plane requires high flexibility (deformation of octahedra) during the formation of the structure shown in Fig. 2.3 (a).

The Rietveld analysis was carried out based on the structure of $Cs_{0.5}[Nb_{2.5}W_{2.5}O_{14}]$ under the assumption that the crystal size was 10 nm×10 nm×300 nm. As shown in Fig. 2.18, observed and calculated diffractions were converged reasonably (Rwp=7.03%) although Rietveld refinement with hexagonal structure did not converge.

Fig. 2.19 illustrates the Raman spectra of hexagonal WO_3 and the complex metal oxides of W and Nb. Hexagonal WO_3 exhibited bands of O-W-O deformation at 252 and 334 cm^{-1}, O-W-O stretching at 648, 688, and 813 cm^{-1}, and W=O stretching at 946 cm^{-1}, respectively.[12] For WO_3/Nb_2O_5, the raman band at 267, 326, 707 and 805 cm^{-1} assigned to monoclinic WO_3.[12] Although the raman bands for $Nb_8W_9O_{47}$ and $Cs_{0.5}[Nb_{2.5}W_{2.5}O_{14}]$ mostly agreed with those of the hexagonal WO_3, the band not ascribed to hexagonal WO_3 was observed at 813 cm^{-1}. Because $Nb_8W_9O_{47}$, $Cs_{0.5}[Nb_{2.5}W_{2.5}O_{14}]$ and hexagonal WO_3 have a common layered arrangement of octahedral units into the *c*-direction, it is suggested that the band at 743 cm^{-1} was assigned to pentagonal $\{(M)M_5O_{27}\}$ unit which is present in $Nb_8W_9O_{47}$, $Cs_{0.5}[Nb_{2.5}W_{2.5}O_{14}]$ and absent in hexagonal WO_3.

Besides, as already shown in Fig. 2.13, I observed an appreciable amount of nitrogen adsorption at p/p_0 in the range of 10^{-6}, indicating the presence of micropores in the material. This supports our postulation that the disordered structure in the *a*-*b* plane might form micro-channel pores as observed in orthorhombic Mo_3VO_x where 7-membered ring forms micropores.

As demonstrated above, it is suggested W-Nb-O (673 K) and $Cs_{0.5}[Nb_{2.5}W_{2.5}O_{14}]$ have common unit such as pentagonal units and 7-membered rings, and similar ordered structure.

2-3-4 Synthesis of W-V-O and W-Ta-O

Fig. 2.20 illustrates the XRD patterns of uncalcined W-V-O (W/V=1.35), W-Nb-O (W/Nb=1.35) and W-Ta-O (W/Ta=1.35) synthesized by hydrothermal method. The diffraction peaks around 23 and 46° due to the layered structure were also observed in W-V-O and W-Ta-O, although low intensity diffractions attributed to hydrated vanadium oxide containing NH^{4+} ion with a layered structure[13] were observed in W-V-O. The peaks ascribed to (001) planes in W-V-O and W-Ta-O appeared at 22.82° and 22.96°, respectively. The *d* spacing between (001) planes of W-V-O and W-Ta-O calculated from these angles were 0.389 nm and 0.387 nm, respectively.

Fig. 2.21 illustrates the nitrogen adsorption isotherms of W-V-O, W-Nb-O and W-Ta-O and these surface areas were listed in Table 2.5. The shape of isotherm of W-Ta-O was similar to that of W-Nb-O and the increase of the adsorption amount below $p/p_0=10^{-6}$ was also observed. Besides, the surface area (118 $m^2 g^{-1}$) was also comparable to W-Nb-O (100 $m^2 g^{-1}$). On the other hand, the adsorption below $p/p_0=10^{-6}$ was hardly observed in W-V-O, and the surface area of W-V-O was less than one fifth of that of the W-Nb-O catalyst.

In the STEM images (Fig. 2.22), all the catalysts were found to have rod-like crystalline morphology. However, dense aggregation of the rod-like crystals was observed in the W-V-O catalyst. Therefore the surface area of the W-V-O catalyst would be lower than those of the W-Nb-O and W-Ta-O catalyst.

2-4 Conclusion

While the simple impregnation and subsequent calcination only produced a mixture of WO_3 and Nb_2O_5, W-Nb-O having layer structure in *c*-direction was obtained by hydrothermal method. The presently applied hydrothermal conditions, which are similar to those used in the synthesis of Mo_3VO_x, could not facilitate the production of crystalline W and Nb materials as with $Cs_{0.5}[Nb_{2.5}W_{2.5}O_{14}]$. It should be noted that the hydrothermal method is in principle an effective method to promote octahedral arrangement of materials even in the case of W‐Nb‐O. The result of Rietveld analysis, Raman and N_2 adsorption suggest that W-Nb-O (673 K) and $Cs_{0.5}[Nb_{2.5}W_{2.5}O_{14}]$ have common unit such as pentagonal units and 7-membered rings, and similar ordered structure. Besides, layer-structured W-V-O and W-Ta-O were also obtained by hydrothermal method.

2-5 References

[1] D. C. Craig, N. C. Stephenson, *Acta Crystallogr. B* **1969**, 25, 2071.

[2] S. M. Montemayor, A. A. Mendez, A. M. la Cruz, A. F. Fuentes, L. M. Torres-Martinez, *J. Mater. Chem.* **1998**, 8, 2777.

[3] F. Krumeich, T. Geipel, *J. Solid State Chem.* **1996**, 124, 58.

[4] M. Lundberg, M. Sundberg, *Ultramicroscopy* **1993**, 52, 429.

[5] T. E. Weirich, J. Portillo, G. Cox, H. Hibst, S. Nicolopoulos, *Ultramicroscopy* **2006**, 106, 164.

[6] A. Simon, E. V. Kondratenko, *Chem. Eur. J.* **2010**, 16, 1765.

[7] J. Barthel, T. E. Weirich, G. Cox, H. Hibst, A. Thust, *Acta Mater.* **2010**, 58, 3764.

[8] M. Sadakane, N. Watanabe, T. Katou, Y. Nodasaka, W. Ueda, *Angew. Chem. Int. Ed*. **2007**, 46, 1493.

[9] F. Wang, W. Ueda, *Catal. Today* **2009**, 144, 358.

[10] M. Sadakane, K. Yamagata, K. Kodato, K. Endo, K. Toriumi, Y. Ozawa, T. Ozeki, T. Nagai, Y. Matsui, N. Sakaguchi, W.D. Pyrz, D.J. Buttrey, D.A. Bolm, T. Vogt, W. Ueda, *Angew. Chem. Int. Ed.* **2009**, 48, 3782.

[11] U. Damien, PhD thesis, Tokyo Institute of Technology, Tokyo, Japan, **2003**.

[12] M. F. Daniel, B. Desbat, J. C. Lassegues, B. Gerand, M. Fjglarz, *J. Solid State Chem.* **1987**, 67, 235.

[13] Y. Oka, T. Yao, N. Yamamoto, *Nippon Seramikkusu Kyokai Gakujutsu Ronbunshi* **1990**, 98, 1365.

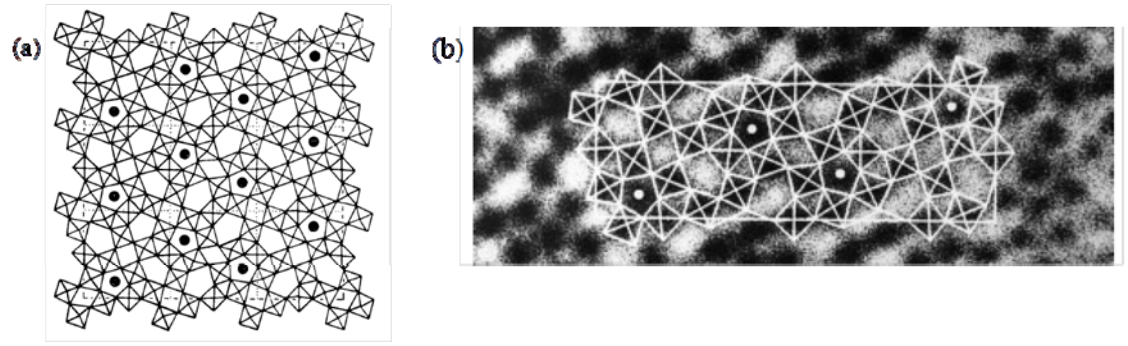


Fig. 2.1 (a): The structure of $Nb_8W_9O_{47}$ projected on to the (001) plane. Each full circle represents a niobium atom at z = 0 together with a superimposed oxygen atom at z = 1/2. The metal atom has seven-fold coordination. (b): TEM image of $Nb_8W_9O_{47}$ projected on to the (001) plane.

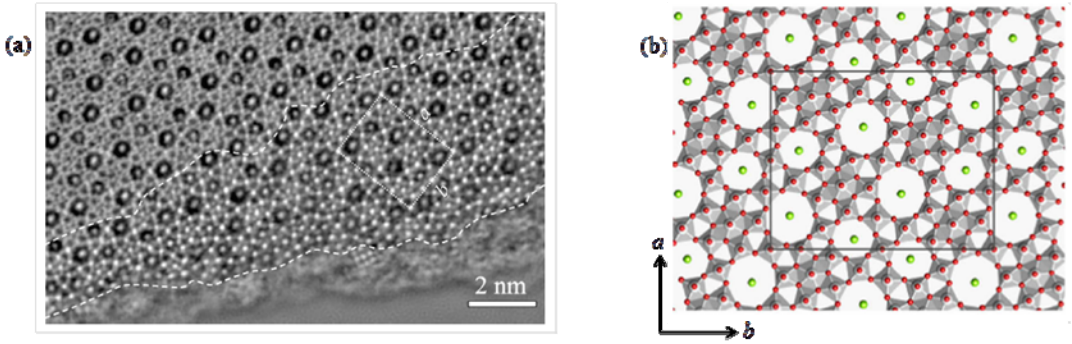


Fig. 2.2 (a): Phase of the reconstructed and aberration-corrected wave function belonging to a thin region near the crystal edge. The average structure of $Cs_{0.5}[Nb_{2.5}W_{2.5}O_{14}]$ was determined from the area enclosed by the dashed curves. The area is 54.4 nm^2 and contains approximately nine projected unit cells. (b): Structure model as derived from the experimentally determined atom positions in projection along the [001] zone axis. Cs = green; Nb, W = light grey; O = red.

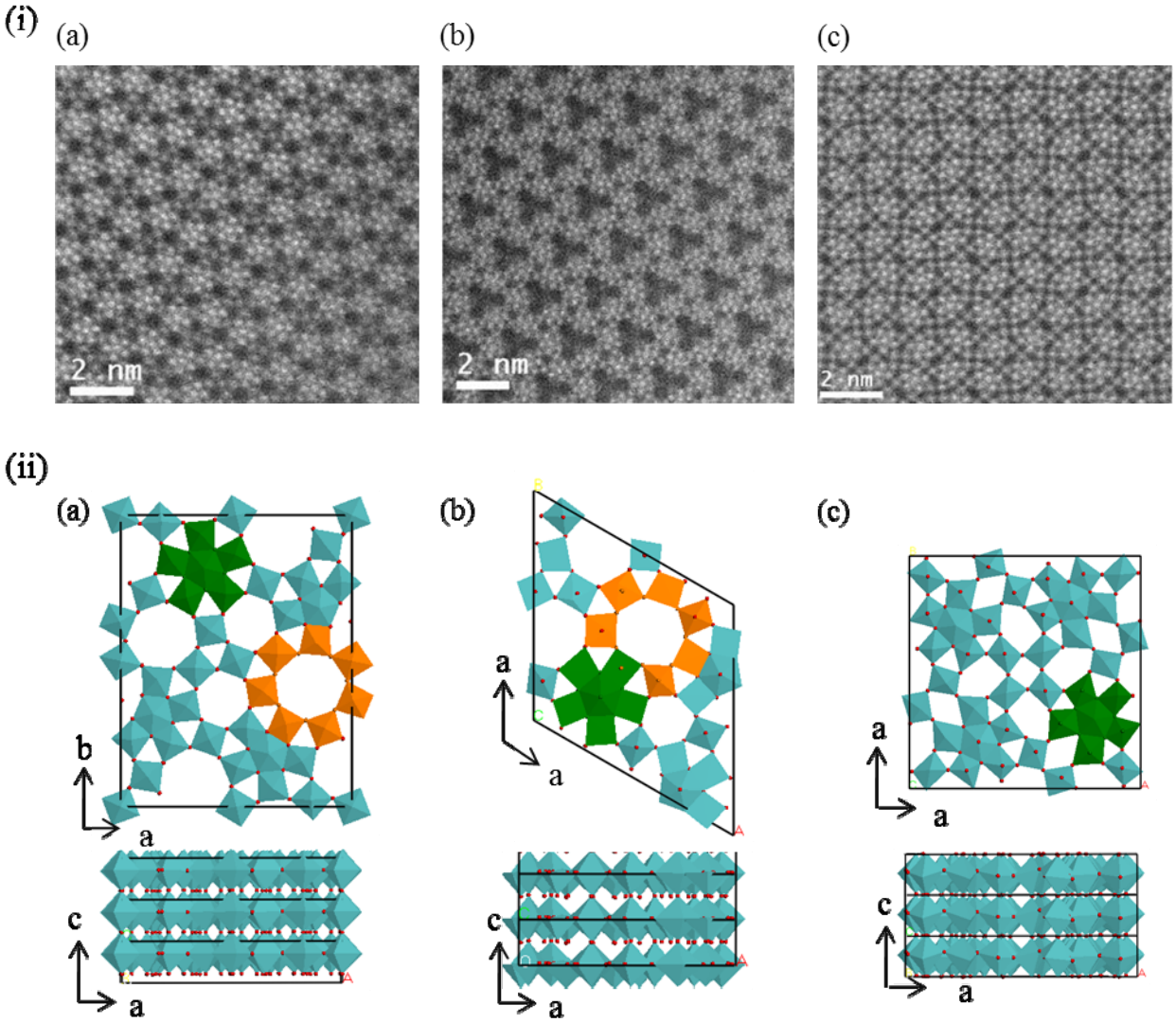


Fig. 2.3 Structures model (i) and HAADF-STEM images (ii) of orthorhombic (a), trigonal (b), and tetragonal (c) Mo_3VO_x.

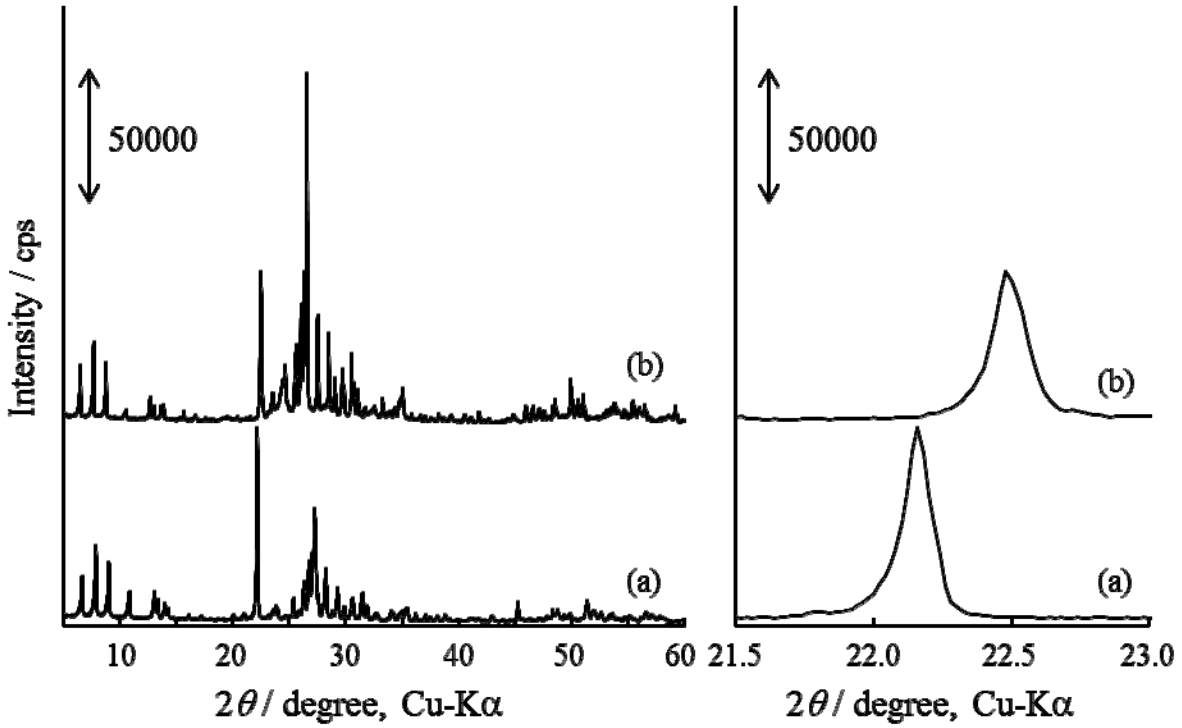


Fig. 2.4 XRD patterns of orthorhombic Mo_3VO_x (a) and $Cs_{0.5}[Nb_{2.5}W_{2.5}O_{14}]$ (b).

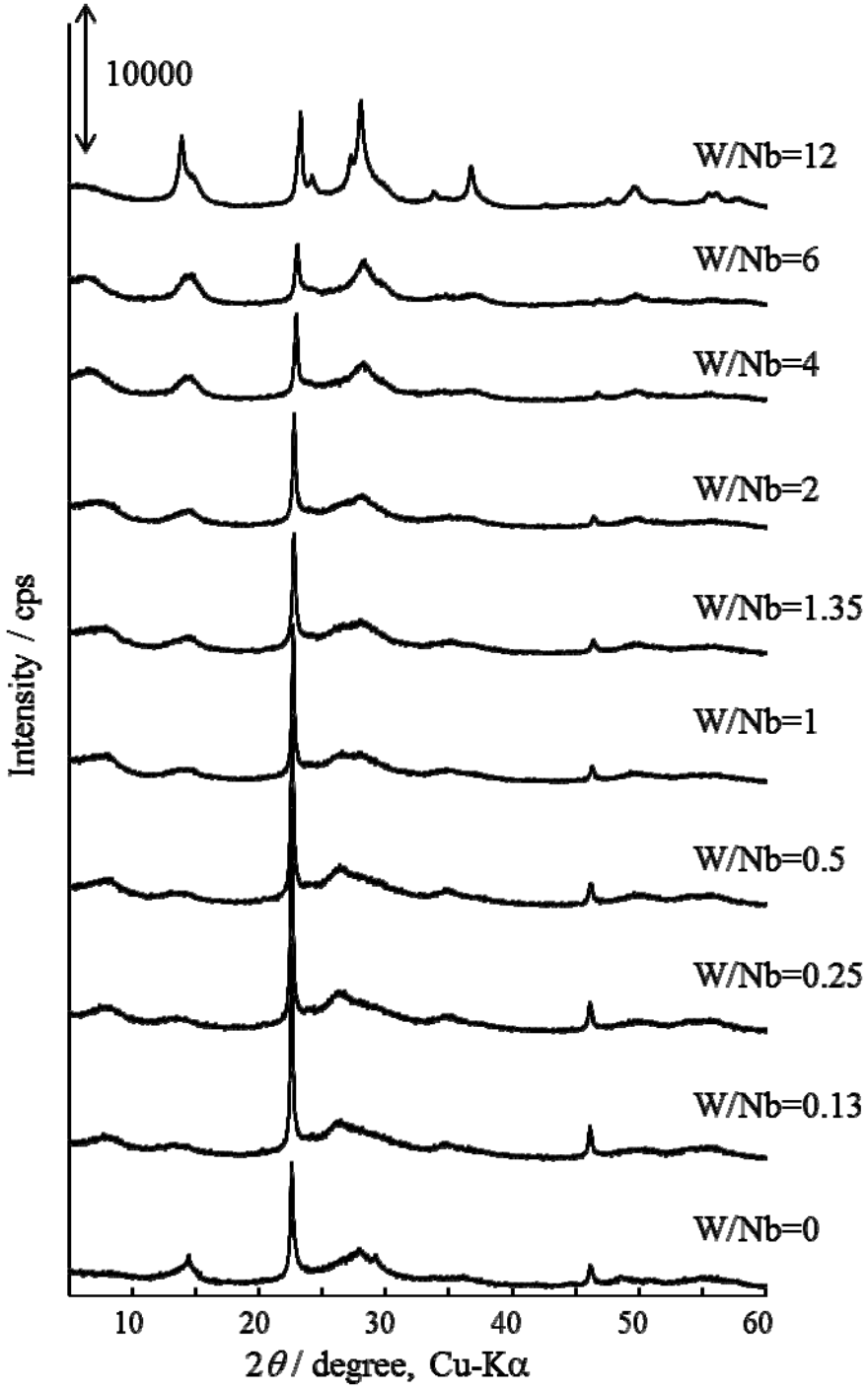


Fig. 2.5 XRD patterns of uncalcined W-Nb-O (W/Nb=0~12).

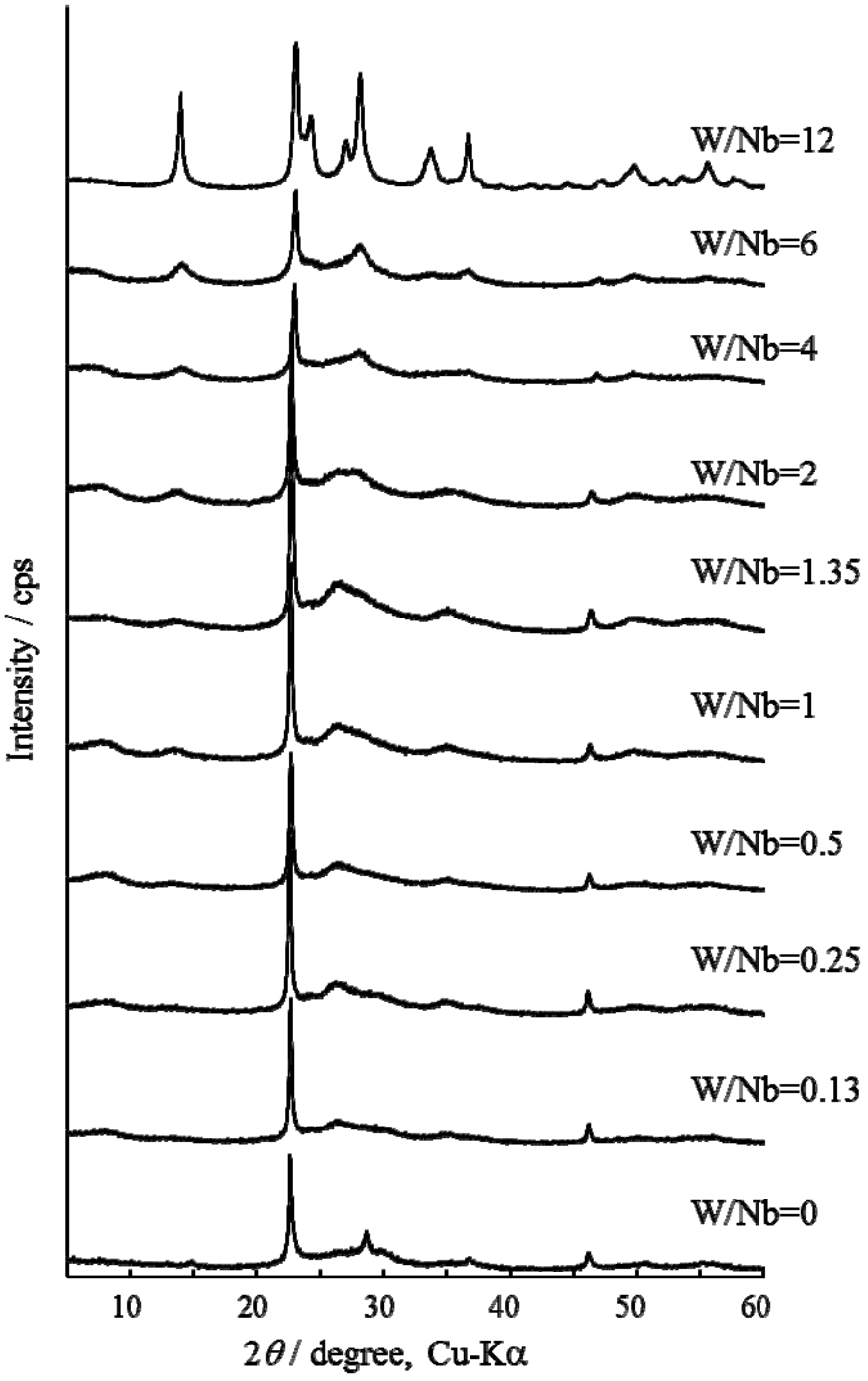


Fig. 2.6 XRD patterns of W-Nb-O (W/Nb=0~12) calcined at 673 K.

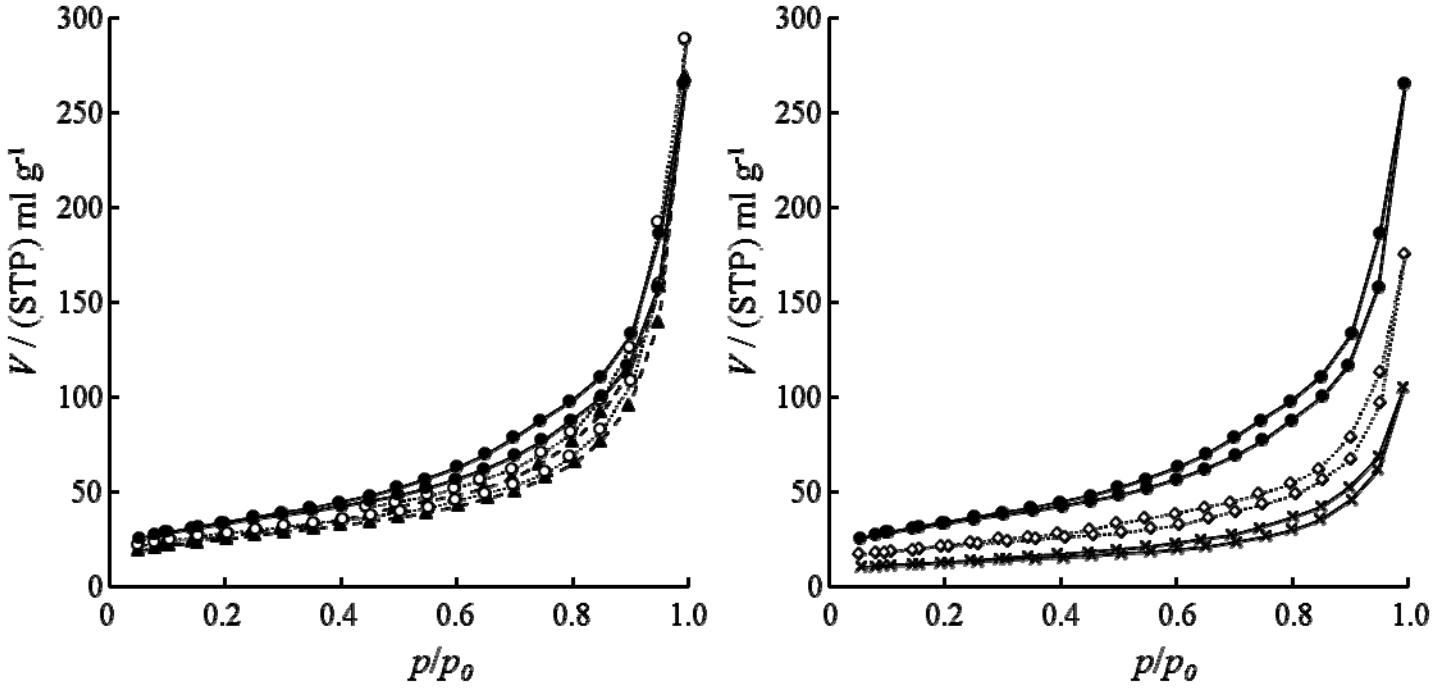


Fig. 2.7 N_2 adsorption isotherms of W-Nb-O calcined at 673 K.
Symbols: W/Nb=0, ▲; W/Nb=0.5, ○; W/Nb=1.35, ●; W/Nb=6, ◇; W/Nb=12, ×.

Table 2.2 Effect of W/Nb ratio on surface area[a]

W/Nb	Surface area / $m^2 \cdot g^{-1}$
0	89
0.13	96
0.25	86
0.5	97
1	111
1.35	118
2	111
4	84
6	72
12	43
h-WO_3	10

[a] Calcination temperature, 673 K.

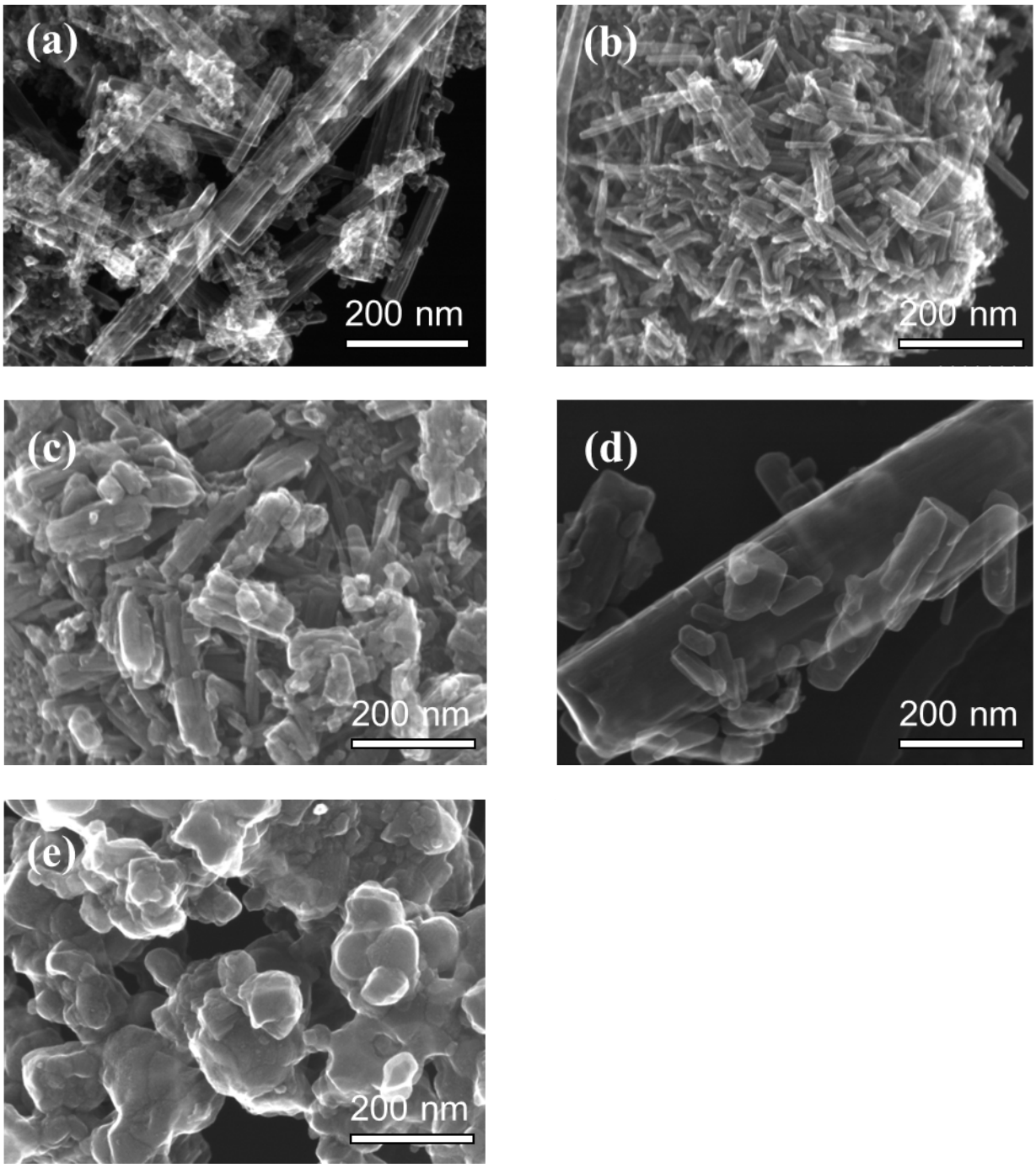


Fig. 2.8 STEM images of Nb-O (W/Nb=0), (a); W-Nb-O (W/Nb=1.35), (b); W-Nb-O (W/Nb=12), (c); hexagonal WO_3, (d), WO_3/Nb_2O_5 (W/Nb=1.35), (e).

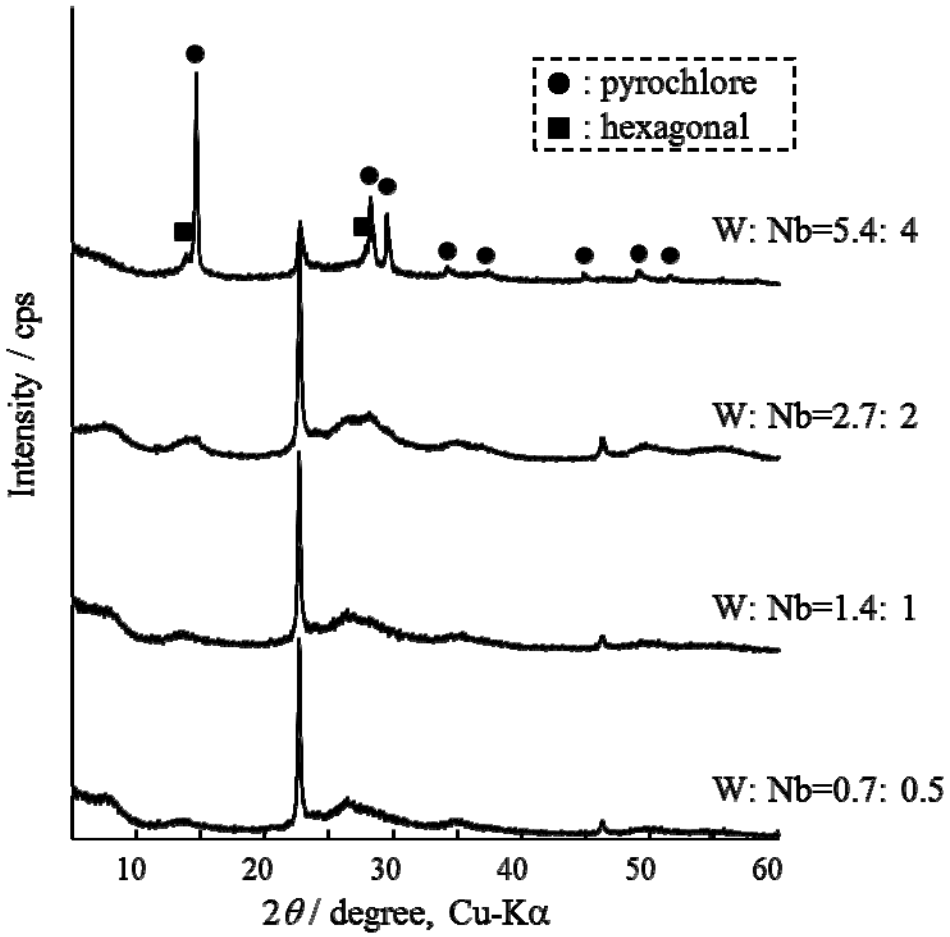


Fig. 2.9 XRD patterns of W-Nb-O prepared from the precursor solution at various concentrations.

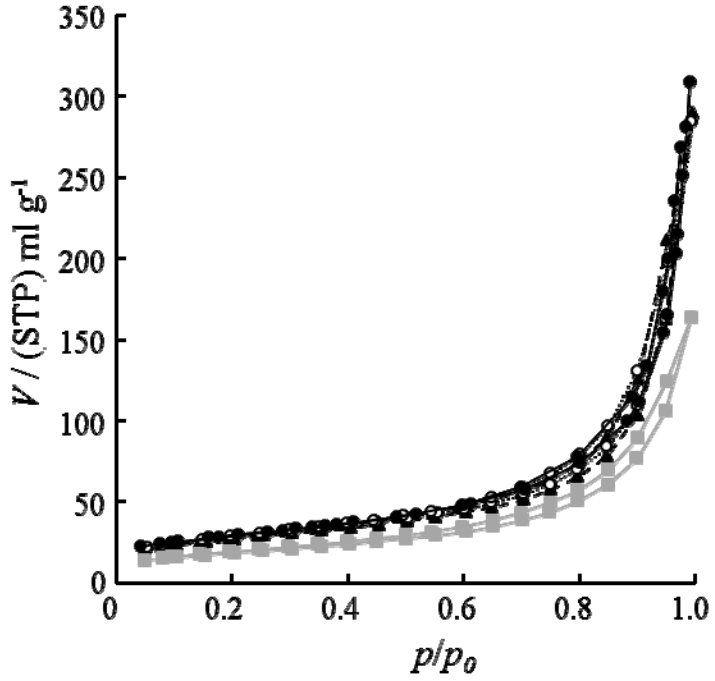


Fig. 2.10 N_2 adsorption isotherms of W-Nb-O prepared from the precursor solution at various concentrations.
Symbols: W: Nb=5.40: 4.00, ■; W: Nb=2.70: 2.00 , ●; W: Nb=1.35: 1.00 , ○; W: Nb=0.63: 0.50 , ▲.

Table 2.3 Effect of concentration of precursor solution on surface area[a]

Concentration / mmol in 45ml of H_2O		Surface area
W	Nb	/ $m^2 \cdot g^{-1}$
0.63	0.50	103
1.35	1.00	102
2.70	2.00	100
5.40	4.00	68

[a] Calcination temperature, 673 K.

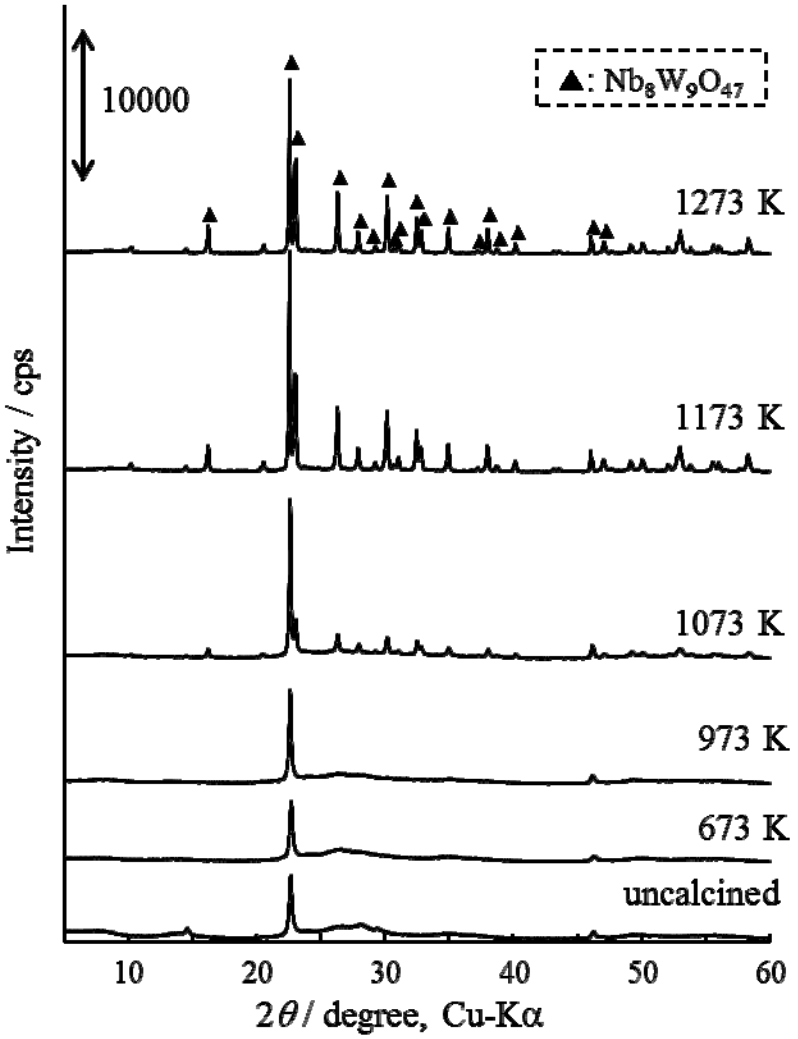


Fig. 2.11 XRD patterns of W-Nb-O (W/Nb=1.35) calcined at various temperature.

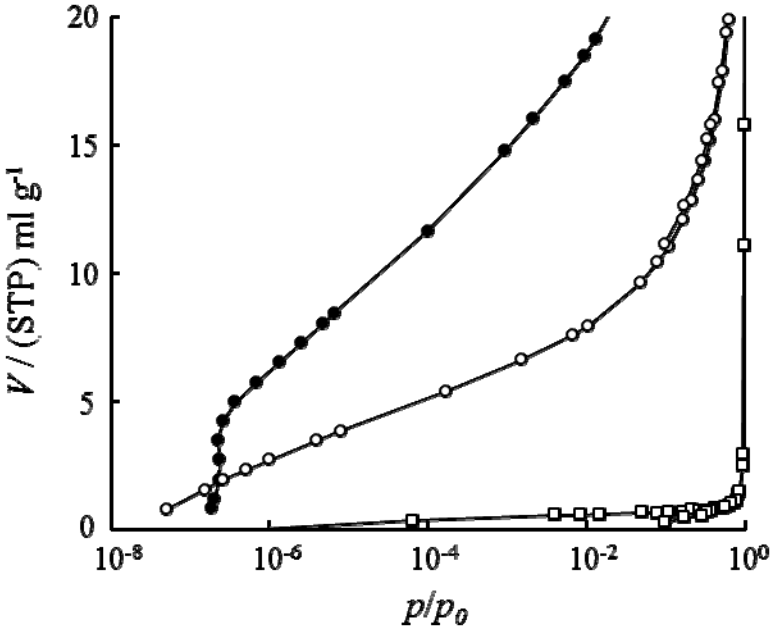


Fig. 2.12 N_2 adsorption isotherms of W-Nb-O complex metal oxides. Symbols: W-Nb-O (673 K), ●; W-Nb-O (973 K), ○; W-Nb-O (1273 K), □.

Table 2.4 Effect of calcination temperature on surface area

Catalyst [a]	Surface area / $m^2 \cdot g^{-1}$
W-Nb-O (673 K)	100
W-Nb-O (973 K)	43
W-Nb-O (1273 K)	2

[a] W/Nb = 1.35.

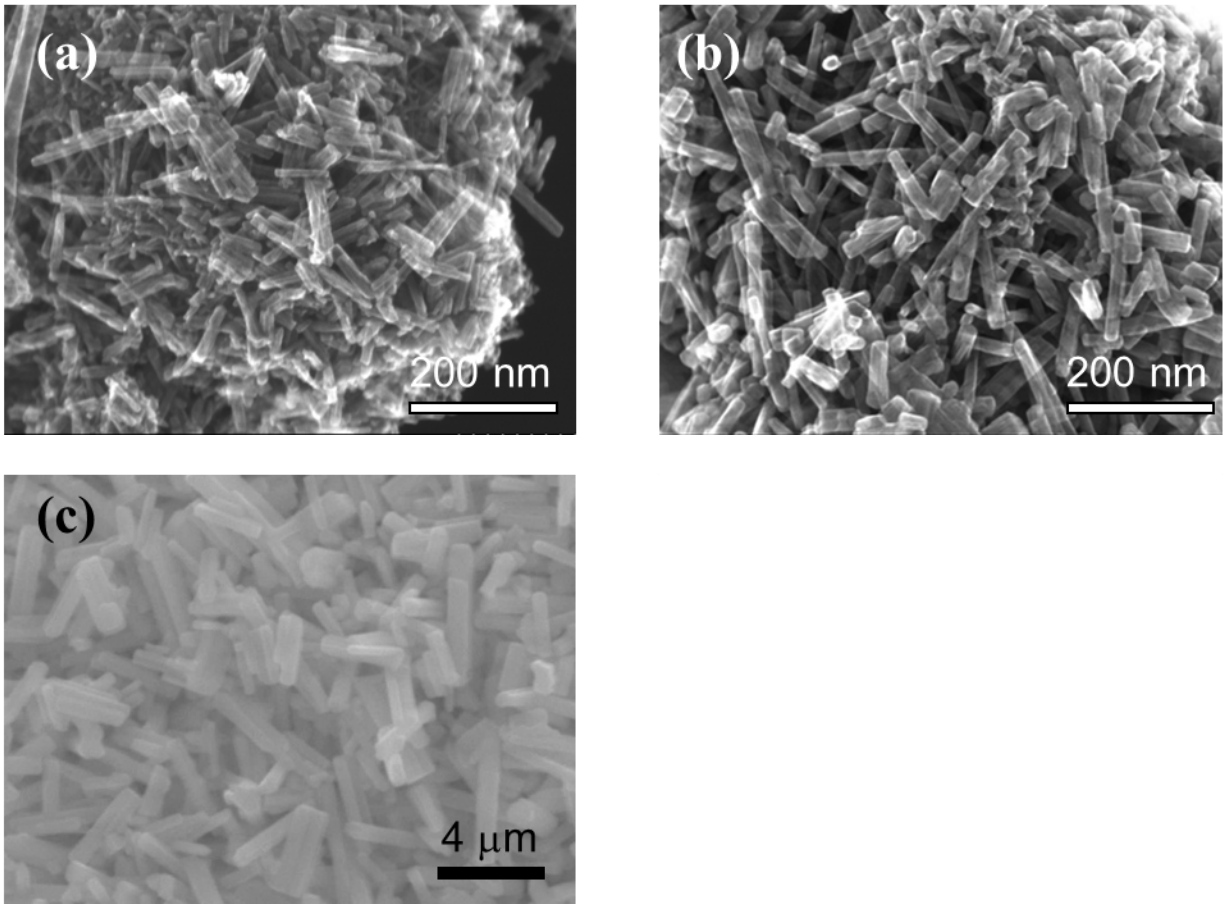


Fig. 2.13 STEM images of W-Nb-O (673 K), (a); W-Nb-O (973 K), (b); and W-Nb-O (1273), (c).

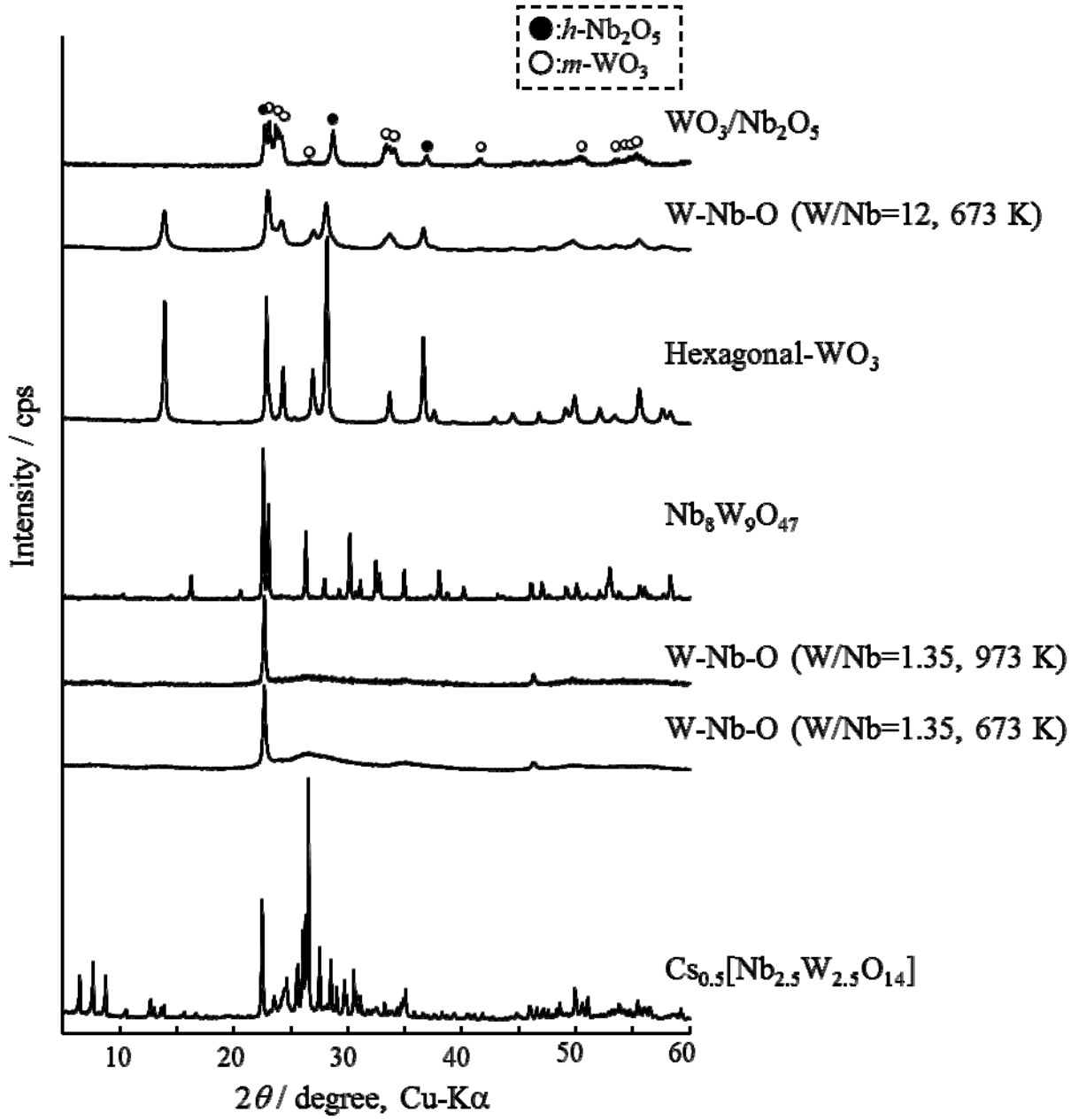


Fig. 2.14 XRD patterns of the complex metal oxides of W and Nb having different structure.

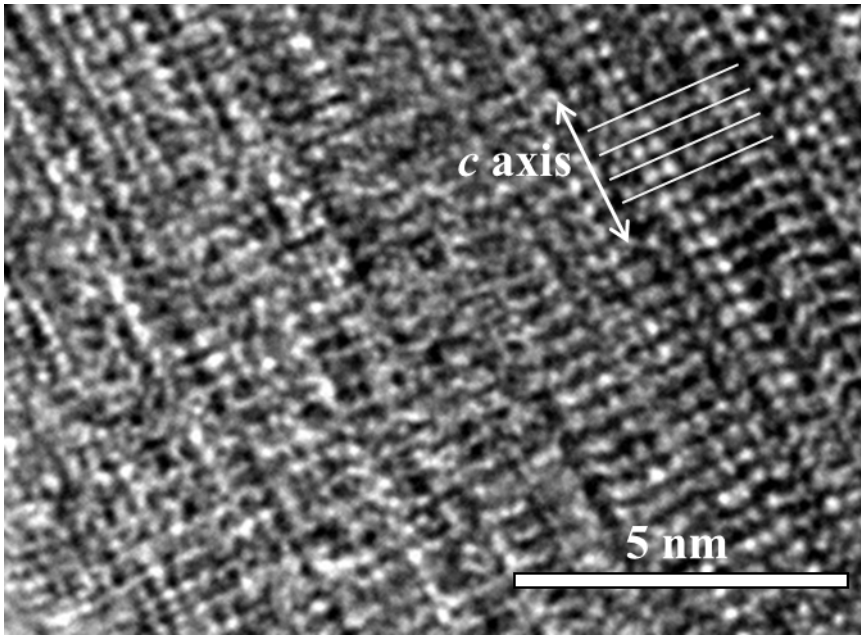


Fig. 2.15 TEM images of W-Nb-O (673 K).

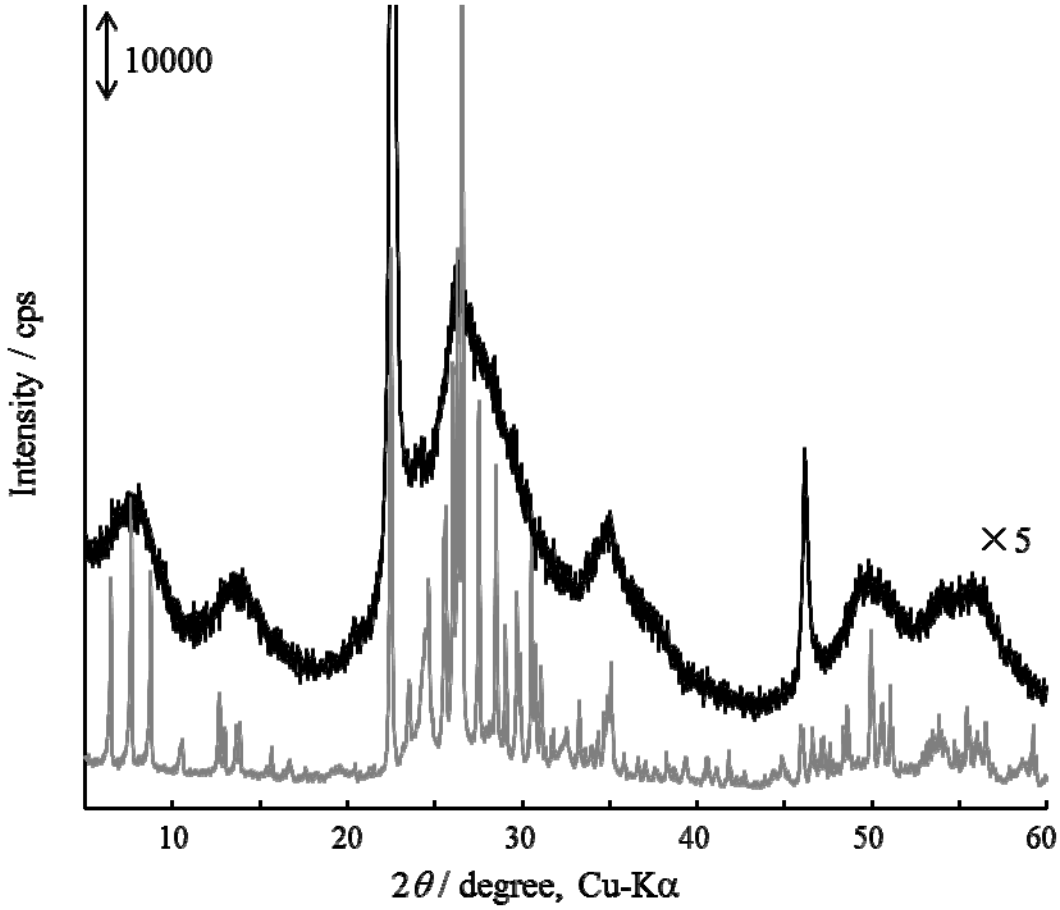


Fig. 2.16 XRD patterns of W-Nb-O (673 K) (black line) and $Cs_{0.5}[Nb_{2.5}W_{2.5}O_{14}]$ (gray line).

.

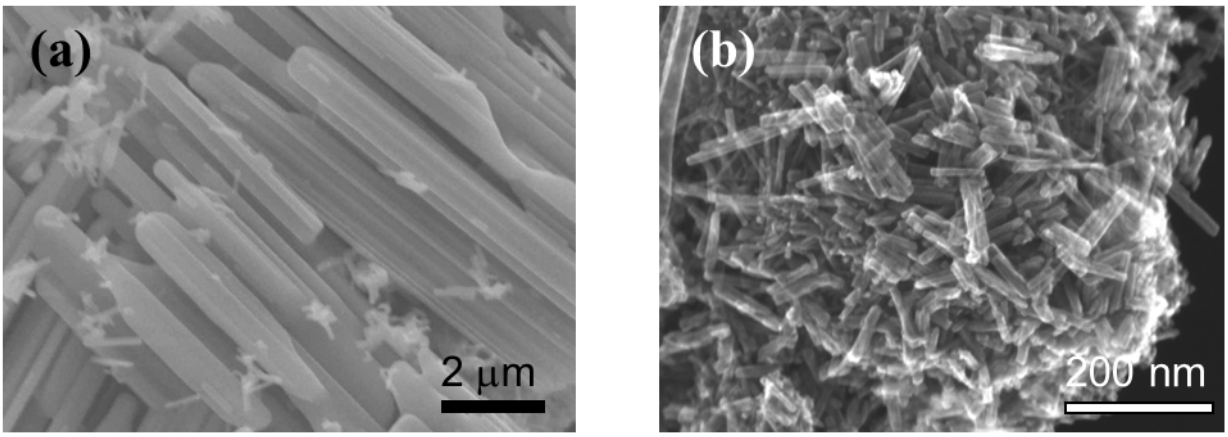


Fig. 2.17 STEM images of $Cs_{0.5}[Nb_{2.5}W_{2.5}O_{14}]$, (a); and W-Nb-O (673), (b).

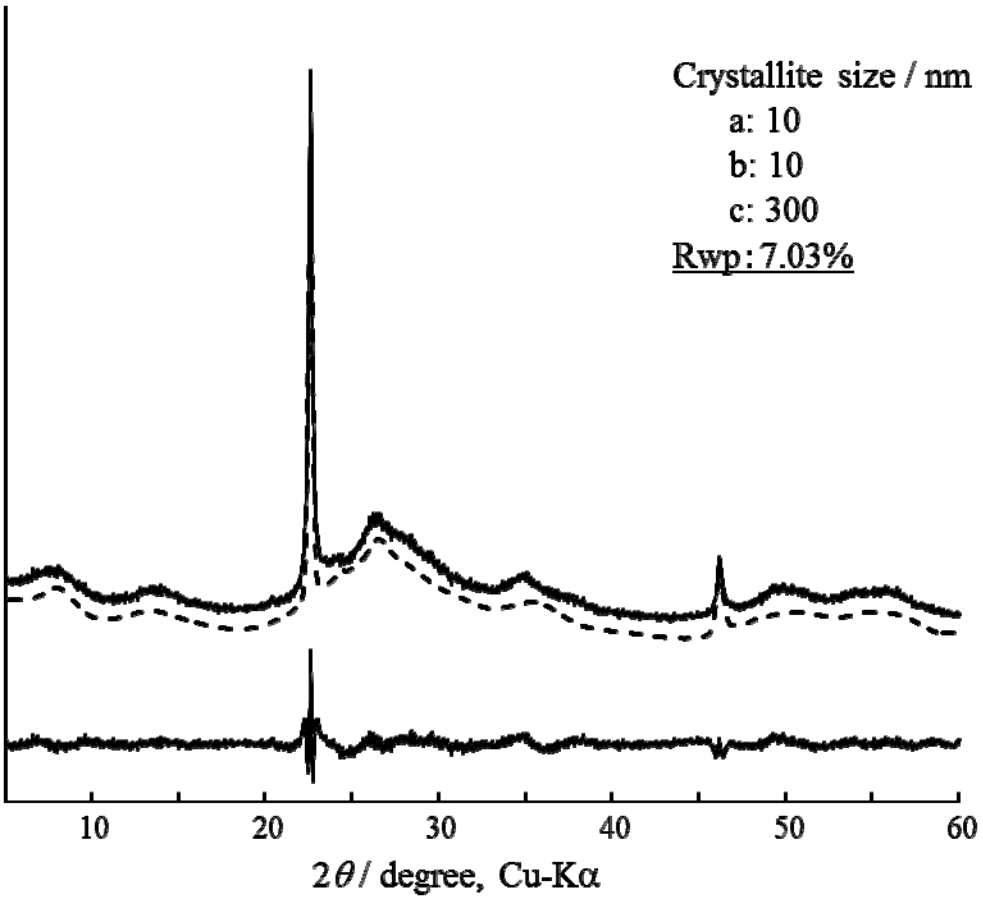


Fig. 2.18 Observed (solid line), calculated (dotted line), and difference pattern (solid line, bottom) from the Rietveld analysis of the XRD data.

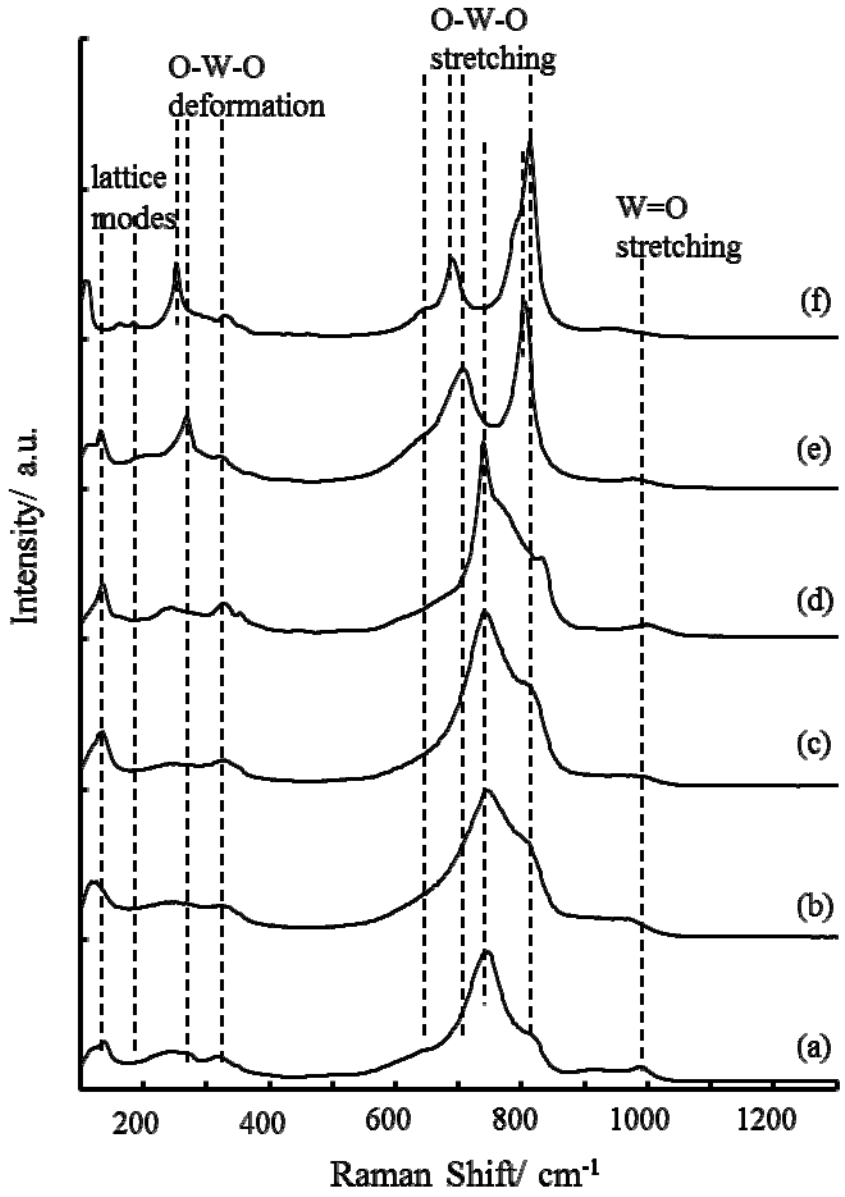


Fig. 2.19 Raman spectra of the complex metal oxides of W and Nb having different structure.
$Cs_{0.5}[Nb_{2.5}W_{2.5}O_{14}]$, (a); W-Nb-O (673), (b); W-Nb-O (973), (c); $Nb_8W_9O_{47}$, (d); WO_3/Nb_2O_5, (e); hexagonal WO_3, (f).

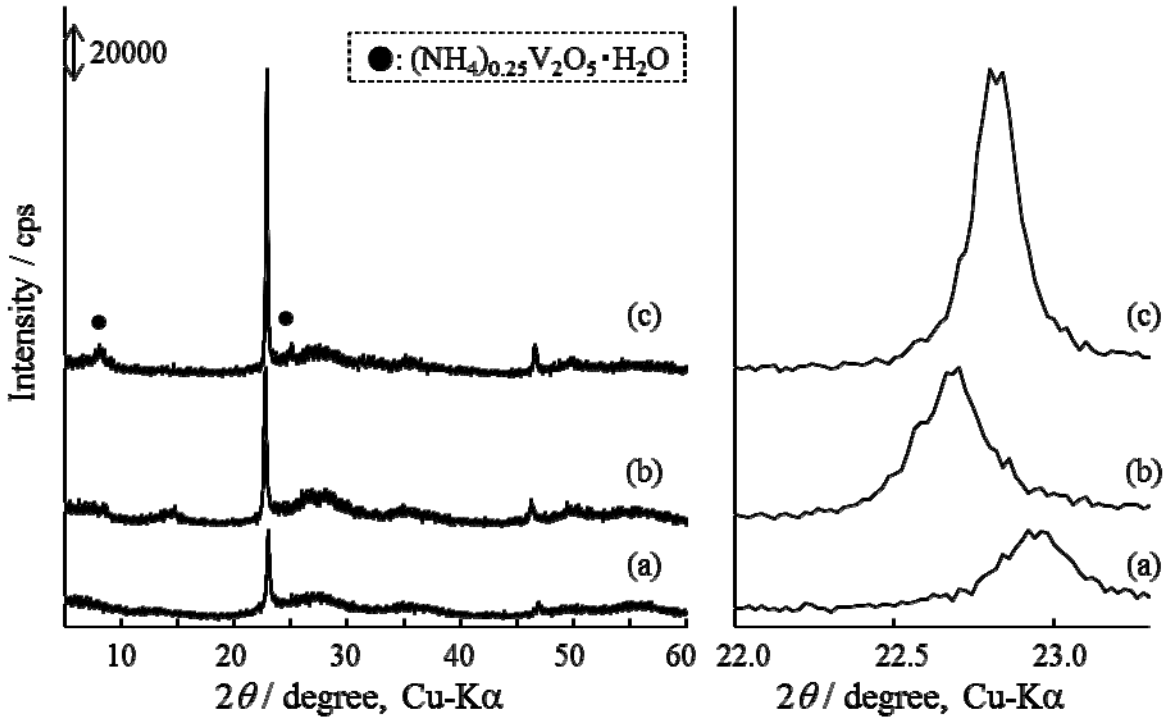


Fig. 2.20 XRD patterns of W-Ta-O, (a); W-Nb-O, (b); and W-Ta-O, (c).

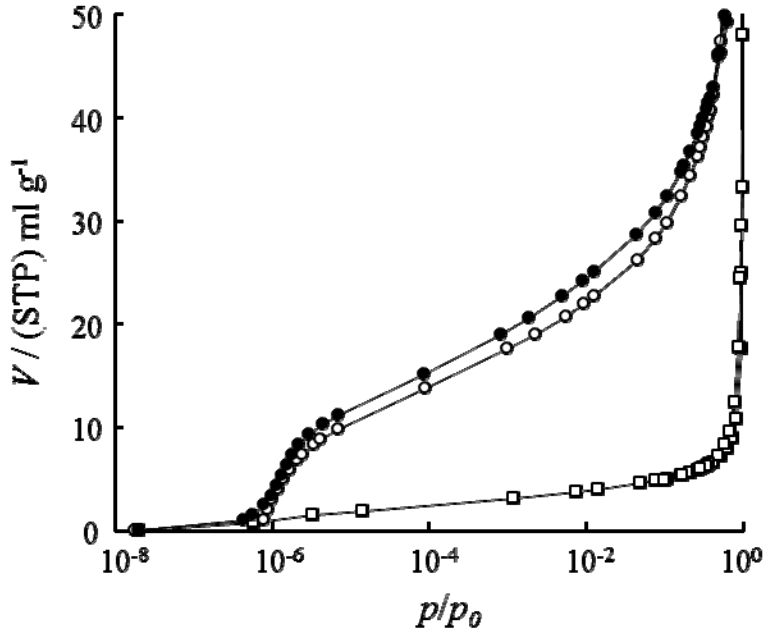


Fig. 2.21 N_2 adsorption isotherms of uncalcined W-V-O, □; W-Nb-O, ●; W-Ta-O, ○.

Table 2.5 Surface areas of uncalcined W-V-O, W-Nb-O and W-Ta-O.

Catalyst	SA_{BET} / $m^2 \cdot g^{-1}$
W-V-O	18
W-Nb-O	100
W-Ta-O	118

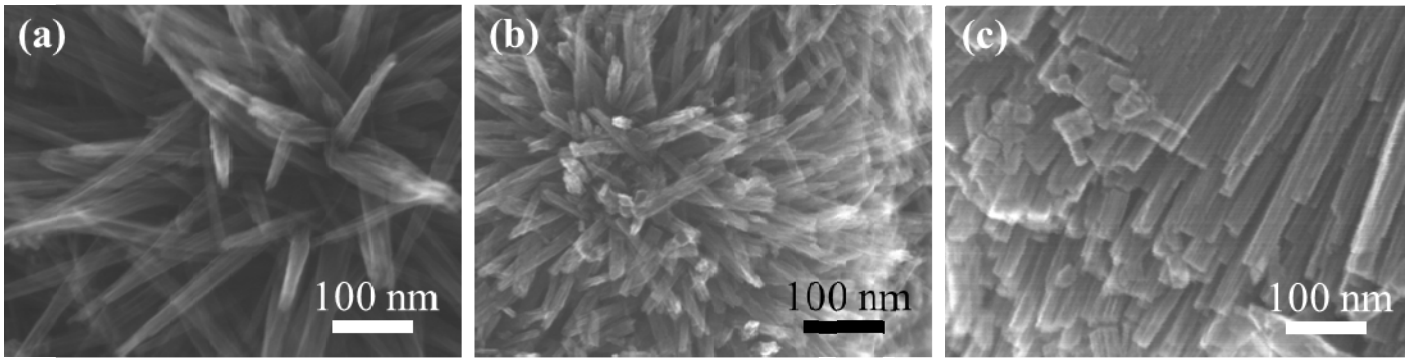


Fig. 2.22 STEM images of W-Nb-O (W/Nb=1.35), (a); W-Ta-O (W/Ta=1.35), (b); W-V-O (W/V=1.35), (c).

Chapter 3

Solid Acid Property of W-based Complex Metal Oxide and Dehydration of Glycerol to Acrolein

3-1 Introduction

As already described in chapter 1, dehydration of glycerol to acrolein, which is an important intermediate for the chemical and agricultural industries is one of the most attractive reactions with respect to effective utilization of biomass-based co-products. To perform this double dehydration reaction, catalysts require both high acidity and water-resisting property due to the presence of steam in the reactant gas.[1] It has been reported that solid acid-catalysts such as niobic acid and H-ZSM-5 are effective under the reaction conditions in the presence of water.[2,3] On the other hand, catalysts such as WO_3–ZrO_2 and 12-tungstosilicic acid, which have high acid strength are known to exhibit high catalytic performance for the reaction.[4,5] These catalysts gave relatively high acrolein yield,[6–9] however, product selectivity and catalyst lifetime were not desirable for practical use. Further catalyst development is obviously necessary to improve the acrolein selectivity and to suppress the catalytic deactivation.

Complex oxides of W and Nb are known as solid acids which exhibit high activity in alkane cracking and dehydration of alcohols. Recently it was reported that mesoporous Nb–W oxide[10] and the fiber-shaped Nb_2O_5–WO_x[11] catalysts showed high activity for Friedel-Crafts alkylation. This is an acid-catalyzed reaction and requires an active site of high acidity. As these catalysts showed higher activity for acid-catalyzed reactions compared with simple composite oxides; crystalline or nano-structured complex oxide based on a combination W and Nb may display high activity for reactions which are acid-catalyzed.

In chapter 2, W-based complex oxide was obtained by hydrothermal synthesis. Although the crystallinity of the synthesized material is low at the present stage, I have attempted here to use the material as catalysts for the dehydration of glycerol to acrolein in the presence of water and oxygen. And effects of structure and the W/Nb ratio of the W-Nb-O catalyst on their acidity and selectivity in glycerol transformation were investigated.

3-2 Experimental

3-2-1 Chemicals

Chemicals used in experiments are listed in Table 3.1.

Table 3.1 List of chemicals

chemical	formula or molar wt.	assay	manufacturer	No.
$Nb_2O_5 \cdot xH_2O$	265.82 (Nb_2O_5)	70.8% (Nb_2O_5)	Soekawa Chemical Co., Ltd.	02275B
$ZrCl_2O \cdot 8H_2O$	322.25	99.0%	Wako Pure Chemical Ind., Ltd.	267-00492
28% ammonia solution	17.03 (NH_3)	28.0~30.0%	Wako Pure Chemical Ind., Ltd.	016-03146
$(NH_4)_6(H_2W_{12}O_{40}) \cdot nH_2O$ ($n \fallingdotseq 6$)	3064	90.8% (WO_3)	Nippon Inorganic Colour and Chemical Co., Ltd.	100114
$HClO_4$	100.46	60%	Kanto Chemical Co., Ltd.	32059-00
glycerol (for reaction)	92.09	97.0%	Wako Pure Chemical Ind., Ltd.	072-00626
glycerol (for calibration)	92.09	99.0%	Wako Pure Chemical Ind., Ltd.	075-00616
2-butanol	74.12	99.0%	Wako Pure Chemical Ind., Ltd.	020-11215
propylenegrycol	76.09	99.5%	Kanto Chemical Co., Ltd.	32458-00
acrolein	56.06	90%	Tokyo Chemical Ind. Co., Ltd.	A0137
hydroxyacetone	74.08	90.0%	Wako Pure Chemical Ind., Ltd.	089-05492
acetaldehyde	44.05	88.0~92.0%	Wako Pure Chemical Ind., Ltd.	015-09576
propionaldehyde	58.08	-	Tokyo Chemical Ind. Co., Ltd.	P0498
acetone	58.08	99.5%	Wako Pure Chemical Ind., Ltd.	012-00343
acetic acid	60.05	99.7%	Wako Pure Chemical Ind., Ltd.	017-00256
acrylic acid	72.06	99%	Tokyo Chemical Ind. Co., Ltd.	A0141
sea sand (50~80 mesh)	-	99.0%(SiO_2)	Miyazaki Chemical Co., Ltd.	M5080KA05

3-2-2 Catalyst preparation

3-2-2-1 Preparation of W-Nb-O by hydrothermal method

The complex metal oxides catalysts of W and Nb were prepared by hydrothermal synthesis method. The mixed solution of $Nb_2O_5 \cdot nH_2O$ and $(NH_4)_6[H_2W_{12}O_{40}] \cdot nH_2O$ was put in a stainless steel autoclave with a Teflon liner and aged at 448 K for 72 h. The molar ratio between W and Nb was set at W/Nb = 1.35. The formed solid was filtered, washed with ion-exchanged water, dried at 353 K and then calcined at

temperature of 673~1273 K for 4 h in air. The catalysts prepared by this method are represented by W–Nb–O (*X*, *Y*). The value *X* and *Y* in the parenthesis means W/Nb ratio and calcination temperature, respectively.

3-2-2-2 WO_3/ZrO_2

WO_3/ZrO_2 was prepared by impregnation method according to Ref. [12, 13]. A solution of $ZrCl_2O \cdot 8H_2O$ was used to produce zirconium hydroxide by precipitation upon addition of 28% NH_3 to pH 10. The precipitate was aged at room temperature for 1 h, and then filtered and washed with ion-exchanged water until no chloride was detected by the $AgNO_3$ test. The solids were then dried at 353 K overnight. The zirconium hydroxide was impregnated with an aqueous solution of $(NH_4)_6(H_2W_{12}O_{40}) \cdot nH_2O$ and dried at 353 K. The content of WO_3 and the calcination temperature were set to be 13 wt.% and 1093 K, respectively.

3-2-2-3 H-ZSM-5

H-ZSM-5(JRC-Z5-90H(1), SiO_2/Al_2O_3 = 90, provided from Süd-Chemie Catalysts Japan, Inc.) was used after calcination at 773 K for 3 h.

3-2-2-4 Treatment of $Cs_{0.5}[Nb_{2.5}W_{2.5}O_{14}]$ with acid

Acidic property of $Cs_{0.5}[Nb_{2.5}W_{2.5}O_{14}]$ was quite low due to the influence of Cs included in its structure. It has been reported that Cs of about 50% could be removed by acid treatment.[14] Therefore, the $Cs_{0.5}[Nb_{2.5}W_{2.5}O_{14}]$ after acid treatment described below was tested for reaction. Exchange of Cs ions in $Cs_{0.5}[Nb_{2.5}W_{2.5}O_{14}]$ with H^+ using $HClO_4$ was carried out. $Cs_{0.5}[Nb_{2.5}W_{2.5}O_{14}]$ was suspended in 1 M $HClO_4$ and refluxed at 353 K for 10 h. The product was filtered, washed with ion-exchanged water until no chloride ion was detected, dried at 353 K, and then calcined at 673 K for 3 h. The $Cs_{0.5}[Nb_{2.5}W_{2.5}O_{14}]$ treated with acid is represented by $Cs_{0.5}[Nb_{2.5}W_{2.5}O_{14}]$ (AT). It was confirmed by XRD that the structure of the $Cs_{0.5}[Nb_{2.5}W_{2.5}O_{14}]$ was not changed by the treatment with $HClO_4$.

3-2-3 Catalyst characterization

3-2-3-1 NH_3-TPD

The acid amount of catalysts was measured by NH_3-TPD with a TPD apparatus (BEL Japan Inc.). Prior to the measurement, the samples were pretreated under He flow at 673 K for 2 h. 100 torr of ammonia was equilibrated with the pretreated sample at 473 K and evacuated for 5 min. The TPD data were collected at temperature ramp rate of 10 K min^{-1} under differentially-pumped He (50 ml min^{-1} (STP)) flow at *ca*.180 torr. A mass spectrometer (ANELVA M-100OA-F) was used to measure the desorbed NH_3 at m/e = 16. The acid amount of catalyst was calculated on the basis of the acid amount of H-ZSM-5(JRC-Z5-90H) (345 μmol g^{-1}).

3-2-3-2 FT-IR spectroscopy of adsorbed pyridine

Acidity of catalysts was measured by FT-IR spectroscopy (PARAGON 1000, Perkin Elmer) of adsorbed pyridine with an evacuable furnace cell with CaF_2 windows, containing a self-supporting disk (with 12 mm diameter) of sample (50 mg) as shown in Fig. 3.1. Prior to the measurement, the samples were pretreated under vacuum at 623 K for 1 h. 4.4 torr of pyridine was adsorbed at 373 K and after evacuation at 423 K for 1 h, and then the adsorption spectrum was recorded.

3-2-3-3 Determination of coke amount

Temperature-programmed oxidation (TPO) measurement of the spent catalyst was conducted on a thermal analyzer (Thermo plus TG8120, Rigaku). The sample was placed in α-Al_2O_3 crucible and heated in flowing air (50 ml・min^{-1}) from room temperature to 1073 K at a rate of 10 K・min^{-1}.

3-2-4 Catalytic testing

3-2-4-1 Transformation of glycerol

Transformation of glycerol was carried out in a vertical fixed-bed reactor (Fig. 3.2). A mixture of 0.02~0.80 g of catalyst powder and sea sand (catalyst + sea sand = 2 ml) was set in a Pyrex glass tube with 12 mm internal diameter and pretreated at 573 K for 0.5 h in flowing 20% O_2/N_2 before the reaction. A glycerol-water 1:5 (mol/mol) solution was fed into the top of reactor with a micro feeder. Pure N_2 or O_2/N_2 was introduced with glycerol vapor with mass flow controllers (KOFLOC). The molar composition of reaction gas was glycerol: N_2: H_2O = 5: 70: 25 (absence O_2) or glycerol: O_2: N_2: H_2O = 5: 14: 56: 25 (presence O_2). Reaction products and unconverted glycerol in both gas and liquid phase were collected hourly in an ice trap (273 K) and a Tedlar bag connected at the end of the trap. Products in the liquid phase were analyzed with FID-GC (GL science GC353, 30 m 0.32 mm TC-WAX capillary column). Products in the gas phase were analyzed with FID-GC (Shimadzu GC14B, Gaskuropak54 column) and TCD-GC (Shimadzu GC8A, Porapak QS and MS-13X column). Glycerol conversion and product selectivities and yields were calculated by Eqs. (3.1) - (3.3).

$$\text{Glycerol conversion } (\%) = \frac{\text{Moles of glycerol reacted}}{\text{Moles of glycerol fed}} \times 100 \qquad (3.1)$$

$$\text{Product selectivity } (\%) = \frac{\text{Moles of carbon in a product defined}}{\text{Moles of carbon in glycerol reacted}} \times 100 \qquad (3.2)$$

$$\text{Product yield } (\%) = \frac{\text{Moles of carbon in a product defined}}{\text{Moles of carbon in glycerol fed}} \times 100 \qquad (3.3)$$

3-3 Results and discussion

3-3-1 Effect of crystal structure on selectivity in glycerol transformation

3-3-1-1 Acid properties

The number of acid sites per gram of the catalysts was determined by NH_3 adsorption and TPD. The results are summarized in Table 3.2. The acid amount of W-Nb-O (673 K) was measured to be 0.190 mmol·g^{-1} and decreased with an increase in calcination temperature as in the case of the surface area. The acid amount of the WO_3/Nb_2O_5, WO_3/ZrO_2 and H-ZSM-5 were found to be 0.008, 0.016 and 0.345 mmol·g^{-1} respectively. Although, there is an observable difference in the acid amount with respect to catalyst weight as illustrated in Table 1, when compared on the basis of catalyst surface area the difference is not large.

3-3-1-2 Catalytic glycerol dehydration

The catalytic results of glycerol transformation are listed in Table 3.3. Acrolein was obtained as main product with all catalysts and accompanied with some byproducts. These include CO_x, acrylic acid (AA) and acetic acid (ACA) which is produced by the oxidation of acrolein were observed, in addition to acetaldehyde (ACAL), propionaldehyde (PRAL) and hydroxyacetone (HACT). 2-oxo-propanal, ethers and traces of unidentified compounds are included in amongst others. Hydroxyacetone, 2-oxo-propanal, and ethers are also dehydration products of glycerol molecules. It was considered that these dehydration products are intermediates of consecutive reactions because the yields of dehydration products increased with a decrease in contact time as described in Chapter 4 in detail.

The W-Nb-O catalysts calcined at 673 K and 973 K gave an acrolein yield of 70%, however, more precisely, the yield of acrolein over W-Nb-O (673 K) was modestly increased over W-Nb-O (973 K). Conversely, the yield of the dehydration products such as hydroxyacetone was found to be slightly lower than that over W-Nb-O (973 K). This result suggests that the subsequent reaction of the primary dehydration products proceeds within the W-Nb-O (673 K) structure due to their longer residence time on

the surface with an increased acid amount and high surface area. Comparison of the two catalysts, W-Nb-O (673 K) and W-Nb-O (973 K), indicates that the XRD pattern for both materials is based on the layer structure and in addition that the product distribution was not substantially different supports a structural effect. In addition, the WO_3/Nb_2O_5 catalyst which is comprised of both Nb_2O_5 and WO_3 which are not layered showed very low acrolein yield compared to W-Nb-O (673 K and 973 K) although the glycerol conversion was relatively high. Considering the observations for the W-Nb-O system, the surface structure sites of the catalysts appear to dominate and control the product distribution of glycerol transformation.

In order to further clarify the observations of the crystalline structure and the effect on product selectivity obtained, the reaction was conducted over catalysts with different structures at iso-conversion of glycerol (Table 3.4). All three catalysts have a layered arrangement of octahedral units into the *c*-direction but different *a*-*b* plane structure; W-Nb-O (973 K) with the disordered arrangement, W-Nb-O (1273 K) with the ordered arrangement based on the $Nb_8W_9O_{47}$ phase (Fig. 2.1) and the $Cs_{0.5}[Nb_{2.5}W_{2.5}O_{14}]$ (AT) with an ordered arrangement based on orthorhombic structure shown in Fig. 2.2. W-Nb-O (973 K) and $Cs_{0.5}[Nb_{2.5}W_{2.5}O_{14}]$ (AT) showed comparable product selectivity, however, the catalytic activity per g_{cat} is significantly different. Conversely, W-Nb-O (1273 K) showed an appreciable trend to give a higher yield of dehydration products such as hydroxyacetone and a lower yield of acrolein compared to W-Nb-O (973 K) and $Cs_{0.5}[Nb_{2.5}W_{2.5}O_{14}]$ (AT). This result suggests that the structure on the *a*-*b* plane affects the product selectivity.

3-3-1-3 Catalytic deactivation

W-Nb-O (673 K) and W-Nb-O (973 K) were superior to WO_3/ZrO_2 (62.1%) and H-ZSM-5 (46.4%) not only in term of acrolein yield (Table 3.3) but also in term of catalyst deactivation. The decreasing rate of acrolein yield in W-Nb-O was appreciably slower than that in WO_3/ZrO_2 or H-ZSM-5 as can be seen in Fig. 3.3. After 5 h on stream from starting the reaction, the acrolein yield of WO_3/ZrO_2 and H-ZSM-5 decreased to less than half. On the other hand, W-Nb-O (673 K) could still achieve an acrolein yield of

about 60%. Because the acid amount of W-Nb-O (973 K) was lower than that of H-ZSM-5, the long lifetime of the W-Nb-O is not due to its large amounts of active sites. These results suggest that the acid sites formed on the W-Nb-O surface structure have not only excellent activity for the dehydration of glycerol to acrolein but also superior property against deactivation.

CO and CO_2 yield and O_2 conversion over W-Nb-O (673 K) was higher than that over W-Nb-O (973 K), suggesting that the oxidative capability of the catalyst suppresses their deactivation. The detail about function of O_2 will be described in 2-3-4-1.

3-3-2 Effect of the W/Nb ratio on activity for glycerol transformation

3-3-2-1 Surface properties of catalysts

Table 3.5 and Fig. 3.4 illustrate the surface areas and acid amounts of the W-Nb-O catalysts having various W/Nb ratios. As already shown in Chapter 2, the surface area of Nb-O without W was 89 m^2g^{-1}, and increased with increasing W/Nb ratio. The maximum surface area of W-Nb-O was 118 m^2g^{-1} with W/Nb=1.35. Further increase of W/Nb ratio decreased the surface area. The surface area of W-Nb-O (W/Nb=12) was 43 m^2 g^{-1}. On the other hand, the acid amount of the W-Nb-O catalysts was 40 μmol･g^{-1} at W/Nb=0, and significantly increased with increasing the W/Nb ratio. W/Nb ratio of 4 or above, the acid amount was about 200 μmol･g^{-1}.

3-3-2-2 Activity for glycerol transformation

Table 3.6 and Fig. 3.5 show the effect of W/Nb ratio on the activity for the glycerol transformation. As illustrated in Fig. 3.5, the conversion of glycerol and the yield of acrolein increased with increasing the W/Nb ratio and stayed constant at the W/Nb ratio of 4 or above. This is corresponding to the change of acid amount (Fig. 3.6). These results indicate that the activity for the dehydration of glycerol depend on only the acid amount, there is no difference in the function of one acid site in the W-Nb-O catalyst.

In Table 3.6, however, while the glycerol conversion over Nb-O without W (41.4%) and W-Nb-O

(W/Nb=0.5) (42.1%) were similar, the acrolein yield over Nb-O and W-Nb-O were 3.7% and 15.9%, respectively. It was clear that the introduction of W increase the acrolein selectivity.

In Fig. 3.7, the acrolein yield over Nb-O and W-Nb-O (W/Nb=1.35 and 12) are plotted against the glycerol conversion. While there is no difference in the aceolein selectivity between W/Nb=1.35 and W/Nb=12, the acrolein selectivity over Nb-O was lower than that over W-Nb-O under the high conversion of glycerol. It is considered that the introduction of W changes their acid property.

The Effect of the introduction of W was investigated with FT-IR of adsorbed pyridine on Nb-O and W-Nb-O. Fig. 3.8 illustrates the IR spectra of pyridine on Nb-O and W-Nb-O (W/Nb=1.35). Both catalysts gave the IR-bands ascribed to the adsorption of pyridine on Lewis and Brönsted acid sites at 1450 and 1540 cm^{-1}, respectively. The ratio of the area of the peak at 1540 to 1450 cm^{-1} in W-Nb-O was larger than that in Nb-O. It was indicated that the introduction of W increases the Brönsted acidity and enhances acrolein selectivity in the glycerol transformation.

3-3-3 Transformation of glycerol over W-V-O and W-Ta-O

3-3-3-1 Acid properties

Fig. 3.9 and Table 3.7 illustrate the TPD profiles of NH_3 adsorbed on W-V-O, W-Nb-O and W-Ta-O at 373 K and 473 K and the acid amount determined the TPD profiles. The acid amount of W-Ta-O was larger than that of W-Nb-O. On the other hand, the acid amount of W-V-O was quite smaller than that of W-Nb-O or W-Ta-O. And the intensity of m/e=16 increased from about 873 K due to reduction of the W-V-O.

3-3-3-2 Glycerol transformation

Catalytic performance of W-based complex metal oxides in the glycerol transformation is listed in Table 3.8. The catalyst performance of W-Ta-O was comparable to that of the W-Nb-O and it showed similar selectivity. On the other hand, in W-V-O oxidation proceeded mainly and the formation of acrolein

was not observed. Because W-V-O has smaller acid amount and contains V which is efficient element for oxidation, the oxidation proceeded in prior to acid reaction.

Fig. 3.10 illustrates the time courses of acrolein yield in the glycerol transformation over W-Nb-O and W-Ta-O caicined at 973 K. The deactivation rate of W-Ta-O was higher than that of W-Nb-O.

Fig. 3.11 illustrates the TG curves of W-Nb-O and W-Ta-O calcined at 973 K after 10 h of the reaction. The coke amount on W-Ta-O (126.7 mg$\cdot g_{cat}$) was lower than that on W-Nb-O (172.3 mg$\cdot g_{cat}$) (Table 3.9), indicating that W-Ta-O is easier not to form the coke but to be affected by the coke. Although W-Ta-O has similar acid sites to W-Nb-O, the density of acid sites per surface area on W-Ta-O is higher than that on W-Nb-O. Therefore, W-Ta-O seems to be seriously affected by the coke.

3-4 Conclusion

The complex metal oxides of W and Nb were synthesized with a layered structure via a hydrothermal method. The W-Nb-O catalysts gave acrolein yield higher than 70% in the glycerol transformation. This catalytic performance was higher than that of the WO_3/ZrO_2 or the H-ZSM-5. In addition, it was observed that the deactivation rate in the W-Nb-O catalyst was less than that in WO_3/ZrO_2 or H-ZSM-5. These results indicate that W-Nb-O is an efficient and potential catalyst of acrolein production from glycerol in high yield. W-Nb-O (1273 K) in $Nb_8W_9O_{47}$ phase and $Cs_{0.5}[Nb_{2.5}W_{2.5}O_{14}]$ with orthorhombic structure in the crystal structure showed different selectivity for glycerol transformation. These results suggest that structure of the *a-b* plane affects not only the activity but also the catalyst selectivity. W-Nb-O synthesized by hydrothermal method seems to assume a similar surface structure as formed in $Cs_{0.5}[Nb_{2.5}W_{2.5}O_{14}]$ and to generate active and selective sites for glycerol transformation to acrolein.

3-5 References

[1] B. Katryniok, S. Paul, V. Belli‘ere-Baca, P. Reye, F. Dumeignil, *Greem Chem.* **2010**, 12, 2079.

[2] K. Tanabe, *Mater. Chem. Phys.* **1987**, 17, 217.

[3] H. Ishida, *Petrotech (Tokyo, Jpn.)* **1996**, 19, 1030.

[4] M. Hino, K. Arata, *J. Chem. Soc. Chem. Commun.* **1987**, 1259.

[5] M. Kimura, T. Nakato, T. Okuhara, *Appl. Catal. A* **1997**, 165, 227.

[6] S.-H. Chai, H.-P. Wang, Y. Liang, B.-Q. Xu, *J. Catal.* **2007**, 250, 342.

[7] Y.T. Kim, K.-D. Jung, E.D. Park, *Microporous and Mesoporous Mater.* **2010**, 131, 28.

[8] A. Ulgen, W. Hoelderich, *Catal. Lett.* **2009**, 131, 122.

[9] S.-H. Chai, H.-P. Wang, Y. Liang, B.-Q. Xu, *Greem Chem*. **2008**, 10, 1087.

[10] C. Tagusagawa, A. Takagaki, A. Iguchi, K. Takanabe, J.N. Kondo, K. Ebitani, S. Hayashi, T. Tatsumi, K. Domen, *Angew. Chem., Int. Ed.* **2010**, 49, 1128.

[11] K. Okumura, T. Tomiyama, S. Shirakawa, S. Ishida, T. Sanada, M. Arao, M. Niwa, *J. Mater. Chem.* **2011**, 21, 229.

[12] G. Larsen, E. Lotero, S. Raghavan, R. D. Parra, C. A. Querini, *Appl. Catal. A* **1996**, 139, 201.

[13] S. Triwahyono, T. Yamada, H. Hattori, *Appl. Catal. A* **2003**, 250, 65.

[14] H. Hibst, F. Rosowski, G. Cox, *Catal. Today* **2006**, 117, 234.

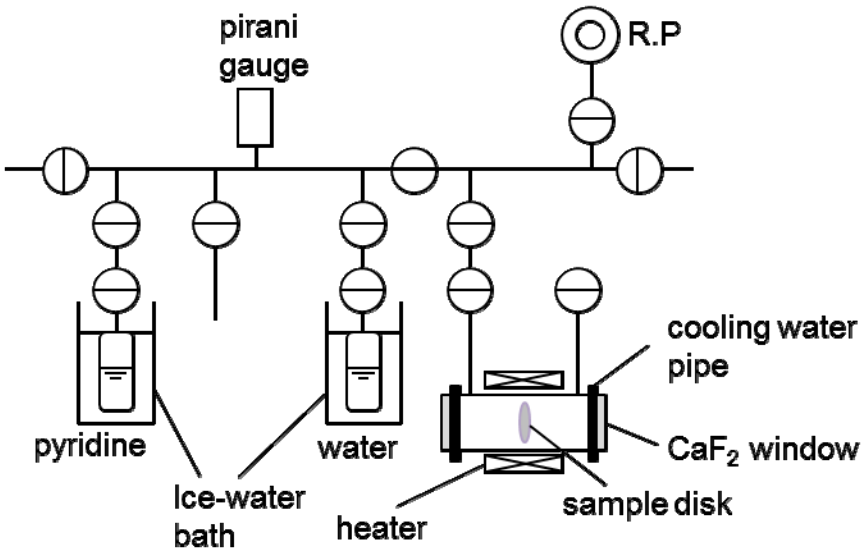


Fig. 3.1 Apparatus for pyridine adsorption.

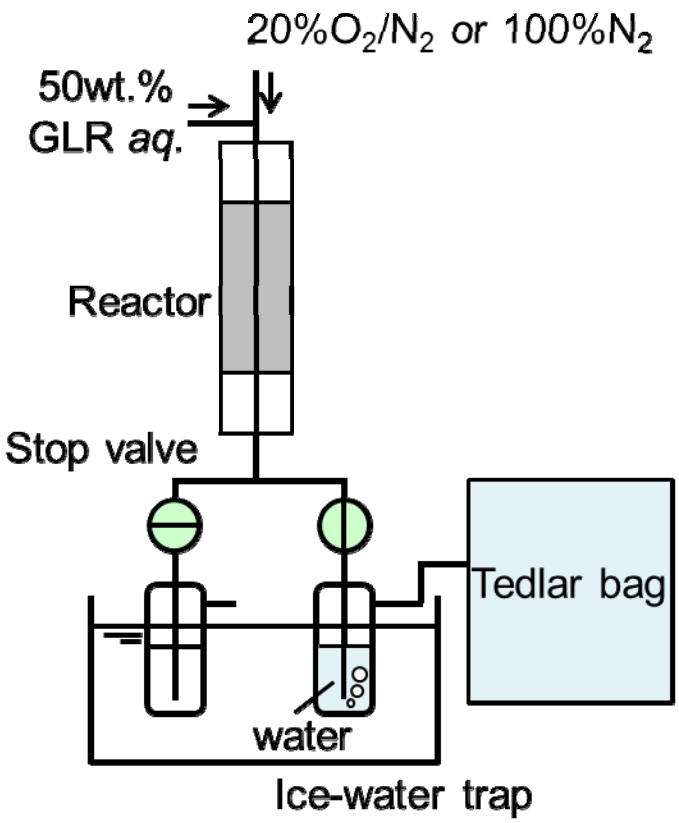


Fig. 3.2 Fixed bed reactor.

Table 3.2 Surface area and acid amount of complex metal oxides tested for glycerol dehydration

Catalyst	Surface area / $m^2 \cdot g^{-1}$	Acid amount / $mmol \cdot g^{-1}$
W-Nb-O (673 K) [a]	100	0.190
W-Nb-O (973 K) [a]	43	0.016
W-Nb-O (1273 K) [a]	2	0.003
WO_3/Nb_2O_5 [a]	9	0.008
Cs-W-Nb-O	3	0.003
Cs-W-Nb-O(AT)	3	0.003
WO_3/ZrO_2 [b]	51	0.016
H-ZSM-5 [c]	347	0.345

[a] W/Nb = 1.35. [b] 13wt.% WO_3. [c] SiO_2/Al_2O_3 = 90.

Table 3.3 Catalytic performance of W-Nb complex metal oxides in the glycerol transformation

Catalyst	Catal. wt. / g	GLR[d] conv.[e] / %	Yield[f] / %							
			ΛCRL	ΛCΛL	PRΛL	HΛCT	ΛCΛ	ΛΛ	CO_x	others
W-Nb-O (673)[a]	0.2	98.9	74.4	2.9	1.0	0.4	0.7	0.1	3.8	15.4
W-Nb-O (973)[a]	0.2	97.9	70.1	1.3	0.8	3.0	0.3	0.5	2.0	19.1
$Nb_8W_9O_{47}$	0.8	64.5	15.4	0.2	<0.1	3.6	0.6	<0.1	0.2	44.0
Cs-W-Nb-O (ΛT)	0.8	59.1	18.0	0.2	0.1	2.3	<0.1	<0.1	0.4	17.5
WO_3/Nb_2O_5[a]	0.8	86.9	37.9	0.8	0.2	3.3	0.2	0.3	0.6	43.5
WO_3/ZrO_2[b]	0.2	89.3	62.1	0.9	0.6	5.0	0.1	0.6	0.7	14.4
H-ZSM-5[c]	0.2	87.3	46.4	1.9	1.4	1.8	0.3	0.3	1.6	33.6

[a] W/Nb = 1.35. [b] 13wt.% WO_3. [c] SiO_2/Al_2O_3 = 90. [d] GLR = glycerol. [e] Reaction conditions: flow rate, 80 ml·min^{-1}; composition of reaction gas, GLR : O_2 : N_2 : H_2O = 4 : 11.2 : 44.8 : 20 (ml·min^{-1}); reaction temperature, 558 K; time on streams, 1 h. [f] ΛCRL = acrolein, ΛCΛL = acetaldehyde, PRΛL = propanal, HΛCT = hydroxyacetone, ΛCΛ = acetic acid, ΛΛ = acrylic acid.

Table 3.4 Conversion of glycerol and products selectivity over W-Nb complex metal oxides

Catalyst	Catal. wt.	GLR conv.[a]	Selectivity / %							
	/ g	/ %	ΛCRL	ΛCΛL	PRΛL	HΛCT	ΛCΛ	ΛΛ	COx	others
W-Nb-O (973 K)[b]	0.05	59.5	29.7	0.3	0.2	2.9	<0.1	<0.1	0.7	66.1
W-Nb-O (1273 K)	0.8	64.5	23.9	0.3	0.1	5.6	0.9	<0.1	0.5	68.2
Cs-W-Nb-O(ΛT)	0.8	59.1	30.5	0.3	0.2	3.9	<0.1	<0.1	0.7	64.5

[a] Reaction conditions: flow rate, 80 ml·min^{-1}; composition of reaction gas, GLR : O_2 : N_2 : H_2O = 4 : 11.2 : 44.8 : 20 (ml·min^{-1}); reaction temperature, 558 K; reaction time, 0~1 h, [b]1~2 h.

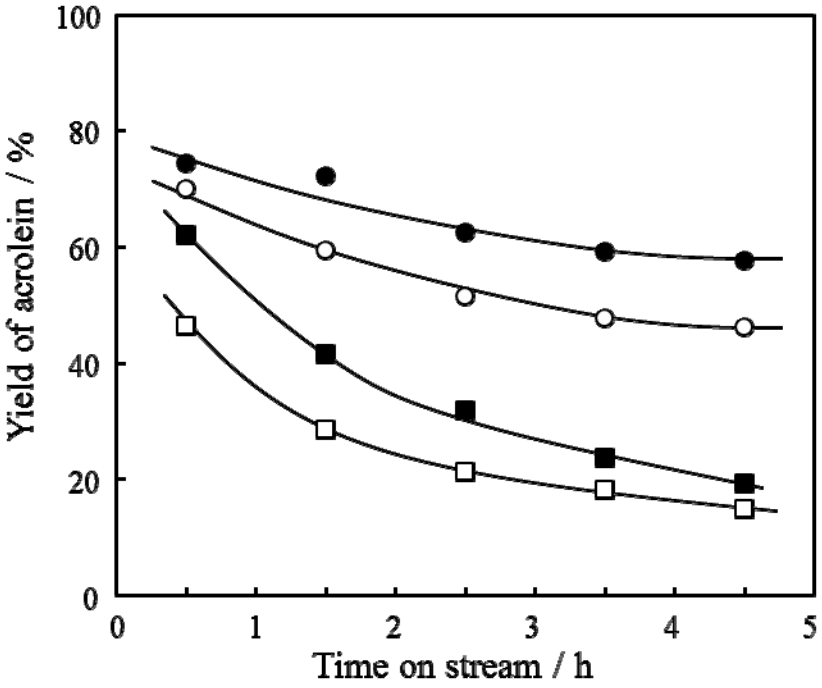


Fig. 3.3 Time courses of glycerol dehydration to acrolein. Symbols: W-Nb-O (673 K), ●; W-Nb-O (973 K), ○; WO_3/ZrO_2, ■; H-ZSM-5, □. Reaction conditions: catalyst weight, 0.2 g; flow rate, 80 ml min^{-1}; reaction temperature, 558 K.

Table 3.5 Surface area and acid amount of W-Nb-O.

W/Nb	SA_{BET} / $m^2 \cdot g^{-1}$	Acid amount[a] / $\mu mol \cdot g^{-1}$
0	89	40
0.5	97	138
1	111	152
1.35	118	136
2	111	171
4	84	194
6	72	193
12	43	210

[a]Determined by NH_3-TPD: NH_3 was adsorbed at 473 K.

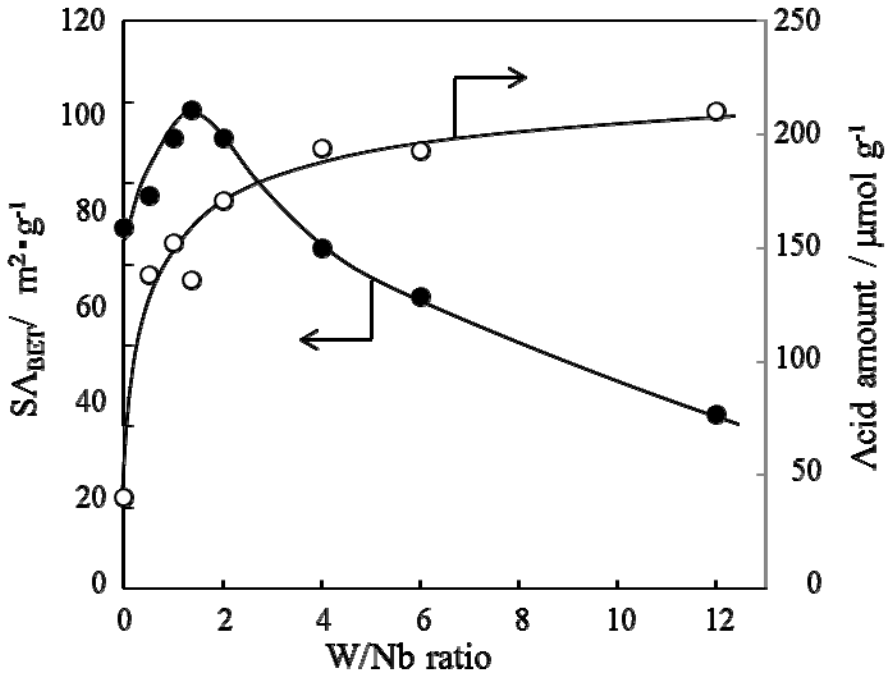


Fig. 3.4 Effect of W/Nb ratio on the surface area (●) and acid amount (○).

Table 3.6 Effect of W/Nb ratio on the performance in glycerol transformation.

W/Nb	GLR conv.[a] / %	O_2 conv. / %	Yield[b] / %									
			ΛCRL	ΛCΛL	PRΛL	HΛCT	ΛCΛ	ΛΛ	PΛ	CO	CO_2	others
0	41.4	<0.1	3.7	0.1	0.1	<0.1	<0.1	<0.1	<0.1	0.1	0.3	37.1
0.5	42.1	<0.1	15.9	0.3	0.1	<0.1	1.5	<0.1	<0.1	0.1	0.3	23.8
1	65.0	2.0	24.6	0.4	0.2	2.0	0.1	<0.1	<0.1	0.3	0.5	37.0
1.35	64.3	1.4	32.4	0.5	0.3	2.5	0.1	0.1	<0.1	0.3	0.5	27.7
2	63.6	3.0	30.7	0.8	0.3	1.7	0.2	<0.1	<0.1	0.7	0.8	28.5
4	82.8	0.9	37.8	0.1	0.3	<0.1	3.1	<0.1	<0.1	0.3	0.4	40.1
6	83.1	1.3	39.3	0.1	0.2	<0.1	2.3	<0.1	<0.1	0.4	0.5	40.3
12	77.3	<0.1	36.5	0.6	0.2	<0.1	2.6	<0.1	0.1	0.5	0.3	36.5

[a] Reaction conditions: catalyst weight, 0.05 g; flow rate, 80 ml·min^{-1}; time on stream, 0~1 h, composition of reaction gas, GLR : O_2 : N_2 : H_2O = 4 : 11.2 : 44.8 : 20 (ml·min^{-1}); reaction temperature, 558 K. [b] ΛCRL = acrolein, ΛCΛL = acetaldehyde, PRΛL = propanal, HΛCT = hydroxyacetone, ΛCΛ = acetic acid, ΛΛ = acrylic acid, PΛ = propionic acid.

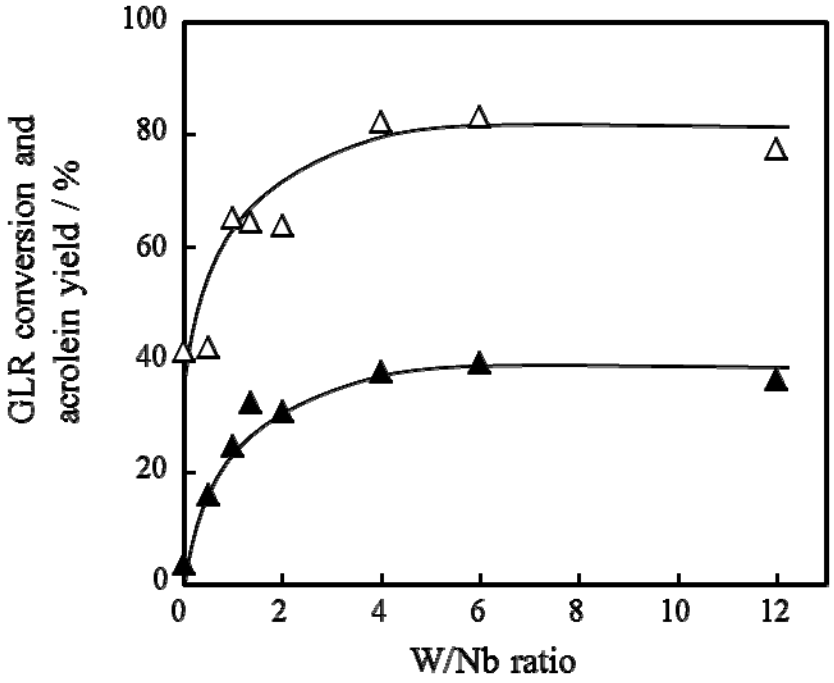


Fig. 3.5 Effect of W/Nb ratio on the activity for the glycerol transformation.
Symbols: glycerol conversion, △; acrolein yield, ▲.

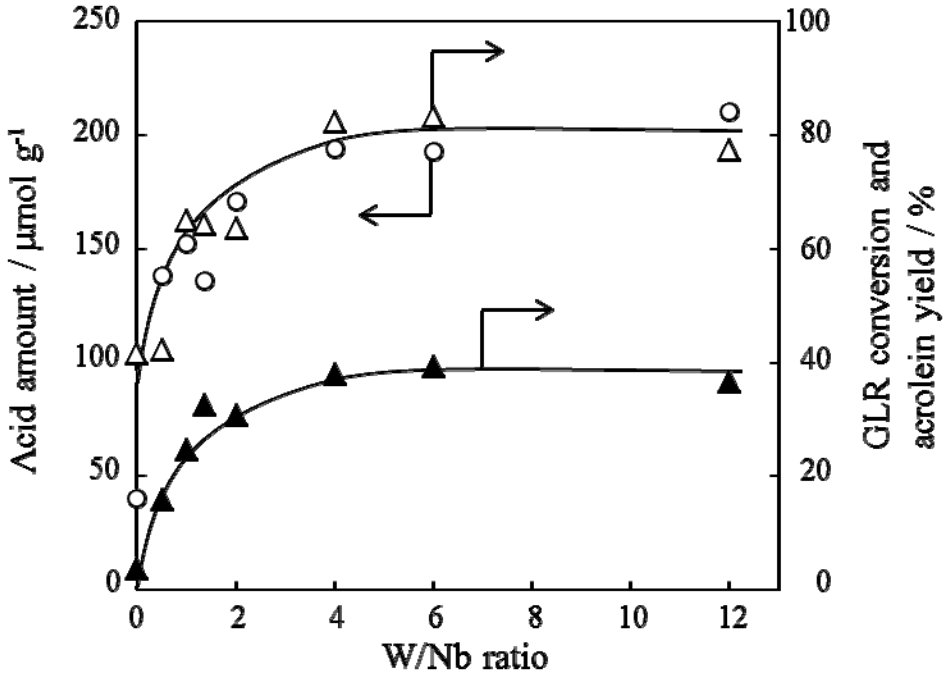


Fig. 3.6 Relation between acid amount and activity for glycerol transformation.
Symbols: acid amount; ○, glycerol conversion, △; acrolein yield, ▲.

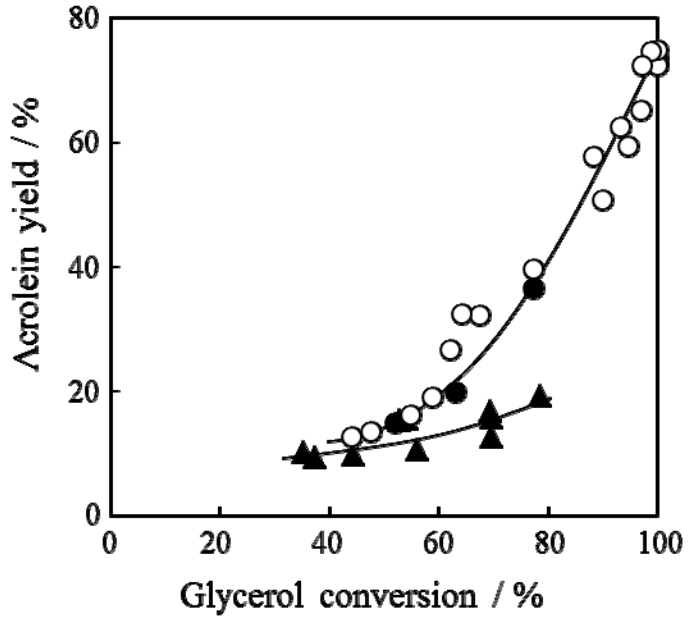


Fig. 3.7 Acrolein yield against glycerol conversion for Nb-O, ▲; W-Nb-O (W/Nb=1.35), ○; and W-Nb-O (W/Nb=12), ●.
Reaction conditions: composition of reactant gas, GLR/ O_2 / N_2/ H_2O = 5/ 14/ 56/ 25 (mol%).

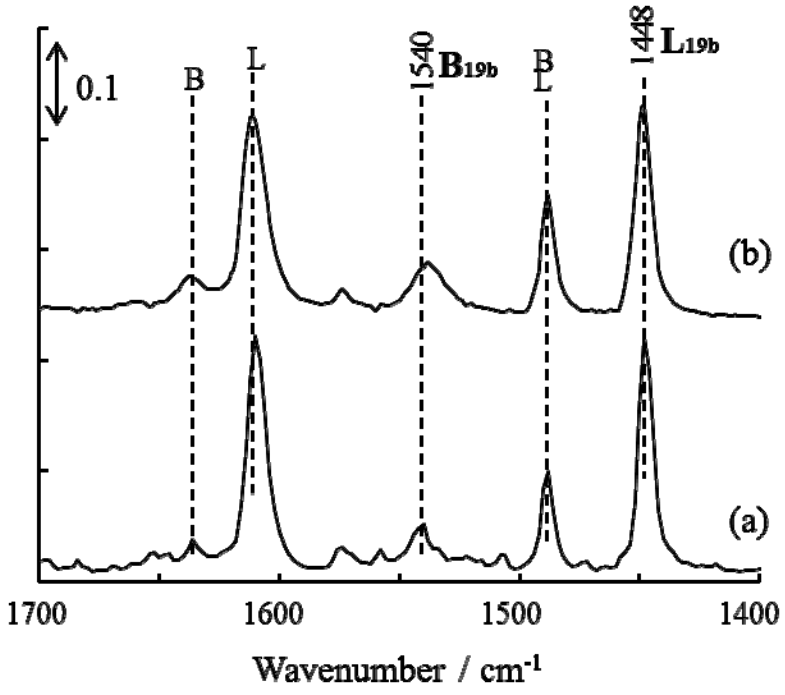


Fig. 3.8 IR spectra of adsorbed pyridine on Nb-O, (a); and W-Nb-O (W/Nb=1.35) ,(b).

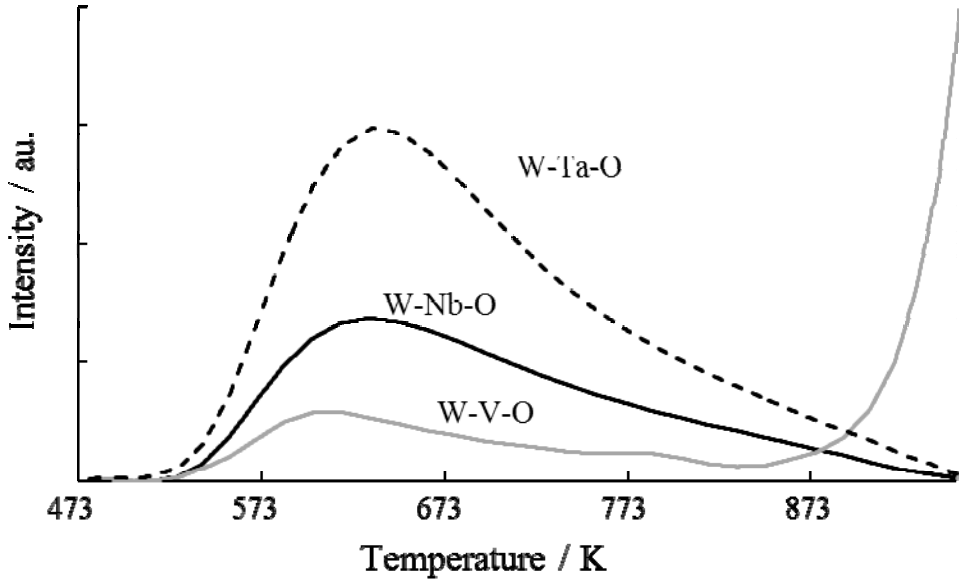


Fig. 3.9 TPD profiles of NH_3.

Table 3.7 Acid amount of W-based complex metal oxides

Catalyst	Acid amount / μmol·g^{-1}	Surface area / m^2·g^{-1}	Acid density / μmol·m^{-2}
W-V-O (673 K)	5	8	0.62
W-Nb-O (973 K)	16	43	0.37
W-Ta-O (973 K)	32	40	0.80

Table 3.8 Catalytic performance of W-based complex metal oxides in the glycerol transformation

Catalyst[a]	Cal. temp / K	GLR conv.[c] / %	Yield[d] / %								
			ΛCRL	ΛCΛL	PRΛL	HΛCT	ΛCΛ	ΛΛ	CO	CO_2	others
W-Nb-O	973	100	70.6	4.8	0.8	<0.1	1.3	0.5	4.5	2.4	15.1
W-Ta-O	973	100	71.7	5.5	1.0	<0.1	1.0	0.3	4.1	2.0	14.4
W-V-O	673	98.2	0.1	<0.1	<0.1	<0.1	11.0	1.6	63.0	22.5	<0.1

[a] Composition determined by EDS, W /Nb = 1.5, W/Ta = 1.4, W/V = 1.4; calcination temperature, 973 K.[b] Calcination temperature, 673 K. [c] Reaction conditions: catalyst weight, 0.8g; flow rate, 80 ml·min^{-1}; composition of reaction gas, GLR : O_2 : N_2 : H_2O = 4 : 11.2 : 44.8 : 20 (ml·min^{-1}); reaction temperature, 558 K. [d] ΛCRL = acrolein, ΛCΛL = acetaldehyde, PRΛL = propanal, HΛCT = hydroxyacetone, ΛCΛ = acetic acid, ΛΛ = acrylic acid.

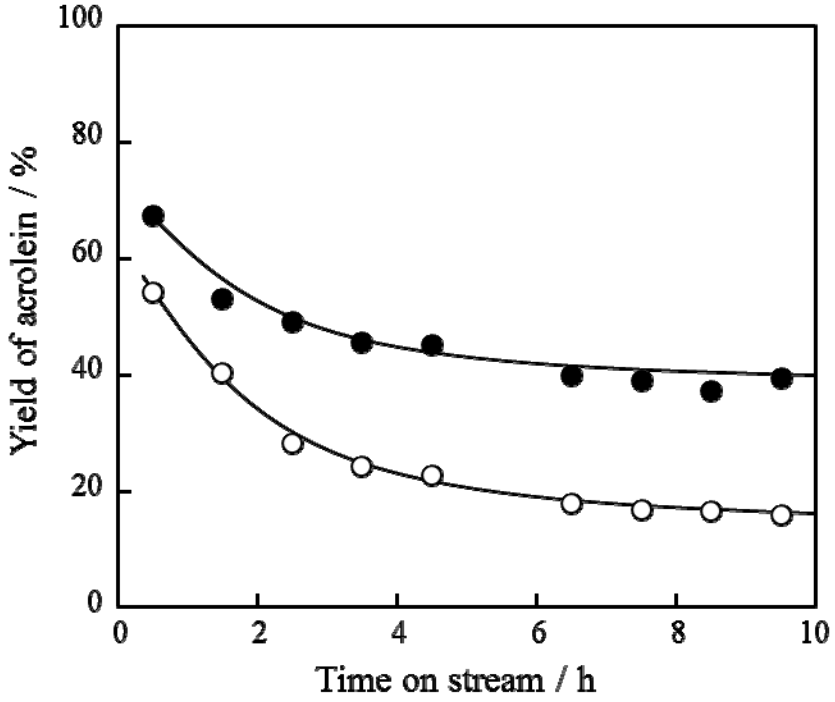


Fig. 3.10 Time courses of acrolein yield in the glycerol transformation over W-Nb-O (●) and W-Ta-O (○) caicined at 973 K.
Reaction conditions: catalyst weight, 0.2 g; flow rate, 80 ml·min^{-1}; composition of reaction gas, GLR/ O_2 / N_2/ H_2O = 5/ 14/ 56/ 25 (mol%).

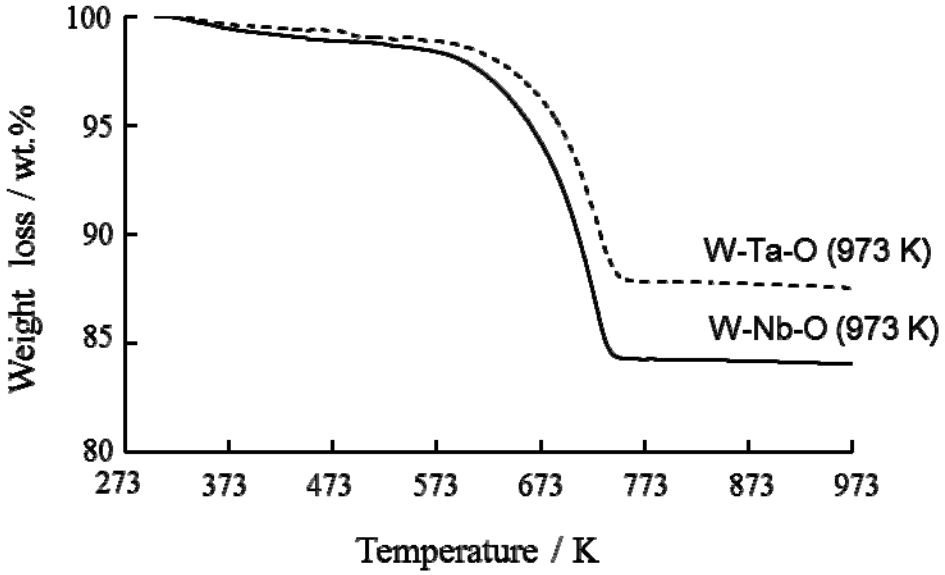


Fig. 3.11 TG curves of W-Nb-O and W-Ta-O calcined at 973 K after 10 h of the reaction.

Table 3.9 Amount of coke formed in the reaction

Catalyst	Amount of coke[a]/ $mg \cdot g_{cat}$
W-Nb-O (973 K)	172.3
W-Ta-O (973 K)	126.7

[a]Reaction time 10h.

Chapter 4

Glycerol Transformation over the W-Nb Complex Metal Oxide Catalyst

4-1 Introduction

As already described in chapter 1, glycerol which has high reactivity is able to be starting material for various reaction. On the other hand, it is hard to obtain desirable materials selectively due to the high reactivity. Therefore, the formation of by-products such as hydroxyacetone, propionaldehyde, cokes and others is one of the most serious problems.

In Chapter 3, it was indicated that the W-Nb-O catalyst gave acrolein in yield of more than 70 % in the glycerol transformation with some byproducts. These byproducts include CO_x, acrylic acid and acetic acid which is produced by the oxidation of acrolein were observed, in addition to acetaldehyde, propionaldehyde and hydroxyacetone. 2-oxo-propanal, ethers and traces of unidentified compounds are included in amongst others. Hydroxyacetone, 2-oxo-propanal, and ethers are also dehydration products of glycerol molecules.

In this chapter, reaction pathway of glycerol transformation over the W-Nb-O catalyst was discussed based on effect of contact time on product distribution and reaction starting from intermediates.

Besides, it has been reported that co-feeding gas changes selectivity or life time of catalyst in glycerol transformation. Wang *et al*.[1] studied the influence of the oxygen concentration on the catalytic performance of vanadium phosphate catalysts. They observed that too little (as well as too much) oxygen has a negative impact on the selectivity for acrolein. In fact, low quantities of oxygen led to larger amounts of acetol, whereas high concentrations induced an increase in the selectivity for acetaldehyde, acetic acid, acrylic acid and carbon oxides, which is explained by the successive over-oxidation of the products. On the other hand, Gu *et al*. [2] have reported that co-feeding of oxygen suppressed deactivation of catalysts in the glycerol deactivation over supported nickel sulfate. Besides, Alhanash *et al.* [3] has been reported that doping cesium 12-tungstophosphate with platinum group metals (PGM) together with co-feeding hydrogen improve catalyst stability to deactivation, while maintaining high selectivity to acrolein.

Because crude glycerol contains water, glycerol transformation has been carried out in the presence

of water in most cases.[4] Besides, water is used for dilution of glycerol which has high viscosity. Witsuthammakul *et al*.[5] has been reported that acrolein selectivity decreased and acetol selectivity increased with increasing the concentration of aqueous solution of glycerol fed in glycerol transformation over H-ZSM-5. They consider that water content plays marked roles in product selectivity, presumably via interaction with glycerol and the active acid sites.

Therefore I examined effect of co-feeding gas such as oxygen and water on catalytic performance of the W-Nb-O catalyst.

4-2 Experimental

4-2-1 Chemicals

Chemicals used in experiments are listed in Table 4.1.

Table 4.1 List of chemicals

chemical	formula or molar wt.	assay	manufacturer	No.
$Nb_2O_5 \cdot xH_2O$	265.82 (Nb_2O_5)	70.8% (Nb_2O_5)	Soekawa Chemical Co., Ltd.	02275B
$(NH_4)_6(H_2W_{12}O_{40}) \cdot nH_2O$ ($n \fallingdotseq 6$)	3064	90.8% (WO_3)	Nippon Inorganic Colour and Chemical Co., Ltd.	100114
glycerol (for reaction)	92.09	97.0%	Wako Pure Chemical Ind., Ltd.	072-00626
glycerol (for calibration)	92.09	99.0%	Wako Pure Chemical Ind., Ltd.	075-00616
2-butanol	74.12	99.0%	Wako Pure Chemical Ind., Ltd.	020-11215
propylenegrycol	76.09	99.5%	Kanto Chemical Co., Ltd.	32458-00
acrolein	56.06	90%	Tokyo Chemical Ind. Co., Ltd.	A0137
hydroxyacetone	74.08	90.0%	Wako Pure Chemical Ind., Ltd.	089-05492
acetaldehyde	44.05	88.0~92.0%	Wako Pure Chemical Ind., Ltd.	015-09576
propionaldehyde	58.08	-	Tokyo Chemical Ind. Co., Ltd.	P0498
acetone	58.08	99.5%	Wako Pure Chemical Ind., Ltd.	012-00343
acetic acid	60.05	99.7%	Wako Pure Chemical Ind., Ltd.	017-00256
acrylic acid	72.06	99%	Tokyo Chemical Ind. Co., Ltd.	A0141
sea sand (50~80 mesh)	-	99.0%(SiO_2)	Miyazaki Chemical Co., Ltd.	M5080KA05

4-2-2 Catalyst preparation

4-2-2-1 Preparation of W-Nb-O by hydrothermal method

The complex metal oxides catalysts of W and Nb were prepared by hydrothermal synthesis method. The mixed solution of $Nb_2O_5 \cdot nH_2O$ and $(NH_4)_6[H_2W_{12}O_{40}] \cdot nH_2O$ was put in a stainless steel autoclave with a Teflon liner and aged at 448 K for 72 h. The molar ratio between W and Nb was set at W/Nb = 1.35. The formed solid was filtered, washed with ion-exchanged water, dried at 353 K and then calcined at temperature of 673 or 973 K for 4 h in air. The catalysts prepared by this method are represented by W–Nb–O (*X*, *Y*). The value *X* and *Y* in the parenthesis means W/Nb ratio and calcination temperature,

respectively.

4-2-3 Catalyst characterization

4-2-3-1 FT-IR spectroscopy of adsorbed pyridine

Acidity of catalysts was measured by FT-IR spectroscopy (PARAGON 1000, Perkin Elmer) of adsorbed pyridine with an evacuable furnace cell with CaF_2 windows, containing a self-supporting disk (with 12 mm diameter) of sample (50 mg) as shown in Fig. 3.1. Prior to the measurement, the samples were pretreated under vacuum at 623 K for 1 h. 4.4 torr of pyridine was adsorbed at 373 K and after evacuation at 423 K for 1 h, the adsorption spectrum was recorded followed by the measurement of the spectrum of adsorbed pyridine on sample in the presence of water vapor (4.6 torr). The spectra of adsorbed pyridine after evacuation at 523 and 623 K were similarly recorded

4-2-4 Catalytic testing

4-2-4-1 Transformation of glycerol

Transformation of glycerol was carried out in a vertical fixed-bed reactor (Fig. 3.2). A mixture of 0.02~0.80 g of catalyst powder and sea sand (catalyst + sea sand = 2 ml) was set in a Pyrex glass tube with 12 mm internal diameter and pretreated at 573 K for 0.5 h in flowing 20% O_2/N_2 before the reaction. A glycerol-water 1:5 (mol/mol) solution was fed into the top of reactor with a micro feeder. Pure N_2 or O_2/N_2 was introduced with glycerol vapor with mass flow controllers (KOFLOC). The molar composition of reaction gas was glycerol: N_2: H_2O = 5: 70: 25 (absence O_2) or glycerol: O_2: N_2: H_2O = 5: 14: 56: 25 (presence O_2). Reaction products and unconverted glycerol in both gas and liquid phase were collected hourly in an ice trap (273 K) and a Tedlar bag connected at the end of the trap. Products in the liquid phase were analyzed with FID-GC (GL science GC353, 30 m 0.32 mm TC-WAX capillary column). Products in the gas phase were analyzed with FID-GC (Shimadzu GC14B, Gaskuropak54 column) and

TCD-GC (Shimadzu GC8A, Porapak QS and MS-13X column). Glycerol conversion and product selectivities and yields were calculated by Eqs. (4.1) - (4.3).

$$\text{Glycerol conversion } (\%) = \frac{\text{Moles of glycerol reacted}}{\text{Moles of glycerol fed}} \times 100 \qquad (4.1)$$

$$\text{Product selectivity } (\%) = \frac{\text{Moles of carbon in a product defined}}{\text{Moles of carbon in glycerol reacted}} \times 100 \qquad (4.2)$$

$$\text{Product yield } (\%) = \frac{\text{Moles of carbon in a product defined}}{\text{Moles of carbon in glycerol fed}} \times 100 \qquad (4.3)$$

4-2-4-2 Cumene cracking

A micro catalytic pulse reactor (Fig. 4.1) was used for the reaction. A mixture of 0.2 g of catalyst powder and sea sand (catalyst + sea sand = 2 ml) was set in a Pyrex glass tube with 12 mm external diameter and pretreated at 573 K for 0.5 h in flowing He before the reaction and cooled down to the reaction temperature. The reaction was carried out at 423~648 K. Pure He or the mixed gas of He and water was used as carrier gas. A dose of cumene, 0.5 μl (0.036 mmol), was passed over the catalyst in a carrier flowing at 50 ml min^{-1}, and the products were trapped at 77 K before being flash evaporated into a gas chromatographic column (PEG-20M, 4 m, 443 K). The intervals between doses were kept constant, 20 min. Reaction products and unconverted cumene were analyzed with FID-GC (SHIMAZU GC-14B). Cumene conversion was calculated by Eqs. (4.4) .

$$\text{Cumene conversion } (\%) = \frac{\text{Moles of formed benzene}}{\text{Moles of unconverte d cumene + Moles of formed benzene}} \times 100 \qquad (4.4)$$

4-3 Results and discussion

4-3-1 Reaction pathway

Fig. 4.2 illustrates the product yields in the glycerol transformation under the various contact times over the W-Nb-O (973 K). The glycerol conversion increased with increasing contact time, and reached 100 % at $W/F = 5.0 \times 10^{-3}$. While the acrolein yield was 25.2% and glycerol conversion was 66.7 % at $W/F = 6.3 \times 10^{-4}$, the acrolein yield was 74.1% and glycerol conversion was 100 %. The yield and selectivity of acrolein increased with increasing the glycerol conversion. Conversely, the yield of hydroxyacetone and others decreased with increasing contact time. This suggested that hydroxyacetone and others sequentially convert to acrolein.

Hydroxyacetone transformation was carried out over W-Nb-O (973 K). As shown in Table 4.2. The conversion of hydroxyacetone was 87.6 % and the yield of 2-oxo-propanal was 66.0 %, indicating that the most of hydroxyacetone formed from glycerol oxidize to 2-oxo-propanal. In fact, 2-oxo-propanal yield increased with decreasing hydroxyacetone yield corresponding to the increase of contact time. The acrolein was hardly formed from hydroxyacetone.

In glycerol transformation (Fig. 4.2), the yield of others was 34.3% at $W/F = 6.3 \times 10^{-4}$. If others does not transform into the acrolein, the maximum yield of acrolein must be below 65.7%. In Fig. 3.5, however, as the maximum yield of acrolein was 74.1% at $W/F = 5.0 \times 10^{-3}$, some of others formed from glycerol seems to convert to acrolein. It is suggested that ethers formed by intermolecular dehydration of glycerol or polymer of unsaturated aldehyde included in others convert to acrolein sequentially.

After glycerol converted completely, in $W/F = 5.0 \times 10^{-3} \sim 1.0 \times 10^{-2}$, although the yield of acrolein was modestly decreased from 74.1% to 70.6%, it was kept above 70%. Besides, in the reaction which acrolein was used as reactant, as shown in Table 4.3 acrolein was hardly converted. It is indicated that acrolein formed from glycerol is stable over the W-Nb-O catalyst.

4-3-2 Effect of reaction atmosphere on catalytic property

4-3-2-1 Effect of water on catalytic activity

4-3-2-1-1 Glycerol transformation

Fig. 4.3 illustrates time courses of acrolein yield (a) and acrolein yield against glycerol conversion (b) in the glycerol transforamtion over W-Nb-O (W/Nb=1.35) under various pressur of water (P_{H2O}/P_{total} = 25). The initial acrolein yield was 57.2 and 60.1% under P_{H2O}/P_{total} = 0 and 2.5, respectively. On the other hand, under P_{H2O}/P_{total} = 25, the initial acrolein yield was 74.5 %. The addition of water to reactant gas increase acrolein yield. After 5 h on stream from starting the reaction, the acrolein yield decreased to less than half under P_{H2O}/P_{total} = 0 and 2.5. On the other hand, under P_{H2O}/P_{total} = 2.5, 80 % of initial acrolein yield remained.

Besides, comparison at iso-conversion of glycerol indicates the addition of water increases the selectivity to acrolein. The product distribution at about 90% of glycerol conversion is listed in Table 4.4. The addition of water increased acrolein yield, on the other hand, decreased others yield. As already described, others seem to be products by intermolecular dehydration. The addition of water decreases concentration of reactant or intermediate and suppressed polymerization. Besides, the yield of hydroxyacetone and propanal were hardly affected by the addition of water. This suggests that the acrolein and hydroxyacetone or propanal were formed on different sites in agreement with the result in 4-3-1.

Under P_{H2O}/P_{total} = 0 and 2.5, the catalytic performance such as activity, selectivity and life time was similar because the amount of water formed in glycerol dehydration (0.315 mmol min^{-1}, at 100% of glycerol convert) was quite large compared to that of additional water (0.079 mmol min^{-1}).

4-3-2-1-2 FT-IR of adsorbed pyridine

Effect of water addition on the acid property of W-Nb-O was investigated by FT-IR of adsorbed pyridine. Fig. 4.4 illustrates the IR spectra of adsorbed pyridine on Nb-O (a) and W-Nb-O (W/Nb=1.35) (b) in presence of water. The water substantially decreased the intensity of the IR-band ascribed to the

adsorption of pyridine on Lewis acid sites and on the other hand increased the intensity of IR-band ascribed to that on Brönsted acid sites. The result indicates that Lewis acid site is hydrated and changes into Brönsted acid site in the presence of water.

Fig. 4.5 illustrates integral intensity (peak area) of the peak at 1540 and 1450 cm^{-1} in Nb-O and W-Nb-O after evacuation at each temperature. The area of peak at 1450 cm^{-1} decreased and that of peak at 1540 cm^{-1} increased with addition of water in both Nb-O and W-Nb-O. However, the ratio of Lewis acid which changed into Brönsted acid was different depending on the presence or absence W. About 29% and 57% of Lewis acid sites changed into Brönsted acid sites in Nb-O and W-Nb-O, respectively. Besides, it is indicated that stronger Lewis acid site is easier to change into Brönsted acid site because Lewis acid site on samples evacuated at 623 K mostly changed into Brönsted acid site.

4-3-2-1-3 Cumene cracking

Effect of water addition on conversion in cumene cracking was investigated. It has been widely reported that cumene cracking proceeds on Brönsted acid sites.[6-8] Fig. 4.6 illustrates the conversion of cumene in the presence or absence of water at the temperature of 423~648 K. The addition of water decreased the cumene conversion from 2.6% to 0.5% at 423 K. As feed of water was stopped, the conversion recovered to 1.0%. The conversion was hardly changed in apparent by the addition of water at 498 K. On the other hand, the addition of water increased the conversion from 16.2% to 27.5% at 573 K. And the conversion decreased to 13.2% by stop of water. At 648 K, the cumene conversion was also increased by the addition of water. It has been widely known that the active sites were poisoned with water. At 423 K, water seems to block the adsorption of reactant by adsorbing on active site strongly. At 573 and 648 K, on the other hand, the enhancement of Brönsted acidity was confirmed by the increase of activity for cumene cracking. Besides, the formation of Brönsted acidity was reversible because the conversion decreased as feed of water was stopped. At 498 K, apparent change of the conversion was not observed, because the decrease of activity due to water poisoning and the increase of activity due to the enhancement of Brönsted acidity balanced each other.

Because the boiling point of glycerol (563 K) was higher than that of cumene (425 K), glycerol was easier to adsorb on the surface of catalysts. Besides, the temperature of catalytic bed in glycerol transformation was about 573 K. Therefore, it was considered that the effect of the increase of Brönsted acidity was dominant compared to that of water poisoning. In fact, the activity or acrolein selectivity did not be decreased by the addition of water as shown in Fig. 3.4. The results of FT-IR of adsorbed pyridine and the cumene cracking indicate that the acrolein yield in the glycerol transformation is improved by water existing in the reaction because the some of the Lewis acid site is hydrated and changes into the Brönsted acid.

In both case of adsorption of pyridine and cumene cracking, the acidity was changed by the addition of about 4.6 torr of water. This is comparable to the amount of water formed in 6% of glycerol conversion. Therefore, it is considered that the acidity is changed by the water formed in reaction without addition of water.

4-3-2-2 Effect of partial pressure of O_2 on catalytic activity

Fig. 4.7 illustrates the time courses of acrolein yield (a) and acrolein yield against glycerol conversion (b) in the presence and absence of O_2 over W-Nb-O (673 K). The initial acrolein yield was 65.1% in the absence of O_2. After 5 h on stream from starting the reaction, the acrolein yield decreased to less than half. On the other hand, initial acrolein yield was 74.5 % and decreased to 57.5% after 5h on stream in the presence of O_2. This result indicates that O_2 supperrssed the deactivation of the catalysts. The difference in initial (0~1 h) acrolein yield between presence and abcense of O_2 because of the deactivation of the catalyst.

Besides, acrolein yield against glycerol conversion was similar in the presence or absence of O_2, indicating that the existence of O_2 does not affect acrolein selectivity. The product distribution was shown in Table 4.5. The yield of others decreased and the yield of CO_x increased by the existence of O_2.

Fig. 4.18 illustrates the TG and DTA curves of W-Nb-O after 5 h of the reaction in the presence (a)

and absence (b) of O_2. The weight loss due to the combustion of deposited carbon with the exothermic peak in DTA was observed in each catalyst. While the single exothermic peak was observed in the temperature range of 673~773 K in the catalyst after the reaction in the presence of O_2, additional exothermic peak was observed at the temperature range of 573~673 K. This result suggests that the materials combusting around 573 K causes deactivation of the catalysts. The oxidative capability of the catalyst promotes the combustion of these materials, and suppresses the deactivation of the catalyst.

The result was agreement Fig. 3.4 which show that the life time of W-Nb-O (673 K) gave higher O_2 conversion and the yield of CO_x was longer than that of W-Nb-O (973 K).

4-4 Conclusion

While the most of hydroxyacetone formed from glycerol oxidize to 2-oxo-propanal, acrolein is stable on the W-Nb-O catalyst. The result of reaction under various contact times suggests that ethers formed by intermolecular dehydration of glycerol or polymer of unsaturated aldehyde included in others convert to acrolein sequentially.

The addition of water increased acrolein yield and suppressed deactivation of catalyst. However, the yield of hydroxyacetone and propanal were hardly affected by the addition of water suggesting that the acrolein and hydroxyacetone or propanal were formed on different sites. Besides, the results of FT-IR of adsorbed pyridine and the cumene cracking indicate that the acrolein yield in the glycerol transformation is improved by water existing in the reaction because the some of the Lewis acid site is hydrated and changes into the Brönsted acid.

The co-feeding of oxygen suppressed deactivation of the catalysts, however, it does not affect acrolein selectivity.

4-5 References

[1] F. Wang, J.-L. Dubois, W. Ueda, *Appl. Catal. A* **2010**, 376, 25.

[2] Y. Gu, S. Liu, C. Li, Q. Cui, *J. Catal.* **2013**, 301, 93.

[3] A. Alhanash, E. F. Kozhevnikova, I. V. Kozhevnikov, *Appl. Catal. A* **2010**, 378, 11.

[4] B. Katryniok, S. Paul, V. Belli`ere-Baca, P. Reye and F. Dumeignil, *Green Chem*. **2010**, 12, 2079.

[5] A. Witsuthammakul, T. Sooknoi, *Appl. Catal. A* **2012**, 413,109.

[6] Y. Oumi, S. Nemoto, S. Nawata, T. Fukushima, T. Teranishi, T. Sano, *Mater. Chem. Phys.* **2002**, 78, 551.

[7] Y. Oumi, R. Mizuno, K. Azuma, S. Nawata, T. Fukushima, T. Uozumi, T. Sano, *Microporous and Mesoporous Mater.* **2001**, 49, 103.

[8] S. Garg, K. Soni, G. M. Kumaran, R. Bal, K. Gora-Marek, J.K. Gupta, L.D. Sharma, G. M. Dhar, *Catal. Today* **2009**, 141,125.

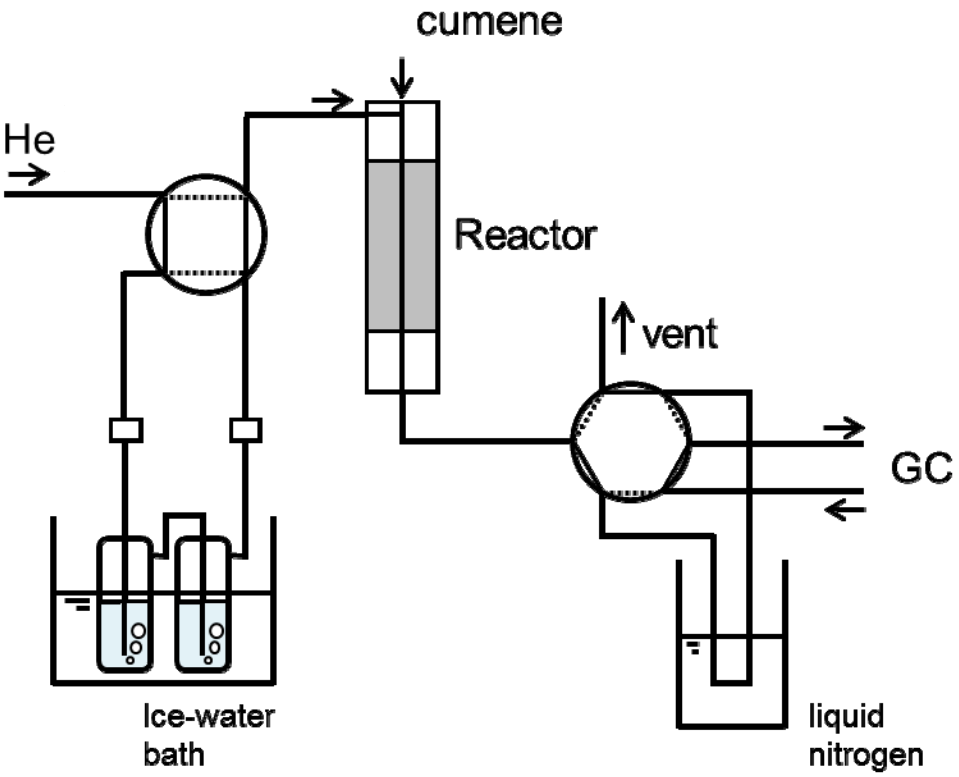


Fig. 4.1 Pulse reactor for cumene cracking.

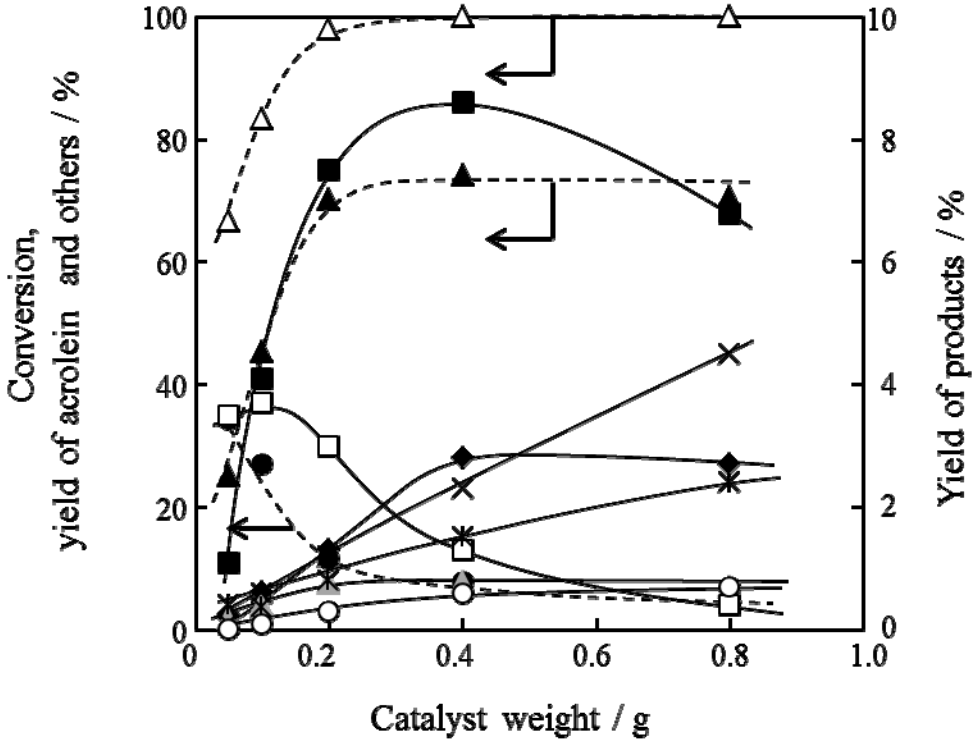


Fig. 4.2 Effect of contact time in the glycerol transformation over the W-Nb-O (973 K) catalyst.
Symbols: conversion of glycerol, △; yield of acrolein, ▲; hydroxyacetone, □; 2-oxo-propanal, ■; acetic acid, ○; propanal, ▲; CO, ×; CO_2, ＊; others, ●.
Reaction conditions: temperature, 558 K; composition of reaction gas, GLR / O_2 / N_2/ H_2O = 5/ 14/ 56/ 25 (mol%).

Table 4.2 Catalytic performance of W-Nb-O (973 K) in the transformation of hydroxyacetone

HACT[a] conv.[b] / %	O_2 conv. / %	Yield[c] / %							
		ACRL	ACAL	PRAL	2-OPAL	ACA	AA	CO_x	others
87.6	16.6	0.2	3.1	0.5	66.0	3.4	<0.1	3.8	10.5

[a] HACT = hydroxyacetone. [b] Reaction conditions: catalyst weight, 0.2 g; flow rate, 80 ml·min^{-1}; composition of reaction gas, HACT : O_2 : N_2 : H_2O = 4 : 11.2 : 44.8 : 20 (ml·min^{-1}); reaction temperature, 558 K. [c] ACRL = acrolein, ACAL = acetaldehyde, PRAL = propanal, ACA = acetic acid, AA = acrylic acid.

Table 4.3 Catalytic performance of W-Nb-O (973 K) in the transformation of acrolein

ACLR[a] conv.[b] / %	O_2 conv. / %	Yield[c] / %							
		ACAL	PRAL	2-OPAL	HACT	ACA	AA	CO_x	others
4.1	0.3	0.3	0.01	<0.1	<0.1	<0.1	<0.1	1.3	2.1

[a] ACRL = acrolein. [b] Reaction conditions: catalyst weight, 0.2 g; flow rate, 80 ml·min^{-1}; composition of reaction gas, ACLR : O_2 : N_2 : H_2O = 4 : 11.2 : 44.8 : 20 (ml·min^{-1}); reaction temperature, 558 K. [c] ACAL = acetaldehyde, PRAL = propanal, 2-OPAL = 2-oxopropanal, HACT = hydroxyacetone, ACA = acetic acid, AA = acrylic acid.

Table 4.4 Effect of water/glycerol (W/G) ratio on the catalytic performance of W-Nb-O (W/Nb=1.35)

P_{O2}/P_{total}	TOS	GLR[a] conv.[b]	Yield[c] / %							
	/ h	/ %	ACRL	ACAL	PRAL	HACT	ACA	AA	CO_x	others
25.0	5	88.5	57.7	1.5	0.5	2.1	0.4	0.1	2.7	23.5
2.5	2	89.5	40.7	1.1	0.5	2.6	<0.1	0.1	2.7	41.8
0	2	90.2	39.1	1.2	0.5	2.5	<0.1	0.1	3.4	43.4

[a] GRL=glycerol. [b] Reaction conditions: temperature, 558 K; catalyst weight, 0.2 g; flow rate, 80 ml·min^{-1}; composition of reaction gas, GLR/ O_2/ N_2/ H_2O = 5/ 14/ 81-x/ x(0~25) (mol%).[c] ACRL = acrolein, ACAL = acetaldehyde, PRAL = propanal, HACT = hydroxyacetone, ACA = acetic acid, AA = acrylic acid.

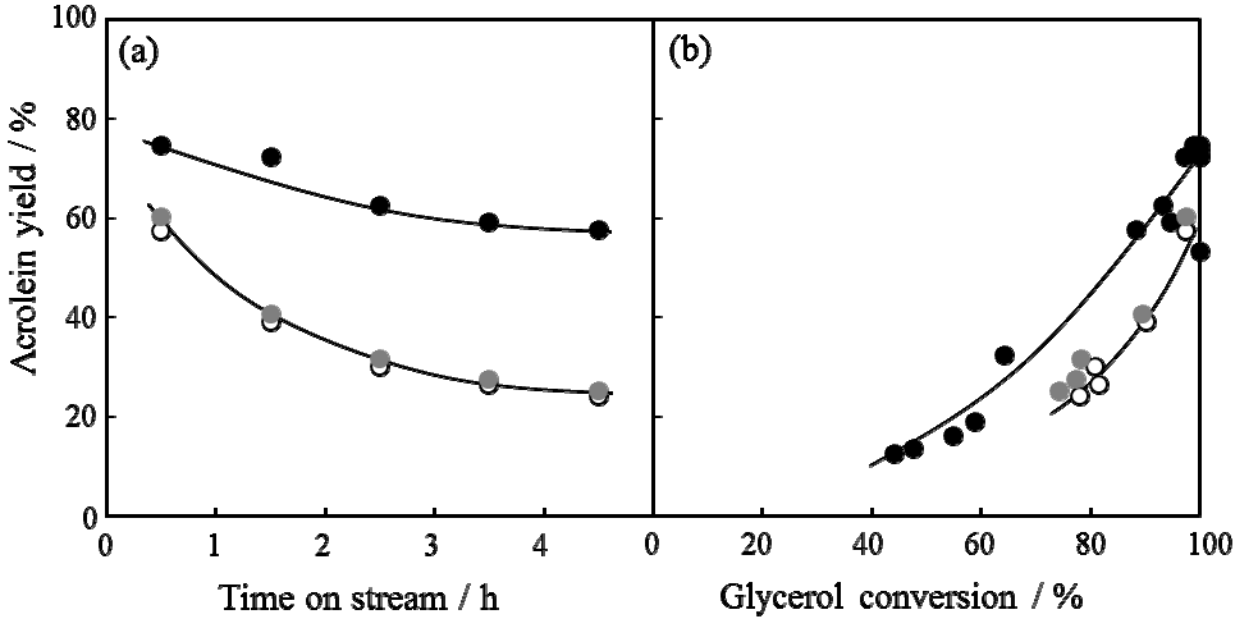


Fig. 4.3 Effect of partial pressure of water on time courses of acrolein yield (a) and acrolein yield against glycerol conversion (b) in the glycerol transforamtion.
Symbols: P_{O2}/P_{total} = 0, ○; P_{O2}/P_{total} = 2.5, ●; P_{O2}/P_{total} = 25, ●.
Reaction conditions: temperature, 558 K; catalyst weight, 0.2 g; flow rate, 80 ml·min^{-1}; composition of reaction gas, GLR/ O_2 / N_2/ H_2O = 5/ 14/ 81-x/ x(0~25) (mol%).

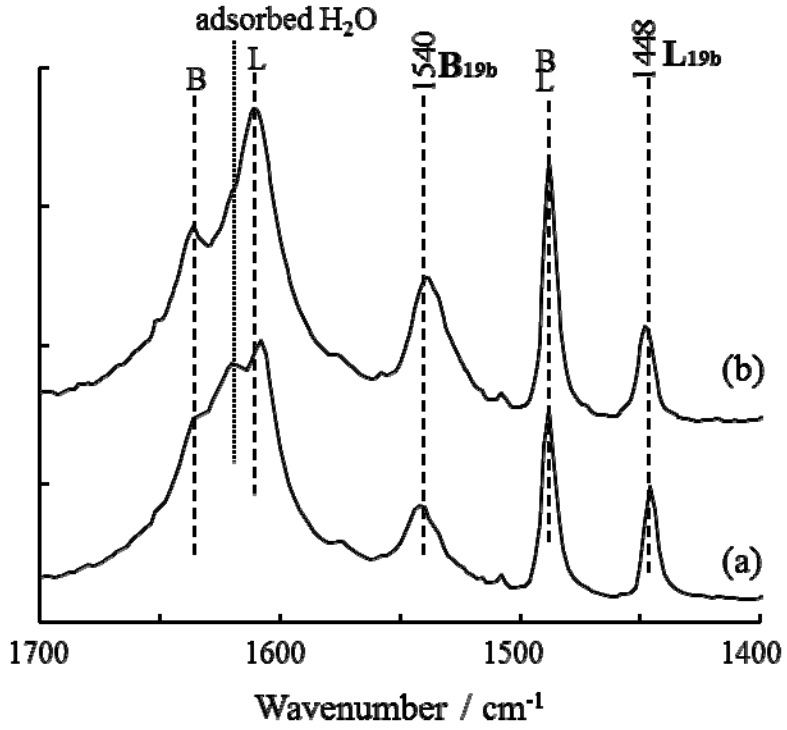


Fig. 4.4 IR spectra of adsorbed pyridine on Nb-O, (a); and W-Nb-O (W/Nb=1.35) ,(b) in presence of water.

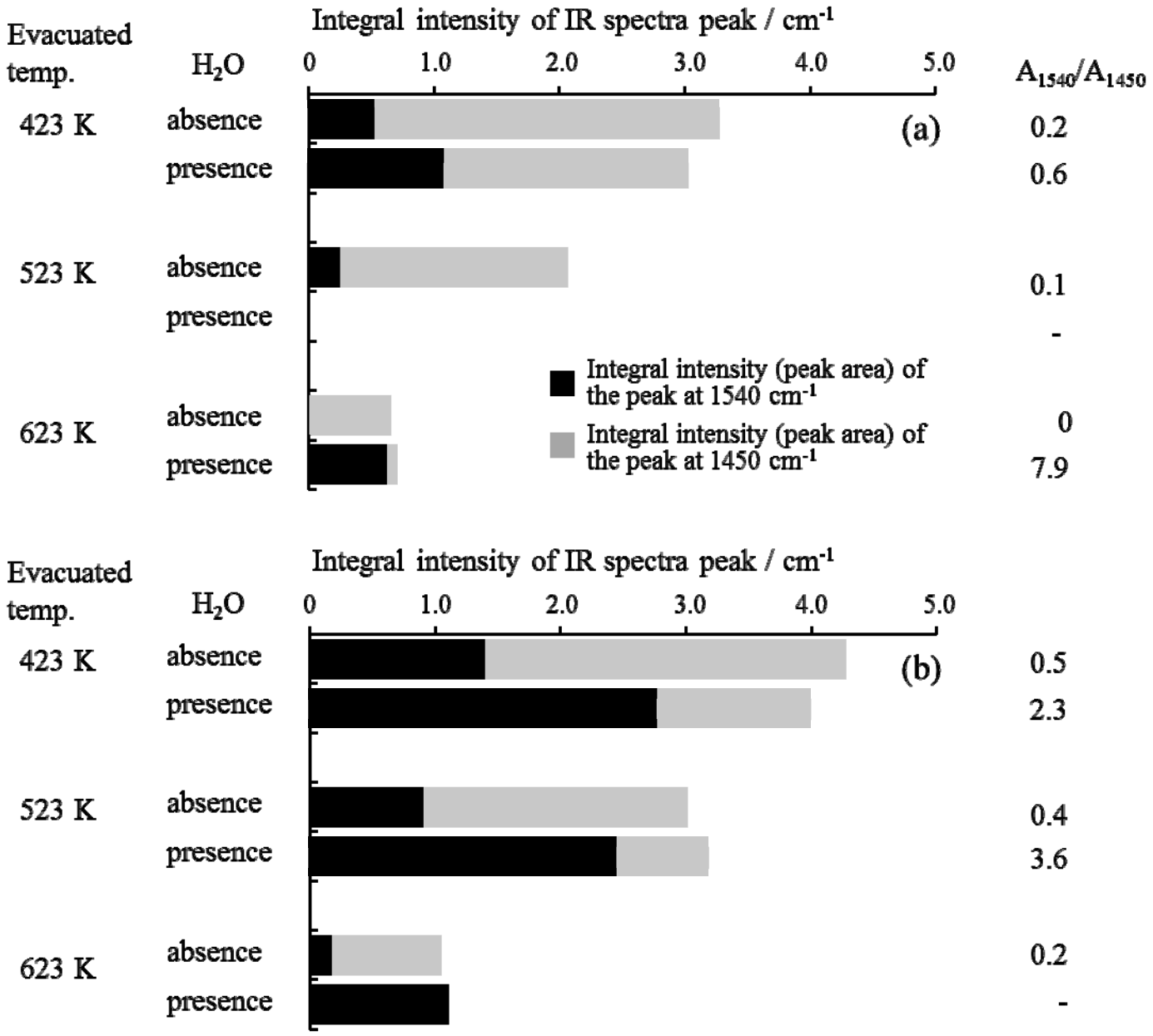


Fig. 4.5 Integral intensity of IR spectra of adsorbed pyridine on Nb-O (a) and W-Nb-O (W/Nb=1.35) (b).

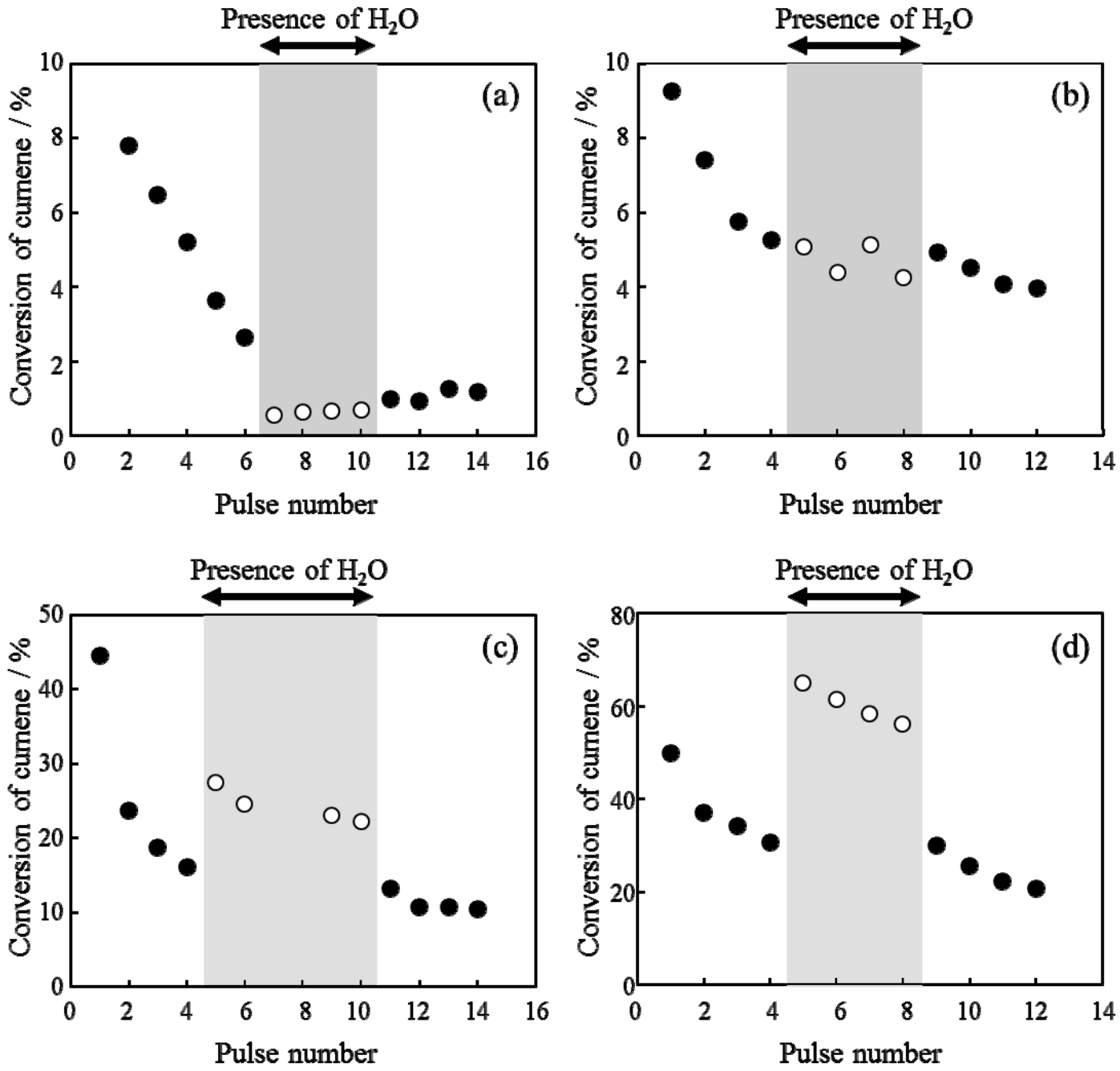


Fig. 4.6 Effect of water addition on conversion in the cumene cracking ovre W-Nb-O (W/Nb=1.35) at 423 (a), 498 (b), 573 (c) and 648 K (d).

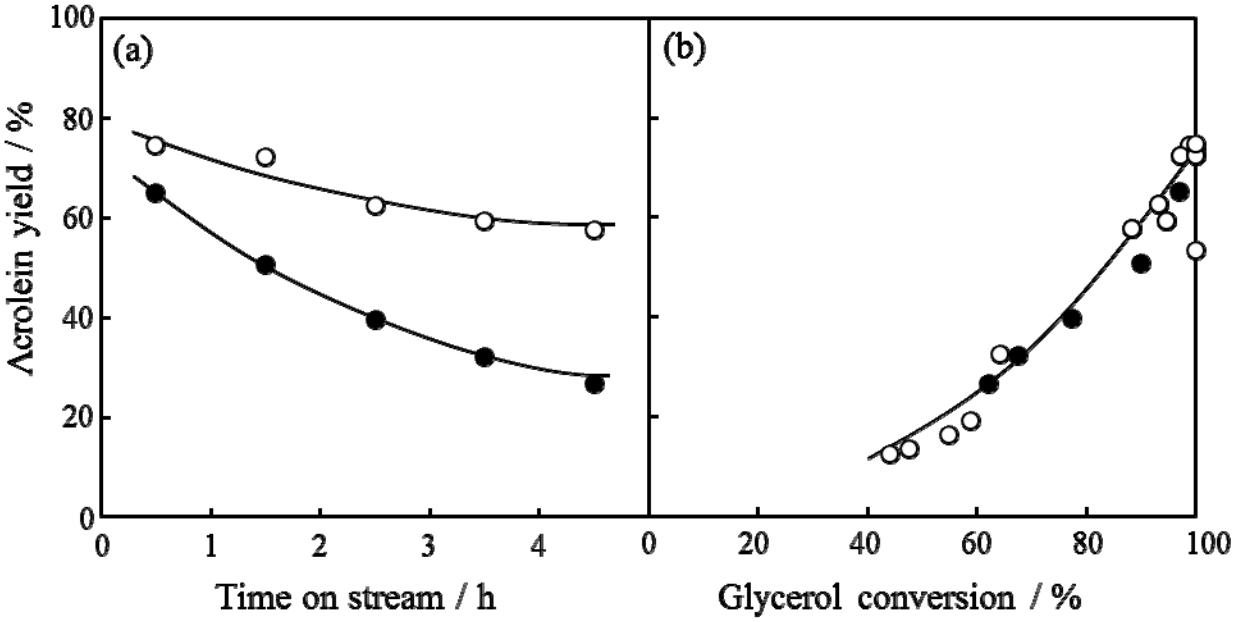


Fig. 4.7 Time courses of acrolein yield (a) and acrolein yield against glycerol conversion (b) in the presence (○) and absence (●) of O_2 over W-Nb-O (673). Reaction conditions: temperature, 558 K; catalyst weight, 0.2 g; flow rate, 80 $ml \cdot min^{-1}$; composition of reaction gas in the presence of O_2, GLR/ O_2/ N_2/ H_2O = 5/ 14/ 56/ 25 (mol%); composition of reaction gas in the presence of O_2, GLR/ N_2/ H_2O = 5/ 70/ 25 (mol%).

Table 4.5 Conversion of glycerol and product yields in glycerol transformation in the presence and absence of O_2

	TOS	GLR conv.[b]	O_2 conv.	Yield[c] / %								
	/ h	/ %	/ %	ΛCRL	ΛCΛL	PRΛL	HΛCT	ΛCΛ	ΛΛ	CO	CO_2	others
presence of O_2 [a, c]	1	98.9	6.5	74.4	2.9	1.0	0.4	0.7	0.1	2.3	1.5	15.4
	5	88.5	4.9	57.7	1.5	0.5	2.1	0.4	0.1	1.5	1.2	23.4
absence of O_2 [a, d]	1	97.1	-	65.1	1.1	2.3	5.4	1.3	0.3	0.3	0.1	21.2
	5	62.1	-	26.7	0.3	0.7	4.7	0.5	0.1	0.1	<0.1	29.0

[a] W /Nb = 1.35. [b] Reaction conditions: catalyst weight, 0.2 g; flow rate, 80 ml·min^{-1}; composition of reaction gas, [c] GLR : O_2 : N_2 : H_2O = 4 : 11.2 : 44.8 : 20 (ml·min^{-1}), [d] GLR : N_2 : H_2O = 4 : 56.0 : 20 (ml·min^{-1}); reaction temperature, 558 K. [c] ΛCRL = acrolein, ΛCΛL = acetaldehyde, PRΛL = propanal, HΛCT = hydroxyacetone, ΛCΛ = acetic acid, ΛΛ = acrylic acid.

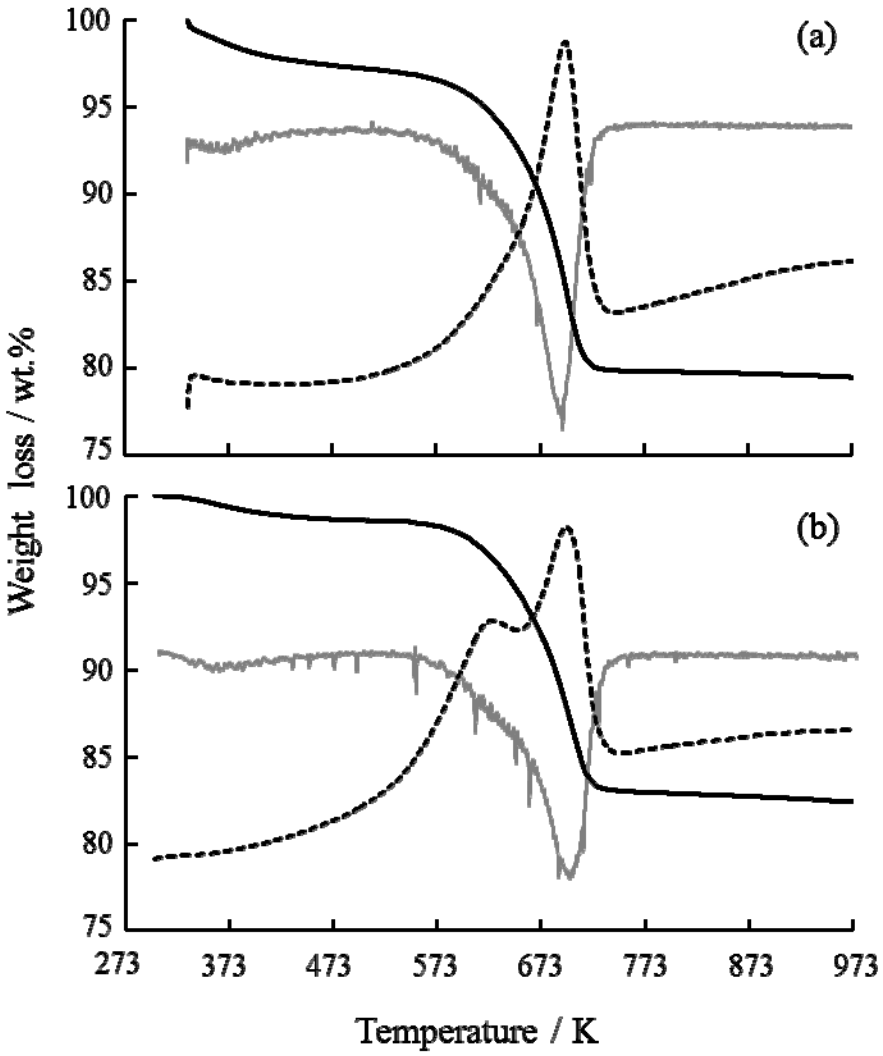


Fig. 4.8 TG (solid line), DTG (gray line) and DTA (dotted line) curves of W-Nb-O after 5 h of the reaction in the presence (a) and absence (b) of O_2.

Chapter 5

Direct Oxidative Transformation of Glycerol to Acrylic Acid over W-based Complex Metal Oxide Catalysts

5-1 Introduction

Acrolein is oxidized to acrylic acid, and then used in the manufacture of plastics, coatings, adhesives and so on. Direct transformation of glycerol to acrylic acid brings about simplification of process and reduction of energy. Standard enthalpy change of the glycerol dehydration to acrolein and the acrolein oxidation to acrylic acid are 18.0 $kJ \cdot mol^{-1}$ and -298.3 $kJ \cdot mol^{-1}$, respectively.[1] The direct transformation of glycerol to acrylic acid may be energy-efficient process if the energy exhausted in the latter reaction can be used for the first reaction.

As catalysts for the direct transformation of glycerol to acrylic acid, Mo-V-Te-Nb-O having an orthorhombic structure,[2] W-V-O[2, 3] and W-V-Nb-O[4] having a hexagonal tungsten bronze structure have been reported. These catalysts gave acrylic acid in yields of ~34%,[2-4] but the values have not come up to that in process separated into the glycerol dehydration and the acrolein oxidation. (For example, $Cs_{2.5}H_{0.5}PW_{12}O_{40}$ catalyst gives an acrolein yield of 98 % in the glycerol dehydration.[5] On the other hand, Mo-V based catalyst gives acrylic acid yield of 98 % in the acrolein oxidation.[6]) The direct transformation of glycerol to acrylic acid is challenging process because not only improvement of selectivity for each reaction but also tune of optimum conditions for each reaction is required to achieve higher acrylic acid yield.

As already described in chapter 2, the complex metal oxides of W and group 5 elements such as V, Nb or Ta synthesized by hydrothermal method have a layered structure similar to orthorhombic Mo-V-O[7, 8] which shows high catalytic activity for various selective oxidations. Besides, in chapter 3, it was found that W-Nb-O catalyst gave acrolein in high yield in gas-phase glycerol dehydration in the presence of water and oxygen.

If the layer-structured complex oxides of W have both enough acidity and acrolein-oxidizing capability similar to orthorhombic Mo-V-O, it is expected to be an efficient catalyst for the direct transformation of glycerol to acrylic acid. In this chapter, I applied the complex metal oxides composed of W, Nb and V prepared by the hydrothermal method as a catalyst for the glycerol transformation. And I

also investigated effects of constituent materials on selectivity, reaction pathway of the glycerol transformation, and conditions to obtain acrylic acid in high yield.

5-2 Experimental

5-2-1 Chemicals

Chemicals used in experiments are listed in Table 5.1.

Table 5.1 List of chemicals

chemical	formula or molar wt.	assay	manufacturer	No.
$Nb_2O_5 \cdot xH_2O$	265.82 (Nb_2O_5)	70.8% (Nb_2O_5)	Soekawa Chemical Co., Ltd.	02275B
$(NH_4)_6(H_2W_{12}O_{40}) \cdot nH_2O$ ($n \fallingdotseq 6$)	3064	90.8% (WO_3)	Nippon Inorganic Colour and Chemical Co., Ltd.	100114
NH_3VO_3	116.98	99.0%	Kanto Chemical Co., Ltd.	
$VOSO_4 \cdot nH_2O$	163.01	61.9%	Mitsuwa Chemicals Co., Ltd.	61595
$Ta_2O_5 \cdot nH_2O$	441.88	82.5% (Ta_2O_5)	Mitsuwa Chemicals Co., Ltd.	59678

5-2-2 Catalyst preparation

5-2-2-1 Preparation of W-V-Nb-O by hydrothermal method

The complex metal oxide catalysts of W, V and Nb were prepared by hydrothermal synthesis method. $(NH_4)_6[H_2W_{12}O_{40}] \cdot nH_2O$, $VOSO_4 \cdot nH_2O$ and $Nb_2O_5 \cdot nH_2O$ were used as raw materials. The mixed aqueous solution of metal salts was put in a stainless steel autoclave with a Teflon liner and heated at 448 K for 72 h. The formed solid was filtered, washed with ion-exchanged water, dried at 353 K and then calcined at 673 K for 4 h in air. V-added W-Nb-O prepared from solution consisting metals with V : W : Nb = x : 1.35 : 1 was denoted by xVWNb. Actual atomic ratios of the catalysts are listed in Table 5.2.

W-Nb-O (W/Nb = 1.35), W-V-O (W/V = 1.35) and V-Nb-O (V/Nb = 0.4) were similarly prepared.

5-2-2-2 Addition of V to W-Nb-O by impregnation method

V added W-Nb-O was also prepared by impregnating uncalcined W-Nb-O or W-Nb-O calcined at 673 K with aqueous solution of NH_4VO_3, followed by calcination at 673 K for 4 h in air. The catalysts using uncalcined W-Nb-O and calcined W-Nb-O as supports are denoted by xV/WNb(pre) and xV/WNb, respectively. x is the V content (V : W : Nb = x : 1.35 : 1).

5-2-2-3 Reference catalysts

V_2O_5 was prepared by calcination of NH_4VO_3 at 773 K for 2 h in air.

5-2-3 Catalyst characterization

5-2-3-1 XRD

Powder X-ray diffraction (XRD) pattern of the catalysts was recorded on RINT2200 (Rigaku) with Cu Kα (λ = 0.154 nm) radiation (tube voltage: 40 kV, tube current: 20 mA).

5-2-3-2 Nitrogen adsorption

Surface area of the catalysts was estimated by BET method where nitrogen adsorption amount was measured at 77 K with a BEL max 00094 (BEL Japan Inc.). Prior to the measurement, the samples were evacuated at 473 K for 2 h.

5-2-3-3 SEM-EDS

Scanning electron microscopy (SEM) images were obtained with a JSM-6360LA (JEOL). Composition of the catalysts was determined by simplified quantitative analysis of EDS with the ZAF method.

5-2-3-4 STEM

Scanning transmission electron microscopy (STEM) images were obtained with a HD-20000 (HITACHI).

5-2-3-5 NH_3-TPD

The acid amount of catalysts was measured by NH_3-TPD with a TPD apparatus (BEL Japan Inc.).

Prior to the measurement, the samples were pretreated under He flow at 673 K for 2 h. 100 torr of ammonia was equilibrated with the pretreated sample at 473 K and evacuated for 5 min. The TPD data were collected at temperature ramp rate of 10 $Kmin^{-1}$ under differentially-pumped He (50 ml min^{-1} (STP)) flow at ca.180 torr. A mass spectrometer (ANELVA M-100OA-F) was used to measure the desorbed NH_3 at m/e = 16. The acid amount of catalyst was calculated on the basis of the acid amount of H-ZSM-5(JRC-Z5-90H) (345 $\mu molg^{-1}$).

5-2-3-6 FT-IR spectroscopy of adsorbed pyridine

Acidity of catalysts was measured by FT-IR spectroscopy (PARAGON 1000, Perkin Elmer) of adsorbed pyridine with an evacuable furnace cell with CaF_2 windows, containing a self-supporting disk (with 12 mm diameter) of sample (50 mg) as shown in Fig. 3.1. Prior to the measurement, the samples were pretreated under vacuum at 623 K for 1 h. 4.4 torr of pyridine was adsorbed at 373 K and after evacuation at 423 K for 1 h, the adsorption spectrum was recorded followed by the measurement of the spectrum of adsorbed pyridine on sample in the presence of water vapor (4.6 torr). The spectra of adsorbed pyridine after evacuation at 523 and 623 K were similarly recorded

5-2-3-7 Raman

The Raman spectra were recorded on an inVia Reflex (Renishaw) with a 2.5 mW semiconducting laser (excitation wavelength 532 nm).

5-2-3-8 ESR

ESR spectra were recorded on an X band (9.14 GHz) spectrometer (JEOL JES-FA200) at 103 K. 0.05 g of the catalyst in a quartz cell (5ϕ) was pretreated at 473 K in a vacuum for 1 h. The g-value and intensity were determined by the Mn^{2+} marker as a reference.

5-2-4 Catalytic testing

5-2-4-1 Transformation of glycerol

Transformation of glycerol was carried out in a vertical fixed-bed reactor (Fig. 3.2). A mixture of 0.02-0.80 g of catalyst powder and sea sand (catalyst + sea sand = 2 ml) was set in a Pyrex glass tube with 12 mm internal diameter and pretreated at 573 K for 0.5 h in flowing 20% O_2/N_2 before the reaction. A glycerol-water 1:5 (mol/mol) solution was fed into the top of reactor with a micro feeder. Pure N_2 or O_2/N_2 was introduced with glycerol vapor with mass flow controllers (KOFLOC). The molar composition of reaction gas was glycerol: N_2: H_2O = 5: 70: 25 (absence O_2) or glycerol: O_2: N_2: H_2O = 5: 14: 56: 25 (presence O_2). Reaction products and unconverted glycerol in both gas and liquid phase were collected hourly in an ice trap (273 K) and a Tedlar bag connected at the end of the trap. Products in the liquid phase were analyzed with FID-GC (GL science GC353, 30 m 0.32 mm TC-WAX capillary column). Products in the gas phase were analyzed with FID-GC (Shimadzu GC14B, Gaskuropak54 column) and TCD-GC (Shimadzu GC8A, Porapak QS and MS-13X column). Glycerol conversion and product selectivities and yields were calculated by Eqs. (5.1) - (5.3).

$$\text{Glycerol conversion } (\%) = \frac{\text{Moles of glycerol reacted}}{\text{Moles of glycerol fed}} \times 100 \qquad (5.1)$$

$$\text{Product selectivity } (\%) = \frac{\text{Moles of carbon in a product defined}}{\text{Moles of carbon in glycerol reacted}} \times 100 \qquad (5.2)$$

$$\text{Product yield } (\%) = \frac{\text{Moles of carbon in a product defined}}{\text{Moles of carbon in glycerol fed}} \times 100 \qquad (5.3)$$

5-2-4-2 Oxidation of acrolein

Oxidation of acrolein was carried out in the same reactor as the transformation of glycerol. Reaction conditions were: catalyst weight, 0.2 g; reaction temperature, 458~658 K; total flow rate, 77 ml·min^{-1}; molar composition of reaction gas, acrolein: O_2: N_2: H_2O = 1: 15: 58: 26. Acrolein conversion and

product selectivities and yields were calculated by Eqs. (5.4) - (5.6).

$$\text{Acrolein conversion (\%)} = \frac{\text{Moles of acrolein reacted}}{\text{Moles of acrolein fed}} \times 100 \tag{5.4}$$

$$\text{Product selectivity (\%)} = \frac{\text{Moles of carbon in a product defined}}{\text{Moles of carbon in acrolein reacted}} \times 100 \tag{5.5}$$

$$\text{Product yield (\%)} = \frac{\text{Moles of carbon in a product defined}}{\text{Moles of carbon in acrolein fed}} \times 100 \tag{5.6}$$

5-3 Results and discussion

5-3-1 W-Nb-O and W-V-O catalysts

X-ray diffraction patterns of W-Nb-O (W/Nb=1.35) and W-V-O (W/V=1.35) synthesized by the hydrothermal method are illustrated in Fig. 5.1 (a) and (b). The diffraction peaks of W-Nb-O and W-V-O were observed around 23° and 46° attributed to (001) and (002) planes of a layered structure, respectively. This result confirmed that W-Nb-O and W-V-O have a layered structure with linear arrangement of corner-shared octahedra in *c*-direction. The peaks ascribed to (001) planes in W-Nb-O and W-V-O appeared at 22.68° and 22.72°, respectively. The *d* spacing between (001) planes of W-Nb-O and W-V-O calculated from these angles were 0.392 nm and 0.391 nm, respectively. Other low intensity diffractions in Fig. 5.1 (b) were also observed in W-V-O. These unknown peaks may be attributed to a type of vanadium oxide which was formed from hydrated vanadium oxide containing NH_4^+ ion with a layered structure[26] (shown in Fig. 2.19) by calcination.

Surface areas and acid properties of these two catalysts are listed in Table 5.3. The surface areas of W-Nb-O and W-V-O were 100 and 8 $m^2 \cdot g^{-1}$, and the numbers of acid sites per gram were 136 and 5 $\mu mol \cdot g^{-1}$, respectively. Introduction of Nb seems to increase the surface area and acid amount. In the STEM images, already shown in Fig. 2.21, both catalysts were found to have rod-like crystalline morphology. Dense aggregation of the rod-like crystals was observed in the W-V-O catalyst. Therefore, the surface area and the acid amount of the W-V-O catalyst would be lower than those of the W-Nb-O catalyst.

The catalytic results of the glycerol transformation both in the absence and in presence of O_2 are listed in Table 5.4. The W-Nb-O and W-V-O catalysts gave acrolein in the yields of 50.7 and 7.2%, respectively, in the absence of O_2. This result is due to the fact that the acid amount of W-V-O is smaller than that of W-Nb-O (Table 5.3). In the presence of O_2, the yield of acrolein over W-V-O decreased to 3.3%, and the yield of acrylic acid increased notably to 18.7%. Over W-Nb-O, on the other hand, the yield of acrolein increased but acrylic acid was not formed. These results indicate that acrolein was

oxidized to acrylic acid on V sites.

5-3-2 Addition of V to W-Nb-O

Effect of V addition to the W-Nb-O catalyst which gave acrolein in a high yield in the glycerol transformation was investigated.

It was confirmed that the layered structure of W-Nb-O was maintained after the V addition by the all methods because the V-added W-Nb-O showed the diffraction peaks attributed to (001) and (002) planes (Fig. 5.1 (d), (e) and (f)). The low intensity diffraction peaks ascribed to V_2O_5 were observed only for 0.4V/WNb. The crystalline V_2O_5 dispersed on W-Nb-O in 0.4V/WNb. In 0.4VWNb, the diffraction peak ascribed to (001) planes shifted to higher angle by 0.04º in 2θ as compared to that of W-Nb-O, indicating that V was incorporated into framework of W-Nb-O. V-Nb-O (V/Nb = 0.4) synthesized by hydrothermal method also had a layered structure according to XRD pattern (Fig. 5.1 (c)). Because the oxides consisted of two metals such as W-Nb-O, W-V-O and V-Nb-O formed the layered structure, it is natural that layer-structured W-V-Nb-O was synthesized by hydrothermal method. On the other hand, in 0.4V/WNb(pre), neither the peaks ascribed to V_2O_5 nor the shift of the diffraction peak ascribed to the (001) planes was observed, suggesting that V species are on the surface of W-Nb-O with high dispersion.

Fig. 5.3 and 5.4 illustrate the STEM images of the V-added W-Nb-O catalysts. It is confirmed that all the V-added W-Nb-O catalysts have rod-like crystalline morphology similar to the W-Nb-O catalyst. However, while the aggregation of the small crystals was observed in the impregnated catalysts in the wide range images (Fig. 5.4), the uniform rod-like crystals separated discretely.

Surface area of the impregnated catalysts was smaller than that of the W-Nb-O catalyst because of the aggregation of crystals (Table 5.5). On the other hand, 0.4VWNb has larger surface area compared to W-Nb-O. Besides, increase of the adsorption amount below $p/p_0 = 10^{-6}$ was also observed. The STEM images and the result of N_2 adsorption indicates that W, Nb and V make complex oxide without impurity phase in agreement with XRD.

Fig. 5.6 illustrates the Raman spectra. The W-Nb-O catalyst and all the V-added W-Nb-O catalysts exhibited the common bands at 743 and 810 cm^{-1}. For 0.4V/WNb, the bands assigned to crystalline V_2O_5 were observed. This result is consistent with the result of XRD (Figure 1). For 0.4V/WNb(pre) and 0.4VWNb, on the other hand, the raman bands of V_2O_5 were not observed. And these catalysts gave the broad bands at 995 and 930 cm^{-1} derived from W-V-O and V-Nb-O, respectively. This result suggests the formation of W-O-V and V-O-Nb bonds in these catalysts.

The catalytic performance of the V-added W-Nb-O catalysts in glycerol transformation was examined (Table 5.6). Acrylic acid yield was increased by the addition of V to the W-Nb-O catalyst. In particular, 0.4VWNb showed a high yield (33.7%) of acrylic acid in comparison with impregnated catalysts.

The acid amount of 0.4V/WNb and 0.4V/WNb(pre) was less than a half that of W-Nb-O (Table 4.8). In these catalysts, as illustrated in Fig. 5.8 (a) and (b), the acid sites on W-Nb-O were covered with V species and accordingly the acid amount was decreased. In contrast, 0.4VWNb had similar acid amount as W-Nb-O, indicating that acid sites of W-Nb-O are maintained by the introduction of V into the framework of W- Nb-O (Fig. 5.8 (c)). In fact, the addition of V to W-Nb-O and Nb-O was hardly affected the activity and selectivity in the glycerol transformation in the absence of O_2 (Table 5.6 and Fig. 5.9). The large acid amount of 0.4VWNb is one reason for the high acrylic acid yield of this catalyst.

Effect of the addition method of V on selectivity in the acrolein oxidation was investigated. Figure 3 shows acrolein conversion and acrylic acid yield in the acrolein oxidation. Acrylic acid was not obtained and CO_x formed as a main product over W-Nb-O. This fact indicates that acrolein is oxidized to CO_x on W-Nb-O sites at a temperature above 573 K. Over the V-added W-Nb-O catalysts, on the other hand, acrylic acid formed. It is confirmed that V is required for the formation of acrylic acid. The V-added W-Nb-O catalysts gave the maximum yield of acrylic acid at about 550 K. 0.4VWNb showed the highest acrylic acid yield (68.0%), followed by 0.4V/WNb(pre) with 53.7% and 0.4V/WNb with 43.9%. It is indicated that V species in the framework show higher selectivity to acrylic acid than that on the surface of W-Nb-O. The acrylic acid selectivity does not depend solely on the amount of V on the surface because

decrease of the V content in impregnated catalysts did not increase but rather decrease acrylic acid selectivity.

Effect of W and Nb on catalytic function of V in the acrolein oxidation was investigated. Acrolein conversion and acrylic acid yield in the acrolein oxidation over 0.4VWNb, W-V-O and V-Nb-O are illustrated in Fig. 5.12. The maximum acrylic acid yield was 63.0% for W-V-O at the same level as 0.4VWNb. Over V-Nb-O, acrolein began to be converted at about 473 K which was about 50 K lower than that observed over W-V-O. However, V-Nb-O showed a maximum acrylic acid yield of 22.3% which was much lower than that observed over W-V-O or 0.4VWNb. This suggests that the introduction of W increases the selectivity to acrylic acid.

It has been widely proposed that acrolein is oxidized to acrylic acid selectively on V^{4+} sites.[9] ESR spectra of the V-containing catalysts are shown in Fig. 5.13. Vertical axis intensity was normalized by total V content per unit weight determined by EDS. The hyperfine structure caused by the vanadium nucleus (I = 7/2) was observed for all the catalysts except for W-V-O, indicating that these catalysts have highly-dispersed V. In W-V-O, the dispersion of V is lower because the V content in W-V-O is higher than that in the other catalysts. Therefore, the hyperfine structure was not observed in W-V-O.

The differential spectra in Fig. 5.13 were transformed into the integral spectra to be compared relative amount of V^{4+} to total V in each catalyst. The area ratios of integral spectra are listed in the table inserted in Figure 5. The relative amount of V^{4+} was higher in the catalysts containing W than in V-Nb-O. It was reported that introduction of W into the framework of V_2O_5 [10] and introduction of V into the framework of hexagonal WO_3 [2] promote the formation of V^{4+}. It is considered that W^{6+} substitutes for V^{5+} or Nb^{5+} in the layered structure, and the V^{4+} is formed by charge compensation (Fig. 5.14). In addition, the relative amount of V^{4+} in 0.4VWNb was about twice as much as that in 0.4V/WNb. This is due to a stronger interaction between V and W in 0.4VWNb which has V incorporated into framework than in 0.4V/WNb which has the crystalline V_2O_5 on the surface of W-Nb-O.

Relation between the relative amount of V^{4+} and the selectivity to acrylic acid from acrolein was considered. The catalyst which has high relative amount of V^{4+} shows high acrylic acid selectivity in the

acrolein oxidation. 0.4VWNb gave a high acrylic acid yield in the acrolein oxidation because of high relative amount of V^{4+}. As an exception, W-V-O showed a similar acrylic acid yield to 0.4VWNb in spite of its lower relative amount of V^{4+}. According to XRD (Fig. 5.1) and Raman (Fig. 5.6), vanadium oxide was observed in the W-V-O catalyst. This suggests that the apparent relative amount of V^{4+} decreases by the effect of the bulk vanadium oxide in W-V-O.

Therefore, high relative amount of V^{4+} which is efficient for the selective oxidation of acrolein to acrylic acid is another reason in addition to a large acid amount for the higher acrylic acid yield in the glycerol transformation over 0.4VWNb.

5-3-3 Effect of V content and reaction conditions on the yield of acrylic acid

The W-V-Nb-O catalysts with different V-contents were synthesized by hydrothermal method. It was confirmed that the 0.1~0.6VWNb catalysts have the layered structure because those catalysts showed the diffraction peaks attributed to (001) and (002) planes (Fig. 5.15). Besides, the diffraction peak ascribed to (001) planes shifted to higher angle with an increase in V content, indicating that V was incorporated into framework of W-Nb-O. STEM images confirmed that the 0.1~0.6VWNb catalysts had rod-like crystalline morphology without impurity phase (Fig. 5.16 and 4.17).

As shown in Fig. 5.18 and Table 5.8, the shape of adsorption isotherms and the surface area was less affected by the V content. Fig. 5.18 illustrates the NH_3-TPD and the acid amount determined by NH_3-TPD is listed in Table 5.9. The differences of both the peak shift in TPD profiles and the acid amount were not observed. Besides, the ratio of Brönsted to Lewis acidity was constant V content with V content. These results indicate that the V content hardly affected the surface area, the acid amount and the acidity (Fig. 5.20 and Table 5.10). It was confirmed that 0.4VWNb showed a similar selectivity to W-Nb-O in the dehydration of glycerol as discussed previously (Table 5.6 and Fig. 5.9).

Fig. 5.21 illustrates the yield of acrolein, acrylic acid and CO_x against the V contents in the glycerol transformation. Acrolein yield decreased and acrylic acid yield increased with increasing the V content.

The maximum acrylic acid yield of 35.8% was achieved over 0.35VWNb under this reaction condition. Acrylic acid yield decreased and CO_x became a main product with a further increase in V content. This result indicates that there exists optimum balance between acid and oxidative capability of the catalysts to obtain acrylic acid.

Fig. 5.22 illustrates the yield of acrolein, acrylic acid and CO_x in the glycerol transformation under the various contact times over the *x*VWNb catalysts. The W-Nb-O catalyst gave maximum acrolein yield at $W/F = 2.5 \times 10^{-3}$ g min ml^{-1}. At a contact time above $W/F = 2.5 \times 10^{-3}$ g min ml^{-1}, the yield of acrolein decreased and the yield of CO_x increased with increasing contact time. Acrylic acid was not observed over the W-Nb-O catalyst. In the acrolein oxidation (Fig. 5.10), acrolein was oxidized to CO_x without formation of acrylic acid over the W-Nb-O catalyst. These results indicate that acrolein formed by the glycerol dehydration was oxidized to CO_x over W-Nb-O catalyst. On the other hand, acrylic acid was formed over the V-containing catalysts. The optimum conditions to obtain the maximum yield of acrylic acid were different depending on the V content. The catalysts containing larger amount of V gave the maximum yield of acrylic acid at shorter contact time. The catalyst which exhibited the maximum yield of acrylic acid was 0.3VWNb and gave an acrylic acid yield of 46.2% at $W/F = 6.7 \times 10^{-3}$ g min ml^{-1}. Activity for the dehydration of glycerol over *x*VWNb catalysts seems to be similar regardless of V content because the V content does not affect much the acidity of *x*VWNb (Table 5.9 and 5.10). Therefore, it is supposed that the selectivity to acrylic acid in the glycerol transformation is determined by the selectivity of acrylic acid in the acrolein oxidation.

Conversion of acrolein and yield of acrylic acid in the acrolein oxidation over the *x*VWNb catalysts are shown in Fig. 5.23. Temperature range of the formation of acrylic acid over *x*VWNb shifted toward lower with increasing the V content. 0.6VWNb, 0.4VWNb and 0.3VWNb gave acrylic acid in yield of about 70% at 529 K, 553 K and 581 K, respectively. In 0.1VWNb, on the other hand, the maximum yield of acrylic acid was about 30%. At a temperature above 600 K, acrylic acid yield decreased. The temperature range in which acrylic acid yield decreased over 0.1VWNb corresponded to the temperature range in which CO_x formed from acrolein over W-Nb-O. This result indicates that 0.1VWNb gave lower

yield of acrylic acid than 0.3~0.6VWNb because of the formation of CO_x from acrolein on W-Nb-O sites. Therefore, acrylic acid yield of 0.1VWNb was lower than those of 0.3~0.6VWNb in the glycerol transformation. However, the yield of acrylic acid over 0.3~0.6VWNb for the glycerol transformation were different in spite of their similar acrylic acid selectivity in the acrolein oxidation.

In Fig. 5.24, the conversion of oxygen and the yields of acrylic acid, acrolein and CO_x are plotted against the glycerol conversion. When glycerol conversion was below 100%, the conversion of oxygen was below 5% over W-Nb-O, 0.1VWNb and 0.3VWNb. That is to say, oxidation is hard to proceed in the presence of glycerol. After the glycerol conversion reached 100%, the oxygen conversion began to increase. In 0.6VWNb, on the other hand, the conversion of oxygen was above 20% under the condition that glycerol conversion was below 100%. Because acrylic acid was formed after glycerol conversion reached 100%, oxygen should be consumed not for the formation of acrylic acid but for the oxidation of glycerol in the presence of glycerol. The oxidation of glycerol which may transform to acrolein should decrease the yield of acrylic acid. The yield of CO_x and acrylic acid increased after glycerol was converted completely. This result suggests that glycerol having high boiling point (563 K) is adsorbed on oxidative site, and suppresses the oxidation of acrolein or other intermediates. 0.3VWNb gave higher acrylic acid yield than 0.4VWNb or 0.6VWNb because glycerol was hardly oxidized over 0.3VWNb.

Reaction pathways of the glycerol transformation on *x*VWNb are shown in Scheme 5.1. On W-Nb-O, pathway 1 where acrolein forms by the dehydration of glycerol (Table 5.4) and pathway 2 where formed acrolein is oxidized to CO_x subsequently (Fig. 5.10, 5.23) proceed. On V sites, pathway 3 where acrylic acid forms by the oxidation of acrolein (Fig. 5.22, 5.23), followed by pathway 4 where acrylic acid is oxidized to CO_x (Fig. 5.22, 5.23) proceed. As pathway 5, the oxidation of glycerol proceeds on V site (Fig. 5.24). Over 0.1VWNb, acrolein forms in a high yield because the reaction rate of the glycerol dehydration to acrolein is much faster than that of the glycerol oxidation. However, the high reaction temperature or the long contact time is required to obtain acrylic acid by the oxidation of acrolein. Under this condition, a high yield of acrylic acid cannot be expected due to occurrence of the direct formation of CO_x from acrolein over W-Nb-O site. On the other hand, 0.6VWNb gave acrylic acid in a high selectivity in the

acrolein oxidation, but the oxidation of glycerol to CO_x proceeds in 0.6VWNb. As a result, 0.3VWNb exhibited the highest yield of acrylic acid. The oxidation of glycerol to CO_x through oxygenated compounds on V sites, the complete oxidation of acrolein on W-Nb-O and the sequential oxidation of the formed acrylic acid to CO_x should be suppressed to increase the yield of acrylic acid in the glycerol transformation.

5-3-4 Effect of V addition on life time

Fig. 5.25 illustrates the time courses of acrolein and acrylic acid yield in the glycerol transformation over *x*VWNb. Over W-Nb-O, acrolein decreased to 80% of initial yield during 5 hours of the reaction. On the other hand 0.2VWNb gave the constant yield of acrolein from 1 to 5 h. Over the 0.4 and 0.6VWNb catalysts which gave acrylic acid mainly, the yield of acrylic acid was kept constant during 5 hours of the reaction. Amount of carbon deposition after the reaction over 0.4VWNb catalyst measured by TG (Fig. 5.26). The weight loss due to the combustion of deposited carbon was observed in all samples. Amount of coke formed in the reaction is listed in Table 5.11. The coke over the catalyst decreased with increasing V content. In particular, the amount of coke over the catalysts which *x* was 0.4 or above (*x* is V content) was less than one sixth of that over the W-Nb-O catalyst. It is clear that V suppresses the carbon deposition causing deactivation of the catalysts.

5-4 Conclusion

The layer-structured complex metal oxides of W, V and Nb synthesized by hydrothermal method were applied to the glycerol transformation. The W-Nb-O catalyst having high acidity gave acrolein in the yield of 72.3% by the glycerol dehydration in the presence of oxygen. Acrylic acid yield was increased by the addition of V to W-Nb-O. The VWNb catalyst synthesized by the addition of V to the starting solution of W-Nb-O showed higher yield of acrylic acid in the glycerol transformation than the catalysts prepared by impregnation method. The VWNb catalyst had similar acid property as W-Nb-O and showed a higher selectivity to acrylic acid in the acrolein oxidation than impregnated catalysts. Activity for oxidation was controlled by changing the V content. Reaction conditions in which acrylic acid forms in a maximum yield varied depending on the V content. The maximum yield of acrylic acid was 46.2% (V: W: Nb = 0.3: 1.35: 1, $W/F = 6.7\times10^{-3}$ g min·ml^{-1}, reaction temperature 580 K).

5-5 References

[1] J. A. Dean, *LANGE'S HANDBOOK OF CHEMISTRY*, **1985**, pp. 9-1f.

[2] J. Deleplanque, J.-L. Dubois, J.-F. Devaux,W. Ueda, *Catal. Today* **2010**,157, 351.

[3] M. D. Soriano, P. Concepci´on, J. M. L. Nieto, F. Cavani, S. Guidetti, C. Trevisanut, *Green Chem.* **2011**, 13, 2954.

[4] A. Chieregato, F. Basile, P. Concepción, S. Guidetti, G. Liosi, M. D. Soriano, C. Trevisanut, F. Cavani, J. M. L. Nieto, *Catal. Today* **2012**, 197, 58.

[5] A. Alhanash, E. F. Kozhevnikova, I. V. Kozhevnikov, *Appl. Catal. A* **2010**, 378, 11.

[6] Y. Moro-oka, W. Ueda, *Adv. Catal.* **1994**, 40, 233.

[7] T. Katou, D. Vitry, W. Ueda, *Catal. Today* **2004**, 91, 237.

[8] M. Sadakane, K. Kodato, T. Kuranishi, Y. Nodasaka, K. Sugawara, N. Sakaguchi, T. Nagai, Y. Matsui, W. Ueda, *Angew. Chem., Int. Ed.* **2008**, 47, 2493.

[9] J. Tichy, *Appl. Catal. A* **1997**,157, 363.

[10] Z.-G. Yan, S. L.T. Andersson, *Appl. Catal.* **1990**, 66, 149.

Table 5.2 Composition of catalysts determined by EDS

Catalyst	W: V: Nb atmic ratio, normalized to Nb					
	In starting solution			In catalysts		
W-Nb-O	1.35:	0:	1	1.50:	0:	1
W-V-O	1.35:	1:	0	1.24:	1:	0
V-Nb-O	0:	0.40:	1	0:	0.36:	1
0.4V/WNb	1.35:	0.40:	1	1.66:	0.62:	1
0.4V/WNb(pre)	1.35:	0.40:	1	1.66:	0.52:	1
0.1VWNb	1.35:	0.10:	1	1.28:	0.05:	1
0.4VWNb	1.35:	0.40:	1	1.36:	0.35:	1
0.6VWNb	1.35:	0.60:	1	1.76:	0.79:	1

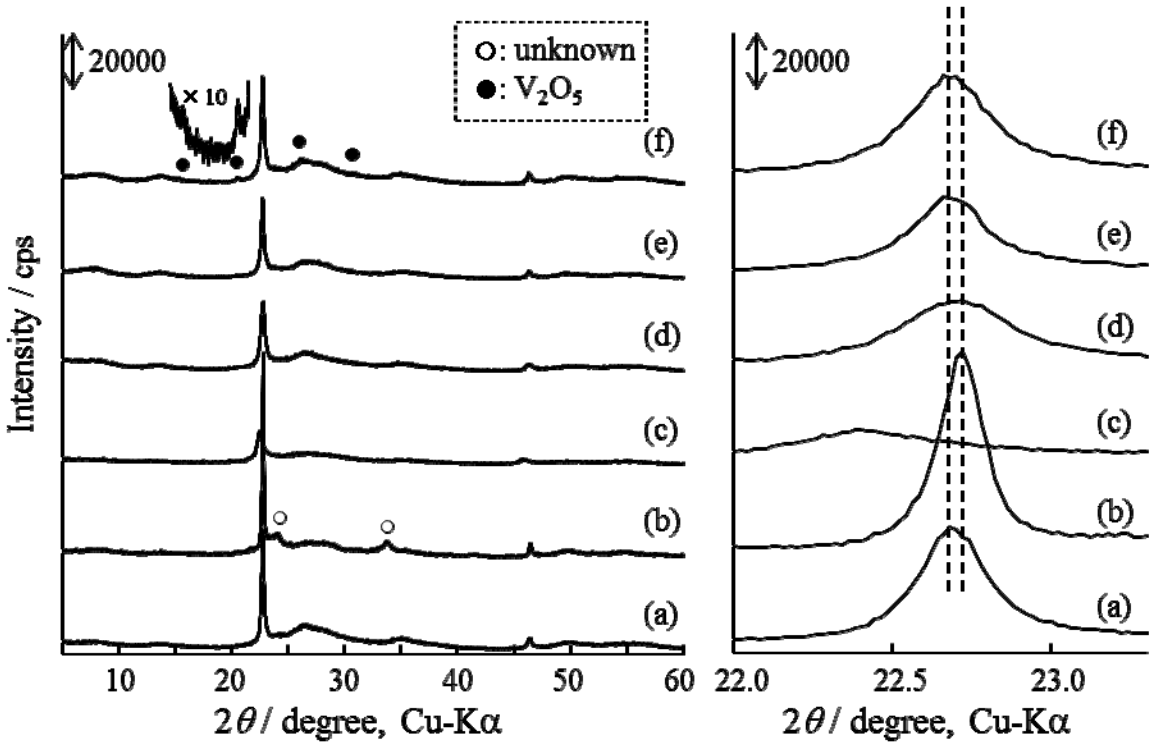


Fig. 5.1 XRD patterns of W-based complex metal oxides.
W-Nb-O, (a); W-V-O, (b); V-Nb-O, (c); 0.4VWNb, (d); 0.4V/WNb(pre), (e); 0.4V/WNb, (f).

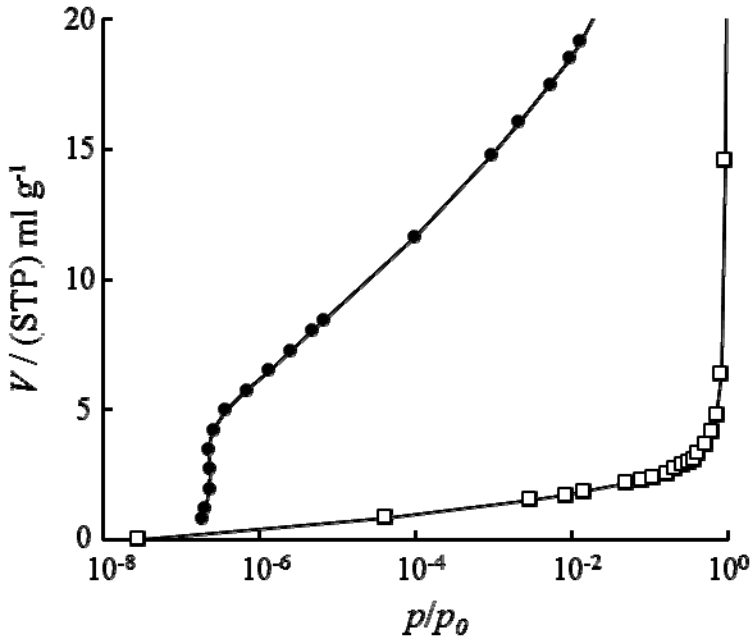


Fig. 5.2 N_2 adsorption isotherms of W-Nb-O (●) and W-V-O (□) calcined at 673 K.

Table 5. 3 Surface area of W-Nb-O and W-V-O

Catalyst	Surface area / $m^2 \cdot g^{-1}$	Acid amount / $\mu mol \cdot g^{-1}$
W-Nb-O (W/Nb=1.35)	100	136
W-V-O(W/V=1.35)	8	5

Table 5.4 Catalytic performance in the glycerol transformation in the absence or presence of O_2

Catalyst	O_2	R. T.[a] / K	GLR[b] conv.[c] / %	O_2 conv. / %	Yield[f] / %							
					ΛCRL	ΛΛ	ΛCΛL	PRΛL	HΛCT	ΛCΛ	CO_x	others
W-Nb-O[d]	absence	562	90.0	-	50.7	0.2	1.1	1.3	6.4	0.9	0.2	29.2
W-V-O[d]	absence	631	25.8	-	7.2	<0.1	1.1	0.3	<0.1	<0.1	0.2	17.0
W-Nb-O[e]	presence	565	97.2	4.9	72.3	<0.1	1.8	0.7	1.6	0.4	2.9	17.5
W-V-O[e]	presence	628	100	55.0	3.3	18.2	0.8	<0.1	<0.1	14.0	53.2	10.5

[a] Reaction temperature. [b] GLR = glycerol. [c] Reaction conditions: catalyst weight, 0.2 g; flow rate, 80 ml·min^{-1}; time on stream, 1~2 h; composition of reaction gas, [d] GLR/ N_2/ H_2O = 5/ 70/ 25 (mol%), [e] GLR/ O_2/ N_2/ H_2O = 5/ 14/ 56/ 25 (mol%). [f] ΛCRL = acrolein, ΛΛ = acrylic acid, ΛCΛL = acetaldehyde, PRΛL = propanal, HΛCT = hydroxyacetone, ΛCΛ = acetic acid.

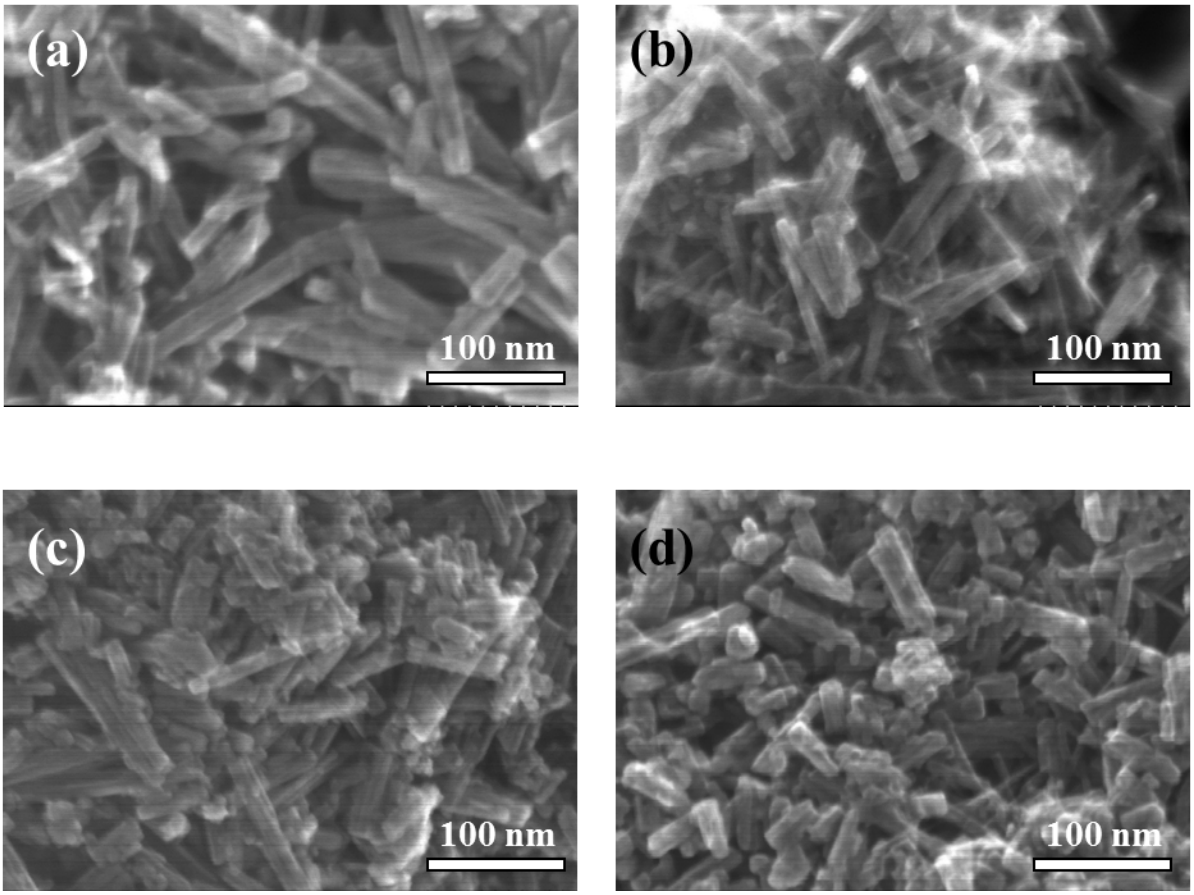


Fig. 5.3 STEM images of W-Nb-O, (a); 0.4VWNb, (b); 0.4V/WNb(pre), (c); 0.4V/WNb, (d).

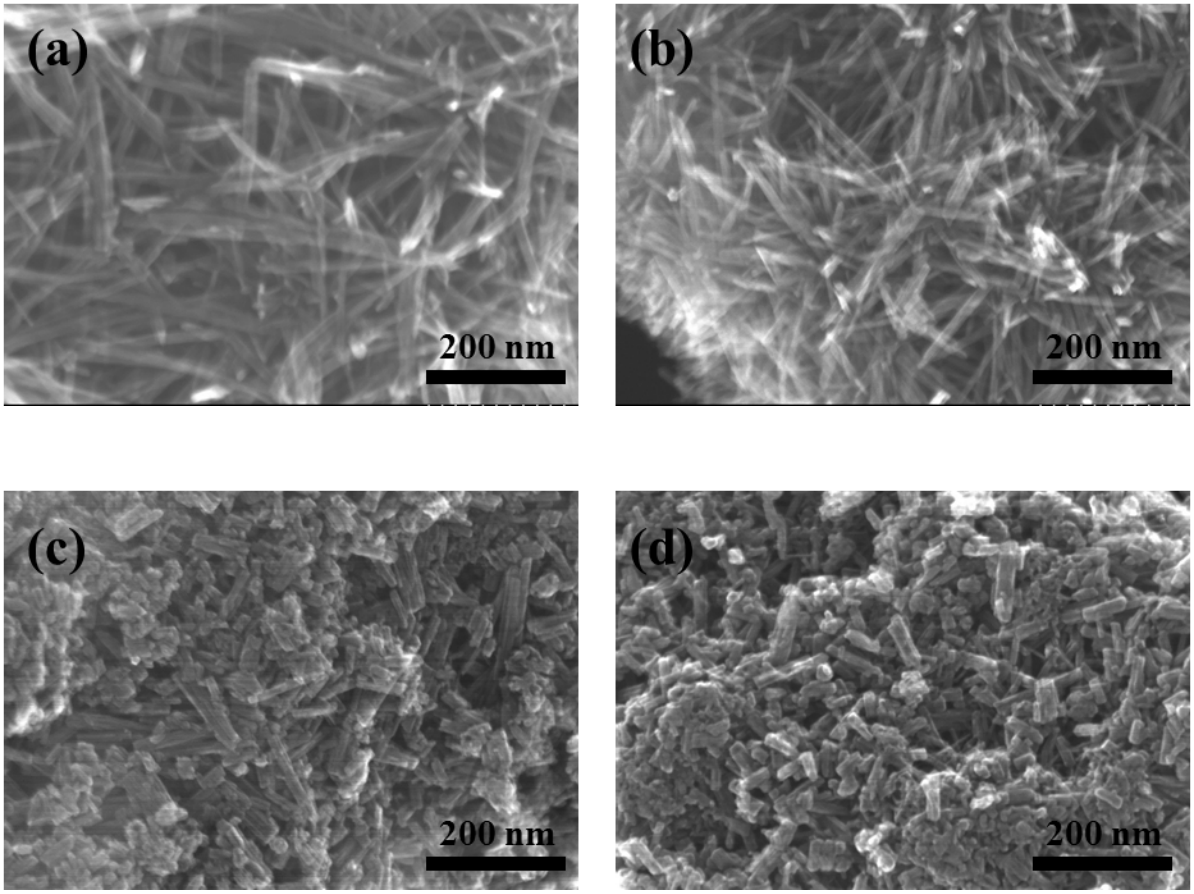


Fig. 5.4 STEM images of W-Nb-O, (a); 0.4VWNb, (b); 0.4V/WNb(pre), (c); 0.4V/WNb, (d).

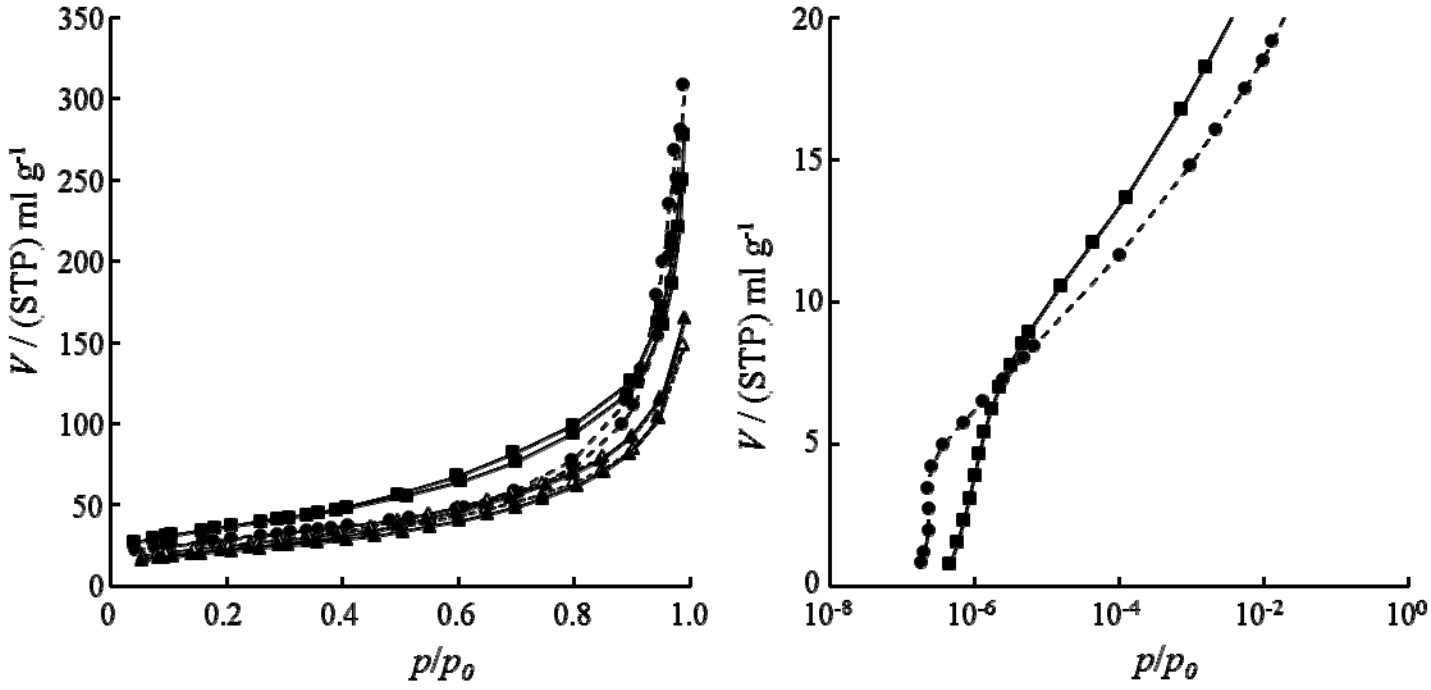


Fig. 5.5 N_2 adsorption isotherms of V-added W-Nb-O.
Symbols: W-Nb-O, ●; 0.4VWNb, ■; 0.4V/WNb (pre), △; 0.4V/WNb, ▲.

Table 5.5 Surface area of V-added W-Nb-O

Catalyst	Surface area / $m^2 \cdot g^{-1}$
W-Nb-O (W/Nb=1.35)	100
0.4VWNb	118
0.4V/WNb (pre)	78
0.4V/WNb	87
W-V-O(W/V=1.35)	8

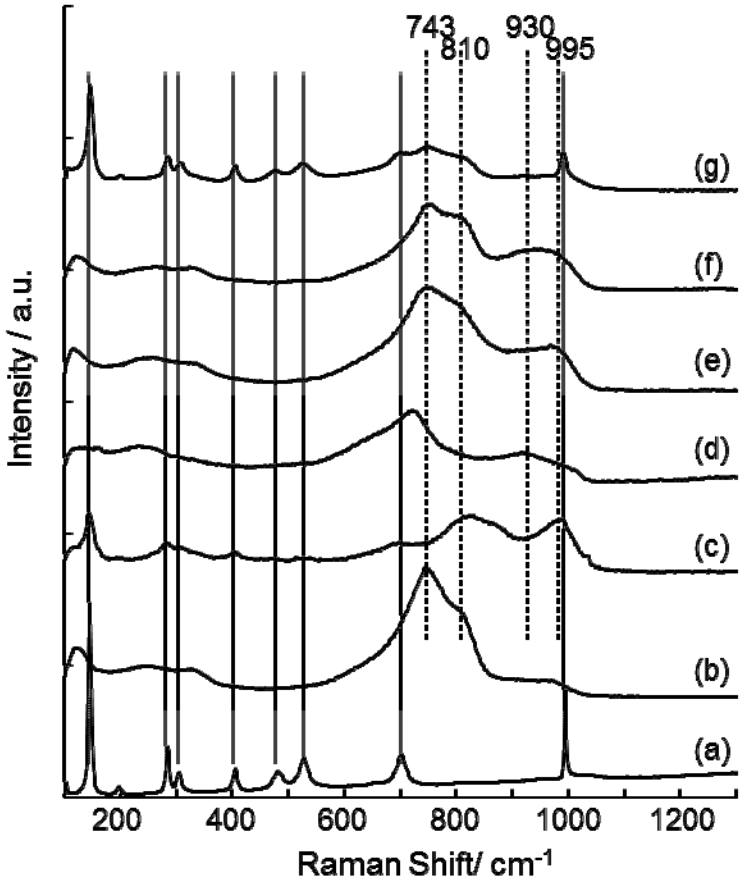


Fig. 5.6 Raman spectra of W-based complex metal oxides. V_2O_5, (a); W-Nb-O, (b); W-V-O, (c); V-Nb-O, (d); 0.4VWNb, (e); 0.4V/WNb(pre), (f); 0.4V/WNb, (g).

Table 5.6 Catalytic performance in the glycerol transformation in the absence or presence of O_2

Catalyst	O_2	R. T.[a] / K	GLR[b] conv.[c] / %	O_2 conv. / %	Yield[f] / %							
					ΛCRL	ΛΛ	ΛCΛL	PRΛL	HΛCT	ΛCΛ	CO_x	others
W-Nb-O[d]	absence	562	90.0	-	50.7	0.2	1.1	1.3	6.4	0.9	0.2	29.2
W-V-O[d]	absence	631	25.8	-	7.2	<0.1	1.1	0.3	<0.1	<0.1	0.2	17.0
0.4VWNb	absence	563	91.7	-	53.8	<0.1	0.8	1.4	7.8	<0.1	0.2	27.7
W-Nb-O[e]	presence	565	97.2	4.9	72.3	<0.1	1.8	0.7	1.6	0.4	2.9	17.5
W-V-O[e]	presence	628	100	55.0	3.3	18.2	0.8	<0.1	<0.1	14.0	53.2	10.5
0.4V/WNb[e]	presence	617	100	68.9	1.4	10.2	0.7	<0.1	<0.1	9.8	68.9	9.0
0.4V/WNb(pre)[e]	presence	612	100	60.8	6.0	11.4	1.9	<0.1	<0.1	8.9	60.1	11.7
0.4VWNb[e]	presence	596	100	51.9	0.9	33.7	0.5	<0.1	<0.1	15.2	42.7	7.0

[a] Reaction temperature. [b] GLR = glycerol. [c] Reaction conditions: catalyst weight, 0.2 g; flow rate, 80 ml·min^{-1}; time on stream, 1~2 h; composition of reaction gas, [d] GLR/ N_2/ H_2O = 5/ 70/ 25 (mol%), [e] GLR/ O_2/ N_2/ H_2O = 5/ 14/ 56/ 25 (mol%). [f] ΛCRL = acrolein, ΛΛ = acrylic acid, ΛCΛL = acetaldehyde, PRΛL = propanal, HΛCT = hydroxyacetone, ΛCΛ = acetic acid.

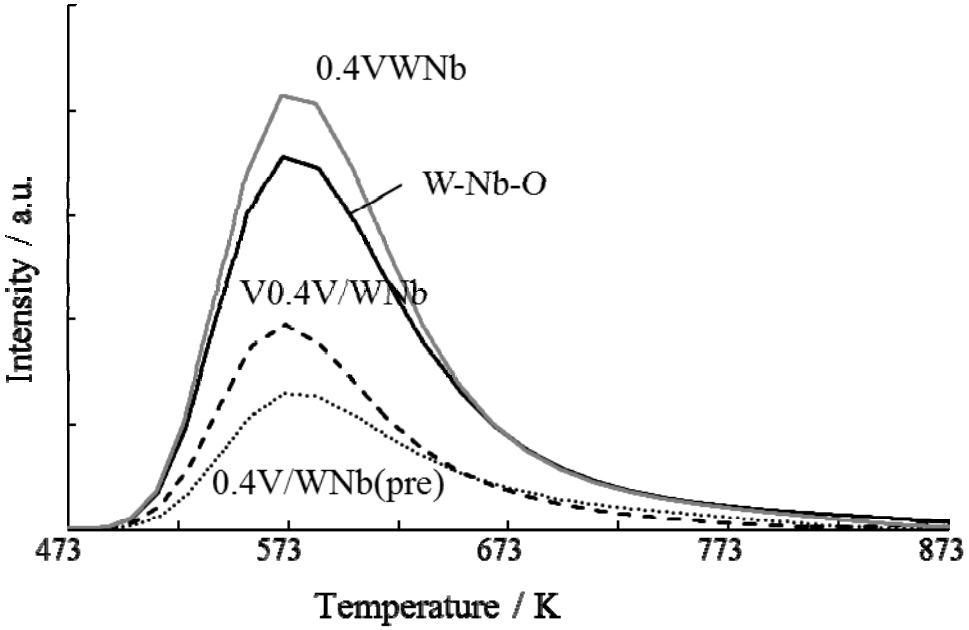


Fig. 5.7 TPD profiles of NH_3.

Table 5.7 Surface area of V-added W-Nb-O

Catalyst	Acid amount / μmol·g^{-1}
W-Nb-O (W/Nb=1.35)	136
0.4VWNb	148
0.4V/WNb(pre)	51
0.4V/WNb	64

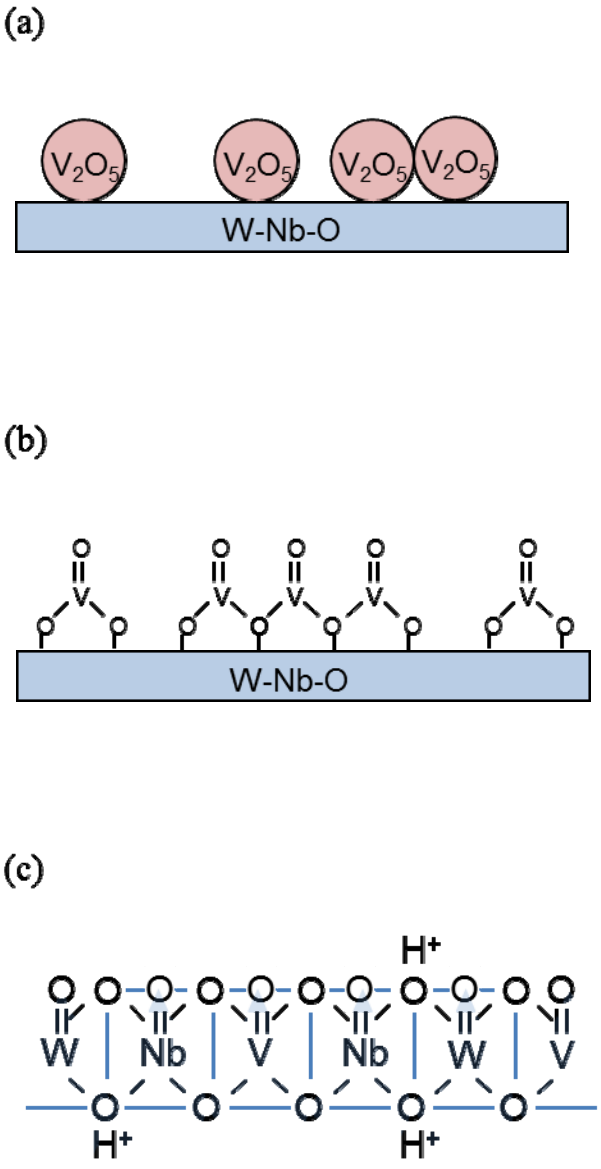


Fig. 5.8 Models for the structure of 0.4V/WNb (a), 0.4V/WNb(pre) (b) and 0.4VWNb (c).

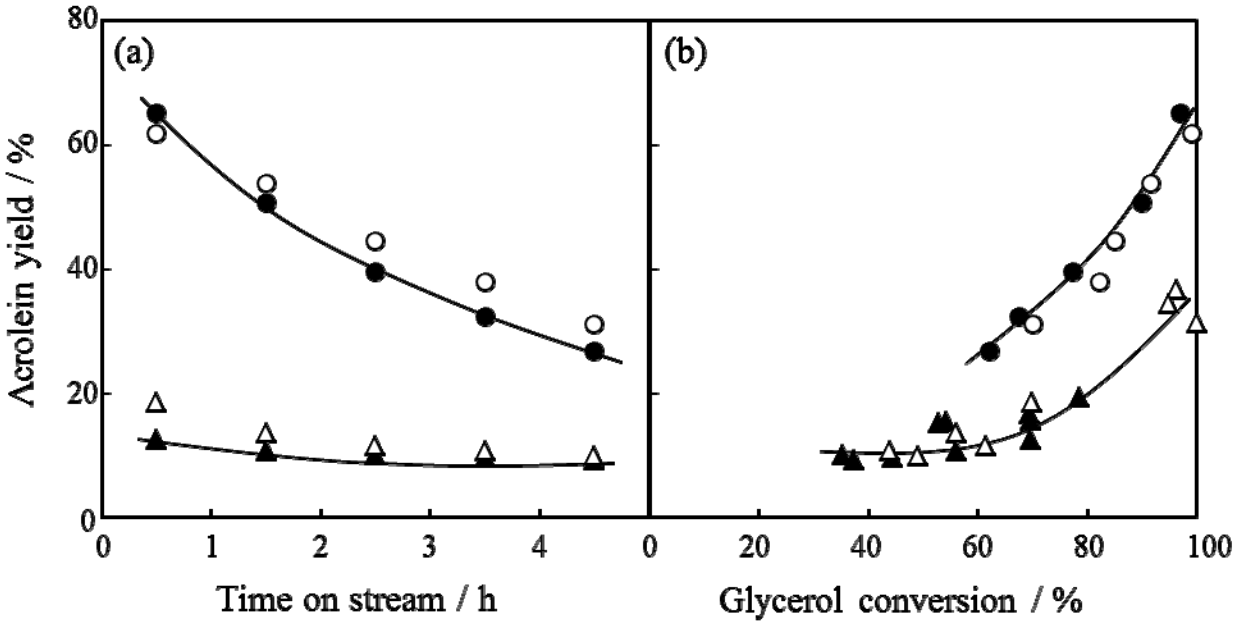


Fig. 5.9 Time courses of acrolein yield (a) and acrolein yield against glycerol conversion (b) in the glycerol transforamtion.
Symbols: W-Nb-O, ●; 0.4VWNb, ○; Nb-O , ▲; V-Nb-O (V/Nb=0.4), △.
Reaction conditions: catalyst weight, 0.2 g; flow rate, 80 ml·min^{-1}; composition of reaction gas, GLR/ N_2/ H_2O = 5/ 70/ 25 (mol%).

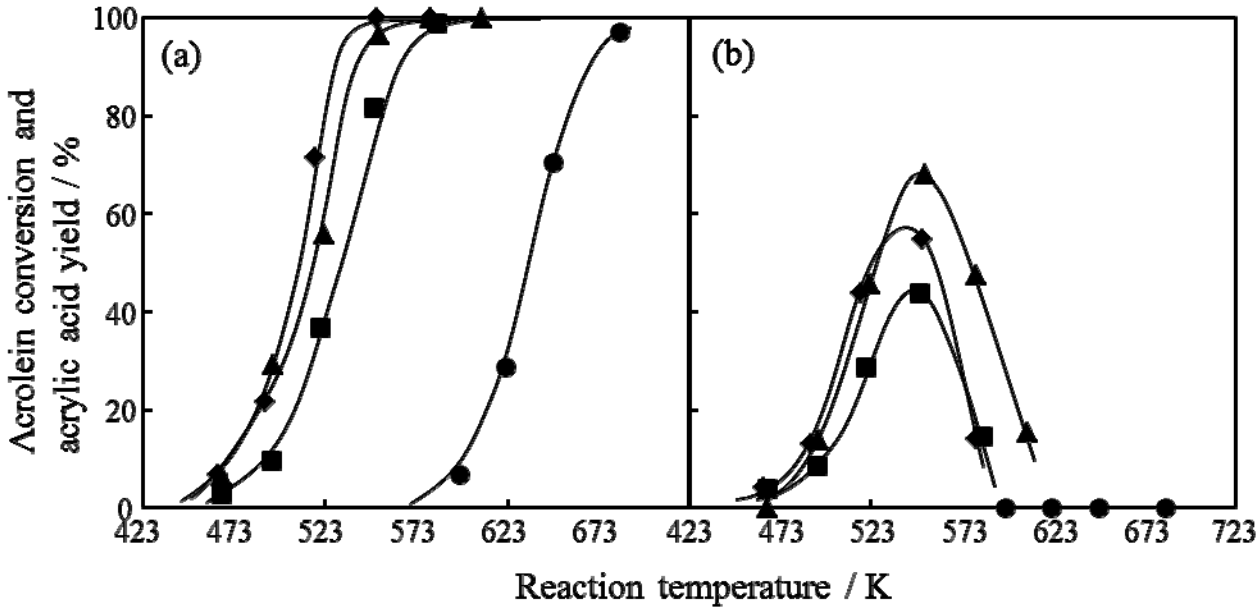


Fig. 5.10 Conversion (a) and acrylic acid yield (b) in acrolein oxidation over W-Nb-O and V-added W-Nb-O.
Reaction conditions: catalyst weight, 0.2 g; flow rate, 77 ml·min^{-1}; composition of reaction gas, acrolein : O_2 : N_2 : H_2O = 1 : 11.2 : 44.8 : 20 (ml·min^{-1}). Symbols: W-Nb-O, ●; 0.4V/WNb, ■; 0.4V/WNb(pre), ◆; 0.4VWNb, ▲.

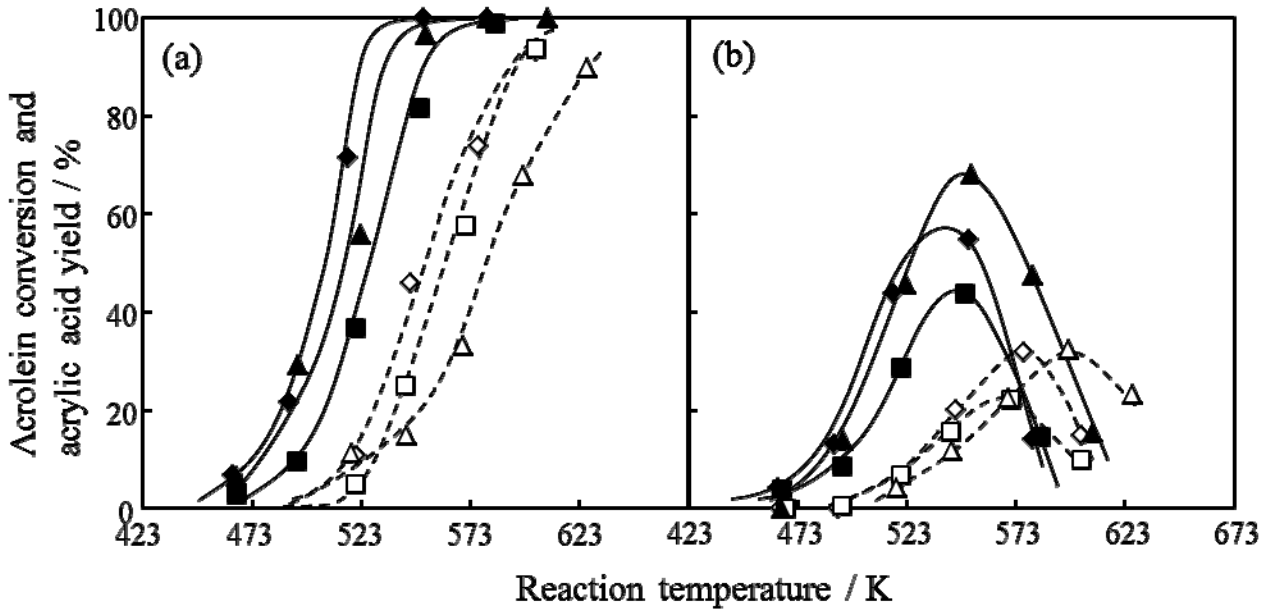


Fig. 5.11 Conversion (a) and acrylic acid yield (b) in acrolein oxidation over W-Nb-O and V-added W-Nb-O.
Reaction conditions: catalyst weight, 0.2 g; flow rate, 77 ml·min^{-1}; composition of reaction gas, acrolein : O_2 : N_2 : H_2O = 1 : 11.2 : 44.8 : 20 (ml·min^{-1}). Symbols: 0.4V/WNb, ■; 0.1V/WNb, □; 0.4V/WNb(pre), ◆; 0.1V/WNb(pre), ◇; 0.4VWNb, ▲; 0.1VWNb, △.

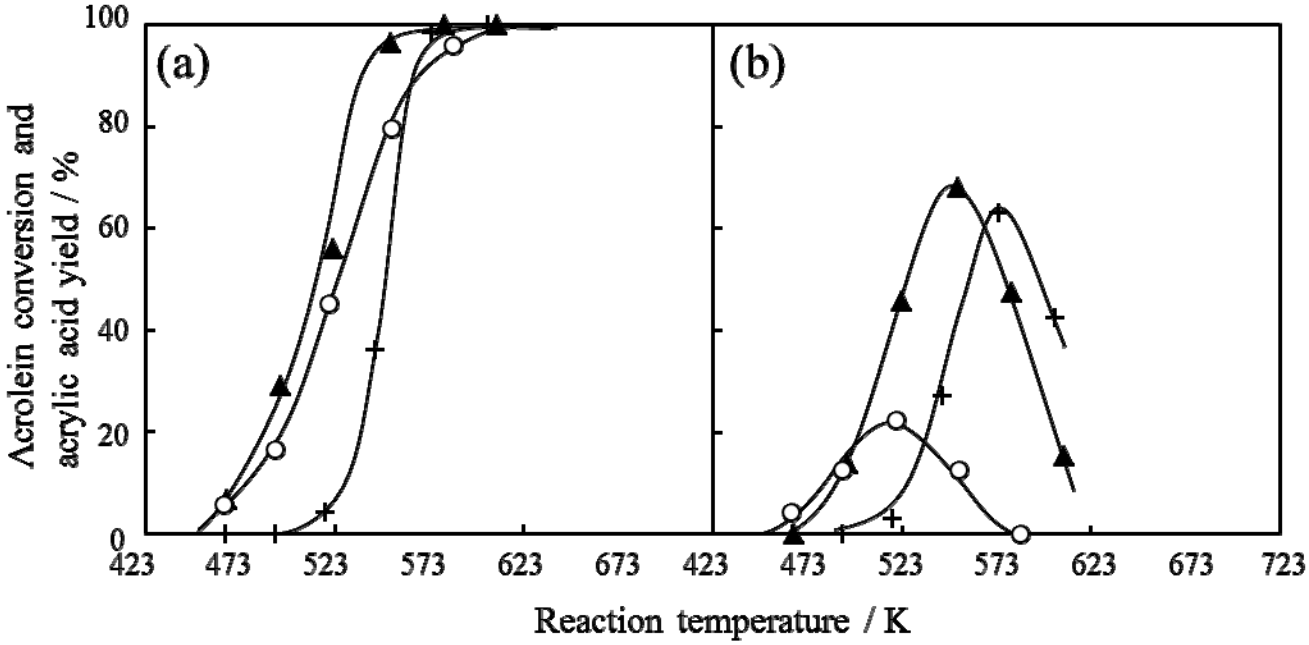


Fig. 5.12 Conversion (a) and acrylic acid yield (b) in acrolein oxidation over 0.4VWNb (▲), W-V-O (+) and V-Nb-O (○).
Reaction conditions: catalyst weight, 0.2 g; flow rate, 77 ml·min^{-1}; composition of reaction gas, acrolein : O_2 : N_2 : H_2O = 1 : 11.2 : 44.8 : 20 (ml·min^{-1}).

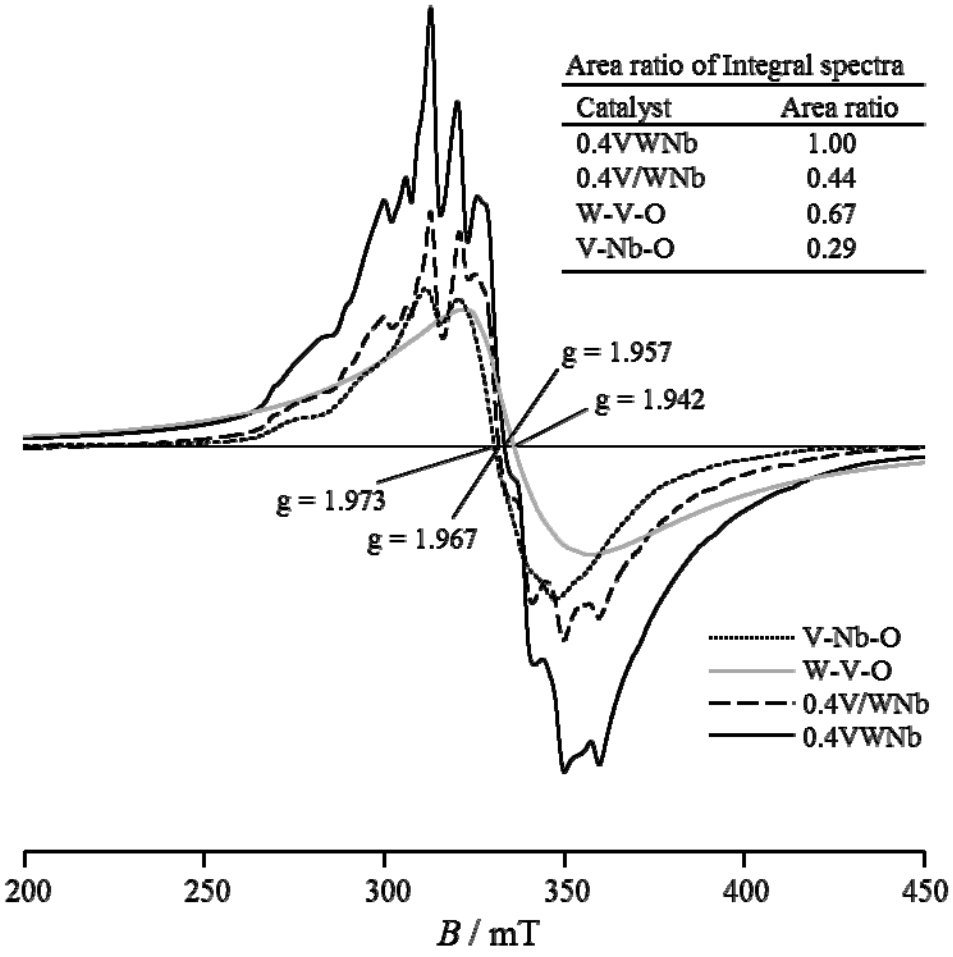


Fig. 5.13 ESR spectra of V containing catalysts.

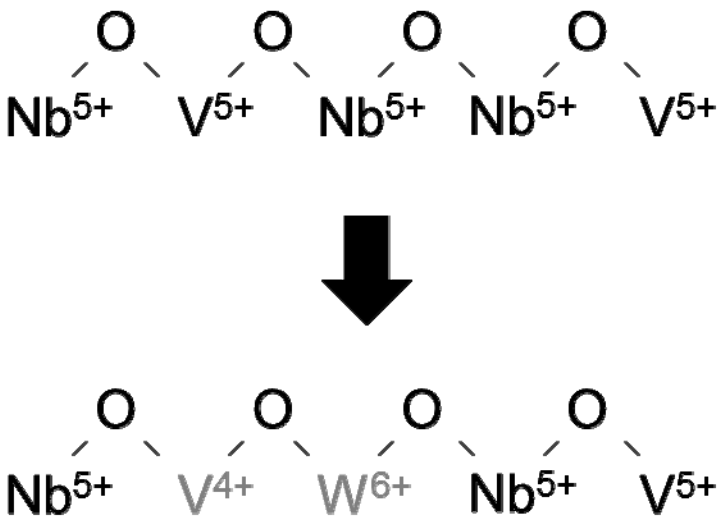


Fig. 5.14 Model for the structure of V-Nb-O influenced by dissolution of W^{6+}.

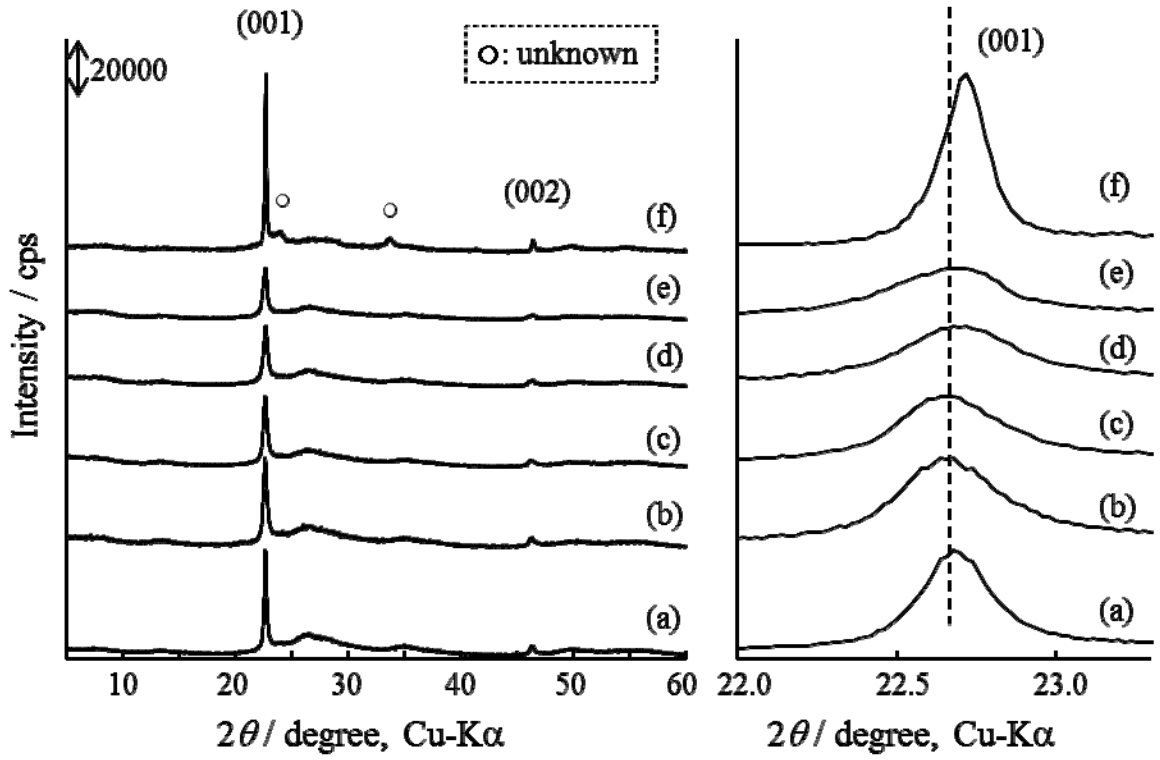


Fig. 5.15 XRD patterns of W-based complex metal oxides.
W-Nb-O (W/Nb=1.35), (a); 0.1VWNb, (b); 0.3VWNb, (c); 0.4VWNb, (d); 0.6VWNb, (e); W-V-O (W/V=1.35), (f).

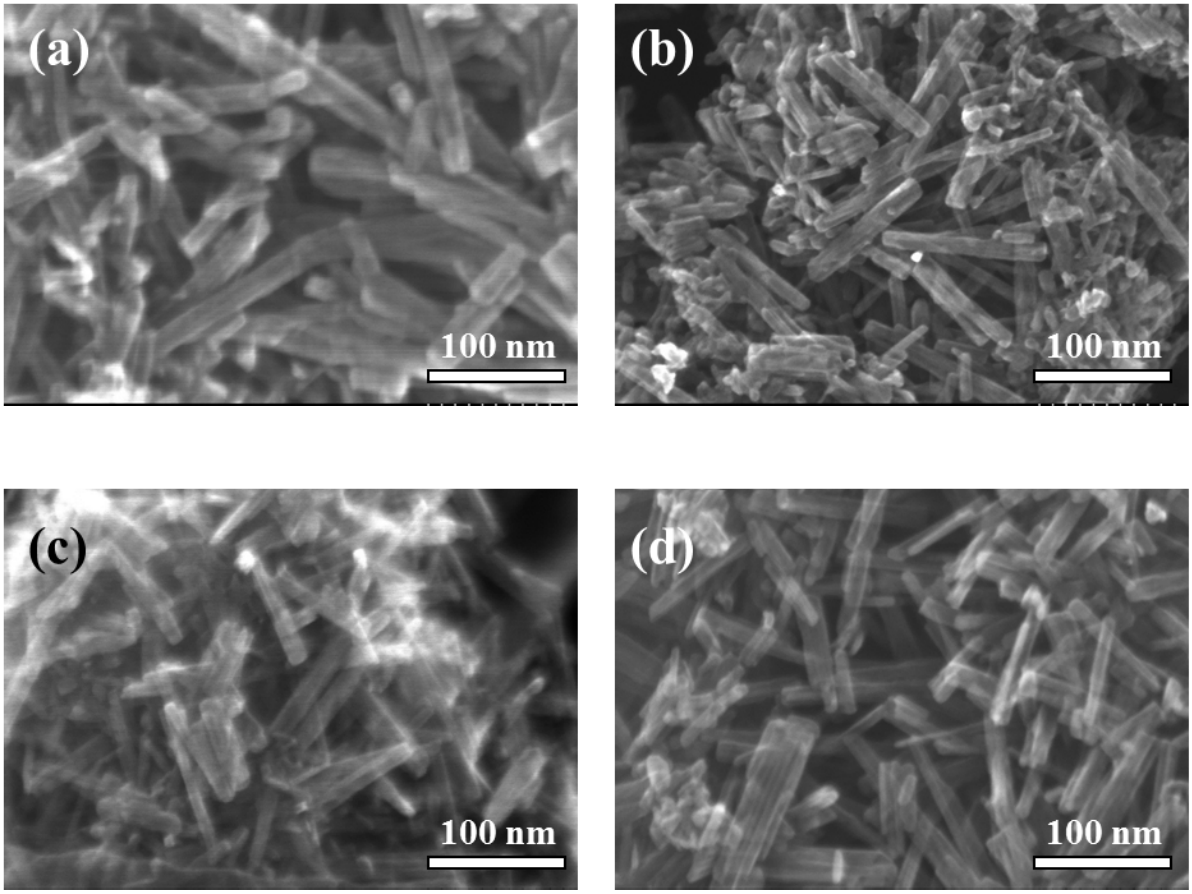


Fig. 5.16 STEM images of W-Nb-O, (a); 0.1VWNb, (b); 0.4VWNb, (c); 0.6VWNb, (d).

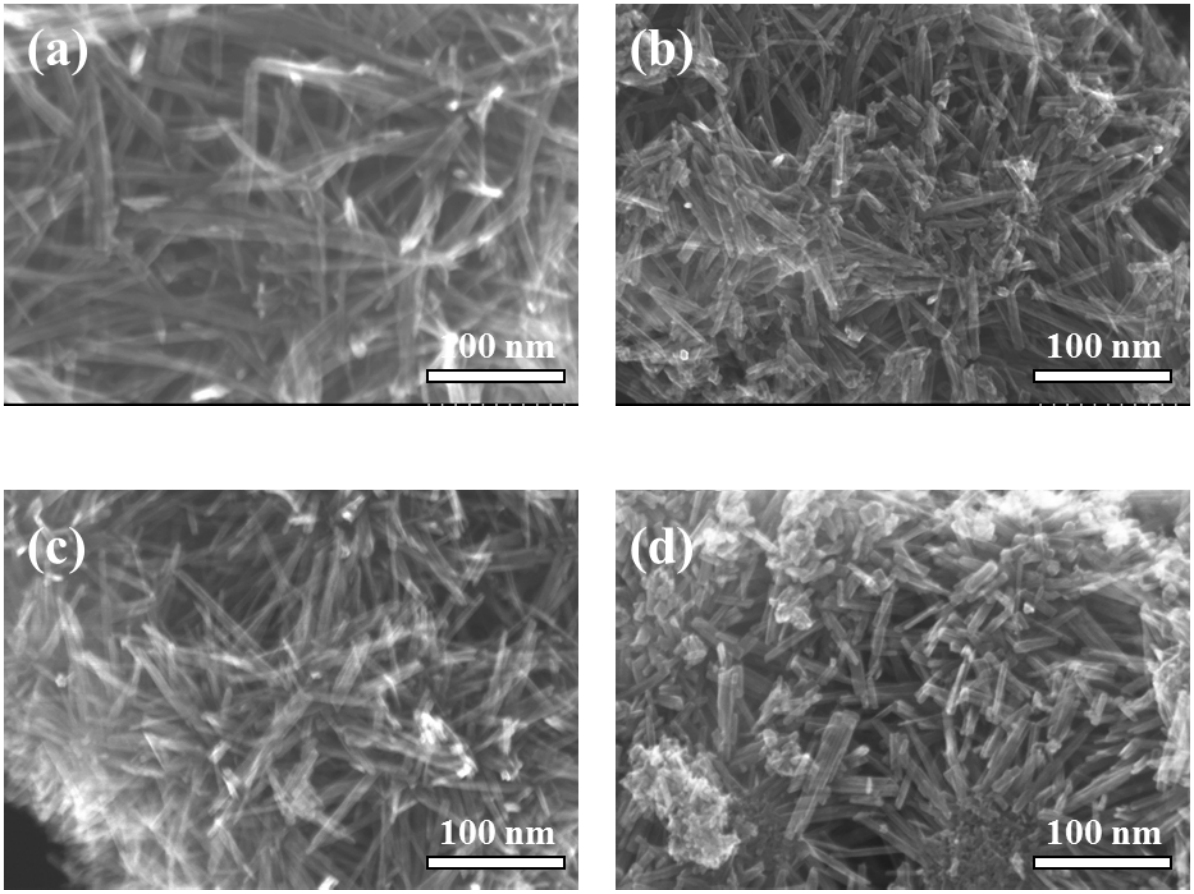


Fig. 5.17 STEM images of W-Nb-O, (a); 0.1VWNb, (b); 0.4VWNb, (c); 0.6VWNb, (d).

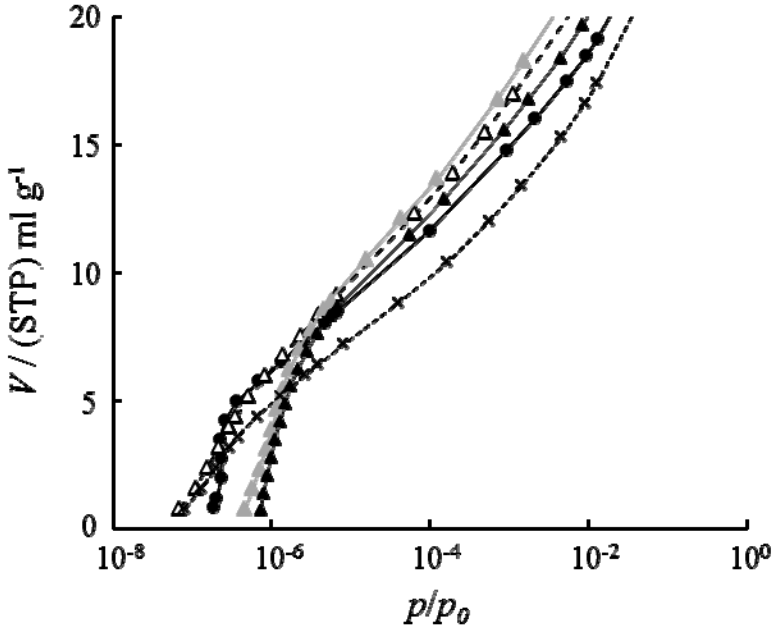


Fig. 5.18 N_2 adsorption isotherms of *x*VWNb.
Symbols: W-Nb-O, ● ; 0.1VWNb, △; 0.3VWNb, ▲; 0.4VWNb, ▲ ;0.6VWNb, ×.

Table 5.8 Surface area of V-added W-Nb-O

Catalyst	Surface area / $m^2 \cdot g^{-1}$
W-Nb-O (W/Nb=1.35)	100
0.1VWNb	118
0.3VWNb	130
0.4VWNb	118
0.6VWNb	112
W-V-O(W/V=1.35)	8

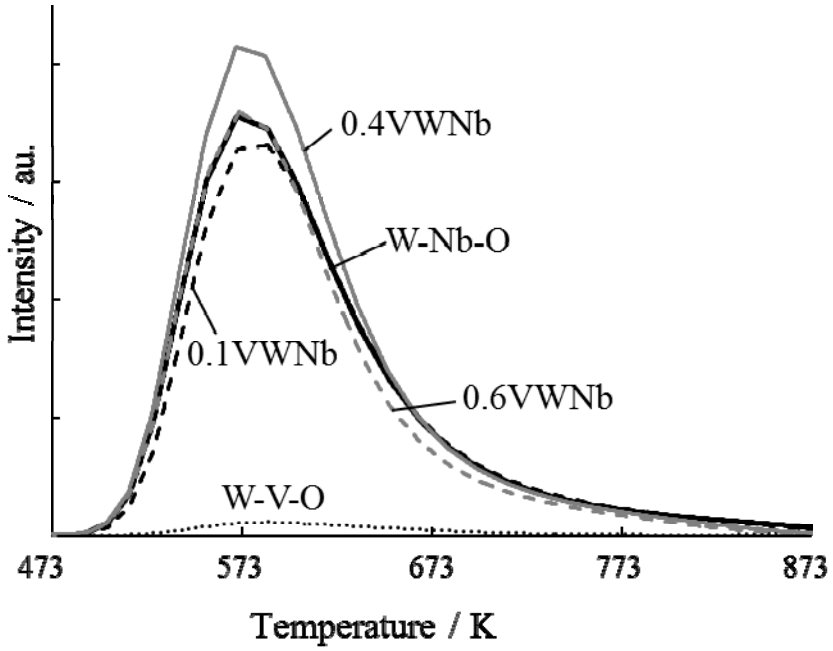


Fig. 5.19 TPD profiles of NH_3.

Table 5.9 Acid amount of V-added W-Nb-O

Catalyst	Acid amount / μmol·g^{-1}
W-Nb-O (W/Nb=1.35)	136
0.1VWNb	128
0.3VWNb	129
0.4VWNb	148
0.6VWNb	127
W-V-O(W/V=1.35)	5

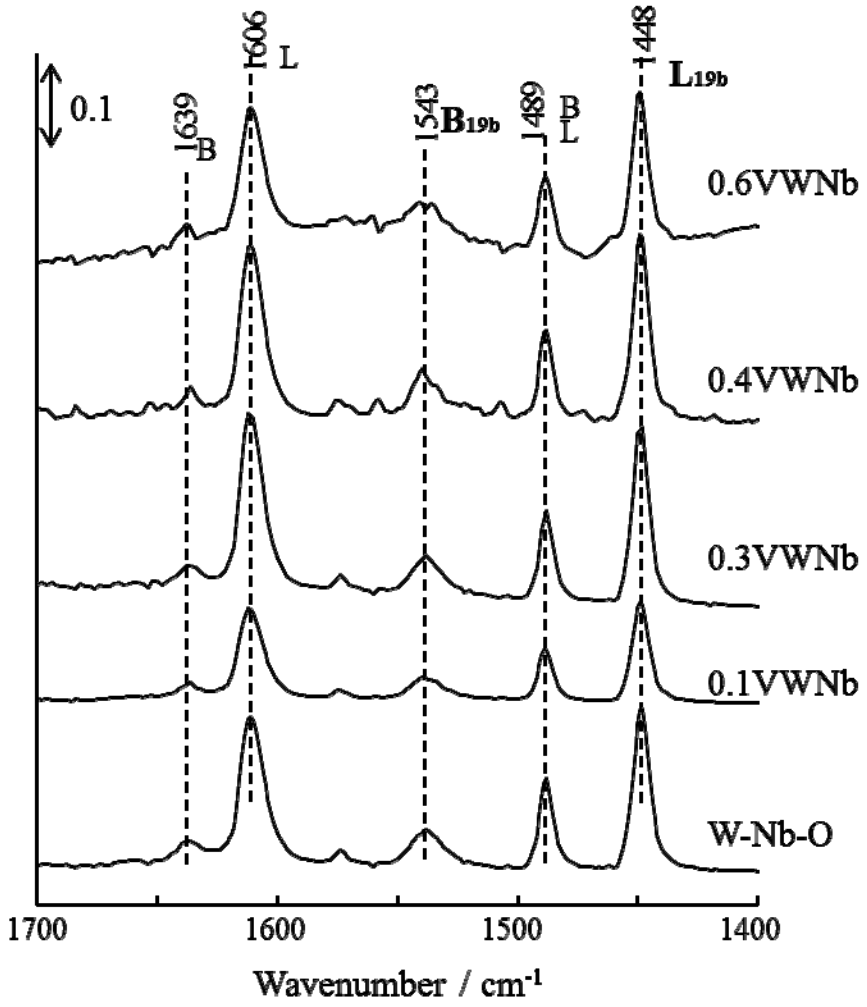


Fig. 5.20 IR spectra of pyridine on *x*VWNb.

Table 5.10 Ratio of Brönsted (B) to Lewis (L) acid amount determined by FT-IR of pyridine adsorption.

Catalyst	B / L[a]
W-Nb-O	0.29
0.1VWNb	0.28
0.3VWNb	0.30
0.4VWNb	0.27
0.6VWNb	0.29

[a] Evacuated at 523 K.

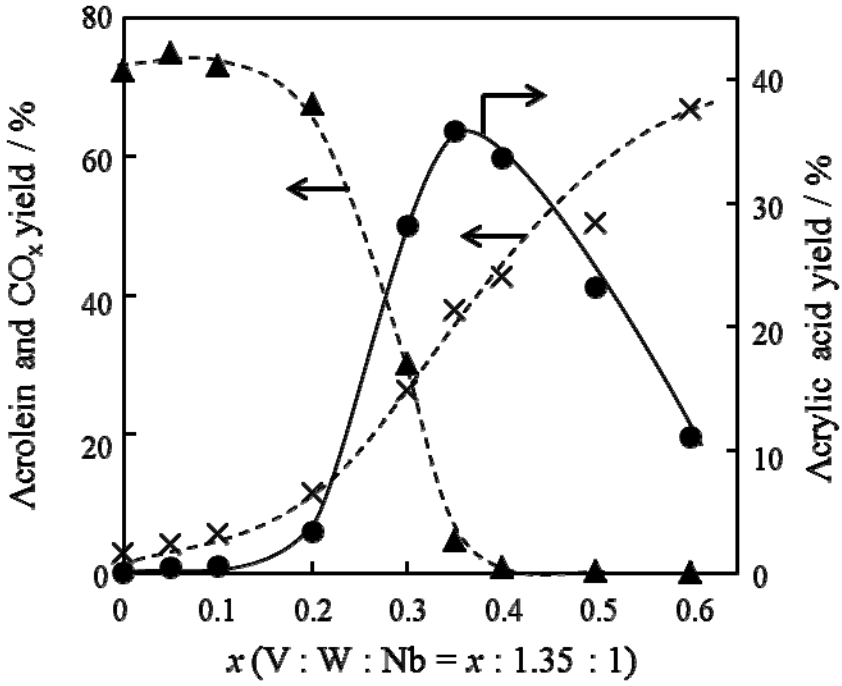


Fig. 5.21 Effect of V content on selectivity in glycerol transformation. Reaction conditions: catalyst weight, 0.2 g; flow rate, 80 ml·min^{-1}; composition of reaction gas, glycerol : O_2 : N_2 : H_2O = 4 : 11.2 : 44.8 : 20 (ml·min^{-1}). Symbols: acrolein, ▲; acrylic acid, ●; CO_x, ×.

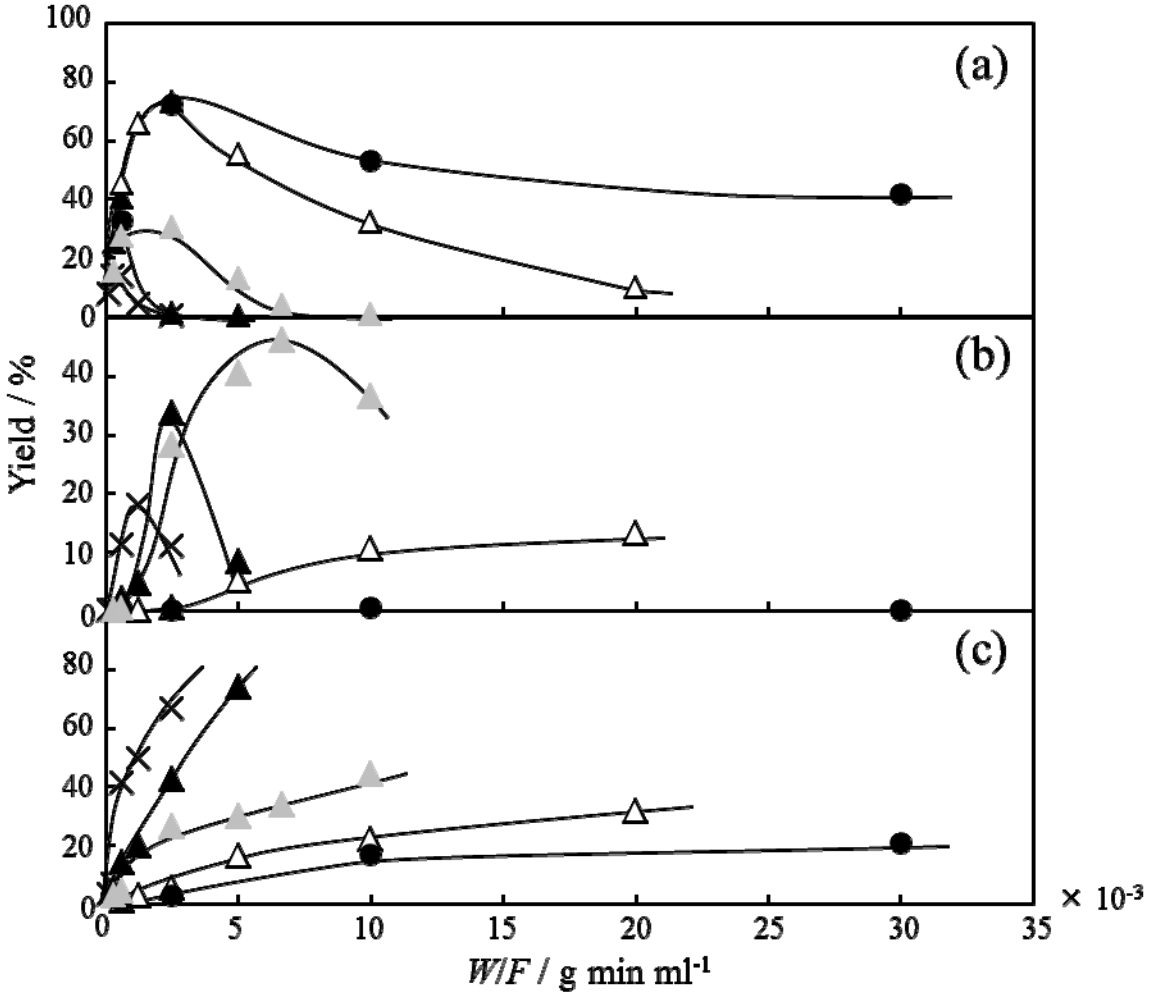


Fig. 5.22 Effect of contact time on yield of acrolein (a), acrylic acid (b) and CO_x (c) in glycerol transformation.
Symbols: W-Nb-O, ● ; 0.1VWNb, △; 0.3VWNb, ▲; 0.4VWNb, ▲ ;0.6VWNb, ×.

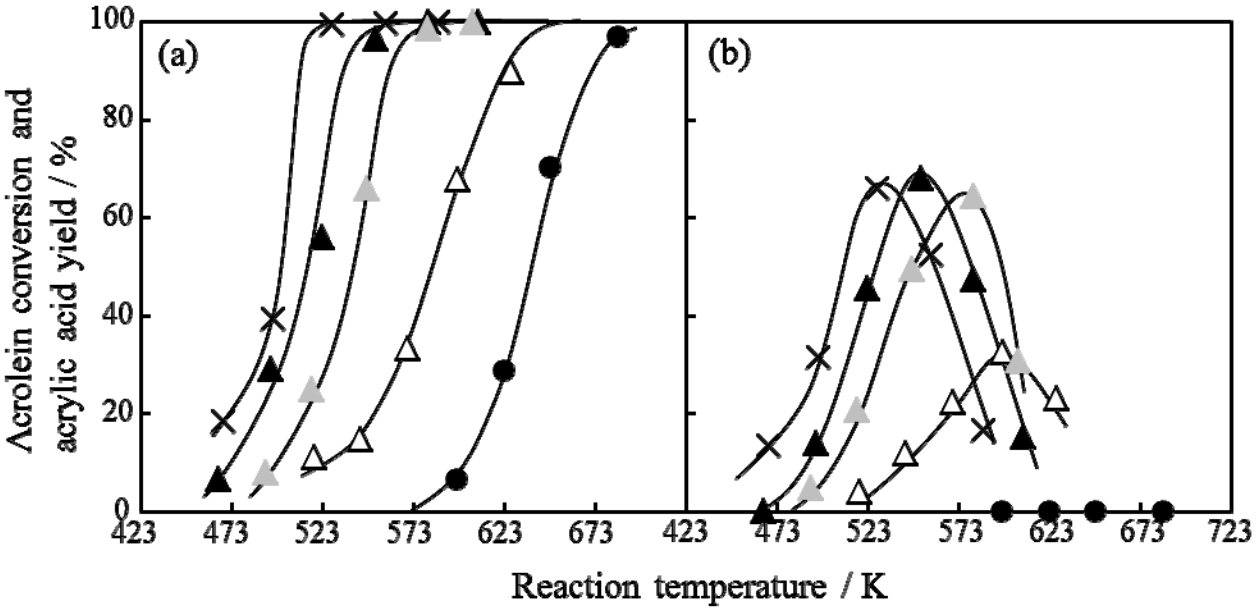


Fig. 5.23 Conversion (a) and acrylic acid yield (b) in acrolein oxidation over *x*VWNb. Reaction conditions: catalyst weight, 0.2 g; flow rate, 77 ml·min^{-1}; composition of reaction gas, acrolein : O_2 : N_2 : H_2O = 1 : 11.2 : 44.8 : 20 (ml ·min^{-1}). Symbols: W-Nb-O, ● ; 0.1VWNb, △; 0.3VWNb, ▲; 0.4VWNb, ▲ ;0.6VWNb, ×.

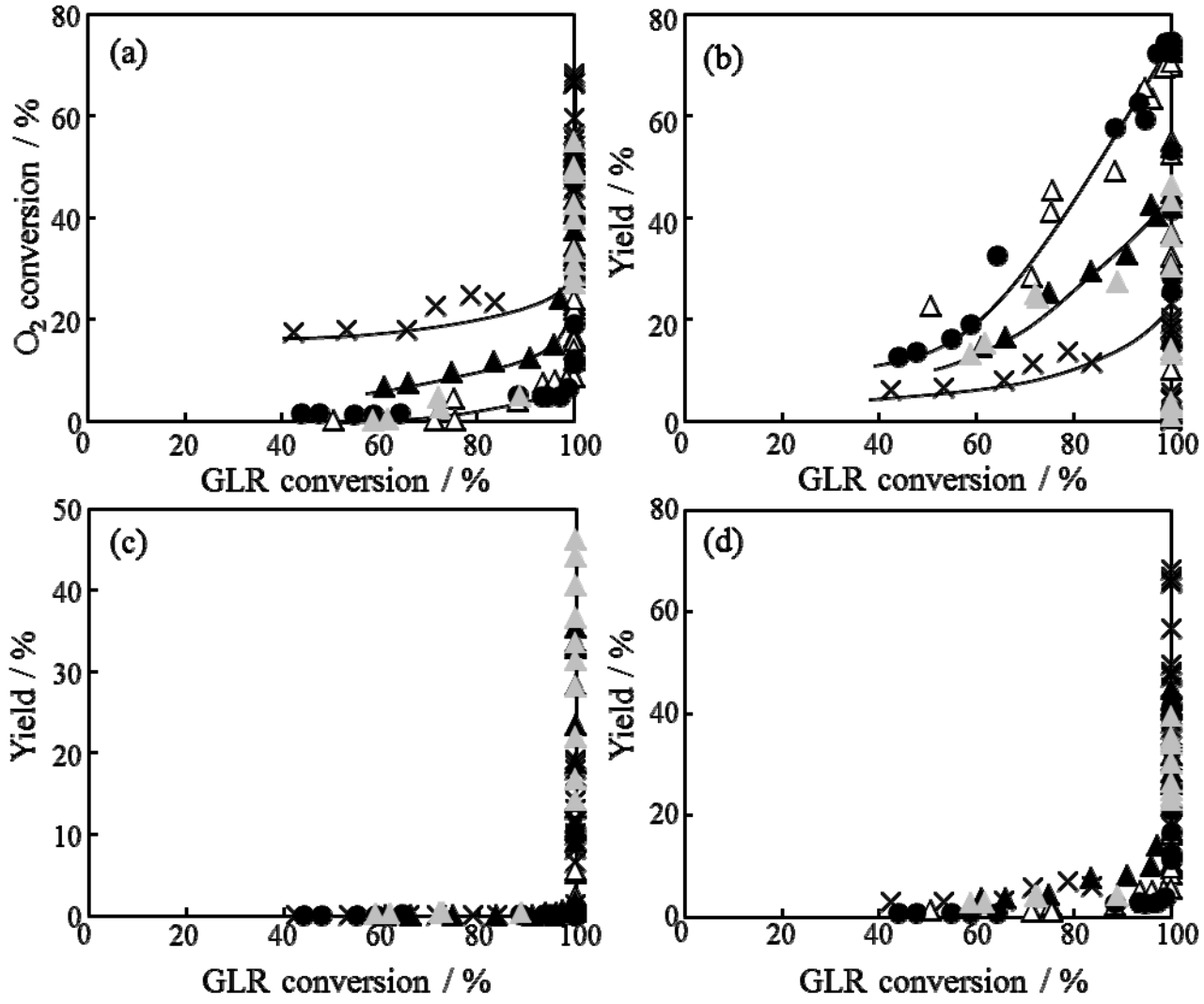
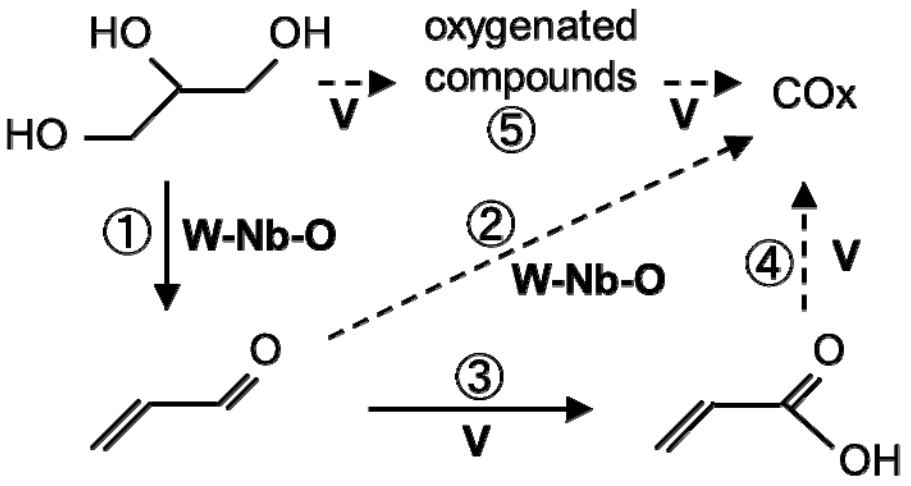


Fig. 5.24 O_2 conversion (a) and yield of acrolein (b), acrylic acid (c) and CO_x (d) in glycerol transformation.
Reaction conditions: temperature, 558 K; composition of reaction gas, glycerol / O_2 / N_2 / H_2O = 5 / 14 / 56 / 25 (mol%). Symbols: W-Nb-O, ●; 0.1VWNb, △; 0.3VWNb, ▲; 0.4VWNb, ▲; 0.6VWNb, ×.



Scheme 5.1 Reaction scheme for transformation of glycerol over *x*VWNb catalysts.

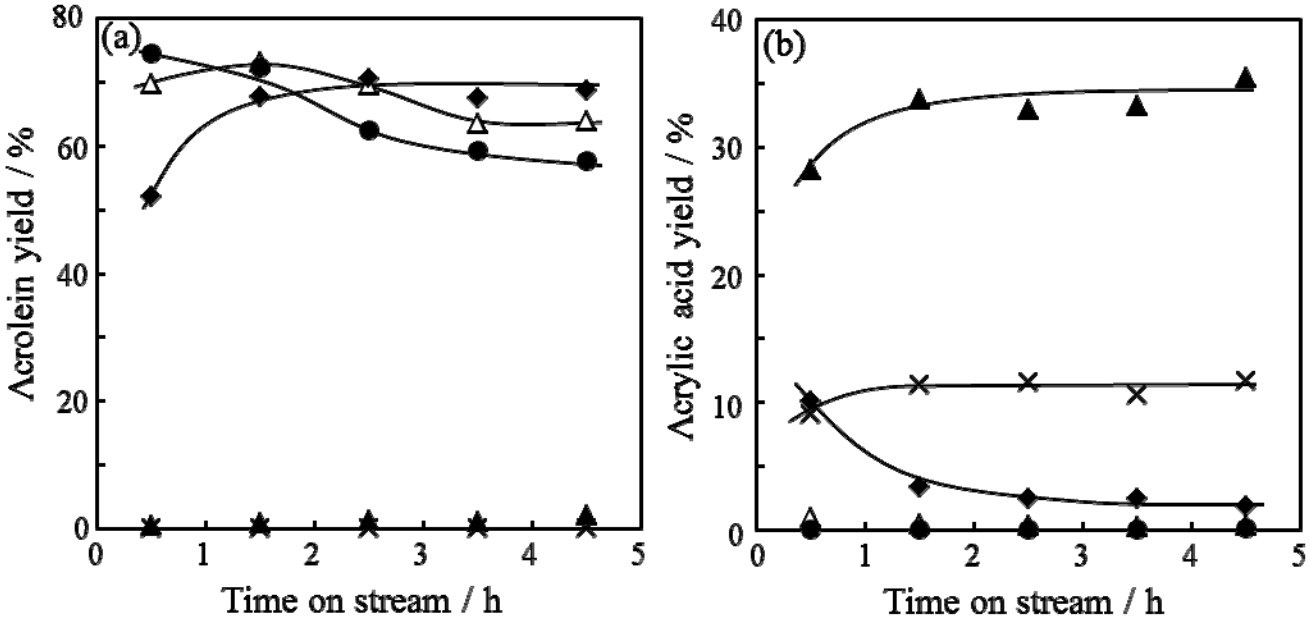


Fig. 5.25 Time courses of acrolein (a) and acrylic acid (b) yield in the glycerol transformation over *x*VWNb
Reaction conditions: set temperature of the furnace, 558 K; composition of reaction gas, glycerol / O_2 / N_2 / H_2O = 5 / 14 / 56 / 25 (mol%). Symbols: W-Nb-O, ●; 0.1VWNb, △; 0.2VWNb, ◆; 0.4VWNb, ▲; 0.6VWNb, ×.

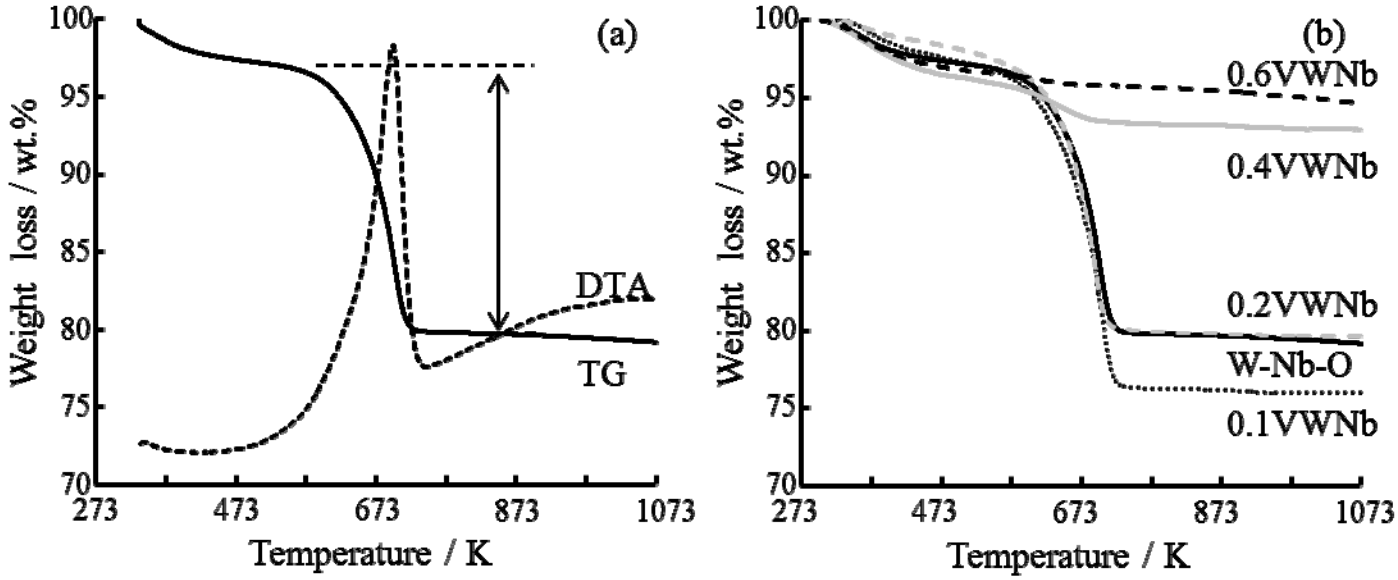


Fig. 5.26 TG and DTA curves of spent W-Nb-O (a) and TG curves of spent *x*VWNb (b).

Table 5.11 Amount of coke formed in the reaction

Catalyst	Amount of coke[a]/ $mg \cdot g_{cat}$
W-Nb-O	193.6
0.1VWNb	272.8
0.2VWNb	186.7
0.4VWNb	30.3
0.6VWNb	10.6

[a]Reaction time 5h.

Chapter 6

Transformation of Glycerol over Phosphoric Acid Added W-based Complex Metal Oxide Catalysts

6-1 Introduction

Glycerol is a main byproduct in biodiesel production by transesterification of plant oils or animal fat with methanol and has been produced heavily at a relatively low price.[1] Because of this situation, transformation of glycerol into other desirable chemicals by various catalytic reactions has been attempted by many researchers.[2] Dehydration of glycerol to acrolein is one of the most valuable reactions, since acrolein is an important intermediate for chemical and agricultural industries. Various solid acid-catalysts have been reported for the dehydration of glycerol.[3] We have reported that layer-structured W-Nb-O catalysts synthesized via hydrothermal method gave acrolein in high yield (75%) in the gas-phase glycerol dehydration.[4] Direct oxidative transformation of glycerol to acrylic acid is also a very important reaction.[5] Achievement of this reaction is, however, challenging because not only improvement of selectivity for both dehydration of glycerol and selective oxidation of acrolein but also tune of optimum catalytic functions for each reaction are required to achieve higher acrylic acid yield. Nevertheless, we have recently found that modification of the W-Nb-O catalyst with vanadium turned out to be an efficient catalyst for the direct transformation of glycerol to acrylic acid6 but the yield of acrylic acid was as low as 45%.

Very recently we found that the addition of phosphoric acid to the W-Nb-O catalyst and the W-V-Nb-O catalysts had pronounced effects both on the transformation of glycerol to acrolein and the direct transformation to acrylic acid, respectively. The achieved single pass yield of acrylic acid was about 60% and is currently the highest amongst the reported results. This paper reports the effects of phosphoric acid addition to the W-Nb-O catalyst and the W-V-Nb-O catalysts on the selectivity in the glycerol transformation.

6-2 Experimental

6-2-1 Chemicals

Chemicals used in experiments are listed in Table 6.1.

Table 6.1 List of chemicals

chemical	formula or molar wt.	assay	manufacturer	No.
H_3PO_4	98.00	85.0%	Wako Pure Chemical Ind., Ltd.	167-02166
glycerol (for reaction)	92.09	97.0%	Wako Pure Chemical Ind., Ltd.	072-00626
glycerol (for calibration)	92.09	99.0%	Wako Pure Chemical Ind., Ltd.	075-00616
2-butanol	74.12	99.0%	Wako Pure Chemical Ind., Ltd.	020-11215
propylenegrycol	76.09	99.5%	Kanto Chemical Co., Ltd.	32458-00
acrolein	56.06	90%	Tokyo Chemical Ind. Co., Ltd.	A0137
hydroxyacetone	74.08	90.0%	Wako Pure Chemical Ind., Ltd.	089-05492
acetaldehyde	44.05	88.0~92.0%	Wako Pure Chemical Ind., Ltd.	015-09576
propionaldehyde	58.08	-	Tokyo Chemical Ind. Co., Ltd.	P0498
acetone	58.08	99.5%	Wako Pure Chemical Ind., Ltd.	012-00343
acetic acid	60.05	99.7%	Wako Pure Chemical Ind., Ltd.	017-00256
acrylic acid	72.06	99%	Tokyo Chemical Ind. Co., Ltd.	A0141
sea sand (50~80 mesh)	-	99.0%(SiO_2)	Miyazaki Chemical Co., Ltd	M5080KA05

6-2-2 Catalyst preparation

6-2-2-1 Addition of phosphoric acid to W-Nb-O and W-V-Nb-O

Phosphoric acid-added catalysts were prepared by impregnation method of uncalcined W-Nb-O or W-V-Nb-O with an aqueous solution of phosphoric acid, followed by calcination at 673 K in air. Phosphoric acid-added W-Nb-O and W-V-Nb-O were denoted by H_3PO_4/WNb and H_3PO_4/WVNb, respectively. The content of P was set to be 2.5 wt.% of the supports after optimization of P-content. XRD analysis confirmed that the layered structure of the W-Nb-O and W-V-Nb-O catalysts was maintained after the phosphoric acid treatment.

6-2-3 Catalyst characterization

6-2-3-1 XRD

Powder X-ray diffraction (XRD) pattern of the catalysts was recorded on RINT2200 (Rigaku) with Cu Kα (λ = 0.154 nm) radiation (tube voltage: 40 kV, tube current: 20 mA).

6-2-3-2 Nitrogen adsorption

Surface area of the catalysts was estimated by BET method where nitrogen adsorption amount was measured at 77 K with a BEL max 00094 (BEL Japan Inc.). Prior to the measurement, the samples were evacuated at 473 K for 2 h.

6-2-3-3 STEM

Scanning transmission electron microscopy (STEM) images were obtained with a HD-20000 (HITACHI).

6-2-3-4 NH_3-TPD

The acid amount of catalysts was measured by NH_3-TPD with a TPD apparatus (BEL Japan Inc.). Prior to the measurement, the samples were pretreated under He flow at 673 K for 2 h. 100 torr of ammonia was equilibrated with the pretreated sample at 473 K and evacuated for 5 min. The TPD data were collected at temperature ramp rate of 10 $Kmin^{-1}$ under differentially-pumped He (50 ml min^{-1} (STP)) flow at ca.180 torr. A mass spectrometer (ANELVA M-100OA-F) was used to measure the desorbed NH_3 at m/e = 16. The acid amount of catalyst was calculated on the basis of the acid amount of H-ZSM-5(JRC-Z5-90H) (345 $\mu molg^{-1}$).

6-2-3-5 FT-IR spectroscopy of adsorbed pyridine

Acidity of catalysts was measured by FT-IR spectroscopy (PARAGON 1000, Perkin Elmer) of adsorbed pyridine with an evacuable furnace cell with CaF_2 windows, containing a self-supporting disk (with 12 mm diameter) of sample (50 mg) as shown in Fig. 3.1. Prior to the measurement, the samples were pretreated under vacuum at 623 K for 1 h. 4.4 torr of pyridine was adsorbed at 373 K and after evacuation at 423 K for 1 h, the adsorption spectrum was recorded followed by the measurement of the spectrum of adsorbed pyridine on sample in the presence of water vapor (4.6 torr). The spectra of adsorbed pyridine after evacuation at 523 and 623 K were similarly recorded

6-2-4 Catalytic testing

6-2-4-1 Transformation of glycerol

Transformation of glycerol was carried out in a vertical fixed-bed reactor (Fig. 3.2). A mixture of 0.02~0.80 g of catalyst powder and sea sand (catalyst + sea sand = 2 ml) was set in a Pyrex glass tube with 12 mm internal diameter and pretreated at 573 K for 0.5 h in flowing 20% O_2/N_2 before the reaction. A glycerol-water 1:5 (mol/mol) solution was fed into the top of reactor with a micro feeder. Pure N_2 or O_2/N_2 was introduced with glycerol vapor with mass flow controllers (KOFLOC). The molar composition of reaction gas was glycerol: N_2: H_2O = 5: 70: 25 (absence O_2) or glycerol: O_2: N_2: H_2O = 5: 14: 56: 25 (presence O_2). Reaction products and unconverted glycerol in both gas and liquid phase were collected hourly in an ice trap (273 K) and a Tedlar bag connected at the end of the trap. Products in the liquid phase were analyzed with FID-GC (GL science GC353, 30 m 0.32 mm TC-WAX capillary column). Products in the gas phase were analyzed with FID-GC (Shimadzu GC14B, Gaskuropak54 column) and TCD-GC (Shimadzu GC8A, Porapak QS and MS-13X column). Glycerol conversion and product selectivities and yields were calculated by Eqs. (6.1) - (6.3).

$$\text{Glycerol conversion } (\%) = \frac{\text{Moles of glycerol reacted}}{\text{Moles of glycerol fed}} \times 100 \qquad (6.1)$$

$$\text{Product selectivity}\,(\%) = \frac{\text{Moles of carbon in a product defined}}{\text{Moles of carbon in glycerol reacted}} \times 100 \qquad (6.2)$$

$$\text{Product yield}\,(\%) = \frac{\text{Moles of carbon in a product defined}}{\text{Moles of carbon in glycerol fed}} \times 100 \qquad (6.3)$$

6-2-4-2 Oxidation of acrolein

Oxidation of acrolein was carried out in the same reactor as the transformation of glycerol. Reaction conditions were: catalyst weight, 0.2 g; reaction temperature, 458~658 K; total flow rate, 77 ml·min^{-1}; molar composition of reaction gas, acrolein: O_2: N_2: H_2O = 1: 15: 58: 26. Acrolein conversion and product selectivities and yields were calculated by Eqs. (6.4) - (6.6).

$$\text{Acrolein conversion}\,(\%) = \frac{\text{Moles of acrolein reacted}}{\text{Moles of acrolein fed}} \times 100 \qquad (6.4)$$

$$\text{Product selectivity}\,(\%) = \frac{\text{Moles of carbon in a product defined}}{\text{Moles of carbon in acrolein reacted}} \times 100 \qquad (6.5)$$

$$\text{Product yield}\,(\%) = \frac{\text{Moles of carbon in a product defined}}{\text{Moles of carbon in acrolein fed}} \times 100 \qquad (6.6)$$

6-3 Results and discussion

The catalytic performance of the W-Nb-O and H_3PO_4/WNb catalysts in the glycerol transformation was first examined and the results are shown in Table 6.1. Both the glycerol conversion and the acrolein yield were clearly increased by the phosphoric acid addition and the H_3PO_4/WNb catalyst gave the acrolein in yield of 81.8% at W/F= 2.5×10^{-3} g_{cat} min·ml^{-1}. The improvement can be explained by changes in the surface acid property because of the following results. As shown in Table 6.2, the number of acid sites per gram largely increased by the addition of phosphoric acid. At the same time, the addition increased the ratio of Brönsted to Lewis acidity. Moreover, it was observed in the FT-IR study that water substantially decreased the intensity of the IR-band ascribed to the adsorption of pyridine on Lewis acid sites and on the other hand increased the intensity of IR-band ascribed to that on Brönsted acid sites. The result indicates that Lewis acid site is hydrated and changes into Brönsted acid site in the presence of water. This change more clearly occur over H_3PO_4/WNb and in fact Lewis acidity was hardly observed on H_3PO_4/WNb in the presence of water vapor. The same effect of the phosphoric acid addition was observed in the case of W-V-Nb-O as shown in Table 6.2. As a consequence, such high Brönsted acid character of H_3PO_4/WNb and H_3PO_4/WVNb should be beneficial for the catalytic reaction, since it is considered that Brönsted acid sites are responsible for the glycerol transformation to acrolein. The observed clear effect of water on the surface acid property in the case of H_3PO_4/WNb is interesting but actual function of surface H_3PO_4 is under investigation.

Next, the catalytic performance of the W-V-Nb-O and H_3PO_4/WVNb catalysts in the direct glycerol transformation to acrylic acid was examined and the results are also shown in Table 6.1. Like as acrolein formation, addition effect of H_3PO_4 is also prominent. The attained maximum yield of acrylic acid was 59.2% at W/F= 1.0×10^{-2} g_{cat} min·ml^{-1}. The performance of this catalyst was the highest in the catalysts reported for the direct transformation of glycerol to acrylic acid.[5] Additional importance is that the yield of acrylic acid was kept almost constant during 5 hours of the reaction; that is, no deactivation within this reaction period, while appreciable deactivation in the transformation of glycerol to acrolein.

Fig. 6.1 illustrates the yield of acrolein and acrylic acid in the glycerol transformation under the various contact time over the W-V-Nb-O and H_3PO_4/WVNb catalysts. Acrylic acid yield increased with decreasing acrolein yield over both W-V-Nb-O and H_3PO_4/WVNb, indicating that acrolein formed on acid sites was consecutively oxidized to acrylic acid on V sites. Over the W-V-Nb-O catalyst, acrylic acid yield reached the maximum value (46.2%) when acrolein was mostly consumed at $W/F = 6.7\times10^{-3}$ g_{cat} min·ml^{-1}. At a contact time above $W/F = 6.7\times10^{-3}$ g_{cat} min· ml^{-1}, the acrylic acid yield decreased because the sequential oxidation to CO_x started. Over H_3PO_4/WVNb, on the other hand, 15.3% yield of acrolein was still sustained at $W/F = 6.7\times10^{-3}$ g_{cat} min·ml^{-1}, and a further increase of the contact time increased the acrylic acid yield. Then the yield of acrylic acid reached 59.2% at $W/F= 1.0\times10^{-2}$ g_{cat} min·ml^{-1}.

The results shown in Fig. 6.1 evidently indicate the sequential reactions from glycerol to acrylic acid via acrolein and ultimately to CO_x. In order to elucidate the role of phosphoric acid in this course of the transformation, we separately conducted acrolein oxidation over W-V-Nb-O and H_3PO_4/WVNb. Fig. 6.2 shows the conversion of acrolein and the yield of acrylic acid and CO_x in the oxidation of acrolein. The difference of acrolein conversion was little observed between W-V-Nb-O and H_3PO_4/WVNb, while the maximum acrylic acid yield was improved from 64.4% (581 K) over W-V-Nb-O to 71.7% (577 K) over H_3PO_4/WVNb. This indicates that phosphoric acid enhances not only the selectivity to acrolein in the glycerol transformation but also the selectivity to acrylic acid in the acrolein oxidation. It should be noted in Fig. 6.2 that over W-V-Nb-O acrylic acid yield decreased drastically at a reaction temperature above 581 K but this decrease was retarded appreciably over H_3PO_4/WVNb. It is clear that the phosphoric acid can suppress the sequential over-oxidation of acrylic acid to CO_x which would inevitably occur on V site of the catalysts.

6-4 Conclusion

The addition of phosphoric acid increased the acid amount and the Brönsted acidity of the W-Nb-O catalyst. In addition to the improvement of the acidity, phosphoric acid interacts with V sites for suppressing the sequential oxidation of acrylic acid to CO_x. As a result, acrylic acid yield in the glycerol transformation increased significantly. The H_3PO_4/WVNb catalyst gave acrylic acid in yield of 59.2% directly from glycerol (W/F = 1.0×10^{-2} g_{cat} min·ml^{-1}, reaction temperature 594 K).

6-5 References

[1] B. Katryniok, S. Paul, V. Belli`ere-Baca, P. Reye and F. Dumeignil, *Green Chem.* **2010**, *12*, 2079.

[2] a) S. Gil, M. Marchena, L. S-Silva, A. Romero, P. Sánchez, J. L. Valverde, *Chem. Eng. J.* **2011**, *178*, 423. b) A. C.-C. Chang, W.-H. Lin, K.-H. Lin, C.-H. Hsiao, H.-H. Chen, H.-F. Chang, *Int. J. Hydrogen Energy* **2012**, *37*, 13110. c) Y. Kusunoki, T. Miyazawa, K. Kunimori, K. Tomishige, *Catal. Commun.* **2005**, *6*, 645. d) M. S. Khayoon, B. H. Hameed, *Appl. Catal. A* **2012**, *433*, 152. e) M. Kapoor, M. N. Gupta, *Process Biochem.* **2012**, *47*, 503. f) H. J. Lee, D. Seung, K. S. Jung, H. Kim, I. N. Filimonov, *Appl. Catal. A* **2010**, *390*, 235. g) A. Martin, M. Richter, *Eur. J. Lipid Sci. Technol.* **2011**, *113*, 100. h) T. Tago, T. Masuda, WO 2011108509, **2011.**

[3] a) Y. T. Kim, K.-D. Jung, E. Duck Park, *Appl. Catal. A* **2011**, *393*, 275. b) C.-J. Jia, Y. Liu, W. Schmidt, A.-H. Lu, F. Schüth, *J. Catal.* **2010**, *269*, 71. c) E. Tsukuda, S. Sato, R. Takahashi, T. Sodesawa, *Catal. Commun.* **2007**, *8*, 1349. d) A. Alhanash, E. F. Kozhevnikova, I. V. Kozhevnikov, *Appl. Catal. A* **2010**, *378*, 11. e) M. Massa, A. Andersson, E. Finocchio, G. Busca, F. Lenrick, L. R. Wallenberg, *J. Catal.* **2013**, *297*, 93. f) A. Ulgen, W. F. Hoelderich, *Appl. Catal. A* **2011**, *400*, 34. g) F. Cavani, S. Guidetti, L. Marinelli, M. Piccinini, E. Ghedini, M. Signoretto, *Appl. Catal. B* **2010**, *100*, 197.

[4] K. Omata, S. Izumi, T. Murayama, W. Ueda, *Catal. Today* 2013, 201, 7.

[5] a) J. Deleplanque, J.-L. Dubois, J.-F. Devaux,W. Ueda, *Catal. Today* **2010**, *157*, 351. b) M. D. Soriano, P. Concepci´on, J. M. L. Nieto, F. Cavani, S. Guidetti, C. Trevisanut, *Green Chem.* **2011**, *13*, 2954. c) A. Chieregato, F. Basile, P. Concepción, S. Guidetti, G. Liosi, M. D. Soriano, C. Trevisanut, F. Cavani, J. M. L. Nieto, *Catal. Today* **2012**, *197*, 58.

[6] K. Omata, K. Matsumoto, T. Murayama, W. Ueda, *ABC-7* **2013**, PA-067.

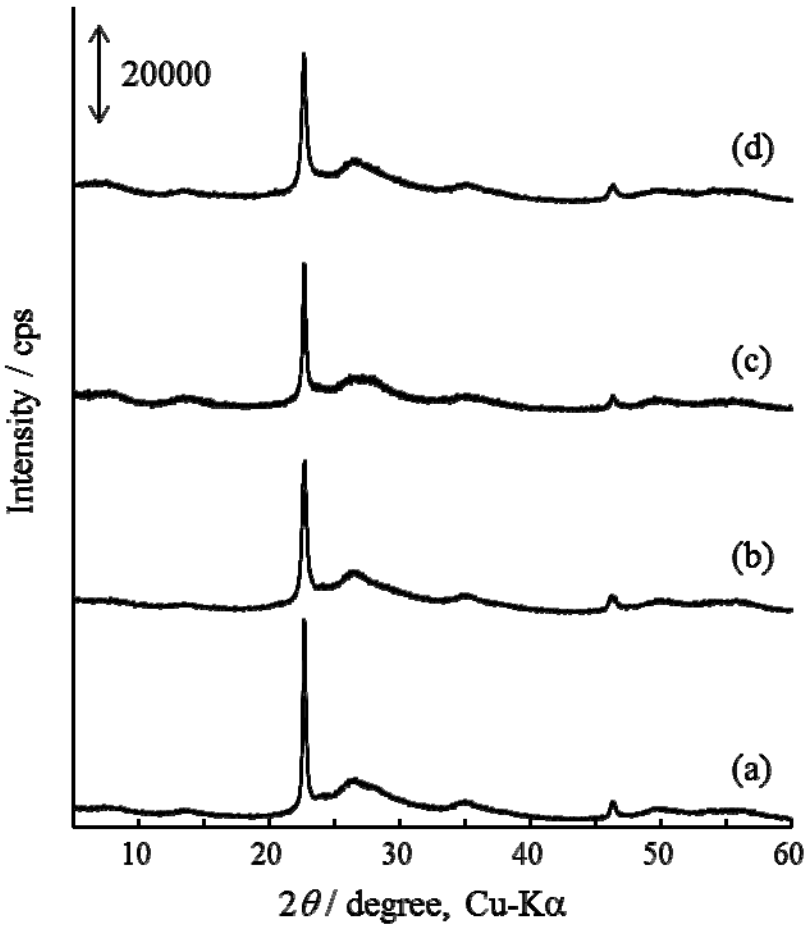


Fig. 6.1 XRD patterns of W-Nb-O (a), H_3PO_4/WNb (b), W-V-Nb-O (c) and H_3PO_4/WVNb (d).

Table 6.1 Effect of phosphoric acid addition on catalytic performance of W-Nb-O and W-V-Nb-O

Catalyst	*W/F*	GLR[a]conv.[b]	O_2 conv.	Yield[c] / %							
	/ g_{cat} min·ml^{-1}	/ %	/ %	**ACRL**	**AA**	ΛCΛL	PRΛL	HΛCT	ΛCΛ	CO_x	others
W-Nb-O	6.3×10^{-4}	64.3	1.4	32.4	0.1	0.5	0.3	2.5	0.1	0.8	27.6
	2.5×10^{-3}	98.9	6.5	74.5	0.1	2.9	1.0	0.4	0.7	3.8	15.5
H_3PO_4/WNb	6.3×10^{-4}	72.3	2.6	43.2	0.1	0.4	0.2	2.6	0.1	0.6	25.1
	2.5×10^{-3}	100	5.6	**81.8**	0.3	2.1	0.6	0.5	0.3	2.7	11.7
W-V-Nb-O	6.7×10^{-3}	100	48.6	3.5	46.2	1.4	<0.1	<0.1	12.7	33.8	2.4
H_3PO_4/WVNb	1.0×10^{-2}	100	45.3	0.5	**59.2**	0.3	<0.1	<0.1	8.2	22.3	9.5

[a]GLR=glycerol. [b]Reaction conditions: set temperature of the furnace, 558 K; composition of reactant gas, glycerol/ O_2/ N_2/ H_2O = 5/ 14/ 56/ 25 (mol%). [c]ΛCRL = acrolein, ΛΛ = acrylic acid, ΛCΛL = acetaldehyde, PRΛL = propanal, HΛCT = hydroxyacetone, ΛCΛ = acetic acid.

Table 6.2 Surface area and acid properties of the W-Nb-O and H_3PO_4/WNb catalysts

Catalyst	Surface area / $m^2 \cdot g^{-1}$	Acid amount / $\mu mol \cdot g^{-1}$	B / L[a]	
			-	$+H_2O$ [b]
W-Nb-O	118	136	0.4	3.6
H_3PO_4/WNb	91	244	1.5	23.4
W-V-Nb-O	120	129	0.4	3.2
H_3PO_4/WVNb	97	250	1.7	25.6

[a] Ratio of the integral absorbance (peak area) of the peak at 1540 cm^{-1} (Brönsted) to 1450 cm^{-1} (Lewis). [b] B / L in the presence of water (4.6 Torr).

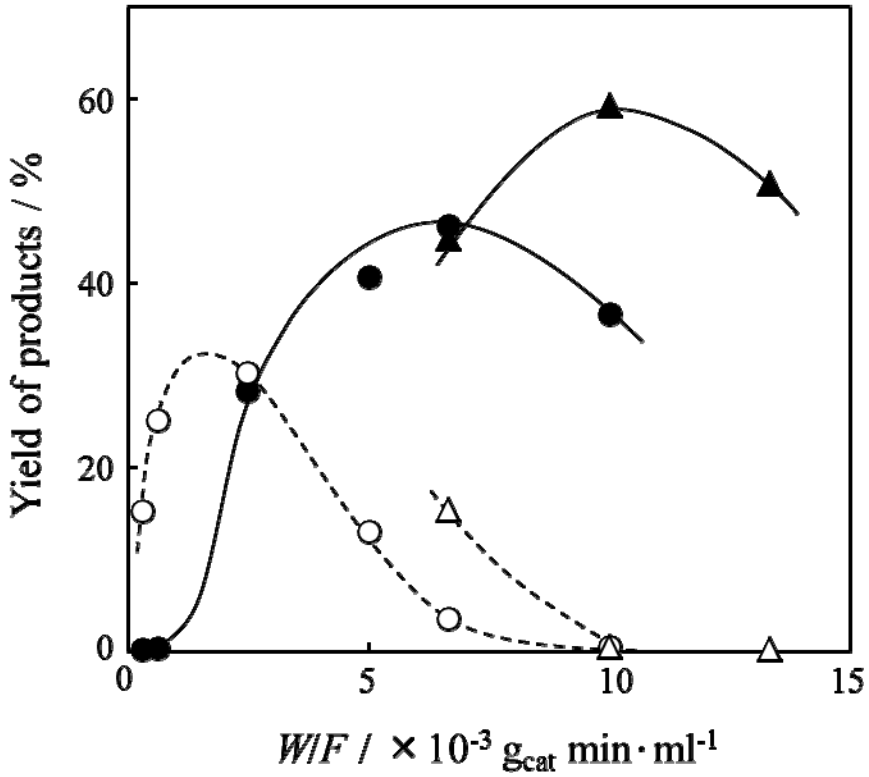


Fig. 6.2 Effect of contact time on the yields of acrolein and acrylic acid in the glycerol transformation over W-V-Nb-O (acrolein, ○; acrylic acid, ●) and H_3PO_4/WVNb (acrolein, △; acrylic acid, ▲).
Reaction conditions: set temperature of the furnace, 558 K; composition of reactant gas, glycerol/ O_2/ N_2/ H_2O = 5/ 14/ 56/ 25 (mol%).

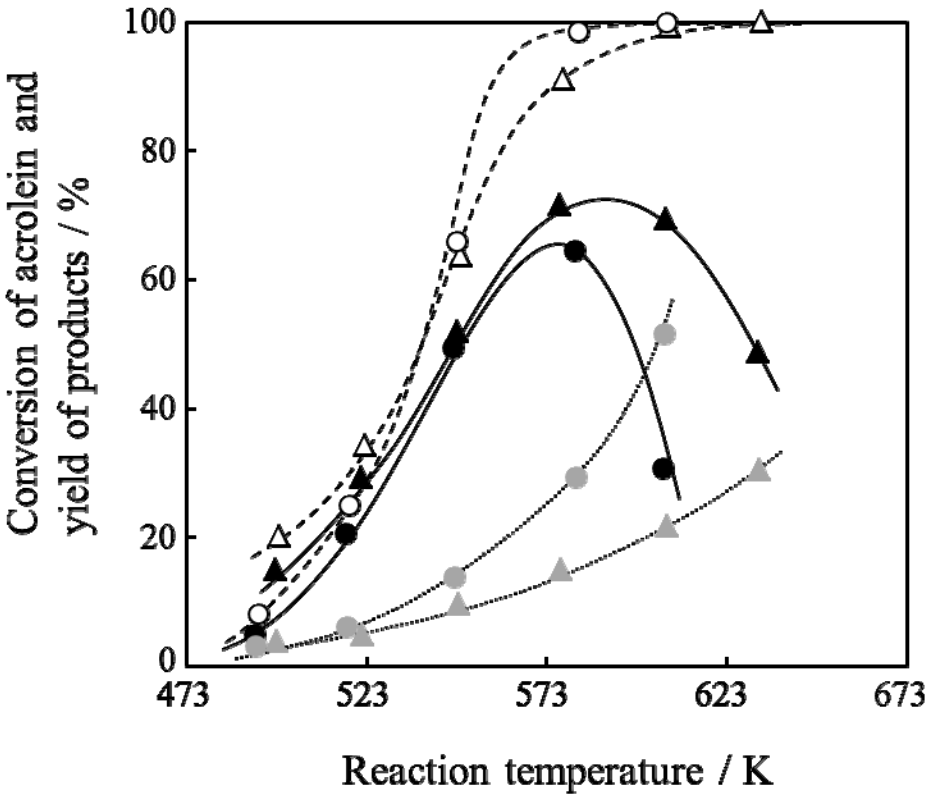


Fig. 6.3 Conversion of acrolein, yield of acrylic acid and CO_x in the acrolein oxidation over W-V-Nb-O (acrolein, ○; acrylic acid, ●; CO_x, ●) and H_3PO_4/WVNb (acrolein, △; acrylic acid, ▲; CO_x, ▲). Reaction conditions: catalyst weight, 0.2 g; flow rate, 77 ml·min^{-1}; composition of reactant gas, acrolein/ O_2/ N_2/ H_2O = 1/ 15/ 58/ 26 (mol%).

Chapter 7

General Conclusion

In this doctoral thesis, I studied on development of new complex metal oxide catalysts composed of W and group 5 elements such as V, Nb or Ta and their application to the synthesis of acrolein or acrylic acid from glycerol.

The main results of this thesis are summarized as follows:

In **Chapter 2**, hydrothermal synthesis of complex metal oxide composed of W and Nb (W-Nb-O) and analysis of their structure were investigated. Effect of preparation conditions such as composition, calcination temperature and concentration of precursor solution on structure of W-Nb-O was examined.

While the simple impregnation and subsequent calcination only produced a mixture of WO_3 and Nb_2O_5, W-Nb-O having layer structure in *c*-direction was obtained by hydrothermal method. It is suggested that the hydrothermal method is in principle an effective method to promote octahedral arrangement of materials. However, the presently applied hydrothermal conditions could not facilitate the crystallization in *a*-*b* plane as with $Cs_{0.5}[Nb_{2.5}W_{2.5}O_{14}]$. Nevertheless, The result of Rietveld analysis, Raman and N_2 adsorption suggest that W-Nb-O (673 K) and $Cs_{0.5}[Nb_{2.5}W_{2.5}O_{14}]$ have common unit such as pentagonal units and 7-membered rings, and similar ordered structure. Besides, layer-structured W-V-O and W-Ta-O were also obtained by hydrothermal method.

Chapter 3 described solid acid property of W-Nb-O and dehydration of glycerol to acrolein over the W-Nb-O catalyst. Effects of structure and the W/Nb ratio of the W-Nb-O catalyst on their acidity and selectivity in glycerol transformation were investigated.

First, catalytic performance of W-Nb-O synthesized by hydrothermal method was compared with those of WO_3/ZrO_2 and H-ZSM-5 which are typical acid catalysts. The W-Nb-O catalysts gave acrolein yield higher than 70% in the glycerol transformation. This catalytic performance was higher than that of the WO_3/ZrO_2 or the H-ZSM-5. In addition, it was observed that the deactivation rate in the W-Nb-O catalyst was less than that in WO_3/ZrO_2 or H-ZSM-5.

Second, product selectivity over W-Nb complex metal oxides, which have the same layered structure

in the *c*-axis direction were tested at comparable glycerol conversion rates. The tetragonal W–Nb–O catalyst ($Nb_8W_9O_{47}$) and the acid-treated $Cs_{0.5}[Nb_{2.5}W_{2.5}O_{14}]$ having orthorhombic structure showed different selectivity for glycerol transformation. However, the hydrothermally synthesized W–Nb–O calcined at a lower temperature had comparable acrolein selectivity to acid-treated $Cs_{0.5}[Nb_{2.5}W_{2.5}O_{14}]$. The results suggest that the structure of *a*–*b* plane affects the product distribution.

Besides, effect of a combination W and Nb on acidity was investigated by the reaction over W-Nb-O having various W/Nb ratio. While W-Nb-O exhibited higher selectivity for acrolein than Nb oxide by hydrothermal method, the W/Nb ratio of W-Nb-O did not affect acrolein selectivity.

In **Chapter 4**, reaction pathway of glycerol transformation over the W-Nb-O catalyst was discussed based on effect of contact time on product distribution and reaction starting from intermediates. While the most of hydroxyacetone formed from glycerol oxidized to 2-oxo-propanal, acrolein was stable on the W-Nb-O catalyst. The result of reaction under various contact times suggests that ethers formed by intermolecular dehydration of glycerol or polymer of unsaturated aldehyde included in others convert to acrolein sequentially.

Effect of co-feeding gas on catalytic performance of the W-Nb-O catalyst was also examined. The addition of water increased acrolein yield and suppressed deactivation of catalyst. However, the yield of hydroxyacetone and propanal were hardly affected by the addition of water suggesting that the acrolein and hydroxyacetone or propanal were formed on different sites. Besides, the results of FT-IR of adsorbed pyridine and the cumene cracking indicate that the acrolein yield in the glycerol transformation is improved by water existing in the reaction because the some of the Lewis acid site is hydrated and changes into the Brönsted acid.

The co-feeding of oxygen suppressed deactivation of the catalysts without affecting acrolein selectivity. The oxidative capability of the catalyst promotes the combustion of materials causing deactivation and suppresses the deactivation of the catalyst.

Chapter 5 indicated direct oxidative transformation of glycerol to acrylic acid over W-based complex metal oxide catalysts. Introduction of V to W-Nb-O aiming at development of the catalyst for direct transformation to acrylic acid was investigated. While the W-Nb-O catalyst synthesized by hydrothermal method gives acrolein mainly in the glycerol dehydration, acrylic acid formed directly from glycerol over the V-added W-Nb-O catalysts. W-V-Nb-O synthesized by the hydrothermal treatment of mixed solution of W, Nb and V exhibited higher yield of acrylic acid than the impregnated catalysts. V was incorporated into framework of W-Nb-O by the hydrothermal treatment. Introduction of V into framework did not affect acid property of W-Nb-O. In addition, V^{4+} which is active site for acrolein to acrylic acid was formed by interaction between V and W. As a result of optimization of the balance between acid and oxidative capability, the maximum yield of acrylic acid was 46.2% over catalyst with composition of V: W: Nb = 0.3: 1.35: 1, under the condition of $W/F = 6.7\times10^{-3}$ g min·ml^{-1}, reaction temperature 580 K.

In **Chapter 6**, the addition of phosphoric acid to the W-V-Nb-O catalyst was attempted toward enhancement of acrylic acid yield. Effect of the phosphoric acid addition on acid properties of W-Nb-O and the catalytic performance of W-V-Nb-O for the acrolein oxidation and the glycerol transformation were investigated. The addition of phosphoric acid increased the acid amount and the Brönsted acidity of the W-Nb-O catalyst. In addition to the improvement of the acidity, phosphoric acid interacts with V sites for suppressing the sequential oxidation of acrylic acid to CO_x. As a result, acrylic acid yield in the glycerol transformation increased significantly. The H_3PO_4/WVNb catalyst gave acrylic acid in yield of 59.2% directly from glycerol ($W/F = 1.0\times10^{-2}$ g_{cat} min·ml^{-1}, reaction temperature 594 K).

Throughout all the studies in this thesis, the following conclusion was drawn.

Orthorhombic-like crystalline W-based complex metal oxides was synthesized by hydrothermal method without introduction of alkali metals and calcination at a high temperature. The diffraction peak ascribed to *a-b* plane was broad because crystallite size was currently not enough. If larger crystal is

obtained by improvement of synthesis method, the structure could be analyzed in more detail.

W-Nb-O synthesized by hydrothermal method exhibited high activity for the dehydration of glycerol to acrolein. The selectivity was different depending on the structure of *a-b* plane of the W-Nb complex metal oxides. However, the structure of active site remains incompletely understood. It is expected to discuss relationship between structure of active site and its catalysis.

Acrylic acid formed from glycerol directly over V-added W-Nb-O. In particular, V spaces in framework of orthorhombic-like W-Nb-O exhibited high acrylic acid selectivity in the acrolein oxidation. Oxidative capability coexists with acidity in the W-V-Nb-O catalyst without the harmful effect on each other; this catalyst is attractive dual-functional catalyst. The functions of constituent elements in the W-V-Nb-O catalyst were concluded by comparison of catalytic performance in the glycerol dehydration and the acrolein oxidation over W-Nb-O, W-V-O and V-Nb-O.

Moreover, the addition of phosphoric acid to the catalytic surface improved the selectivity for both of the glycerol dehydration to acrolein and the acrolein oxidation to acrylic acid. As a result, the achieved single pass yield of acrylic acid was about 60% and is currently the highest amongst the reported results. The addition of phosphoric acid enhanced Brönsted acidity which is efficient for the formation of acrolein. However, the effect on oxidative capability should be investigated.

The effective catalyst for the direct oxidative transformation of glycerol was developed by the control of structure and composition of catalysts, optimization of reaction conditions and the addition of third component.